Operational impacts of large-scale wind power generation in the German power system and effects of integration measures – Analyses with a stochastic electricity market model

Von der Fakultät Energie-, Verfahrens- und Biotechnik der Universität Stuttgart zur Erlangung der Würde eines Doktor-Ingenieurs (Dr.-Ing.) genehmigte Abhandlung

Vorgelegt von
Bernhard Hasche
geboren in München

Haubtberichter:	Prof. Dr.-Ing. Alfred Voß
Mitberichter:	Prof. Mark O'Malley

Tag der Einreichung:	19. Oktober 2011
Tag der mündlichen Prüfung:	27. September 2012

Institut für Energiewirtschaft und Rationelle Energieanwendung, Stuttgart
Prof. Dr.-Ing. A. Voß
Abteilung Elektrizitäts- und Gasmarktanalysen (EGA)

2012

Acknowledgements

This work would not have been possible without the support of many people. First and foremost, I wish to express my sincere gratitude to Prof. Alfred Voß for his supervision and guidance. My deepest gratitude is also due to Prof. Mark O'Malley for accepting the co-examination of the thesis and for his tremendous generosity that he showed on many occasions.

My grateful thanks are extended to Dr.-Ing. Derk Swider for his valuable advice at the beginning of the project and to Rüdiger Barth for three great years in the same office. Special thanks are given to Heike Brandt, Prof. Christoph Weber and Prof. Peter Meibom for their support, above all with regard to the applied model.

All colleagues of the "Institut für Energiewirtschaft und Rationelle Energieanwendung" at University of Stuttgart are thanked for numerous memorable moments. The same applies to all members of the "Electricity Research Centre" at University College Dublin who gave me such a friendly welcome. An honourable mention goes to Robert Küster and to the football players of both groups who helped me to keep physically active.

Finally, I would like to thank my family and friends for all the personal support over the last years. I am forever indebted to my parents, Angela and Helmut Hasche, for everything they have done for me and to my wife Mélanie for her understanding and love.

Contents

Symbols

Parameters

ϕ^{max} . . . . . .maximal angle difference between regions

π . . . . . .probability of a scenario

b^{reg} . . . . . .susceptance between regions

c^{fuel} . . . . . .relative fuel price

c^{heat} . . . . . .cost for external negative heat use

$c^{inst,heat}$ . . . . .installed heat capacity

$c^{inst,load}$ . . . . .installed loading capacity

c^{inst} . . . . . .installed capacity

$c^{o\&m}$ . . . . . .relative operation and maintenance cost

$c^{onl,prev}$ . . . . .capacity on-line as planned in the last optimization

$c^{opp,onl}$ . . . . . .opportunity cost for being online

$c^{opp,res}$ . . . . . .opportunity cost for reservoir

$c^{opp,sto}$ . . . . . .opportunity cost for storage

c^{pen} . . . . . .relative penalty costs for slack variables

c^{start} . . . . . .relative start-up cost

c^{tax} . . . . . .relative emission tax

d^{heat} . . . . . .CHP heat demand

$d^{prim,+}$ . . . . .positive primary reserve requirement

$d^{prim,-}$ . . . . .negative primary reserve requirement

$d^{sec,+}$ . . . . . .positive secondary reserve requirement

$d^{sec,-}$ . . . . . .negative secondary reserve requirement

$d^{ter,+}$ . . . . . .positive tertiary reserve requirement

d . . . . . .electricity demand

e^{gen} . . . . . .efficiency related to generation

e^{onl} . . . . . .efficiency related to capacity being online

e^{start} . . . . . .relative start-up fuel consumption

i^{res} . . . . . .inflow in hydro reservoirs

k^{chp} . . . . . .chp relation index

l^{loss} . . . . . .load loss

lf^{min} . . . . . .minimal load factor

p^{pv} . . . . . .photovoltaic power generation

p^{ror} . . . . . .run-of-river power generation

$p^{wind,day}$ . . . . .day-ahead forecast of wind power generation

$p^{wind,intra}$ . . . .intraday wind power forecast

t^{minop} . . . . . .minimal operation time

t^{minsd} . . . . . .minimal shut-down time

t^{minst} . . . . . .minimal start-up time

t^{reg} . . . . . .transmission capacity between regions

Sets and Elements

$\mathbf{A}$ . . . . . .set of areas

$\mathbf{R}$ . . . . . .set of regions

$\mathbf{S}$ . . . . . .set of scenarios

$\mathbf{T}$ . . . . . .considered time period

$\mathbf{U_a}$ . . . . . .power plants in area a

$\mathbf{U_r}$ . . . . . .power plants in region r

$\mathbf{U_{rs}}$ . . . . . .reservoir hydro power plants without loading capacity

$\mathbf{U_{sp}}$ . . . . . .power plants qualified as spinning reserves

$\mathbf{U_{st}}$ . . . . . .pump storage power plants

$\mathbf{U_{tr}}$ . . . . . .power plants qualified as fast activating reserves

$\mathbf{U}$ . . . . . .set of power plants

$\mathbf{X}$ . . . . . .set of regions pairs where tertiary reserve can be transmitted

a . . . . . .area

r . . . . . .region

s . . . . . .scenario

t_{last} . . . . . .last time step in time period

t . . . . . .time steps

u . . . . . .power plant

Variables

C^{online} . . . . .online capacity

$F^{reservoir}$ . . . .fill level of reservoir

$F^{storage}$ . . . . .fill level of storage

L^{+} . . . . . .up-regulation of loading

L^{-} . . . . . .down-regulation of loading

L^{day} . . . . . .loading day ahead

P^{+} . . . . . .up-regulation of generation

P^{-} . . . . . .down-regulation of generation

P^{day} . . . . . .power generation day ahead

P^{heat} . . . . . .heat generation

P^{start} . . . . . .started capacity

$R^{sp,+}$ . . . . . .positive primary and secondary reserve

$R^{sp,-}$ . . . . . .negative primary and secondary reserve

$R^{sp,stor,+}$ . . . .positive primary and secondary reserve by decreased storage loading

$R^{sp,stor,-}$ . . . .negative primary and secondary reserve by increased storage loading

$R^{ter,+}$ . . . . . .positive tertiary reserve

T^{day} . . . . . .transmission scheduled at day-ahead market

T^{intra} . . . . . .transmission scheduled at intraday market

T^{res} . . . . . .transmission of tertiary reserve

V^{day} . . . . . .slack variable for day-ahead equation

V^{heat} . . . . . .slack variable for heat equation

V^{intra} . . . . . .slack variable for intra-day equation

V^{spill} . . . . . .spilling of water

$W^{shed,day}$ . . . .wind shedding at the day-ahead market

$W^{shed,intra}$ . . .wind shedding at the intraday market

Φ^{delta} . . . . . .intraday change of regional angle

Φ . . . . . .voltage angle

Zusammenfassung

Ein starker Ausbau der Windenergie, onshore und offshore, ist ein erklärtes politisches Ziel in Deutschland und anderen Ländern. Der Windenergieanteil nimmt folglich in immer mehr Stromsystemen zu. Die Stromerzeugung durch Windenergie weist andere Eigenschaften auf als sie beim Betrieb konventioneller Kraftwerke gegeben sind. Die Erzeugung beruht auf der natürlichen Ressource Wind und ist daher fluktuierend. Die meteorologische Abhängigkeit führt auch zu einer begrenzten Prognostizierbarkeit des verfügbaren Stromes. Ein dritter Aspekt ist die Konzentration der Windenergieanlagen an windreichen Standorten wie im Norden Deutschlands.

Die Arbeit verfolgt zunächst das methodische Ziel, diese drei Aspekte bei der Analyse des Strombetriebs greifbar zu machen und geeignete Ansätze für die Strommarktmodellierung zu entwickeln. Dies betrifft insbesondere die Simulation der Windstromerzeugung und Windstromprognosen und die Anwendung eines stochastischen Optimierungsmodells zur Systemanalyse. Außerdem wird das anwendungsorientierte Ziel verfolgt, verschiedene Szenarien des deutschen Stromsystems für das Jahr 2020 zu untersuchen. Vielversprechende Systemanpassungen für eine verbesserte Integration der Windenergie und einen effizienteren Strombetrieb sind dabei zu identifizieren.

Vor der Methodenentwicklung und Anwendung des Strommarktmodells wird zunächst die Bedeutung der drei obengenannten Aspekte erörtert und die Grundlage für die spätere Modellierung gelegt. Es ergibt sich, dass die Windstromeinspeisung die Fluktuation der Residuallast vor allem in Relation zu den vorliegenden Residuallastniveaus verstärkt. Die Flexibilität thermischer Kraftwerke wird in diesem Zusammenhang ebenfalls analysiert. Eine Untersuchung von Systemunsicherheiten zeigt die verstärkte Bedeutung der Windprognosefehler im Vergleich zu Lastprognosefehlern auf. Der DC Lastfluss wird als ein allgemeiner Ansatz für die Netzabbildung in der Strommarktmodellierung vorgestellt.

Eine systembezogene Analyse der Windstromintegration wird durch die Vorstellung eines stochastischen Strommarktmodells vorbereitet. Ein Merkmal des Optimierungsmodells ist die Verwendung einer rollierenden Planung, die eine detaillierte Berücksichtigung von Prognosefehlern ermöglicht. Die in der Arbeit durchgeführte Weiterentwicklung des Modells besteht hauptsächlich in der Erfassung von Netzengpässen. Dazu wird ein Netzreduktionsansatz entwickelt, der das Übertragungsnetz auf die im Marktmodell gewählte Regionenabbildung reduziert. Der Reduktionsansatz beruht auf einem Vergleich der Lösungen des DC-Lastflusses im

reduzierten und unreduzierten Netz. Des Weiteren wird eine Methode zur Berechnung der benötigten Tertiärreserve in Abhängigkeit von der Windenergieprognose entwickelt, die probabilistische Ansätze mit einer Optimierung kombiniert.

Die Simulation der Windstromeinspeisung und Windstromprognosen führt verschiedene Analysen und Methoden zusammen. Zunächst wird allgemein ein quantitativer Bezug zwischen der Variabilität der Windstromeinspeisung und der Regionengröße hergestellt. Die ermittelten Zusammenhänge werden bei der Simulation der Windstromerzeugung, die auf einer Anpassung von Leistungskennlinien beruht, verwendet. Die modifizierten Leistungskennlinien bilden bei der Transformation von Windgeschwindigkeit zu Windleistung den Glättungseffekt ab, der sich bei regionaler Einspeisung einstellt. Die Simulationsergebnisse zeigen die erhöhte Variabilität der Stromerzeugung in den Offshore-Gebieten. Zur Simulation der Windstromprognosen wird ein Szenariogenerierungsansatz auf Grundlage des Moment Matching Verfahrens eingesetzt, der sowohl Korrelationen der Prognosefehler als auch Abweichungen von der Normalverteilung berücksichtigt. Die Simulation erfolgt auf Basis einer statistischen Analyse gemessener Prognosefehler, die unter anderem einen empirischen Zusammenhang zwischen Fehlerkorrelation und geographischer Distanz liefert. Die für 2020 simulierte deutschlandweite Prognosegüte ist, bezogen auf die installierte Kapazität, trotz einer unterstellten Prognoseverbesserung von 20% vergleichbar zu der heutigen aufgrund der räumlichen Konzentration der Anlagen auf See.

Für die Szenarioanalyse des Stromsystems im Jahre 2020 werden die Kraftwerksportfolios von zwölf deutschen Regionen und weitere Parameter anhand verschiedener Quellen ermittelt. Dazu gehören die Reserveanforderungen und Parameter des reduzierten Stromnetzes, die anhand obiger Modelle berechnet werden. Die Modellanwendung demonstriert, dass in dem betrachteten Szenario 3% der jährlichen Windenergie fast ausschließlich aufgrund von Netzengpässen abgeregelt werden muss. Die stark unterschiedlichen regionalen Elektrizitätspreise weisen ebenfalls auf Netzengpässe hin. Die jährlichen Kosten der Windprognosefehler belaufen sich auf circa 180 Millionen Euro oder 1% der betrieblichen Systemkosten. Die Modellergebnisse zeigen dabei ein großes Potential für Kosteneinsparungen durch den Einsatz von Risikomanagement auf.

Anhand von Szenariovariationen werden Systemanpassungen hinsichtlich des Einsatzes von CAES Speicherkraftwerken, Demand Side Mangagement und flexiblerer Kraftwerke sowie Änderungen der Infrastruktur durch Netzausbauten und einer angepassten geographischen Allokation von Kraftwerken untersucht. Die Ergebnisse belegen die Vorteile eines stochastischen Marktmodellierungsansatzes für die Evaluierung flexibilitätsbezogener Integrationsmaßnahmen. Der Vergleich der Integrationsmaßnahmen identifiziert infrastrukturelle Maßnahmen als wirksamste Systemverbesserung, während der Nutzen zusätzlicher CAES Speicherkapazitäten gering ist. Unter der Annahme eines Netzes ohne Übertragungsengpässe reduzieren sich die jährlichen Systembetriebskosten um eine Milliarde Euro. In einem

moderateren Netzausbauszenario lassen sich nur 10% dieser Einsparung realisieren. Eine Kostenreduktion in ähnlicher Höhe wird durch eine angepasste Standortwahl neuer Kraftwerke erreicht. Eine Anpassung der Stromerzeugung an die Netzsituation ist demnach eine vielversprechende Alternative zu Netzausbauten, die vor allem auch wegen der langwierigen Prozesse beim Bau neuer Netzleitungen interessant ist. Ein regionales Preismodell würde dafür Anreize schaffen.

Abstract

A strong increase of onshore and offshore wind power capacities is an official political target in Germany and other countries. The wind energy shares therefore rise in many power systems. Wind power generation has other characteristics than the power generation by conventional power plants. The wind is a natural resource that is fluctuating. The meteorological dependency leads to a limited predictability of the available power. A third aspect is the concentration of wind farms at locations with high wind yields as in the North of Germany.

From a methodological point of view, the thesis focuses on the analysis of the three aspects with regard to the power system operation and the development of related modelling approaches. This especially refers to the application of a stochastic optimization model for the system analysis and to the simulation of wind power generation and wind power forecasts. The application orientated focus is on a scenario analysis of the German power system in 2020. The analysis aims at the identification of promising system adaptations that lead to an improved wind power integration and a more efficient power system operation.

Before the model presentation, the importance of the three aspects above is discussed giving the basics for the latter modelling. It is shown that the residual load fluctuations are increased by the wind power generation, especially if they are related to the residual load levels. The flexibility of thermal power plants is also regarded here. An analysis of operational uncertainties shows the importance of wind power forecast errors in relation to load forecast errors. The DC load flow model and characteristics of the transmission grid are explained.

A stochastic market model is presented that allows an integrative analysis of the wind power integration. One characteristic of the optimization model is the application of a rolling planning so that forecast errors can be specifically considered. A main modification of the model compared to earlier model versions is given by the representation of grid constraints. A grid reduction approach is developed that reduces the transmission grid to a simplified structure that is applied in the market model. The grid reduction approach is based on a comparison of DC load flow solutions in the reduced and unreduced grid. Additionally, an approach for the calculation of tertiary reserves is given. The approach considers the wind forecast quality and combines probabilistic elements with an optimization.

The simulation of wind power generation and forecasts combines different analyses and methods. General quantitative relations between the variability of wind power generation and the geographical region size are derived. The equations are

applied in the simulation of wind power generation that is based on adapted wind power curves. The adapted power curves consider regional smoothing effects in the transformation of wind speed to wind power. The simulation results reflect the high variability of the concentrated offshore wind power. For the simulation of the wind power forecasts, a scenario generation method based on moment matching is presented that allows simulating non Gaussian distributed forecast errors and their correlations. The results of a statistical analysis of measured forecast errors are used in the simulation. An empirical relation between error correlation and geographical distance is for example given. The German forecast quality that is simulated for 2020 assuming an improvement of forecasting by 20% is, related to the installed capacity, similar to the one of today due to the high spatial concentration of the offshore capacities.

For the scenario analysis of the power system in 2020, the power plant portfolios of twelve German regions and other parameters are derived based on different sources. This includes reserve requirement values and reduced grid parameters that are calculated by the methods mentioned above. The results show that, in the regarded scenario, 3% of the yearly wind energy cannot be integrated into the system. They are curtailed nearly exclusively due to transmission constraints. The network congestions also lead to high differences between the regional electricity prices. The yearly costs of wind forecast errors amount to circa 180 million Euros or 1% of the operational system costs. The model results thereby indicate a large cost saving potential by risk management methods.

Based on scenario modifications, integration measures related to CAES capacities, demand side management and more flexible power plants as well as infrastructural changes by grid expansions and an adapted geographical allocation of power plants are analysed. The importance of a stochastic modelling approach for the evaluation of flexibility related scenarios is shown. The comparison of the integration measures identifies infrastructural changes as most efficient system improvements whereas the benefits of CAES capacities are small. Assuming a grid without any transmission constraints, the yearly system costs are reduced by one billion Euros. A limited grid upgrade leads to 10% of this cost reduction. Similar cost savings are achieved by adapting the geographical locations of the power plants. Adjusting the generation to the grid is therefore a promising alternative to grid expansions especially considering the long processes that are involved with new transmission lines. A market design with regional electricity prices would give related incentives.

1. Introduction

Over the last decade renewable energy has become an important part of the power system. In the future, its share will further rise as the European governments have defined high renewable energy targets. Among the renewable energy sources, wind energy is one of the most successful ones and has outrun hydro power in some countries. Even though many wind farms have been built until now, additional potential is predicted for the future. Especially offshore wind energy is promising as higher wind yields can be achieved. Also the replacement of older wind farms by newer, larger ones could lead to additional capacities. The potential of wind power is therefore still important.

The specific characteristics of wind power however lead to challenges for the operation of the power system. Wind power, being based on the natural resource wind, is a fluctuating power source. In an electric system, a continuous balance between generation and demand is necessary and the operation of the power and storage plants is always adapted to the demand level. The fluctuating wind power in combination with the fluctuating demand may lead to new requirements for the flexible operation of the power plants. Wind is a meteorological phenomenon and the prediction of the future wind is subject to uncertainties. As the generation of most of the power plants has to be planned in advance, the maintenance of the balance between generation and load can be more challenging with high wind power shares. A third aspect is the regional concentration of wind farms in windy regions. In Germany, higher wind yields are for example possible in the North and most of the capacities are located there. Offshore wind farms are naturally restricted to specific geographical areas. The transmission of power may therefore become more important depending on the wind resources in the regarded system.

These aspects outline the topic of the thesis. A potential future German power system with high shares of on- and off-shore wind power is analysed. The focus is thereby on the dispatch of the power plants and the techno-economical performance of the power system. A large part of the analysis is model-based. The core model is an optimization model of the power system. An additional simulation model is related to the wind power generation and short-term wind forecasts. General analyses of wind power integration issues are considered in the model concept and its input parameters. Only operational aspects that are related to the dispatch and the transmission are examined. The geographical scale is Germany under consideration of its regional differences and the European neighbour countries. The temporal scale is the hourly operation of the power system over one

year. Technical questions that are related to the short-time domain are not considered here. This does not apply to the topic of reserves that is situated between the two time domains and therefore important for the dispatching. Long-term aspects related to the system planning and the analysis of investment effects are also not part of this work.

The different parts of the thesis aim to give explicit and implicit answers to the following questions that are related to the modelling of power systems and to potential future scenarios of the German power system. The simulation of wind power generation and wind power forecasts is one principal topic of the work. The variable character of wind power was mentioned. Different measures are introduced to define this variability. The variability thereby depends on the region size and the number of wind farms in the region. A general analysis shows how the variability is influenced by these two factors. The derived relations are also used in a simulation approach that gives regional wind power time series for given wind speed data. In the approach, multi-turbine power curves can be generated according to defined statistics. The statistics of wind speed forecasts are derived by an analysis of measured forecast data. Forecast quality and parameters describing the distributions of the forecast errors are thereby considered. A moment matching approach is presented to apply these statistics. Thus, forecast errors can be simulate that take into account both forecast quality and the frequency of extreme events.

The variability of wind load has to be considered in combination with the electricity demand leading to the residual load (the demand minus the wind power generation). The question is whether the variability of the residual load is affected by the wind power generation. This topic is explicitly addressed by an statistical analysis of the residual load with and without wind power showing why variability can be an issue with high wind power shares. The residual load is implicitly considered in the application of the power system model. The flexibility of the power plants is thereby important and an literature research leads to the related input parameters for the model. Uncertainties in the dispatch are also considered in two ways. On the one hand, the influence of wind power forecasts and other uncertainties on reserve requirements is analysed. The tertiary reserve requirements are thereby calculated by an probabilistic approach. On the other hand, intraday rescheduling of the dispatch is considered in the power system model. Wind forecast scenarios, derived by the wind simulation approach, are applied in the intraday optimizations.

The transmission issues are addressed by a representation of the transmission grid in the power system model. The consideration of complete transmission grids is challenging in large-scale dispatch models due to computational and data issues. A grid reduction approach is therefore developed. The approach reduces a complete representation of the transmission grid to a regional one. The reduction is based on a DC load flow. The reduced grid is compared to the complete grid

and to a grid representation that considers thermal transmission capacities only. The transmission parameters of the reduced grid can then be applied in the power system model.

The model is applied for the analysis of the power system in 2020. A possible scenario of the power plant portfolio and electricity demand is derived, mainly based on a UCTE system forecast. German regions and neighbour countries are thereby modelled in order to capture the influence of hydro-dominated systems. The developed wind power simulation leads to the generation and forecast data of on-shore and off-shore wind power. The application of the model shows the operational performance of the power systems. Parameters as system costs, curtailment, electricity prices and exchanges are for example presented. The integration of high shares of wind power is thus evaluated. The importance of the stochastic representation of forecast errors in the dispatch model is also discussed. The influence of high wind years and high fuel prices are thereby analysed by two additional scenarios.

Finally, the power system model is used to compare different integration measures. A main feature of the work is that the integration measures are evaluated applying the same power system model and scenario. They can therefore be directly compared. This is possible as the dispatch model considers both uncertainty and transmission issues. The regarded measures are related to forecasting, improvement of flexibility and infrastructure changes. The power system model can be run in a stochastic optimization mode. The dispatch optimizations are then based not only on expected value forecasts of the wind power generation but also on possible forecast error scenarios. This allows to simulate hedging of forecast errors in the dispatch process and to assess the benefits of hedging. The flexibility measures are defined by additional CAES power plants, by a basic representation of demand side management and by an increased flexibility of conventional power plants. Infrastructure changes relate to additional transmission lines and to a different regional allocation of power plants. The later can be seen as an alternative way to deal with transmission congestion. The differences between the related scenarios are thereby explicitly derived. The following has to be considered in the interpretation of the model results. In the dispatch model, an exogenously given power system is applied and no optimal power plant portfolio is calculated. The analyses are therefore scenario analyses and the results can only be indicative for other power systems.

The thesis is organized as follows. Some principles of wind power generation and forecasting are given in Section 2.1 as a general basis for the rest of the work. The variability of the residual load is analysed in Section 2.2.1 motivating the application of a dispatch model. The parameters that are related to power plant flexibility and that are later applied in the model are also presented in Section 2.2.1. Uncertainties in the dispatch and related mechanisms are explained in Section 2.2.2 supporting the differentiated consideration of uncertainties in the

model. The transmission grid and the later required DC load flow are introduced in Section 2.2.3. The power system model is defined in Section 3.1. The general concept is first presented followed by the mathematical description. The main parameters of the applied power system scenario as for example the regional distribution of the installed capacities are derived in Section 3.2.1. In Section 3.2.2 and Section 3.2.3, two methods are developed to derive the model input parameters that are related to reserves and transmission. The tertiary reserve requirements and a reduced grid are thereby calculated. A principal input parameter of the model is the wind power. An overview to the related simulation approach and the applied data is given in Section 4.1.1, followed by the main results in Section 4.1.2. The variability of wind power is generally analysed in Section 4.2.1. The derived relations are then used in the simulation of wind power generation in Section 4.2.2. The simulation of wind power forecasts is addressed by an analysis of speed forecast errors in Section 4.3.1 and a scenario generation method in Section 4.3.2. The power system model in combination with the simulated wind power generation and forecasts is then applied. The scenario analysis starts with the main scenario plus a high wind and a high fuel price scenario in Section 5.1. Based on these scenarios, the integration measures related to forecasting, flexibility and infrastructure are analysed in Section 5.2, 5.3 and 5.4. All integration measures are compared in Section 5.5. The main results of the thesis are resumed in the conclusion.

2. Wind power in the electricity system

General technical aspects of wind power generation, grid connection and forecasts are analysed in the following chapter. In the first section, the transformation of wind to power and forecasting of wind are considered. Some aspects of grid connection are also given. The three topics are reflected by the aspects of wind power integration that are discussed in the second section of the chapter. First, the variability of the residual load and the flexibility of conventional power plants are analysed. Secondly, the uncertainties due to forecast errors or outages and the mechanisms to cope with them are compared. Finally, the transmission grid and its transmission constraints are regarded.

2.1. Grid-connected wind power

Some principles of wind power generation are here addressed first followed by some aspects of the grid connection of wind farms. The process of wind power forecasting and some challenges for forecast improvements are explained in the second part.

2.1.1. Wind power generation and grid connection

The wind power output and its fluctuations are mainly determined by the fluctuation of the wind. The relation between wind and power is defined by the power curve that is considered in the following. After that, some aspects of grid connection are given indicating for example at which voltage levels the wind farms are normally connected.

Power output

The power curve gives the relation between wind speed and power generation. There are two cases where the wind farm does not generate any power. Below a minimal wind speed, the cut-in speed, the wind energy is not sufficient for the inertia forces of the wind farm system (phase A in Figure 2.1-(a)). On the contrary, the rotor is blocked to avoid that the generator of the farm operates in motor mode and that energy is drawn from the grid [1]. Above a maximal

frequency power generation is also stopped (phase D). These cut-out wind speeds occur in events of severe weather. The pitch control automatically turns the blades out of the wind to avoid strong mechanical stresses. With the blades out of the wind and the rotor blocked, only the small surface of the blades is opposed to the wind and not the total rotor surface. Between these two points, there is an increase of the power generation with rising wind speeds until the nominal power output at the so-called rated speed is reached (phase B). A steady phase follows where the wind farm generates at name plate capacity (phase C).

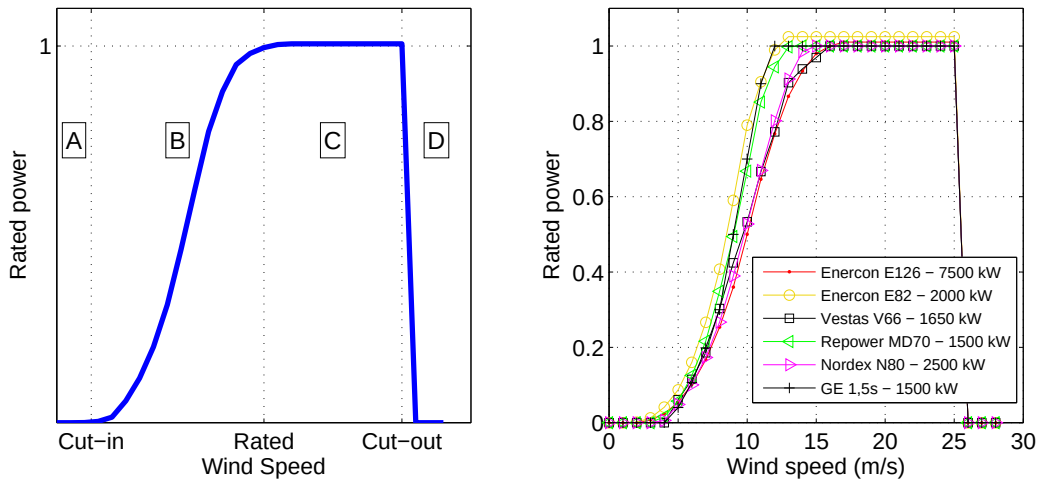

Figure 2.1.: Relation between wind speed and power output

The typical curve slightly differs between the turbine types and producers. For the German market, the following producers are especially important: Enercon, Vestas, Repower, Nordex, General Electric, Siemens, Fuhrländer and Gamesa. Between these, Enercon and Vestas are the most important delivering more than 70% of the wind farms that were installed in 2006 and 2007, and Repower being third [2, 3]. The power curves are often given in the product sheets of producers. Some example power curves are presented in Figure 2.1-(b) showing that there are small differences between them. The cut-in speed for example differs between 2 and 5 m/s. The nominal power output is reached between 15 and 19 m/s. The cut-out point is not always reached as abruptly as shown here. Pitch controlled wind farms can have a storm control system that prevents an automatic shut down. The power generation is smoothly stopped by turning the rotor blades out of the wind in a controlled way. The right end of the power curve then reflects the left end of the curve, but with a much steeper slope.

The power curves are derived by measurements in wind tunnels. It is important that the curves only give a statistical relation between wind speed and power. The real data points can be significantly below or above the curve. This is due to other influencing factors that can be related both to the wind and to the turbine.

The generation is for example also influenced by the air density or turbulences and the control system of the turbine. The power curves therefore refer to standard conditions like an average turbulence intensity of 12% and an air density of 1.225 kg/m^3.

For an optimal energy yield, the wind farm has to generate at or near to nameplate capacity as often as possible. To evaluate the productivity of a wind farm, the energy that is generated over a selected time period is related to the capacity of the wind farm. Two kinds of values are used: the full load hours and the capacity factor. The capacity factor is defined by the ratio between the energy generated over a period of time and the energy that would have been generated by constant operation at nameplate capacity. The capacity factor multiplied by 8760 gives the full load hours. As the wind is stronger at higher heights, bigger wind farms are built in order to maximise the energy yields. In 1980, the typical capacity of a wind farm was 30 kW [4]. In 2009, only 16% of the new build farms had a capacity below 2 MW, 5% of the farms had a capacity of 3 MW or higher, and 2% had a capacity of 5 MW [5]. Wind farms with 6 MW or higher are already built and tested, for example the Enercon E-126 with 7.5 MW. The same development can be seen with the rotor diameter and turbine heights. In 1980, the typical rotor diameter and turbine height was 15 m and 30 m. For a 2 MW wind farm, the typical rotor diameter and turbine height are 80 m and 95 m. The E-126 has a rotor diameter of 127 m and a turbine height of 135 m.

The figures show that repowering can increase the potential of wind power. Repowering means that older wind farms are replaced by newer models. Repowering is supported by the German Renewable Energy Law that, under certain conditions, guarantees a bonus to the feed-in tariff of repowered wind farms [6]. Next to the higher power output, bigger wind farms have the advantage of reduced noise emissions. Repowering can be limited as the height of constructions is often limited to 100 m by communal regulation [4]. The minimal distance between the farms is also larger for higher wind farms. In 2009, 55 wind farms were repowered [5].

Grid connection

Only grid-connected wind farms are of interest in the context of this work. Grid connection imposes some requirements on the wind farm design. The grid frequency of 50 Hz and the voltage level have to be respected. The wind power is transformed to electrical power by synchronous or asynchronous generators [1]. A basic design is thereby given by an asynchronous generator that is directly connected to the grid. In this case, the constant frequency of the grid enforces a constant (but, due to the gear, different) speed of the rotor (typically 1000 to 1500 revolutions per minute [7]). The elasticity between grid frequency and rotor speed is for example increased by asynchronous generators with slip regulation. In modern wind farms, variable rotor speeds are possible by applying double-fed asynchronous generators or synchronous generators with frequency convertors.

The voltage levels in the wind farms are typically below 1000 V. Low voltage levels are chosen for security and cost reasons [8]. The wind farms therefore require transformers for the grid connection. Either the low voltage cables of several wind farms are connected to one transformer or each wind farm is equipped with its own transformer. Due to the high-losses in the low-voltage cables and the increased capacities of modern wind farms, the second option is in general chosen. The transformer is thereby located in the base of the tower or in the power house next to the tower. The transformation level is determined by the local grid the wind farm is connected to. In Germany, the typical generator outage voltage of 690 Volt is often transformed to the 20 kV of the medium-voltage grid. But wind farms are also connected to the high voltage levels of the transmission grid. At the end of 2008, 2.6 GW or about 10% of the (onshore) wind power capacity was connected to the transmission grid and 20.8 GW or about 90% were connected to the distribution[1] grid [9]. In 2008, 23% of the newly installed capacities in 2008 was connected to the transmission grid. These figures indicate that, in the future, more wind farms will be connected to the transmission grid due to the increasing size of the farms.

Especially offshore wind farms are connected to the transmission grid as the transmission to the mainland requires special solutions in any case. The offshore wind farms are internally connected by medium voltage cables to a central transformer station. The connection to the main land is done by high voltage cables, typically at 110 kV, as medium-voltage would lead to unacceptable losses. The wind park is then connected to the transmission grid, for example at the 110 kV level. The future large offshore parks with capacities of 1000 MW will be connected to the 220 kV and 380 kV levels [10]. In the first German offshore park "alpha-ventus" the wind farms are internally combined at 30 kV and the 60 km long connection to the mainland has a voltage of 110 kV. The described connections refer to alternating current. For long distances, transmission by alternating current leads to increased losses. High-voltage direct current (HVDC) systems are therefore considered to connect the offshore parks. These systems require additional electrical components with higher costs that have to be compared to the reduced losses. HVDC systems are estimated to be economical for distances above 60 km, [11], to 100 km, [10]. With a HVDC mainland connection, it could also become advantageous to use direct current for the internal connection of the wind farms in the park.

2.1.2. Wind power forecasting

The power system operation is based on forecasts of the available generation and the load in order to realize the dispatch. Reliable wind power forecasts are therefore important for a successful integration of wind power into the power system. In the

[1] See Section 2.2.3 for distribution and transmission grid.

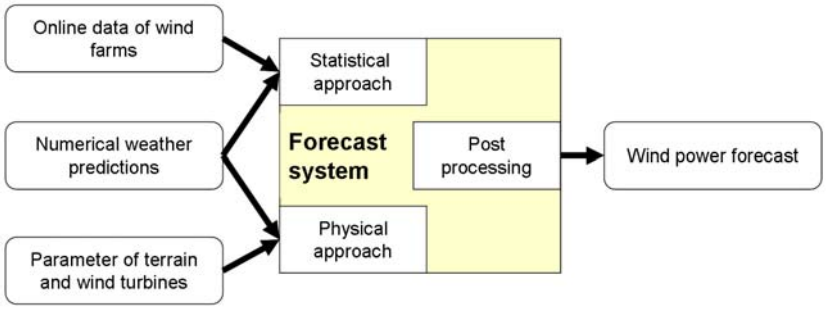

Figure 2.2.: Process of wind power forecasting

following, general principles of wind power forecasting are explained. A statistical analysis of the forecasts is given in Chapter 4.

General set-up

One parameter of wind power forecasting is its temporal horizon. Most forecast systems cover forecast horizons from some hours to a few days. These forecast horizons are given by the planning of the power system operation and the day-ahead and intraday markets. If trading at the day-ahead market takes place at noon, forecasts horizons of more than 36 hours are necessary to cover the next day. If the day-ahead market on friday covers the total weekend forecasts with forecast horizons of up to three days are required. Longer forecast horizons are no longer related to the dispatch and unit-commitment problem. They can be helpful in the mid and long term planning, for example to coordinate maintenance actions at power plants with high wind periods. However, the forecast quality significantly decreases for forecast horizons above five to seven days [12]. In the following, the focus is on forecast systems with forecast horizons of up to two days. The principal set-up of a wind power forecast is a transformation of input data to power forecasts as shown in Figure 2.2. The input data can include information about the surrounding terrain and the technical characteristics of the wind turbines, measured time series of past realizations and numerical weather forecasts. The data is transformed to wind power forecasts by means of physical and/or statistical models.

Input data The input data of forecasts systems can be divided into three groups. Measured wind speeds and/or power outputs of the precedent hours or days can be considered if available. Statistical methods are typically based on such autoregressive approaches. If the wind or power realizations are measured and made available online, so immediately, the data is directly used to produce an updated forecast. Online data is not always available and it normally does not cover all wind farms. Numerical weather predictions (NWP) are another important input. Most forecast systems are based on these predictions. Models for NWP are complex

models that are based on supercomputers and operated by national meteorological services like the "Deutscher Wetterdienst". The models cover large regions like continents or the world. The normal geographical resolution is between 5 to 25 kilometres. Every 6 to 12 hours a new NWP is given with a forecast horizon of 48 hours. The predictions are transferred to the wind forecaster by emails or ftp-servers [13]. Statistical treatment of the received weather data can improve the quality of the wind power forecasts [14]. The geographical resolution of the NWPs is an important criterion for the wind power forecast quality. If the geographical resolution is too coarse, additional models are applied to determine the meteorological conditions at the wind farms. These models require parameters that describe the surrounding terrain of the wind farms like the surface roughness. Technical data of the wind farms and turbines are applied to transform the local wind speed forecasts to power forecasts. A basic input data for the forecasts is therefore given by the power curves of the turbines.[2] As the power curve gives a non-linear relation between wind speed and power output, the statistical analysis of wind speed forecasts has to be differentiated from the statistical analysis of wind power forecasts.

Components Two principal methods of wind power forecasting exist: statistical and physical approaches. Normally, a combination of the two approaches is applied. The statistical approach directly transforms numerical weather predictions and/or online data of past realizations to power forecasts. Typical approaches are regression models or neural networks. Physical approaches are based on the physical and technical characteristics of the wind farms and their surroundings. Flow models allow to derive the wind speed at the wind turbine from the numerical weather prediction. Starting with a geographical resolution of more than 5 kilometres in the NWPs, mesoscaled models lead to a resolution of 500 meters, exploiting information about the surrounding terrain. Microscaled models then increase the resolution even more. As the NWPs only give meteorological data at certain heights, it is also important that the wind speeds at turbine heights are derived by physical flow models. Once the wind characteristics at turbine height are known, the power output is calculated applying the technical parameters of the turbine. In a wind park with several wind farms, the positioning of the wind farms leads to additional wind flow effects that have to be considered. In the evaluation of the wind power forecasts, systematic errors may be detected that can be reduced by a statistical post-treatment without knowing their physical origins. A simple example is the addition of an offset to the results in order to to correct a bias, so a permanent mean deviation of the forecasts.

For large-scale power system, the wind power generation in a certain area or

[2]The power curve only gives a statistical relation between wind speed and power output and, for single moments, the speed/output pairs can be significantly different to the power curve. The forecast at single turbines is more difficult due to this.

region is normally more important than the generation at a single wind farm. The forecasts for single wind farms are therefore upscaled to regional forecasts in case that the forecast system does not cover all wind farms of the region. Balancing effects with regard to the generation and with regard to the forecast errors have to be considered in the upscaling process. The size of the region and the number of wind farms is thereby important. Forecast systems based on physical models normally perform better for forecast horizons greater than three to six hours. For very short forecast horizons, purely statistical approaches can lead to better results [15]. In general, forecast systems that are based both on physical approaches and statistical approaches perform best [12].

Improvement of wind power forecasts

Over the last years many forecast systems have been developed in different countries [12, 13, 16]. Often system operators apply more than one forecast system to assure the planning. Known systems are for example the in Denmark developed Prediktor and WPPT (Wind Power Prediction Tool) that were combined to the Zephyr model. In Germany, there are for example the WPMS (Wind Power Management System or also AWPT for Advanced Wind Power Prediction Tool) and Previento. Sipreolico is a Spanish system. For Crete in Greece, a system called MoreCare was developed. The eWind model is applied in California. These are only a few examples for the existing systems. Forecasting has been improved over the last years but there is still potential for improvement. This is especially true for the fields that are not only related to forecast quality but also to more general aspects of wind power integration. Interesting points are for example offshore forecasting, density forecasts, forecast for special grid nodes or forecasts for intraday trading.

Offshore forecasts The forecast systems are mostly based on onshore locations as experiences with offshore farms and related data are still rare. Offshore forecasting has some special characteristics. The thermal layering of the atmosphere is different due to the high heat storage capacity of water. This requires an adaption of the micro-scaled models that are applied in order to derive the wind characteristics at turbine height. There are also different atmospheric flows due to the water-land border. The water surface is in general flat and flat terrain is advantageous for forecasting [17]. However, due to the waves, the surface can be moving, which adds another speciality to offshore forecasting. Another topic is slipstream effects that become more important in the big offshore wind parks and in flat terrain. Losses due to these effects are estimated to be above five percent [18].

The high spatial concentration of offshore wind farms is also to mention. The planned wind parks with up to two gigawatt of installed capacity enclose a large number of wind farms in a small area. Additionally, the German zones in the Nordic and Baltic sea that are suitable for offshore wind parks are relatively small.

The resulting high spatial concentration of wind farms makes forecast errors more important as there are less balancing effects. Due to the short distances, the wind characteristics and the forecast errors are very similar at the different offshore farms. The errors are therefore highly correlated and balancing effects between errors at different locations are relatively weak.

Forecasts with error estimation (density forecasts) The standard result of a forecast system is the forecast of the wind power generation that can be expected. Next to this, estimations of the possible error range are also helpful for the planning of the power plant operation. Such estimations are given by density forecasts. Density forecasts give an estimation of the error distribution next to the actual expected value forecast. In the ideal case, the distribution of the possible errors is then known. This information is useful to hedge the power plant operation. For example, it may be decided that a power plant stays online to be available in the case of a larger forecast error even though, looking only at the expected value forecast, it would be switched off. Different studies show that the consideration of density forecasts is advantageous for the power plant operation and trading activities [19, 20]. Confidence intervals are therefore an important aspect of forecasts and the output of error quantiles is already implemented in some of the existing forecast systems [21, 22]. Typically, the possible errors are especially high in the area between twenty and eighty percent of the installed capacity. This is due to the shape of the power curves, see Figure 2.1. A small wind speed forecast error at the steep slope of the power curve leads to a bigger power forecast error than at the horizontal sections of the power curve.

Other improvement potential The forecast quality is improved by the combination of different forecast systems and model approaches. A combination of different numerical weather predictions also leads to better forecasts by improving the input data basis significantly [15]. The quality of the numerical weather predictions themselves may have improvement potential. More online wind measurement stations and an increased use of online data can also increase the forecast quality. Another topic is forecasts for special grid nodes. In the future, additional stresses on the transmission grids are expected due to energy sources that are far away from the demand centres and due to increased trading activities. For the operation of the power systems, node specific forecasts may therefore be useful [15]. Forecasts with forecast horizons of one week would be useful to do maintenance work at offshore wind farms that cannot be done in rough weather conditions. Short-term operation planning and intraday trading are supported by improving the frequency and quality of short-term. Finally, forecast systems are often unreliable in the following situations that also indicate potential for improvement: abruptly changing and locally limited weather conditions, shut-downs of wind farms due to storms or delayed input data [16].

2.2. Challenges for the system operation

High shares of stochastic power sources in the power system can be challenging for several reasons. Potential issues are for example related to grid stability, generation system adequacy, dispatch and transmission. In this work, the power system operation is analysed with regard to its techno-economical characteristics. The following chapter therefore focuses on three challenges: balancing a fluctuating generation and demand, balancing issues that are due to uncertainties and transmitting power in the transmission grid.

2.2.1. General dispatch

The balance between generation and load is a basic principle of power systems. With restricted storage capacities, the power plants must be flexible to follow the load profile that is demanded by the consumers. The flexibility of most types of power plants is however restricted due to thermal constraints. With increasing wind penetrations, the residual load profile may become more variable and the flexibility requirements may increase. The increase of load variability is here analysed first. In the second section, the flexibility of thermal power plants is discussed.

Variability of the net load

One characteristic of wind energy is its fluctuating nature. The wind power generation follows the wind resource. Curtailing can be a possibility to adapt the wind power generation to the demand but it comes at the price of lost energy. In general, wind power generation will therefore be as fluctuating as the wind resource. The variability of wind power itself is analysed in detail in Section 4.2. Here, the variability of the net load is of interest. The net or residual load is given by subtracting the wind power generation from the demand. The variability of the net load determines how much flexibility is required in the power system. The net load variability is therefore an important parameter to assess the grid-integration of wind power.

The change in the net load variability is shown by wind and load data from 2006. The German wind power data is published by the transmission system operators and the load data is given by the UCTE. In order to highlight some effects, the wind power data is scaled to higher capacities. The linearly scaled data is denoted by “56 GW wind” referring to an assumed capacity of 56 GW. This scaling approach can only serve to show some tendencies as it does not consider the regional dispersion of the future wind power portfolio, in particular the impact of offshore wind power. In Chapter 4.2 a more sophisticated simulation method is therefore developed.

An index for the impact of wind on the net load variability could be the correlation between wind and load. The data gives a correlation of 0.15 between load and wind. This low positive correlation could suggest a decrease of the net load variability. However, looking at each day separately, the average daily correlation is -0.08. So, over a day the load and wind are normally negatively correlated. The higher general correlation is due to a positive seasonal correlation. The correlation of the daily mean values of load and wind (so 365 values of load and wind) is 0.22. Concluding, both wind and load are stronger in the winter, but the variability of the net load may still be increased by wind power. In general, correlation is not a good measurement of variability as the order of the values, being significant for the variability, is not considered in the correlation coefficient. In the following, the jumps of the net load are therefore analysed.

Table 2.1.: Variability of German net load (GW)

	1h Jumps			**4h Jumps**		
	StaDev	**Mean+**	**Max+**	**StaDev**	**Mean+**	**Max+**
Original (GW)	2.6	2.3	11.2	8.4	7.7	25.4
Increase with wind (%)	1.4	-1.5	-0.5	1.4	0.5	0.4
Increase with "56 GW wind" (%)	8.9	4.0	0.3	8.5	5.6	18.4

Table 2.1 shows some statistics of one-hour and four-hour jumps. The standard deviation ("StaDev"), the average positive jump ("Mean+") and the maximal positive jump ("Max+") are given. In 2006, the wind power generation did not cause an increase of the variability. The standard deviation is only increased by 1.4%, but the mean and maximal one-hour jumps are even slightly lower. The penetration of the power system by wind energy is therefore not important enough to lead to any significant changes, at least not on a national scale. In single regions, this may be different. The increase of variability becomes clearer by assuming a "56 GW" wind scenario. In this case, all statistics show an increase of variability. Especially the maximal four-hour load jump is now 30 GW, so 18% higher than without wind. Overall, according to these statistics, the change of variability may however be considered as moderate (again, variability on a national scale is analysed only).

The importance of changed variability becomes clearer relating the jumps to the net load level. As a matter of fact, the absolute jumps of the net load are likely to become smaller with wind power as the general load level decreases. However, a lower load also means that less thermal power plants are activated and that fewer power plants are generally installed. The jumps, even though being smaller in absolute terms, may therefore be more difficult to realise. The jumps and their relation to the load level is shown by Figure 2.3. Figure 2.3-a shows the hourly jumps in relation to the load level without wind power. The same plot for the case of "56 GW wind" is given by Figure 2.3-b. The jumps are only slightly larger but they occur at much lower net load levels. Statistics of the jumps normalised

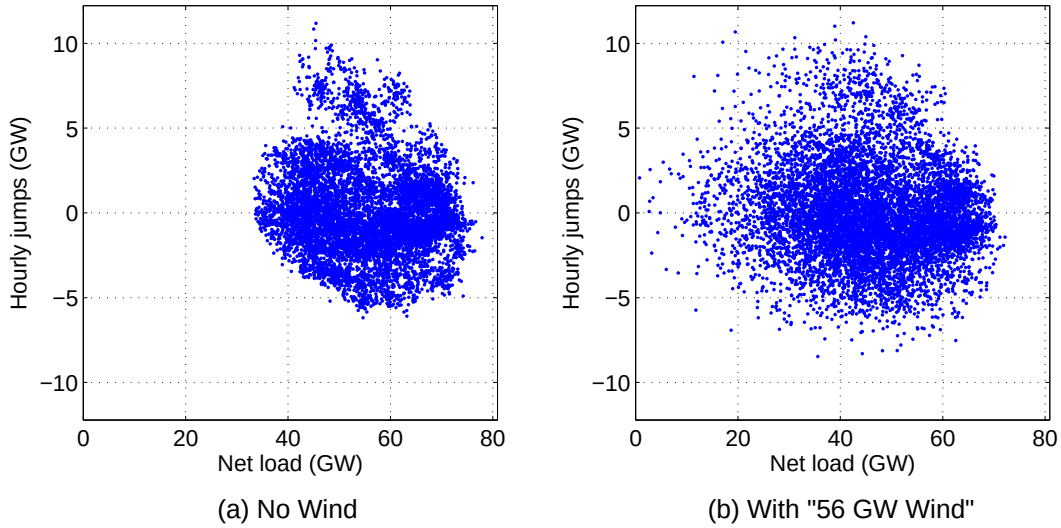

Figure 2.3.: Net load and hourly jumps of net load

Table 2.2.: Variability of German net load normalised by mean net load

	1h Jumps			4h Jumps		
	StaDev	**Mean+**	**Max+**	**StaDev**	**Mean+**	**Max+**
Original (percentage of mean net load)	4.7	4.2	20.0	15.1	13.8	45.5
Increase with wind (%)	8.6	5.5	6.5	8.5	7.6	7.5
Increase with "56 GW wind" (%)	32.6	26.8	22.2	32.2	28.7	44.3

by the mean net load are given in Table 2.2. According to these statistics, more flexibility was required from the activated power plants already in 2006. In the case of "56 GW wind", the increased variability becomes more obvious. For instance, the mean positive four-hour jump is now 17.8% of the average net load whereas it is 13.8% without wind, so there is an increase of 28.7%. The four-hour jumps are in general more affected by the wind power than the one-hour jumps. This in particular applies to the maximal four-hour jump that rises by 44%.

This leads to the general question at which temporal resolution the wind power integration has the highest impact on the variability. Especially the impact at higher temporal resolutions would be interesting, also with regard to the model formulation in Chapter 3. Higher temporal resolutions could not be analysed by the German data. Especially load data was not available in higher resolutions[3] and relating quarter-hourly wind data to hourly load data, for example, will not show the variability of the net load, but only reflect the variability of the wind. Quarter-hourly data of load and wind power generation was available for Ireland (year 2008). The Irish wind power data is here scaled to 1.69 GW in order to have

[3]The "vertical gird load", published by the German TSOs in a quarter-hourly resolution, is here not applicable as it already represents a consumer load that is reduced by a part of the wind power generation.

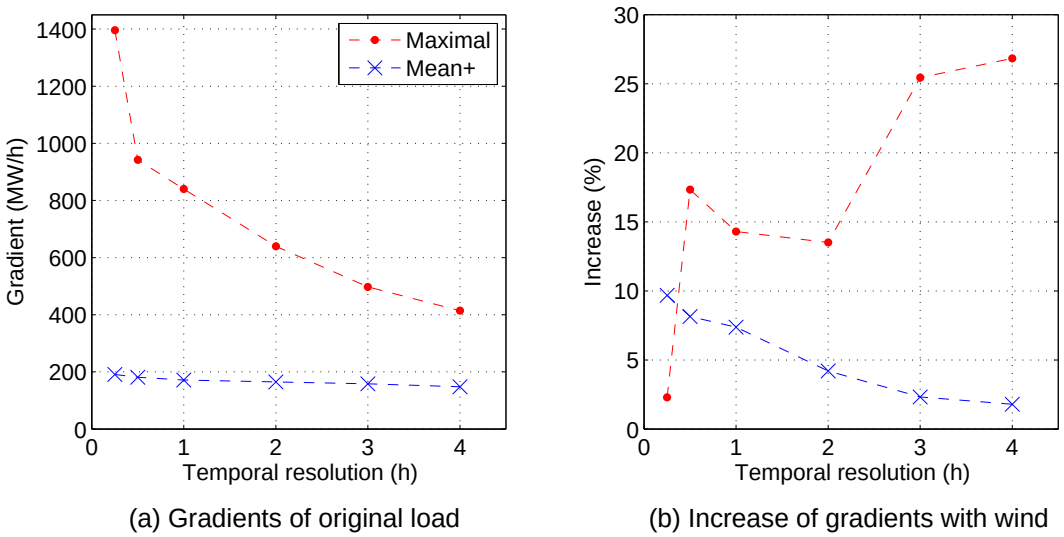

(a) Gradients of original load (b) Increase of gradients with wind

Figure 2.4.: Variability of Irish net load depending on temporal resolution

the same wind energy penetration as in Germany with the "56 GW wind" scenario (18% of the total demand is then covered by wind energy).

Figure 2.4-a shows mean and maximal gradients of the original load depending on the temporal resolution. For the purpose of comparison, no jumps are analysed but gradients in MW/h. The gradients are naturally higher with higher temporal resolutions. The maximal gradient based on hourly data is for example much lower as the one based on quarter-hourly data as the maximal quarter-hour jump does not occur four times in a row. Correspondingly, the mean positive gradients ("Mean+") also increase with higher temporal resolutions (170 MW/h based on hourly data and 190 MW/h based on quarter-hourly data). The impact of wind on variability is shown by Figure 2.4-b for the different temporal resolutions. The impact on the maximal gradients decreases with higher temporal resolutions. Based on quarter-hourly data the maximal gradient for example rises by 2.5%, whereas it rises by 27.5% in the case of four-hour lags. In contrast, the impact on the mean gradients is stronger with higher temporal resolutions. The difference is especially important comparing hourly and two-hourly data. These statistics indicate that, at low temporal resolutions, high shares of wind power can lead to very large jumps of the net load if the wind and the load are trending in opposite directions over several hours. At high temporal resolutions, the net load becomes generally jumpier due to the wind but the extremes are not affected so much. Concluding, a good part of the increased variability is captured applying an hourly resolution. To see the full impact of wind on variability higher temporal resolutions are however required.

These results for Ireland can only be indicative for Germany as the systems are different. For example, the general correlation between wind and load is 0.16, similar to the German one. However, the average daily correlation, being more

important for the variability, is equal to 0.06, so positive, whereas it was negative in the German system (equal to -0.08, see above). The impact of wind on the German net load is therefore subject to further analyses.

Flexibility of power plants

The variability of the net load must be reflected by the flexibility of the power plant portfolio (and by other flexibility options like DSM). Some power units are more capable of a flexible operation than others. Hydro power plants are for example well suited for frequent operation changes, whereas the flexibility of thermal power plants is normally seen as restricted. It is however important to note that flexibility restrictions are never fixed limits. Rather, cycling is likely to cause higher costs both in the short and long term. Cycling here refers to on-load cycling (ramping), on/off operations and operation at low load levels. Higher costs derive for several reasons. The cycling may reduce the lifetime of the equipment increasing the capital costs. Thermal stresses can for example cause premature cracks in the material. The risk of severe damages like boiler explosions also leads to higher forced outage rates. Boilers are often the limiting factor on power plant flexibility and account for a significant proportion of unplanned availability losses [23]. In general, maintenance costs increase. Ramping processes also require additional manpower as the operation is less automatic making human failure more likely. Additional manpower and extra start-up fuel are required for unit start-ups. Usually the most critical part of the start-up process is the synchronization to the power system. Part-load efficiency is normally lower than the full-load efficiency. Even in the offline state costs may arise as the equipment that normally runs sits idle at ambient temperatures and must be carefully 'laid up' to avoid potential damage caused by corrosion or condensation [24]. Essentially, cycling will cause additional operational costs (fuel, auxiliary start-up fuel, personnel, chemicals, maintenance), opportunity costs (lower availability) and capital costs (loss of equipment life) [25, 26].

Due to these multiple effects of cycling, the assessment of the related costs is extremely difficult. The influential plant-specific factors are for example the overall-design of the plant, the size and age of the plant, the way the plant is operated, the quality of water chemistry and the previous maintenance philosophy. The inclusion of power plant flexibility and cycling costs in dispatch models is therefore a challenging task. Different parameters are used to define the flexibility of a power plant in dispatch models. Start-up costs and part-load efficiency are direct indications of the costs that are caused by cycling. Then there are parameters that restrict the operation of the power plant as start-up times, shut-down times, ramping rates and minimal operation and down times. It is clear from the previous paragraph that most of these technical restrictions are not absolute. It is for example possible to achieve short start-up times if really wanted. However, this will result in higher stresses on the different unit parts and reduce their lifetime.

The given parameters can therefore only be general indications which operation modes are normally tolerated.

Start-up times The temperature increase due to a start causes large stresses on the material. The boiler can for example expand by 30 cm [27]. Other parameters like rotational speed and pressure undergo large changes as well during the start-up process [28]. The shorter the starting times are the larger the gradients and the stresses on the material become.

Starts of power plants are usually categorized in hot, warm and cold starts depending on the previous down-time and the temperatures of the turbine metal. Warm starts are typically characterized by off-line times between 8 and 48 hours and turbine metal temperatures between 200°C and 400°C. Cold and hot starts are defined by off-line times over 48 hours and temperatures below 200°C respectively off-line times below 8 hours and temperatures above 400°C [29, 30]. Cold starts are sometimes also characterized by off-line times of more than 120 hours or 60 hours instead of more than 48 hours and hot starts can be defined by offline times below 24 hours or 12 hours instead of 8 hours [24, 26, 31]. The time periods also vary largely between unit types and unit sizes. For coal, oil steam and combined cycle power plants, average times from hot to warm can be between 10 and 13 hours, whereas there are only around one and two hours for gas turbines [32]. For nuclear power plants, the cold state normally refers to a subcritical reactor state after off-line times of more than 120 hours. In combined cycle power plants, the gas turbine can be operating before the steam turbine [33].

Table 2.3 gives start-up times for power plant types depending on the state of the power plant. “IEEE” stands for values from the IEEE reliability test system with 8 thermal units, [34]. “PJM” stands for values collected by the market monitoring unit of the transmission organization PJM, [32]. Additionally, values from [35], denoted by “Hundt”, and values based on [33] and [36], denoted by “Fisch./DVG”, are shown. “Vollmer” refers to indications for an Alstom power plant [31]. Gas turbines require the shortest start times, followed by combined cycle plants, oil or gas steam plants and coal power plants. Nuclear power plants only require long start times if coming from a subcritical state.

Ramping rates The ramping or load following of a power plant is also limited due to the thermal stresses. The maximal up-ramping for different power plant types is given in Table 2.4, using the sources above and data from Ireland. Technical parameters of the Irish power plants (50 thermal units, 69 units in total) were validated for their use in the single electricity market model on behalf of the Regulatory Authorities. The validated data is published on the Internet [37]. These parameters were here analysed, grouping the plants by type. The resulting parameter ranges are shown in the “Eire” column. The average results are given in round brackets.

Table 2.3.: Start-up times (h) of thermal power plants

		IEEE	PJM	Hundt	Fisch./DVG	Vollmer
Coal	hot	3 - 8	6.1 - 8.9[a]	2	< 2[b]	-
	warm	-	9.1 - 11.7[a]	-	< 3[b]	-
	cold	11 - 12	12 - 14.6[a]	-	< 5[b]	-
Oil/Gas	hot	2 - 4	3	1	-	-
(Steam)	warm	-	4.8	-	-	-
	cold	4 - 7	7.1	-	-	-
Combined	hot	-	2.6	1	-	< 0.8
Cycle	warm	-	3.6	-	< 0.3 - 0.8[c]	1.8 - 2.5
	cold	-	4.5	-	< 0.3 - 2[c]	2.4 - 2.8
Gas	hot	0	0.3 - 0.7[d]	0	< 0.3	-
Turbine	warm	-	0.3 - 0.7[d]	-	< 0.3	-
	cold	0	0.3 - 0.7[d]	-	< 0.3	-
Nuclear	hot	-	-	-	< 3	-
	warm	-	-	-	< 6	-
	subcr.	-	-	-	< 25	-

[a]larger value applies to super-critical coal
[b]includes lignite
[c]lower value only for gas turbine
[d]larger value applies to large turbines

Table 2.4.: Ramp rates (up-ramping) of thermal power plants (% of installed capacity per minute)

	Eire	IEEE	PJM	Hundt	Fisch.
Coal	0.5 - 2.5 (1.2)[a]	1.1 - 2.6	0.6 - 1.8	3 - 4[b]	2 - 6[b]
Oil/Gas (Steam)	0.7 - 2.9 (1.6)	1.5 - 8.3	2.7	6	-
Combined Cycle	1.9 - 7.8 (4.2)	-	1.6	6	8 - 10
Gas Turbine	2.3 - 20.7 (11.8)	15	6.6 - 21.3[c]	20	8 - 20
Nuclear	-	5	-	3.8 - 10[d]	5 - 10

[a]includes peat
[b]includes lignite
[c]lower values for large turbines
[d]larger values for full-load operation (power output larger than 80% of installed capacity)

The results indicate that the limitations by ramping rates can be neglected if the power operation is simulated in an hourly resolution. As ramping applies to the operating status of a unit, it applies to capacities between the minimal part load and the full load. Assuming typical minimal part loads of about 40% of the installed capacity, the capacity range covered by ramping becomes 60% of the installed capacity. As nearly all values in Table 2.3 are above 1, ramping rates are not limiting in an hourly resolution.

Minimum operation and down times Parameters for minimum operation and down times are used in unit-commitment problems to simulate a realistic operation [38]. Like the other operation parameters, they only give indications for the operation of the power plants. In reality, these constraints might be redundant as the operational constraints are already expressed by ramping rates, start-up times and shut-down times [35]. Nevertheless, they are often used to simulate a realistic power plant operation.

Table 2.5.: Minimum operation times of thermal power plants (h)

	Eire	**IEEE**	**PJM**	**Hundt**
Coal	0 - 6 (3.8)[a]	8 - 24	9.8 - 24[b]	4 - 6[c]
Oil/Gas (Steam)	0 - 5.5 (3.3)	4 - 12	6.3	4
Combined Cycle	0 - 4 (3.6)	-	5.5	4
Gas Turbine	0 - 4 (0.3)	1	1.3 - 3.3[d]	1
Nuclear	-	1	-	-

[a] includes peat
[b] larger value applies to super-critical coal
[c] includes lignite
[d] larger values for large turbines

Typical values of minimum operation times are given in Table 2.5. Steam and combined cycle power plants have the longest minimum operation times, whereas the on-line time of gas turbines can be below one hour. A very low operation time is also given for the nuclear power plant in the IEEE reliability test system.

Table 2.5 gives minimum down times. The values are mostly in the same order as the minimum operation times.

Minimum load factors The cycling capacity of power plants is also determined by their minimum load factors. They determine at which capacity level a power plant can start to produce power in part-load operation. Table 2.7 shows values from the already introduced sources. The values in round brackets are the average values. Parameters used in the German Dena study, "Dena", are also given [39]. These values are only general indications. A boiling water reactor (BWR) can

Table 2.6.: Minimum down times of thermal power plants (h)

	Eire	IEEE	PJM	Hundt
Coal	0 - 5 (2.9)[a]	4 - 48	5.2 - 62.8[b]	2 - 6[c]
Oil/Gas (Steam)	0 - 4 (2.6)	2 - 10	5.3	2
Combined Cycle	0 - 4 (2.4)	-	4	2
Gas Turbine	0.3 - 0.8 (0.5)	1	1.1 - 2.7[d]	0
Nuclear	-	1	-	-

[a]includes peat
[b]larger value applies to super-critical coal
[c]includes lignite
[d]larger values for large turbines

for example be operated at power levels below 60% of the maximal power, but a manual adjustment of the control rod positions is then required [24].

Table 2.7.: Minimum load factors (% of maximum power)

	Eire	IEEE[a]	Dena	Hundt	Fisch.
Coal	22.8 - 80.2 (48)[b]	20 - 40	38 - 40[c]	38 - 40[c]	35 - 60
Oil/Gas (Steam)	16.6 - 51.1 (34.4)	20 - 35	-	38	-
Combined Cycle	45.7 - 87.5 (56.4)	-	33	33	20
Gas Turbine	3.8 - 53.6 (15.2)	79	20	20	55
Nuclear	-	25	40	20 - 60[d]	30 - 50

[a]lowest values of given heat rate curve
[b]includes peat
[c]includes lignite
[d]lower values for PRW; highest value for BWR

Costs and fuel usage The causes of cycling costs and their types were discussed at the beginning of the section. A straight-forward quantification of these costs is only partially possible. The required amount of start-up fuel or the part-load efficiency are parameters that allow a cost quantification. Other costs, for example related to damages, are much more difficult to assess. In general, cost estimations are extremely varying. For example, an assessment of individual units resulted in cold start costs between 15,000 and 500,000 US dollars and hot start costs between 4,000 and 90,000 [40]. Lefton and Besunder point out that cycling costs are generally underestimated. According to them, the typical industry value for the costs per cycle and unit is 100$ for a gas turbine and 10,000$ for a large super-critical unit, whereas the true costs could be in the range between 300 and 80,000$ respectively 15,000 and 500,000$ [30].

Table 2.8.: Start-up costs of thermal power plants ($Euro_{2009}$/MW)

		Dena[a]	**EPRI**[b,c]	**Gostl.**[b]	**Thomp.**[b]
Coal	hot	-	-	6	53 - 63
	warm	-	-	7	91 - 106
	cold	3.3 - 5.4[d]	-	118	188 - 220
Oil/Gas	hot	-	311 - 380	-	32 - 115[e]
(Steam)	warm	-	407 - 448	-	45 - 192[e]
	cold	-	597 - 666	-	81 - 411[e]
Combined	hot	-	-	-	-
Cycle	warm	-	-	-	-
	cold	11.2	-	-	-
Gas	hot	-	-	-	-
Turbine	warm	-	-	-	-
	cold	11.2	-	-	-
Nuclear	hot	-	-	-	-
	warm	-	-	-	-
	cold	1.9	-	-	-

[a] without fuel costs
[b] includes costs due to increased heat rate
[c] best estimate costs
[d] includes lignite
[e] gas units with more than 500 MW

Table 2.8 gives estimations of start-up costs by the Dena study ("Dena"), [39], by an EPRI report ("EPRI") from 2001, [40], by Gostling ("Gostl."), [29], and by Thompson and Wolf ("Thomp.") [24]. The values show the large range of estimations. These costs are due to component replacement, higher maintenance costs, lower availability due to increased forecast outage rates, start-up fuels and chemicals and from non optimum heat rates. The costs are mainly attributed to maintenance, reduced availability and capital costs [40]. Only 25% of the total costs is due to increased fuel usage. Start-up fuels thereby represent only about 5% of the total costs and the heat rate increase accounts for not more than 20%.

Table 2.9.: Start-up fuel of thermal power plants (MWh/MW)

		Eire	**IEEE**	**Dena**
Coal	hot	0.9 - 4.3 (2.3)[a]	0.5 - 2.3	-
	warm	1.2 - 6.9 (3.7)[a]	-	-
	cold	1.5 - 14.5 (7.0)[a]	1.8 - 3.7	6.2[b]
Oil/Gas	hot	0.7 - 1.5 (1.2)	0.7 - 0.9	-
(Steam)	warm	1.5 - 2.5 (2.2)	-	-
	cold	1.9 - 4.9 (3.3)	1.2 - 1.7	-
Combined	hot	0.1 - 1.7 (0.8)	-	-
Cycle	warm	0.1 - 2.3 (1.3)	-	-
	cold	0.1 - 5.2 (2.3)	-	3.5
Gas	hot	0 - 0.2 (0.1)	0.1	-
Turbine	warm	0 - 0.2 (0.1)	-	-
	cold	0 - 0.2 (0.1)	0.1	1.1
Nuclear	hot	-	-	-
	warm	-	-	-
	cold	-	-	16.7

[a] includes peat
[b] includes lignite

Indications for the required amount of start-up fuel are given in Table 2.9. The average values of the Irish power plants are given in round brackets. Little start-up fuel is needed in the case of gas turbines. The values also indicate that a gas turbine start-up does not depend on the temperature state. In contrast, for coal power plants, cold starts are twice as costly as warm starts.

Part-load efficiency is another parameter that quantifies the costs of cycling. Typical values of minimal-load efficiencies are shown in Table 2.10. The "Eire" and "IEEE" values are thereby derived from the heat rate curves that are given in the studies. Typically, efficiency is reduced by about 5 percentage points (so, for example, 35% instead of 40%). The efficiency loss is significantly higher at gas turbines, equal to about 20 percentage points. Consequently, it is also slightly higher at combined cycle power plants. The "IEEE" gas turbine shows an untypically low

Table 2.10.: Loss of efficiency at minimal capacity (percentage points)

	Eire	**IEEE**	**Dena**	**Hundt**
Coal	0.9 - 15.8 (5.6)[a]	2.5 - 8.5	5 - 6[b]	5 - 6[b]
Oil/Gas (Steam)	1.9 - 12.5 (5.2)	3.8 - 7.1	-	6
Combined Cycle	1.0 - 11.0 (6.2)	-	11	11
Gas Turbine	6.5 - 24.1 (17.5)	0.9	22	22
Nuclear	-	7.4	5	-

[a]includes peat
[b]includes lignite

loss of efficiency as it refers to a minimal capacity of 80%, so nearly full capacity (see Table 2.7).

The range of values given in the section shows the versatility of power plants and the difficulty to define parameters that quantify the restrictions and costs of cycling. However, the formulation of unit-commitment models depends on specified values for these parameters. The values that are used for the model in this work are given in Section 3.2.1. They are derived from the analyses above and can be seen as approximate indications for the different parameters, even though such indications must be treated with care as the range of published values has shown.

2.2.2. Coping with uncertainty

Power plant operation has to be planned in advance in order to optimize unit-commitment and dispatch. In the planning process, there are uncertainties on the supply and the demand side. On the demand side, the future demand can not be perfectly predicted. On the supply side, power plant outages can occur and forecast errors related to stochastic generation have to be considered. Wind power therefore adds uncertainty to the system and the balancing requirements may become more important. In the following, the uncertainties related to outages and forecast errors are discussed and a comparison between wind and load forecast errors is given. Finally, reserve capacities and intraday markets are presented as mechanisms that prevent imbalances.

Uncertainties

The uncertainties on the generation side related to outages and forecast errors are analyzed first. Load forecasts are then explained and their relevance is compared to the one of wind forecasts. At the end of the section, values for typical reliability levels are given. Uncertainties originating from transmission failures, for example cutting off a power plant connection, are not considered here.

Unplanned outages of power plants Power plants are not absolutely reliable and there is always the possibility that capacity is out of service. Outages can be planned or forced. Forced outages are unplanned outages that occur due to events like equipment failures. The forced outage rate (FOR) stands for the percentage of time a power plant is out of service due to forced outages. For the assessment of reserve requirements, the FOR is not important but the occurrence probability of a forced outage. The occurrence probability can be estimated if the FOR and the mean time to repair (MTTR) are known. The MTTR stands for the average time required to repair the power plant. The probability of an outage per hour, POH, is then calculated by Equation (2.1), cf. [41]. The number of outages in one year is thereby given by x and the total outage time is equal to the product of x and MTTR. The relative outage frequency serves as an estimate for the outage probability.

$$\frac{x \cdot \mathrm{MTTR}}{8760h} = \mathrm{FOR} \qquad \text{and} \qquad \mathrm{POH} \approx \frac{x}{8760h} = \frac{\mathrm{FOR}}{\mathrm{MTTR}} \tag{2.1}$$

Until now, no differentiation was made between relocatable and non-relocatable outages. Relocatable outages are outages that can be postponed for a certain period of time. In the context of reserve requirements only the probabilities of non-relocatable outages are important and Equation 2.1 should be applied with forced outages rates related to non-relocatable outages. In practice, general forecast outage rates can also be applicable, as a VGB report shows that explicitly gives the forecast outage rates for non-relocatable outages [42]. In average, about 90% of the forecast outages are non-relocatable forecast outages. For some power plants, relocatable outages are more important but they never represent more than 25% of the total forced outage rate.

Table 2.11.: Estimated yearly number of outages of thermal power plants

	VGB,Br.	**VGB,Ha.**	**VGB,E.**	**Eire**
Coal	9.4	6.6	14.8	8
Lignite	14.1	4.5	12.6	8.7[a]
Oil / Gas (Steam)	2.2	3.9	9.1[b]	34.5
Combined Cycle	11.8	12.1	32.8	6.8
Turbine	4.3	2.5	48.7	6.9
Nuclear	5.2	1.1	4.5	-
Hydro	-	-	-	4.3

[a] refers to peat
[b] only oil

Table 2.11 gives indications for the yearly number of outages. The values denominated by "VGB.,Br." are derived from the forced outage rates in the VGB report, [42], in combination with MTTR values, taken from Brückl's work, [43],

applying Equation (2.1). Additionally, outage numbers used by Haubrich, [44], are shown ("VGB,Ha."). Data suggested for the EWI reserve model, [45], also allows a calculation of the outage number ("VGB,E."). The values in both sources are based on VGB data. The values used by Haubrich are thereby based on the newest data and it is recommended to use these values in future studies. FORs and MTTRs proposed for the modelling of Irish power plants, [37], lead to a fourth set of outage values ("Eire").

The values in Table 2.11 show that the occurrence probability of an outage is generally far below 0.01. High number of outages can be seen at combined cycle power plants due to their relatively complex design. Hydro and nuclear power plants have lower outage probabilities than fossil thermal power plants. Nuclear power plants are subject to high security standards and hydro power plants being non-thermal are also highly reliable (see also [43]).

Load uncertainties Forecasts of the future load are always subject to uncertainties. On the one hand, the influencing factors, for example weather conditions or human behaviour, are subject to uncertainties. On the other hand, not all influencing factors and not all dependencies between influencing factors and load can be captured. But short-term load forecasts have been used and developed over a long time and their quality is relatively high. Typical techniques for short-term load forecasting, often used in combination, are similar-day approach, regression methods, time series analysis or neural networks [46, 47, 48]. Similar-day approaches make use of typical load profiles in combination with typical model days. In regression methods causal relations between the load and input parameters such as weather parameters are derived. The load forecast is then based on forecasts of the input parameters. Time series analyses exploit temporal patterns of the load. Significant autocorrelations in the time series of load are therefore identified. Neural networks are mathematical models imitating biological networks. They are trained by historical data to simulate complex and non-linear relations between input parameters and load.

Load forecasts are used by electricity suppliers respectively trading companies to assess the future load of their clients. It is therefore difficult to assess the quality of a load forecast for a country or a control area. In the literature, the following indications are given for the standard deviation of load forecast errors related to the four German control areas: 1.67% of the yearly peak load [49], 2% to 2.5% of the yearly peak load [39, 45], 2% to 5% of the current load [50]. An empirical analysis of deviations of control areas leads to 1.27% to 1.8% of the yearly peak load [44]. A similar analysis by the author in 2004 led to values ranging from 0.8% to 2.1% of the peak load whereby 0.8% applies to the forecast for total Germany [51]. In Ireland, a standard deviation of 75 MW is indicated for a day-ahead forecast, 60 MW for a four-hour forecasts and 40 MW for an one-hour forecast, which corresponds to about 1.7%, 1.3% and 0.9% of the yearly peak

load [52, 41]. In larger systems, the relative forecast quality is in general higher as balancing effects become more important. According to this, the German standard deviations will be smaller than the Irish ones as the Irish system is considerably smaller than the German control areas. This suggests that the lower values in the range of indications above are more realistic. For Germany, the forecast quality will again be higher as the areas partially level each other. In the following, a standard deviation of 1.2% of the peak load is therefore used for Germany.

Next to the actual forecast error, there is also a permanent oscillation of load that leads to discrepancies between load and generation. Additionally, discrepancies occur due to commercial steps in the exchange schedules between different balancing areas. As power plants cannot realise instantaneous generation changes, such steps are converted to ramps over several minutes in the nominal exchange schedules. However, the power plants do not exactly follow the same ramp rates and imbalances occur [53].

Forecast errors of stochastic generation The outages of conventional power plants are one example of uncertainty at the supply side. Additional uncertainty is given by stochastic power sources like wind or solar energy. For these technologies, the outage of one generating unit can be neglected due to the relatively small size of the units, their higher technical availability and their spatial distribution [54, 43]. The uncertainty is rather given by the fluctuations of the underlying natural resource that affects all units.

Wind power forecasting and its statistics are analyzed in detail in Section 2.1.2 and Section 4.3. Solar power forecasting is based on similar concepts that the ones used for wind power forecasting. Forecasts of the underlying resource are transformed to power forecasts applying the technical characteristics of the power plant. Some general statistical characteristics of solar and wind power forecasts are therefore similar. The forecast errors at different locations are not perfectly correlated and the correlation decreases considerably with distance [55]. Hence, forecast quality increases with larger region sizes and larger number of stations as in the case of wind power forecasting. Solar power forecasting becomes challenging in situations with inhomogeneous clouds, whereas clear sky forecasts are more straightforward [56, 57]. Short-term uncertainties can also arise in relation with fluctuating stream flows and reservoir inflows at hydro power plants [58, 59, 60]. Ocean power will also be subject to some short-term uncertainties.

Comparison of load and wind forecasts Power systems have always dealt with uncertainties about the future load. It is therefore interesting to compare wind power and load forecasts. The question is whether the uncertainty in the system is significantly increased by the wind forecast errors or whether the wind and load forecast errors are of the same order. In the following comparison, both forecast errors are assumed to be normally distributed and to be independent from each

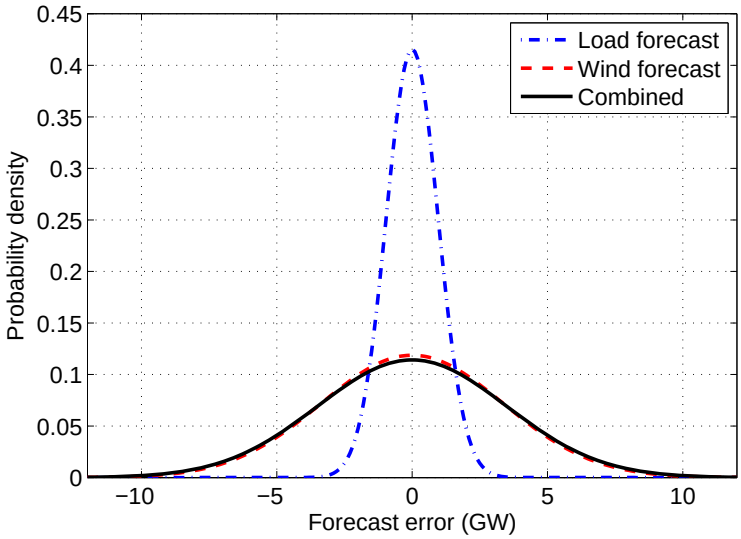

Figure 2.5.: Comparison of wind and load forecast errors by probability functions

other. Normal distributions are assumed as the orders of the forecast errors are only relevant for this comparison. For a first approach independency can also be assumed as the wind and load forecasts derive from completely different forecast systems (in reality, correlations may exist due to the influence of common weather patterns). The comparison refers to day-ahead forecasts. The standard deviation of the German load forecast errors is set to 1.2% of the peak load (see above). The standard deviation of the German wind power forecast errors is set to 6% of the installed capacity (as it is derived in Chapter 4 for the year 2020). Assuming a peak load of 80 GW and 56 GW of installed wind power capacities, the standard deviations of the forecast errors are 0.96 GW and 3.36 GW.

Figure 2.5 shows the resulting probability distributions of the forecast errors. Larger forecast errors exceeding 5 GW only have a relevant probability if there are wind forecast errors. As independence is assumed, the standard deviation of the combined forecast error (wind plus load) is equal to the root of the sum of the squared single standard deviations (3.5 GW). The standard deviation of the combined forecast error is only 5% larger than the standard deviation of the wind power forecast errors. Correspondingly, the probability distributions of the wind power forecast errors and the combined error, given by the dashed and solid line, are nearly equal. This shows that, in a German power system with high wind power shares, the main forecast uncertainties will be due to wind power forecasting (neglecting other fluctuating power sources).

Security of supply To cope with uncertainties, reserve capacities are hold back. Unacceptable changes of system frequency or the necessity of load shedding are thus prevented. As a system with perfect reliability would be too expensive, a low

probability of loss of load incidents is generally accepted. For a German balancing area, a loss of load probability (LOLP) of 0.1% is a commonly assumed value [39, 53]. This corresponds to 8.76 hours per year. As there are four German balancing areas that can support each other, the actual loss of load probability in Germany is far lower and a value of 0.0028% equivalent to one quarter-hour per year can be assumed. This value is proposed as a very conservative assumption and higher values of loss of probability could be justified in the future [44].

Coping with uncertainties

The general method to deal with uncertainties is to keep reserves as standby capacities. Reserves are capacities that are able to react fast in case of imbalances in the system and they are activated as an immediate or shortly delayed reaction to any disturbance in the system. Additionally, the scheduled dispatch of the power plants can be adapted in foresight. In a liberalised market, the adaptation of the dispatch is coordinated by intra-day markets.

Reserves Reserves are needed to maintain the balance between generation and load and to guarantee a stable system frequency. Three types of reserves are discerned according to the UCTE operation guidelines: primary control, secondary control and tertiary control. Any imbalance in the system is equivalent to a change of the stored kinetic energy. For example, a higher load leads to a reduction of the stored kinetic energy and a decrease of the system frequency. The change of frequency is stopped by the primary control. The primary reserves are then replaced by secondary reserves that restore the reference frequency and that are finally replaced by manually activated tertiary reserves.

Primary reserves are responsible for the primary regulation after a frequency deviation. After a positive load jump, the frequency declines according to the difference between the load and the generation. The relation between frequency decline and load imbalance thereby depends on the grid "stiffness" that gives the sensitivity of grid frequency to changes in input power. At the power plants, the imbalance is first measured by a change in the turbine speed and the regulating steam valves are adjusted accordingly. 50% of the primary reserves is deployed at latest 15 seconds and they must be completely activated within 30 seconds. The primary reserves are fully activated at the maximally allowed deviation of system frequency of 200 mHz [61, 62]. The primary control stabilizes the turbine speeds and system frequency but they are not yet back to their reference values. This is achieved in the second control system that is controlled by the system frequency [63].

Secondary reserves are automatically activated by the central secondary controller that measures the grid frequency. The central controller also controls the share of the different power plants in the secondary control and it also

considers exchanges with connected neighbouring grid zones [11]. The primary control is provided by the primary reserves in the total grid. If a load imbalance occurs in a grid zone, the primary reserves in the other grid zones also react. This support from the other grid zones is corrected by the secondary control. The secondary control overlaps the primary control but it reacts more slowly to avoid interactions between the two control types. The secondary reserves must start their controlling action within 30 seconds and they must be completely activated within 5 minutes. They are automatically activated by the transmission system operator and the reference frequency is restored within the order of minutes [61, 62].

Tertiary reserves replace the secondary reserves once the free secondary reserve capacities diminish due to increased load changes. Tertiary reserves can also serve to support the secondary reserves in restoring the system frequency after large incidents. They are manually activated after a call from the system operator and they have to be completely activated 15 minutes after the phone call [61, 62].

An estimation of the required amount of reserves is presented in Section 3.2.2.

Reserve and Intra-day market The provision of reserves is organized by the transmission system operator. He is responsible for the provision of reserves but he does not possess any reserve capacities. The reserve capacities are bought by the system operator at reserve markets where power plant operators can offer reserve capacities for defined time periods. The four German system operators have established an internet platform, where they buy the reserve capacities in a combined tender procedure (apart from a technically required amount of reserves in the home control area) [61].

Each electricity supplier in the control area has its own balancing area that he coordinates (the balancing areas are not to be understood as geographical areas). In each balancing area, imbalances can occur due to the uncertainties in the planning process. The imbalances of all balancing areas are summed up and the resulting net imbalance of the control area is balanced by the TSO by activating reserve capacities. Each electricity supplier has then to pay or is remunerated for the balancing energy he receives. The supplier has to pay if his imbalance and the net imbalance of the control area are both positive or both negative. The price for the balancing energy is set by the reserve activation costs [64, §8(2)].

The imbalances in the balancing areas are balanced by the TSO actions for maximal one hour. Longer imbalances have to be controlled by the electricity supplier himself [64, §5(2)]. There is therefore no centrally organised provision of a reserve type for longer imbalances, a so-called “hours reserve”. There is one exception to this. The TSOs are responsible for the imbalances that come from power sources that are classified under the “Erneuerbare-Energien-Gesetz (EEG)”

(Renewable Energy Law). These power sources are coordinated by the TSO in the EEG balancing area [64, §11)]. To optimize the balancing of their EEG balancing areas, TSO may tender special "hours reserve" capacities, the so-called EEG reserve, that can have activation times of 45 minutes or longer.

To avoid imbalances, the electricity suppliers can participate at the intraday market. The day-ahead market is closed at 12 am. Intraday trading is then possible from 3 pm up to 75 minutes before the physical delivery [65]. Successful intraday trading leads to changes in the schedules. There is a schedule for each balancing area that has to be balanced and that is reported to the TSO until 14:30 pm the day before. Intra-day schedule modifications (both within a control area and cross-control-area) have to be reported to the TSO at least three quarter-hours before physical delivery. In the case of modifications of the cross-control-area schedule, the TSO can reject the modification to prevent congestion in the grid. The TSOs are responsible for the physical realisation of the schedules in the grid. They can use active load flow management techniques (network switcher, transformer taps) or market base methods as load management, use of reserves or other congestion management measures [66, §13]. The legal implications in the context of curtailment and prioritized feed-in of renewable energy are thereby yet to be clarified [67].

2.2.3. Transmission

High shares of wind power can have congesting effects in the transmission grid. Even though wind power is often mentioned in the context of distributed generation, it has normally different characteristics. Large wind parks are connected at transmission voltage levels and not at distribution voltage levels, see Section 2.1.1. Independent from the connection voltage, it is obvious that wind power will centralize in regions with high wind potential. Especially offshore wind energy is naturally located in near coastal areas. It may therefore be that there are large geographical distances between the centres of high demand and the wind power centres, which motivates a more detailed look at the transmission grid. A potential scenario of the future German allocation of power capacities and demand requirements follows in Chapter 3. Here, the transmission grid and the related concepts are presented. First, the general design of the transmission grid is explained. After that, transmission line parameters are given and the DC load flow concept is explained.

Grid structure

Transmission of power is always subject to transmission losses due to the electrical resistance of the transmission lines. The energy loss is proportional to the length of the line and to the square of the intensity of current [7]. At constant power, an increase of the voltage level leads to a reduction of the intensity of current. A

high voltage level is therefore preferred for the transmission over long distances. In Germany, the following voltage levels are use. Voltage levels of 230 V or 400 V are defined as low voltage. Voltage levels of 10 kV or 20 kV are defined as medium voltage. High voltage is given by 110 kV and extremely high voltage is given by 380 kV. Other levels, like 30 kV, 60 kV and 220 kV, are also in use. Their exact classification depends on their structure and function, [68], whereby 220 kV is normally classified as extremely high voltage and 60 kV as high voltage, [69].

There is no clear technical definition which voltage levels belong to the transmission grid. For example, Schwab, [1], defines transmission systems ("Transportnetze") by 220 kV and 380 kV voltages, whereas subtransmission systems ("Übertragungsnetze") are defined by 110 kV lines. In other sources all high voltage levels form the transmission grid ("Übertragungsnetz") [68]. A possibility is to define the transmission grid by the lines the transmission grid operators are responsible for. The transmission grid operators are identified by their duties and responsibilities as prescribed by the corresponding national energy laws. This means that the transmission grid may not contain the same voltage levels in different control areas and that the contained voltage levels may change with the time (if for example a new line is built). In Germany, there are currently four transmission grid operators (50Hertz, Amprion, Transpower, EnBW) and they mainly operate the 220 kV and 380 kV lines.

Figure 2.6 shows the German transmission grid in 2007 (map published by the Verband der Netzbetreiber - VDN, Berlin). The red and green lines represent the 380 kV and 220 kV lines. High density of transmission lines can be seen in the populous Ruhr area and in the South-West at the border to Switzerland (around the "Stern von Laufenburg"-node connecting the German, French and Swiss transmission grid). The former border between the German Democratic Republic and the Federal Republic of Germany is noticeable by a low density of transmission lines. The German transmission grid covers an area of about 350,000 km^2. The length from North to South is about 900 km and from West to East about 600 km. The transmission over such distances can be covered by overhead lines. Overhead lines are normally considered to be practical for distances up to 1000 km [1]. A general rule of thumb is that the voltage level of the transmission line indicates the distance for that it is normally used [68]. The voltage levels of the German transmission lines and the distances between the German regions correspond to these indications.

Transmission line parameters

In the following, technical characteristic of transmission lines are given. In the case of overhead lines, transmission lines have to be supported by wood or steel poles or towers. Many different types of tower designs exist and they can carry several circuits. It is also usual that circuits with different voltage levels are on the same towers. Depending on the terminology, transmission lines represent one

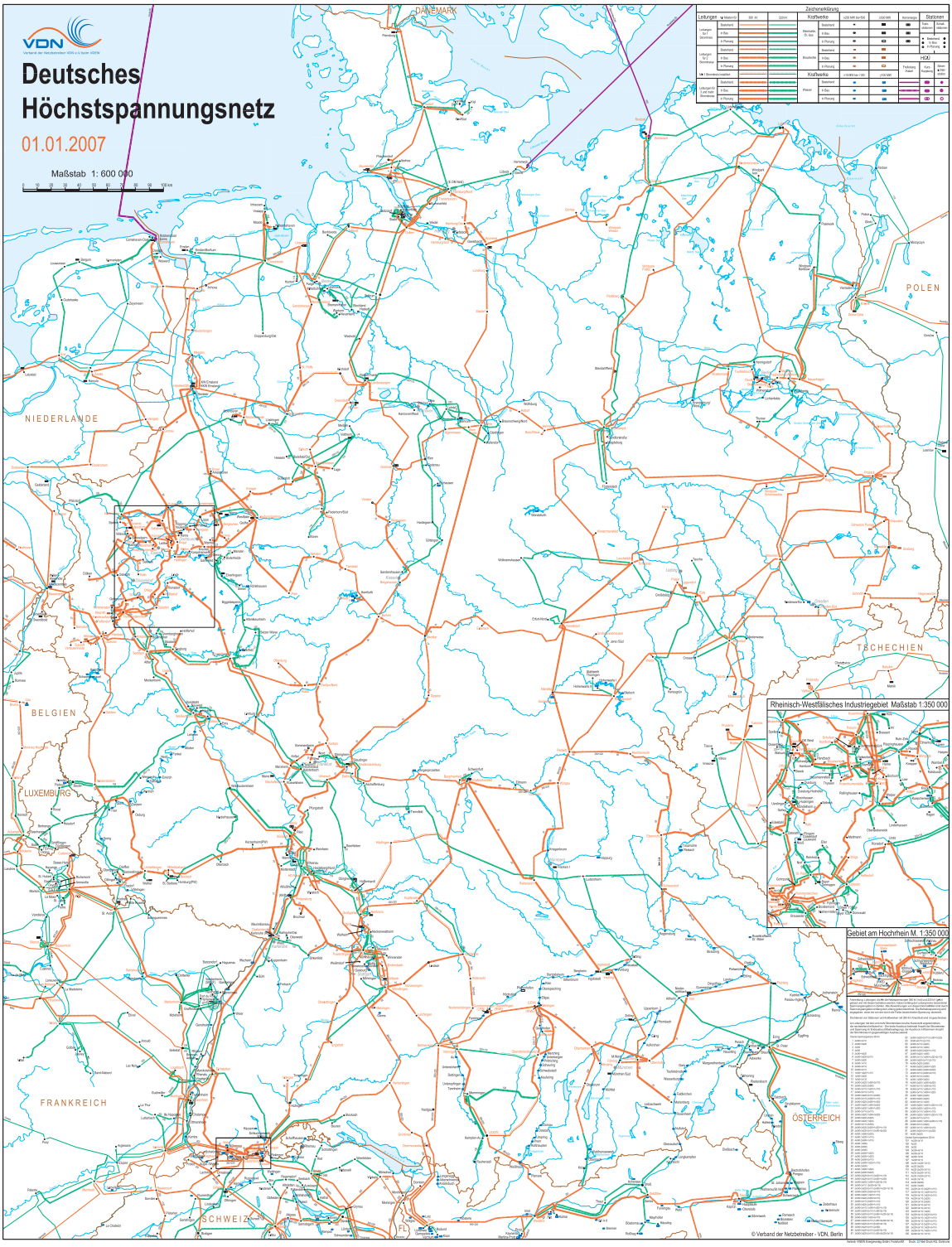

Figure 2.6.: VDN map of the German transmission grid in 2007

or all circuits of a connection. Each circuit consists of three conductors as the transmission of power is based on three-phase voltage (each conductor supplies one phase). In the case of extremely high voltage lines, these conductors are often bundled meaning that the conductors consist of separated wires. The wires of one conductor bundle are held apart by a few inches by non-conducting spacers (arranged approximately every 50 meters). Two-conductor bundles are normally used for 220 kV circuits and three- or four-conductor bundles for 380 kV circuits. Reasons to use conductor bundles are increasing heat dispersion, reducing corona losses and reducing inductance [69, 70]. The wires themselves are typically made of aluminium alloys and a steel core to increase the mechanical strength [68].

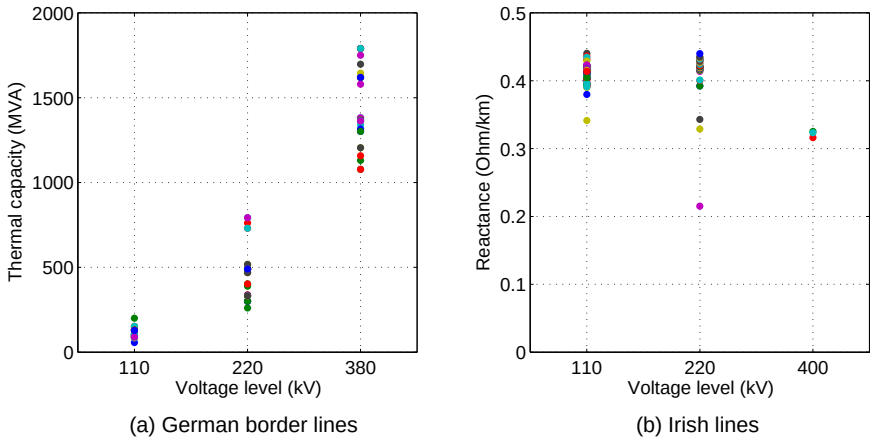

Figure 2.7.: Thermal transmission capacities and reactances of transmission lines (one circuit)

In Figure 2.7, different parameters of the transmission lines (including 110 kV lines) are given. For economic electricity models, the maximal power transmission capacity of a line is of interest. The thermal transmission capacity is one limiting parameter for the maximal transmission capacity. The thermal transmission capacity of a line depends on its technical characteristics like type of conductor bundle and material as well as on external factors like ambient temperature or wind conditions [69]. A range of possible capacities for one circuit is given by Figure 2.7-(a). The values are published by the UCTE, [71], and refer to the transmission lines at the German borders. They are calculated for ambient temperatures of 35°C and wind velocities of 0.56 m/s at a right angle to the line. The given values correspond to literature indications, see for example [72, 73]. The large differences between the values is mainly due to different conductor bundles. For example, the transmission capacities exceeding 1600 MW in the 380 kV case are related to four-conductor bundles, whereas the lower values are related to two- or three-conductor bundles. There is therefore no linear relation between the capacity and the number of conductors in the bundle. In the case of 110 kV, the range of transmission capacities is smaller as the 110 kV lines generally consist of

non-bundled single conductors. It is important to note that the thermal capacity gives no indication for the real capacity of the line as it depends on "(...) many other factors, such as load flow distribution, upholding of voltage, real ambient conditions, limits of stability, n-1 security, etc." [71]. N-1 security is a general principle of power transmission and it is respected if any element in the system can fail without overloading another element [62].

The load flow can be estimated by a DC load flow approach that is presented in the next section. The reactances of the transmission lines are therefore needed. Exemplary reactances of transmission lines, published by the Irish transmission system operators, are shown in Figure 2.7-(b) for voltage levels of 110 kV, 220 kV and 400 kV[4]. An important factor is the type of conductor bundle. In the case of 110 kV, only single conductors are used and the difference between the reactances is small. In the case of 220 kV, the values at 0.4 Ω/km refer to single conductors. The values slightly above 0.3 Ω/km can be explained by a mixture of overhead line and underground cable. The values of two-conductor bundles are typically 30% lower ranging from 0.28 to 0.3 Ω/km [68]. Four-conductor bundles have low reactances of about 0.2 Ω/km. In the case of 400 kV, reactances above 0.3 Ω/km refer to two-conductor bundles. The reactances of four-conductor bundles at 400 kV are in general 25% lower than the ones of two-conductor bundles and values of 0.25 Ω/km apply [68]. Other factors for the reactances are the width and material of the conductors and the number of circuits of the transmission line. For German transmission lines, similar values as in Figure 2.7-(b) are indicated [74, 68, 75]. Hence, the reactances increase with the voltage level and decrease with the size of the conductor bundle (and the section of the cables) and they range from 0.2 Ω/km to 0.45 Ω/km.

DC load flow

The calculation of the power flows in combination with the dispatch is known as optimal power flow model. In this optimization problem, the generation costs are minimized and all power systems constraints are considered as restrictions. The optimal power flow is a large and difficult mathematical problem if all constraints are considered in detail. Different simplifications of the problem have therefore been proposed. The DC power flow model is one of them that is especially suitable for large economic models as it reduces all network constraints to linear restrictions.

In a network, the complex power, S_k, at a node k, being composed of the active power P and reactive power Q, is given by the product of the complex voltage, E_k, and the conjugate-complex current, I_k^*, at the node. I_k is given by the voltages

[4]The values for 400 kV can be considered representative for 380 kV lines as the influence of the voltage level on the reactance is not as significant as in the case of thermal transmission capacities

and admittances, $Y_{m,n}$, in the network [76, 77].

$$S_k = P_k + jQ_k = E_k \cdot I_k^* = E_k \sum_l Y_{k,l}^* E_l^*$$

With $Y_{k,l} = G_{k,l} + jB_{j,k}$, and with θ_k as phase angle at node k, the power is calculated as follows [38].

$$P_k + jQ_k = \sum_l |E_k||E_l|(G_{k,l} - jB_{k,l}) \exp j(\theta_k - \theta_l)$$

With $V_k = |E_k|$, the real power P_k is:[5]

$$P_k = \sum_l V_k V_l (G_{k,l} \cos(\theta_k - \theta_l) + B_{k,l} \sin(\theta_k - \theta_l))$$

Looking only at one branch between two nodes, the transmitted power is equal to:

$$P_{kl} = V_k V_k G_{k,k} - V_k V_l (G_{k,l} \cos(\theta_k - \theta_l) + B_{k,l} \sin(\theta_k - \theta_l))$$

In the following the DC load flow assumptions are applied [38, 78, 79]. First, the losses are assumed to be zero and the resistance of each branch is negligible compared to its reactance. The conductance G is then zero and the susceptance B is equal to $-1/x$ with x as reactance.

$$P_{kl} = V_k V_l \frac{1}{x_{k,l}} \sin(\theta_k - \theta_l)$$

Secondly, the difference of the phase angles is considered as small so that the small angle approximation can be applied:

$$P_{kl} = V_k V_l \frac{1}{x_{k,l}} (\theta_k - \theta_l)$$

Finally, the voltage differences are taken as negligible and all voltages are equal. In any electrical network, all quantities can be formulated in the per-unit system [1]. In the per-unit system, all values are related to two base (reference) values. For example, a base apparent power and a base voltage are chosen as reference values. If the base apparent power is set to 1 and the base voltage is set equal to the unique voltage at all nodes, the transmitted power is:

$$P_{kl} = \frac{1}{x_{k,l}} (\theta_k - \theta_l)$$

The problem is therefore linearised. In the optimization, the reactance of each

[5] The reactive power Q_k, being eliminated by the subsequent assumptions, is not considered any more.

branch is given as a parameter and the voltage angles at each node are variables.

For large-scale economic models, the DC load flow is an useful approximation of the transmission. The losses are neglected but the effects of the constraints are normally much more significant than the effects of the losses [38]. Detailed comparisons of AC and DC load flow representations are given in several studies [80, 81, 79].

3. A stochastic optimization model of the power system

The operational effects of high shares of wind power are analyzed by a stochastic electricity market model that is presented in the following. The model formulation is based on the Joint Market model that was originally developed in the Wilmar project from 2002 to 2005 [82, 83, 84, 85, 86]. Since then, the model has been used and improved in several projects [87, 88, 89, 90]. For this work, the model was adapted in several points. Main enhancement is a more detailed representation of transmission restrictions. A DC load flow representation of the electricity exchanges was therefore added. In the load flow restrictions, the susceptances of the transmission lines are considered. Another major change is the assessment of the storage value that is now calculated by a deterministic pre-run of the model. The provision of reserves was updated so that tertiary reserve requirements can now be met by spinning and non-spinning units. In order to focus on the power supply, the heat market representation was adapted. Only CHP power plants and the related heat demand are considered and additional heat demand is covered by a simplified boiler representation. A minor change is for example given by the distinction between stochastic and deterministic regions. The model concept and the model equations are presented in the first section of this chapter.

The derivation of the input parameters is given in the second section of the chapter. Germany is thereby divided into 14 model regions and future power plant portfolios are required for all regions. These power plant portfolios are developed based on a power plant database and literature. The other data assumptions are related to the power plant parameters (based on the flexibility analysis in the previous chapter), the demand and the fuel prices. Additionally, an approach for reserve calculation and a grid reduction approach are presented. Tertiary reserve requirements are calculated by a probabilistic method based on the forecast errors and power plant outages. The grid reduction approach allows to derive transmission parameters for a reduced grid starting from the complete grid.

3.1. General model description

A main feature of the model is the stochastic representation of wind power forecasts. The forecasts are considered by a rolling planning approach. The rolling planning approach is explained in the following after a short general description

of the model and its input and output. The equations including the objective function and the constraints are presented in the rest of the section.

3.1.1. Model concept

The model is a linear optimization model that minimizes the total operational system costs. All technical restrictions in the system operation like capacity limits are thereby considered by constraints. The calculated optimum can be interpreted in two ways. It can be interpreted as an operation that is planned by a hypothetical single system operator that is responsible for the total power system, so the power plant operation and the power transmission. The result can also be interpreted as the solution that is realized by an ideal electricity market with pure competition that respects the transmission restrictions. In the concept of pure competition, market distortions like market power or irrational behaviour of the market participants are neglected. The model only optimizes the operational system costs and investment costs or renewable feed-in tariffs are not considered. The model has an hourly resolution.

Table 3.1 shows the input and output of the model. The power plant portfolio is defined by the generation capacities in the model regions. For CHP and storage plants, the maximal heat or pumping capacity is also needed. The power plants are also defined by parameters that describe their technical operation like their efficiency or maximal storage content. Flexibility is described by parameters as minimal operation times, start up costs and others. The technical capability to provide primary, secondary or tertiary reserve is another characteristic of a power plant. The fuel prices and CO2 prices are required. No other taxes than the CO2 price are considered in the model. The transmission between the model regions is restricted by the thermal capacities and susceptances of the connecting lines. For each model region the reserve requirements are indicated. The heat and power demand as well as the generation from fluctuating renewable sources are given in an hourly resolution. In the case of wind power, not only the generation but also forecasts of the wind power generation are required for each optimization. The wind power generation and forecasts are simulated as described in Chapter 4. The simulation has its own input parameters that are for example related to forecast quality.

The results of the optimization model can be analyzed in different ways. Some examples are given in Table 3.1. The two basic results are the system costs (the value of the objective function) and the operation of the power plants (the variables in the optimization). Other values can be deduced as the curtailment or the emissions. The transmission between the model regions is another result. The marginal values of the balance equations are interpreted as market prices. The optimization model in combination with the simulation in Chapter 4 therefore allows to analyze the effects of high wind power shares on the power system operation

Table 3.1.: Input and output of the optimization model

Input data	Output examples
• Installed capacities (power, heat, pumping) • Plant parameters (efficiency, operation costs, emissions, flexibility, storage, CHP, reserve) • Prices (fuel prices, CO_2 tax) • Transmission (capacities, susceptances) • Demand (power, heat) • Reserve requirements • Wind power (generation, forecasts) • Other fluctuating power generation	• Generation and curtailment • Operational costs • Storage operation • Fuel usage • Emissions • Transmission • Market prices

for different system configurations.

The wind power forecasts are considered by a stochastic rolling planning approach. Power plant operators have to decide on the plant operation before the precise wind power production is known.[1] As wind power forecasts are not perfect, recourse actions are necessary when the delivery period is in the nearer future and the wind power forecasts become more accurate. Hence, there is a continuous alternation of first decisions based on first forecasts and re-dispatch actions at a later date based on updated forecast information. Differences between former forecasts and updated forecasts are balanced by changes in the power plant operation. The rescheduling of the plant operation can be interpreted as the result of intraday trading. The intraday optimizations therefore update the results of the day-ahead optimization and precedent intraday optimizations.

There are two ways how wind power forecasts can be considered in the intraday optimizations of the model. In the first mode, deterministic optimizations are executed that only consider the actual predicted wind power production (expected value forecast). This decision structure is illustrated in Figure 3.1-(a). The

[1]Next to wind forecasts, there are other uncertainties in the system as described in Section 2.2.2. It was shown that, for day-ahead forecasts, load forecast errors are negligible compared to wind forecast errors. Load forecast errors and uncertainties resulting from unplanned power plant outages are considered in the calculation of tertiary reserve requirements.

rolling planning is thereby based on an intraday optimizations taking place every 3 hours.[2] The optimizations cover the hours until the end of the next day and, in each optimization, the forecast for the first two hours is assumed to be perfect. The forecast errors related to forecast horizons with one or two hours are only considered in the calculation of the tertiary reserve capacities.

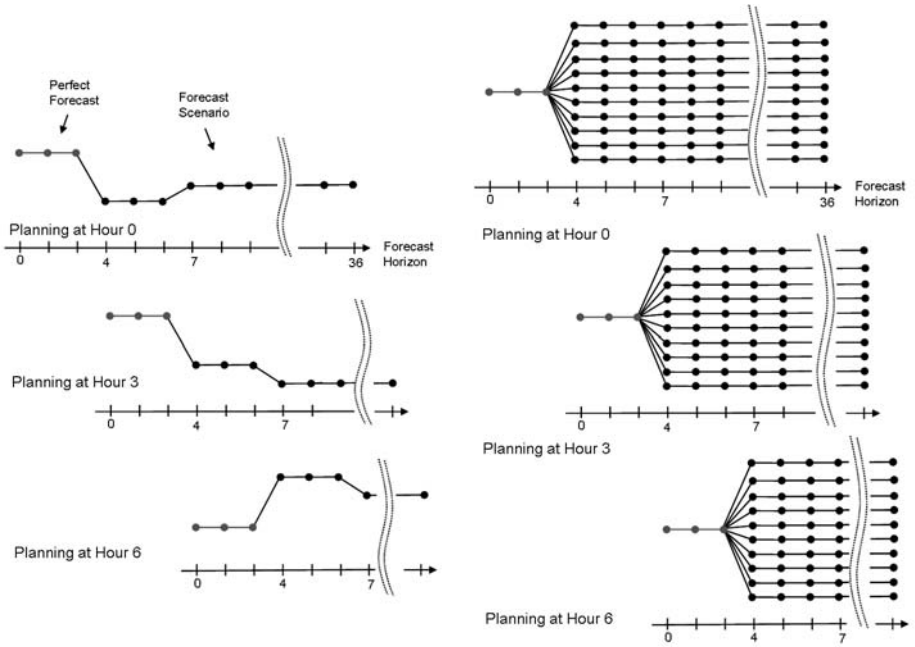

(a) Deterministic optimizations (b) Stochastic optimizations

Figure 3.1.: Two modes of rolling planning

In the second model mode, not only the expected value forecast but also possible forecast errors are considered in the intraday optimizations. This allows to hedge possible forecast errors. In these stochastic optimizations, the random variable "forecast error" is represented by several discrete scenarios (or scenario paths as more than one forecast hour is considered). Each scenario is weighted by its probability in the objective function and the constraints are respected for all scenarios. Thus, an optimal solution is found that also considers possible forecast errors. This approach is illustrated in Figure 3.1-(b). The number of considered scenarios is a trade-off between calculation time and a good statistical representation of the forecast error. Calculation time is above all critical due to the rolling planning. The calculation of one year for example demands 2920 successive optimizations (one every three hours). The generation of the error scenarios and their statistical characteristics are presented in Chapter 4.

Concluding, the model is defined by (stochastic) optimizations of the power plant operation under uncertain wind power forecasts, [92, 93], combined with a

[2]The intraday trading at the EEX takes place every hour but the wind power forecasts are updated only every four hours [91].

rolling planning approach, [94], where the recourse decisions of former optimizations become continuously the root decisions of the following ones.

3.1.2. Objective function

As explained in the precedent section, the general concept of the model is given by linear optimizations embedded in a rolling planning. In each optimization, the operational costs over the time steps t of the forecast horizon and over the forecast scenarios s are minimized. The optimizations are called deterministic if only one forecast scenario (the expected value forecast) is considered and they are called stochastic if several forecast scenarios are considered, weighted by their probabilities π.[3] The length of the considered forecast horizon $\mathbf{T}$ depends on the rolling planning step. Each day at 12 am, for instance, the rest of the day and the following day are considered which corresponds to 36 hours. In the next optimization, taking place three hours later, only 33 hours are considered. The optimization at 9 am only considers the remaining 15 hours of the day.

Objective function The objective function, minimizing the operational costs, is given by Equation (3.1). The operational costs are composed of fuel costs and emission taxes, operational maintenance costs, start-up costs, opportunity costs and penalties.

$$\min \Bigg\{ \sum_{s \in \mathbf{S}} \pi_s \cdot$$

optimization over all scenarios weighted by probabilities

$$\Big(\sum_{t \in \mathbf{T}} \sum_{u \in \mathbf{U}} (c_u^{fuel} + c_u^{tax}) \cdot (e_u^{gen}(P_{u,t}^{day} + P_{s,u,t}^{+} + P_{s,u,t}^{-} + k_u^{chp} P_{s,u,t}^{heat}) + e_u^{onl} C_{s,u,t}^{online}) \tag{3.1a}$$

fuel costs and emission taxes

$$+ \sum_{t \in \mathbf{T}} \sum_{u \in \mathbf{U}} c_u^{o\&m} \cdot (P_{u,t}^{day} + P_{s,u,t}^{+} + P_{s,u,t}^{-} + k_u^{chp} P_{s,u,t}^{heat}) \tag{3.1b}$$

operational maintenance costs

$$+ \sum_{t \in \mathbf{T}} \sum_{u \in \mathbf{U}} (c_u^{start} + c_u^{fuel} e_u^{start}) \cdot P_{s,u,t}^{start} \tag{3.1c}$$

start-up costs and start-up fuel consumption

$$+ \sum_{u \in \mathbf{U}} c_{u,t_{last}}^{opp,onl} C_{s,u,t_{last}}^{online} + c_{u,t_{last}}^{opp,sto} F_{s,u,t_{last}}^{storage} + c_{u,t_{last}}^{opp,res} F_{s,u,t_{last}}^{reservoir} \tag{3.1d}$$

opportunity costs for being online, storage content and hydro reservoir

[3] This differentiation refers to the intraday optimizations. The optimization that represents the day-ahead market always takes only the expected value forecast into account.

$$+\sum_{t\in\mathbf{T}}\Big(\sum_{r\in\mathbf{R}}(c^{pen}\cdot(V^{day}_{r,t}+V^{intra}_{s,r,t}))+\sum_{a\in\mathbf{A}}(c^{heat}V^{heat}_{s,a,t})\Big)\Bigg\} \tag{3.1e}$$

penalty costs for system violations and heat boiler use

The different components of the objective function are explained in the following.

Power generation and fuel consumption

The fuel consumption is determined by power generation, by heat generation and by having capacity online. The power generation is given by the sum of P^{day} and P^{+} minus P^{-}. P^{day} stands for the day-ahead dispatch that is found in the day-ahead market. The day-ahead market is only optimized in the optimization at 12 am. In the following intraday optimizations (up to 9 am at the next day) the day-ahead dispatch stays is corrected by intraday actions. Up-regulation of generation is thereby denoted by P^{+} and down-regulation by P^{-}. The fuel consumption caused by heat generation is considered by transforming the heat generation, P^{heat}, to an equivalent power generation. For each CHP plant type, the parameter k^{chp} gives the iso-fuelline, so the relation between heat generation increase and power generation reduction. The fuel consumption caused by having capacity online is calculated applying the parameters e^{gen} and e^{onl}. The parameters allow to estimate the fuel consumption that is related to the online status of a power plant group. This representation results from the aggregation of power plants to fleets and the linearization of the binary online status variable, see [95]. The two parameters are thereby derived by two known relations: the power plant efficiency at full and at minimal load. At full load, the fuel consumption is now written as $e^{gen}P + e^{onl}C^{online} = c^{inst}/\eta$. At minimal load, it is $e^{gen}P + e^{onl}C^{online} = c^{inst}lf^{min}/\eta^{min}$ with lf^{min} as minimal load factor and η^{min} as part load efficiency. The online capacity is then set equal to the installed capacity c^{inst} (corresponding to 1 in the binary case), the generation P is equal to the installed capacity or the minimal load and the remaining unknown parameters e^{gen} and e^{onl} can be calculated.

Costs and penalties

Three cost types are considered in the objective function: operational costs, opportunity costs and penalties.

Operational costs Operational fuel costs are given by the fuel consumption in combination with the fuel prices and CO_2 emission tax. Each power plant type therefore has a fuel cost factor c^{fuel} and an emission tax factor c^{tax}. Operational maintenance costs are defined by $c^{o\&m}$ and related to the equivalent power generation. In the start-up process, additional fuel, defined by e^{start}, is consumed leading to additional start-up costs. Start-up processes also cause additional general costs

given by c^{start}. The start-up costs are related to a positive change of the online capacity.

Opportunity costs Opportunity costs are required as the time horizon of each optimization in the rolling planning process is limited. The model calculates one year by consecutive optimizations, but only one to two days are considered in each optimization. There would therefore be a maximal use of storage without consideration of later time periods even though the storage content may then be of a higher value. The same applies to the online status of thermal units. It can be of value that a thermal unit is running so that no start-up process is required.

The following approach is here developed to calculate the opportunity costs. A pre-run of the model leads to the marginal costs of the relevant constraints for every hour. In the pre-run, the time periods of the optimizations are lager, covering one week (without consideration of forecast errors). The opportunity costs then play a less important role due to the longer time periods so that approximate opportunity costs can be applied in the pre-run. The hourly marginal costs that result from the pre-run are then used in the main run to represent the opportunity costs. For storage plants, the opportunity costs are set to the average pre-run marginals of all hours that follow after the optimization period. A potentially higher storage value later in the year is thus considered in the optimization. For the online status, the opportunity costs are set to the average pre-run marginals of the day after the optimization period. This reflects that the online status is more important in a short-term context.

Penalties The slack variables (V^{day}, V^{intra}, V^{heat}) are used to identify system violations and to consider additional heat demand. They allow to violate the related constraints but under high penalty costs, so that slack variables are only used if there is no other option. One exception is the heat slack V^{heat}. Only combined heat and power (CHP) plants are considered in the model and no heat plants. The modelled heat demand therefore represents only the CHP heat demand. As the CHP heat demand could also be partially covered by heat plants, the model has the possibility to use the heat slack variable. The related costs are calculated by a typical boiler efficiency in combination with the gas and oil fuel price. Due to the high efficiency of CHP, the model normally avoids to use the heat slack variable.

The penalty costs (except the heat costs) are considered separately in the final analysis of the model results. As the penalty level is set in an arbitrary way, their consideration in the cost analysis would not be meaningful. However, the slack variables indicate the situations when the model cannot fulfil the demand requirements. Their use is therefore registered and regarded separately from the other results giving an indication of the adequacy of the power system.

3.1.3. Restrictions

The main constraints are presented in the following. They are related to the balances on the day-ahead, intraday and heat market, capacity restrictions, transmission constraints, inter-temporal restrictions, the representation of hydro and storage power plants and the consideration of reserve requirements.

Market balances

The power balance at the day-ahead market is represented by Equation (3.2). The power is generated by all dispatched power plants, P^{day}, and the fluctuating resources (wind, photovoltaic and run of river). Negative generation is given by pumping, L^{day}, and shedding of fluctuating resources, $W^{shed,day}$. In the case of wind power, only day-ahead forecasts, $p^{wind,day}$, are considered and not the actual generation. The demand d can be reduced by the slack variable V^{day}. Imports and exports are considered by T^{day}.

$$\sum_{u \in \mathbf{U_r}} (P^{day}_{u,t} - L^{day}_{u,t}) + p^{wind,day}_{r,t} + p^{pv}_{r,t} + p^{ror}_{r,t} - W^{shed,day}_{r,t} + \sum_{r*} T^{day}_{r*,r,t} = d_{r,t} - V^{day}_{r,t}$$
$$\forall r \in \mathbf{R}, \forall t \in \mathbf{T} \qquad (3.2)$$

Changes in the planned wind power generation due to forecast errors are balanced on the intraday market according to Equation (3.3). The intra-day wind forecast, $p^{wind,intra}$, gives updated information about the wind power generation. The generation and pumping can be up- or down-regulated (P^+,P^-,L^+ and L^-) or additional shedding, $W^{shed,intra}$, can be applied in order to balance the errors. The transmission schedules are changed by T^{intra}.

$$\sum_{u \in \mathbf{U_r}} (P^{+}_{s,u,t} - P^{-}_{s,u,t} + L^{-}_{s,u,t} - L^{+}_{s,u,t}) - W^{shed,intra}_{s,r,t} + \sum_{r*} T^{intra}_{s,r*,r,t} =$$
$$p^{wind,day}_{r,t} - W^{shed,day}_{r,t} - p^{wind,intra}_{s,r,t} - V^{intra}_{s,r,t} \qquad \forall s \in \mathbf{S}, \forall r \in \mathbf{R}, \forall t \in \mathbf{T}, \quad (3.3)$$

If forecast errors are only modelled in selected regions, intraday changes are only possibly in these regions. The heat balance is given by Equation (3.4).

$$\sum_{u \in \mathbf{U_a}} P^{heat}_{s,u,t} = d^{heat}_{a,t} - V^{heat}_{s,a,t} \qquad \forall s \in \mathbf{S}, \forall a \in \mathbf{A}, t \in \mathbf{T} \qquad (3.4)$$

In each area a, the CHP plants have to generate heat according to the heat demand, d^{heat}. The areas thereby have a higher geographical resolution than the regions. Heat generation from heat boilers is considered by the slack variable V^{heat} as described above.

Capacity restrictions

The power generation is restricted by the installed capacity c^{inst} according to Equation (3.5). The power generation is thereby equal to the day-ahead scheduling P^{day} under consideration of up-regulation and down-regulation, P^{+} and P^{-}. Capacity margins are kept for the potential use of spinning reserves, $R^{sp,+}$, and non-spinning reserves, $R^{ter,+}$.

$$P^{day}_{u,t} + P^{+}_{s,u,t} + P^{-}_{s,u,t} + R^{sp,+}_{u,t} + R^{ter,+}_{s,u,t} \leq c^{inst}_{u} \qquad \forall s \in \mathbf{S}, u \in \mathbf{U}, t \in \mathbf{T} \tag{3.5}$$

The power generation is not only restricted by the installed capacity. It must also be smaller than the online capacity, C^{online}, according to Equation (3.6). In this case, only a margin for the use of spinning reserves is kept as tertiary reserve capacities are defined as being offline (see below).

$$P^{day}_{u,t} + P^{+}_{s,u,t} + P^{-}_{s,u,t} + R^{sp,+}_{u,t} \leq C^{online}_{s,u,t} \qquad \forall s \in \mathbf{S}, u \in \mathbf{U}, t \in \mathbf{T} \tag{3.6}$$

The power generation must be higher than the minimal load given by the minimal load factor lf^{min} and the online capacity according to Equation (3.7). In this case, a margin for the use of negative spinning reserve, $R^{sp,-}$, is considered.

$$P^{day}_{u,t} + P^{+}_{s,u,t} + P^{-}_{s,u,t} - R^{sp,-}_{u,t} \geq lf^{min}_{u} \cdot C^{online}_{s,u,t} \qquad \forall s \in \mathbf{S}, u \in \mathbf{U}, t \in \mathbf{T} \tag{3.7}$$

An additional equation, not shown here, assures that the capacity online plus the non-spinning reserves is not higher than the installed capacity. Equation (3.8) assures that the heat generation does not exceed the installed heat generation capacity, $c^{inst,heat}$.

$$P^{heat}_{s,u,t} \leq \cdot c^{inst,heat}_{u} \qquad \forall s \in \mathbf{S}, u \in \mathbf{U}, t \in \mathbf{T} \tag{3.8}$$

There are two types of CHP plants in the model: back pressure plants and extraction plants. In back pressure plants the heat generation and the power generation are tightly coupled and there is only one degree of freedom. In extraction plants, the heat generation can partially be chosen independently of the power generation. The related equations are as given in [86].

Transmission

The transmission between two regions cannot exceed the installed transmission capacity t^{reg}. The transmission scheduled at the day-ahead market, T^{day}, intraday changes, T^{intra}, and the transmission of tertiary reserves, T^{res}, are thereby considered according to Equation (3.9). Tertiary reserves can only be transmitted between regions within Germany and the related region pairs are defined by the

set $\mathbf{X}$.

$$T^{day}_{r*,r,t} + T^{intra}_{s,r*,r,t} + T^{res}_{s,(r*,r)\in\mathbf{X},t} \leq t^{reg}_{r*,r} \qquad \forall s \in \mathbf{S}, \forall r*, r \in \mathbf{R}, \forall t \in \mathbf{T} \quad (3.9)$$

Additional equations, not shown here, assure that the transmission capacities are also not exceeded at the day-ahead market and that the transmissions are symmetrical.

Within the German regions (given by $\mathbf{X}$) the transmission is defined by the regional "voltage" angles Φ and the regional susceptances b^{reg}. The regional susceptances are connection line parameters that are derived by the approach in Section 3.2.3. The "voltage" angles are variables and there is one angle for each region. The relation between angles and power exchanges on the day-ahead market is given by Equation (3.10). The intraday transmission changes are realized by changes of the angles according to Equation (3.11).

$$T^{day}_{r*,r,t} = b^{reg}_{r*,r} \cdot (\Phi_{r*,t} - \Phi_{r,t}) \qquad \forall r*, r \in \mathbf{X}, t \in \mathbf{T} \quad (3.10)$$

$$T^{intra}_{s,r*,r,t} = b^{reg}_{r*,r} \cdot (\Phi^{delta}_{s,r*,t} - \Phi^{delta}_{s,r,t}) \qquad \forall s \in \mathbf{S}, \forall r*, r \in \mathbf{X}, t \in \mathbf{T} \quad (3.11)$$

Both at the day-ahead market and after intraday changes the difference between the angles cannot exceed the maximally allowed angle difference, ϕ^{max}, according to Equation (3.12) and Equation (3.13). The maximally allowed angle difference is thereby derived by the approach in Section 3.2.3.

$$(\Phi_{r*,t} - \Phi_{r,t}) \leq \phi^{max} \qquad \forall r*, r \in \mathbf{X}, t \in \mathbf{T} \quad (3.12)$$

$$(\Phi_{r*,t} + \Phi^{delta}_{s,r*,t}) - (\Phi_{r,t} + \Phi^{delta}_{s,r,t}) \leq \phi^{max} \qquad \forall s \in \mathbf{S}, \forall r*, r \in \mathbf{X}, t \in \mathbf{T} \quad (3.13)$$

Inter-temporal restrictions

There are several inter-temporal equations in the model. In order to calculate the start-up costs in the objective function, the started capacity, P^{start}, is required. It is defined by the change of the online capacity according to Equation (3.14).

$$P^{start}_{s,u,t} \geqq C^{online}_{s,u,t} - C^{online}_{s,u,t-1} \qquad \forall s \in \mathbf{S}, u \in \mathbf{U}, t \in \mathbf{T} \quad (3.14)$$

The power plant operation is constraint by minimal operation times, t^{minop}, according to Equation (3.15). The online capacity at $(t-1)$ minus the online capacity at t gives the capacity that is shut down at t. The condition for shutting down capacity at t is that the capacity has been online before t for the time period

t^{minop} at least.

$$C^{online}_{s,u,t_{op}} \geqq C^{online}_{s,u,t-1} - C^{online}_{s,u,t} \qquad \forall s \in \mathbf{S}, u \in \mathbf{U}, t \in \mathbf{T}, t_{op} \in \mathbf{T} \mid t - t^{minop}_u \leq t_{op} \leq t-1 \tag{3.15}$$

In a similar manner minimal shutdown times, t^{minsd}, are considered by Equation (3.16). The online capacity at t minus the online capacity at $t-1$ gives the capacity that is started at t. The condition for starting capacity at t is that the capacity has been offline before t for the time period t^{minsd} at least.

$$C^{online}_{s,u,t_{sd}} \leqq c^{inst}_u - (C^{online}_{s,u,t} - C^{online}_{s,u,t-1}) \qquad \forall s \in \mathbf{S}, u \in \mathbf{U}, t \in \mathbf{T}, t_{sd} \in \mathbf{T} \mid t - t^{minsd}_u \leq t_{sd} \leq t-1 \tag{3.16}$$

The consideration of start-up times has two aspects. On the one hand, the process to start-up a power plant takes some hours and the power plant can not be immediately online again after having turned it off. This is considered by the minimal shutdown (offline) times. On the other hand, the decision to start-up a power plant may be spontaneous and not be planned in forehand. A start-up time should then be respected even if the power plant has been offline for many hours. In the first hours of each optimization, the online capacity can therefore not be higher than the capacity that was planned to be online by the last optimization, given by $c^{onl,prev}$ in Equation (3.18). The number of the affected hours is thereby defined by the start-up time, t^{minst}, of the power plant.

$$C^{online}_{s,u,t} \leqq c^{onl,prev}_{u,t} \qquad \forall s \in \mathbf{S}, u \in \mathbf{U}, t \in \mathbf{T} \mid t \leq t^{minst}_u \tag{3.17}$$

Hydro and storage power plants

Some extra equations are given for hydro power plants next to the constraints that apply to all power plants. There are three types of hydro power plants. Pump storage power plants, hydro power plants with a reservoir but without pumping capacities and run of river hydro power plants. Pump storage power plants are defined by $\mathbf{U_{st}}$. The storing of electricity, L^{day}, is scheduled at the day-market but rescheduling can take place leading to an up-regulation, L^{+}, or down-regulation, L^{-}, of the storing. Storage power plants can also provide reserve capacities by a potential decrease or increase of the storing. A potential increase of storing stands for negative spinning reserve, $R^{sp,stor,-}$. The total storing plus the reserve can not exceed the total storing capacity, $c^{inst,load}$.

$$L^{day}_{u,t} + L^{+}_{s,u,t} - L^{-}_{s,u,t} + R^{sp,stor,-}_{u,t} \leqq c^{inst,load}_u \qquad \forall s \in \mathbf{S}, u \in \mathbf{U_{st}}, t \in \mathbf{T} \tag{3.18}$$

Positive spinning reserve, $R^{sp,stor,+}$, can be provided by a potential decrease of storing. The provision of positive spinning reserve respectively a decrease of storing is only possible to the extent storing is in process.

$$R^{sp,stor,+}_{u,t} \leqq L^{day}_{u,t} + L^{+}_{s,u,t} - L^{-}_{s,u,t} \qquad \forall s \in \mathbf{S}, u \in \mathbf{U_{st}}, t \in \mathbf{T} \tag{3.19}$$

The storage content, $F^{storage}$, is subject to the following equation. The content is increased by pumping and decreased by generation under consideration of the losses l^{loss}. The storage content at the beginning is thereby set to the value resulting from the previous optimization.

$$F^{storage}_{s,u,t} - F^{storage}_{s,u,t-1} = (1 - l^{loss}_{u}) \cdot (L^{day}_{u,t} + L^{+}_{s,u,t} - L^{-}_{s,u,t}) - (P^{day}_{u,t} + P^{+}_{s,u,t} - P^{-}_{s,u,t}) \tag{3.20}$$
$$\forall s \in \mathbf{S}, u \in \mathbf{U_{st}}, t \in \mathbf{T}$$

Further restrictions, not shown here, assure that the storage level respects the capacity of the storage reservoir and that there is a margin for the potential use of negative or positive reserve.

Hydro power plants with large natural reservoirs but without pumping capacity ($\mathbf{U_{rs}}$) are refilled by natural inflows, i^{res}. Their power generation and reservoir content are related by Equation (3.21).

$$F^{reservoir}_{s,a,t} - F^{reservoir}_{s,a,t-1} = i^{res}_{a,t} - V^{spill}_{s,a,t} - \sum_{u \in (\mathbf{U_a} \cap \mathbf{U_{rs}})} P^{day}_{u,t} + P^{+}_{s,u,t} - P^{-}_{s,u,t} \tag{3.21}$$
$$\forall s \in \mathbf{S}, a \in \mathbf{A}, t \in \mathbf{T}$$

The variable V^{spill} gives the possibility to spill water without producing electricity. The reservoir content $F^{reservoir}$ is also restricted by a maximal fill level and a minimal fill level (not shown here). The power generation of run of river hydro power plants can not be scheduled. It is directly considered in Equation (3.2).

Reserves

Different kind of reserve capacities have to be kept in the system. Primary and secondary reserves in positive and negative direction are considered by Equations (3.22) and (3.23). The reserve requirements are defined per region and the reserves can only be provided by power plants that are capable of it, defined by the unit set $\mathbf{U_{sp}}$, and that are located in the region, defined by the unit set $\mathbf{U_r}$. An equal distribution of the reserve capacities over all regions can so be considered, see Section 2.2.2. ; It was shown in Section 2.2.2 that these reserve types can normally be provided by the same power plant types. The positive primary and secondary reserve requirements, $d^{prim,+}$ and $d^{sec,+}$, are thereby summed up. The same applies to the negative primary and secondary reserve, $d^{prim,-}$ and $d^{sec,-}$. The positive and

negative reserve capacities are denoted by $R^{sp,+}$ and $R^{sp,-}$. Pump storage plants, defined by $\mathbf{U_{st}}$, can also provide reserves by changing the storing process. The potential decrease of storing represents positive spinning reserve, $R^{sp,stor,+}$, and the potential increase represents negative spinning reserve, $R^{sp,stor,-}$.

$$\sum_{u \in (\mathbf{U_r} \cap \mathbf{U_{sp}})} R_{u,t}^{sp,+} + \sum_{u \in (\mathbf{U_r} \cap \mathbf{U_{sp}} \cap \mathbf{U_{st}})} R_{u,t}^{sp,stor,+} \geqq d_r^{prim,+} + d_r^{sec,+} \qquad \forall t \in \mathbf{T}, \forall r \in \mathbf{R} \tag{3.22}$$

$$\sum_{u \in (\mathbf{U_r} \cap \mathbf{U_{sp}})} R_{u,t}^{sp,-} + \sum_{u \in (\mathbf{U_r} \cap \mathbf{U_{sp}} \cap \mathbf{U_{st}})} R_{u,t}^{sp,stor,-} \geqq d_r^{prim,-} + d_r^{sec,-} \qquad \forall t \in \mathbf{T}, \forall r \in \mathbf{R} \tag{3.23}$$

The reserve capacities do not depend on the forecast scenarios s as they are only scheduled at the day-ahead market. In the following intraday optimizations they are fixed to the day-ahead schedule and changes are not possible. Thus, it is taken into account that primary and secondary reserves are normally tendered in constant shares for a longer period in the future.

Tertiary reserves can be provided both by fast activating off-line plants such as gas turbines and by spinning power plants. In general, the use of off-line plants will be preferred as there are no direct costs involved. Nevertheless, capacities that are normally used for primary and secondary reserves can also provide tertiary reserves. The sum of primary and secondary reserve capacities, $R^{sp,+}$, and off-line tertiary reserve capacities, $R^{ter,+}$, must therefore cover the sum of primary, $d^{prim,+}$, secondary, $d^{sec,+}$, and tertiary, $d^{ter,+}$, reserve requirements according to Equation (3.24). Off-line tertiary reserve capacities can only be provided by appropriate power plants like gas turbines or hydro plants, defined by $\mathbf{U_{tr}}$. The power plants must also be located in the right region, so belonging to $\mathbf{U_r}$, but it is possible to exchange tertiary reserves between the German regions by T^{res}. Negative tertiary reserves are not considered in the model.

$$\sum_{u \in (\mathbf{U_r} \cap \mathbf{U_{sp}})} R_{u,t}^{sp,+} + \sum_{u \in (\mathbf{U_r} \cap \mathbf{U_{tr}})} R_{s,u,t}^{ter,+} + \sum_{u \in (\mathbf{U_r} \cap \mathbf{U_{sp}} \cap \mathbf{U_{st}})} R_{u,t}^{sp,stor,+} + \sum_{r* | (r*,r \in \mathbf{X})} T_{s,r*,r,t}^{res} \geqq d_r^{prim,+} + d_r^{sec,+} + d_r^{ter,+} \qquad \forall s \in \mathbf{S}, r \in \mathbf{R}, t \in \mathbf{T} \tag{3.24}$$

The reserve requirements are calculated in the second part of the following section.

3.2. Specific model parameters

Next to the model formulation, the analysis is determined by the model input. The derivation of important input parameters is presented in the following. The

power plant assumptions are explained in the first section after a short description of the model regions. Price assumptions are also given. The second section explains the calculation of reserve requirements. For the primary and secondary reserve, a literature based approach is chosen. For the tertiary reserve, a probabilistic calculation model considering the load and wind forecast quality and the power plant outages is developed. A grid reduction model is presented in the third section in order to consider the transmission constraints in Germany. Transmission parameters between the European countries are given at the end.

3.2.1. Model regions, demands, capacities and other parameters

The following model regions are defined by their electricity demands and the installed power plants. Technical parameters of the plants are then indicated and fuel and CO_2 price are assumptions are then given.

Model regions

The analysis focuses on the power system and the wind power in Germany. The consideration of cross-border exchanges is important in this context. International trading activities in Europe are increasing. The influence of wind power and hydro-dominated systems as Switzerland, Austria or the Scandinavian countries is also important with regard to wind power integration. All neighbouring states of Germany as well as Norway, Finland, Sweden and Italy are therefore modelled. Figure 3.2-a shows the considered countries.

Germany is represented in more detail as transmission grid constraints can only be captured by a higher spatial resolution. Ideally, each transmission grid node is represented by a model "region" giving a full representation of the grid. However, next to the computational burden, difficult data issues would arise as supply and demand data is needed for each node. Moreover, not only the transmission grid but also distribution grids would have to be considered at such a high spatial resolution. For these reasons, Germany is divided into 12 subregions according to the German Federal Lands. Small lands as Berlin or Hamburg are allocated to their neighbouring lands. Additionally, there are two offshore areas in the Nordic and Baltic Sea. Figure 3.2-b shows the resulting German regions.

The German and non-German regions are modelled with a different level of detail. In all countries the power operation and international power exchanges are calculated once a day for the following day according to the European day-ahead markets. In the German regions, uncertainty due to wind forecast errors is considered in the model and intraday rescheduling takes place every three hours. In the non-German countries, forecast errors are not considered and perfect wind power forecasts are applied in the optimizations. A CHP heat demand is also not considered in these countries.

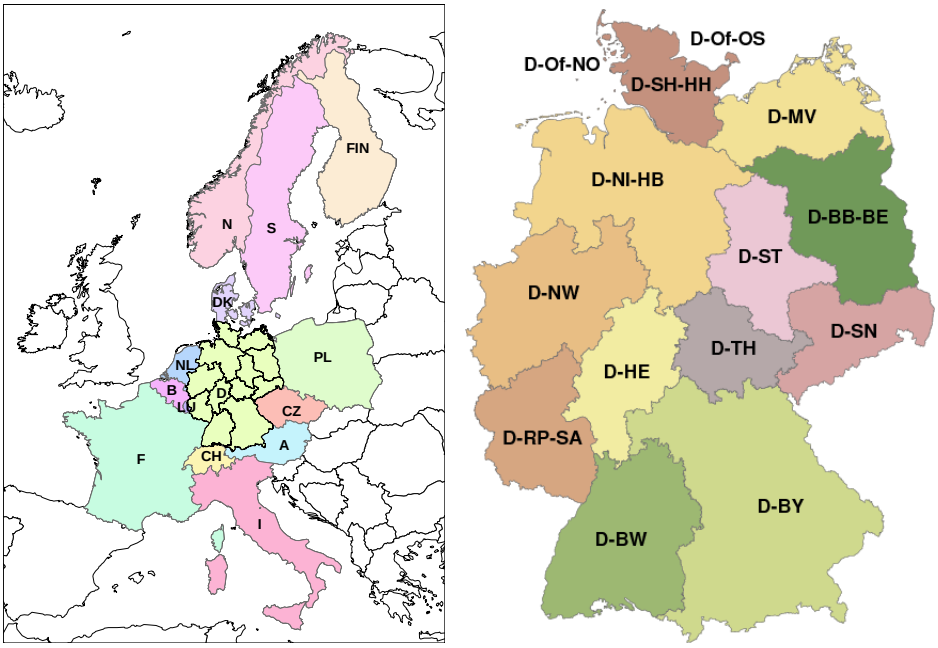

(a) European countries (b) German regions

Figure 3.2.: Model regions

Demand

The yearly electricity demands in 2020 are shown in Figure 3.3. They are based on the demand growth rates of the UCTE system adequacy forecast and they stand for the net consumption including network losses [96, 97]. The hourly load profiles from 2006 are applied in the model [98]. As the UCTE system adequacy forecast is also applied to estimate the installed capacities, see below, the assumptions for demand and installed capacities are coherent. The regional demand distribution in Germany is taken as it was in 2005 neglecting uneven growth rates [99]. Figure 3.3-a shows the large differences in electricity consumption between the different regions. High consumption levels can be seen in Bayern, Baden-Württemberg and Nordrhein-Westphalen, the most populous land. The northern and eastern regions have lower consumption levels. For the non-UCTE countries in the model (Scandinavian countries), the demands and capacities are modelled based on the baseline scenario in the European energy trends [100].

For Germany, the CHP heat demand is required. In the model, this demand is covered by CHP plants or by standardized heat plants as explained in Section 3.1.2. There are 19 German heat areas, one for each land and one for Frankfurt, München and Köln. The CHP demand is estimated based on the CHP heat production in 2006 according to the AGFW report [101]. An increase of 16% of CHP heat production is assumed until 2020 as suggested by the baseline scenario in the European energy trends [100].

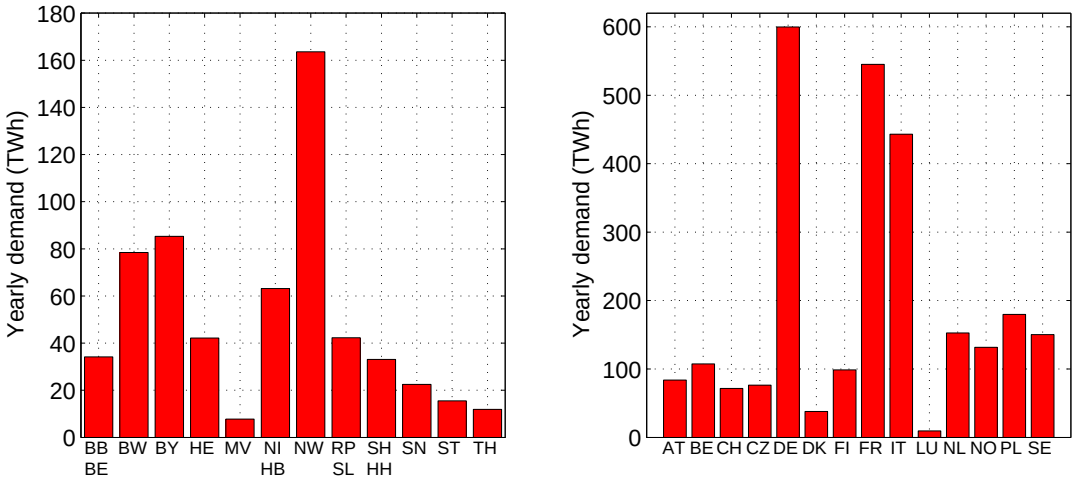

(a) German regions (b) European countries

Figure 3.3.: Net electricity demand (2020)

Installed capacities

The installed capacities are shown in Figure 3.4. They are according to the best estimate scenario in the UCTE system adequacy forecast. The scenario takes into account future power plants that are likely to be commissioned until 2020 [97]. The report states that these capacities are sufficient to maintain generation system adequacy in 2020 for the assumed demand growth rates. For the non-UCTE countries, the capacities are modelled according to the baseline scenario in the European energy trends [100]. The future wind power capacities are analysed in detail in Chapter 4.[4]

The power plant portfolio of each country has its own characteristics. Finland shows a well diversified portfolio whereas the Scandinavian countries Norway and Sweden as well as the Alpine countries Switzerland and Austria are hydro dominated. Switzerland and Sweden also rely on important shares of nuclear power. France is a prominent example for a nuclear dominated supply that is also supported by large amounts of hydro capacities. Italy, another country near to the Alps, also benefits from hydro power. The systems in Germany, Poland and the Czech Republic are characterized by coal and lignite power. In Belgium and especially in the Netherlands gas power plants play an important role. The highest shares of wind power can be seen in Germany and Denmark. Important amounts of wind power in absolute terms are also expected in France and Italy.

The installed capacities in the German regions are modelled based on internal

[4]More wind and photovoltaic capacities are modelled than the UCTE system adequacy forecast suggests. This has only a marginal influence on the generation system adequacy as the capacity value of wind power is limited, especially in the case of wind power capacities that are added to an already well developed wind power portfolio (see for example [102] by the author). The same applies to photovoltaic with its relatively low capacity factors in the winter.

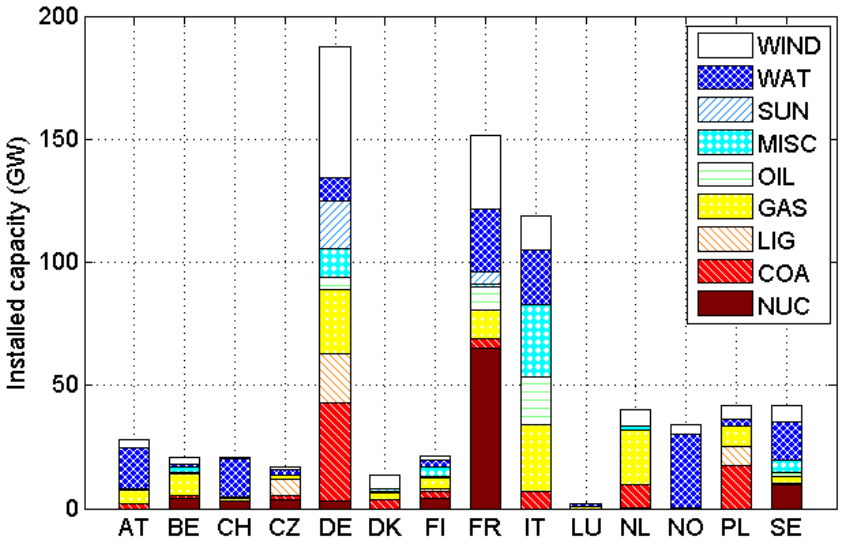

Figure 3.4.: Installed capacities (2020)

databases of the IER[5]. The lifetimes of existing power plants as well as future power plants and their locations are considered in order to derive the conventional capacities in 2020. The calculated portfolio corresponds well to the UCTE figures. The differences in the case of coal, lignite and gas are below 2%. The derived oil power capacity is 11% lower than in the UCTE forecast. In consistence with the UCTE forecast, a nuclear phase-out is assumed and only two nuclear power plants, Neckarwestheim 2 and Brokdorf, are operating. The wind power capacities are according to Section 4.1.2. The photovoltaic capacities are assumed to 19 GW (corresponding to the average of two studies from 2009 [35, 103]). The geographical distribution of the PV and other renewable energy capacities is based on different sources [104, 105].

Figure 3.5 shows the resulting capacities for the German regions. The North Sea offshore wind capacities are here added to Niedersachsen (NI) and the Baltic ones to Mecklenburg-Vorpommern (MV). The number of installed capacities strongly differs between the regions, especially due to the concentration of wind power in the North. The black bars show the capacities that would result from a hypothetical capacity distribution according to the yearly electricity demand of each region (keeping the same total capacity for Germany). This illustrates the discrepancy between the Northern wind power concentration, for example in Niedersachen (NI), and load centres like Bayern (BY) or Nordrhein-Westphalen (NW) in South and Middle Germany. It is however important to note that the load factor of the conventional capacities is in general higher than the one of wind power. The discrepancy between generation and load is therefore attenuated to some extent.

[5]Institut für Energiewirtschaft und Rationelle Energieanwendung (IER), Universität Stuttgart

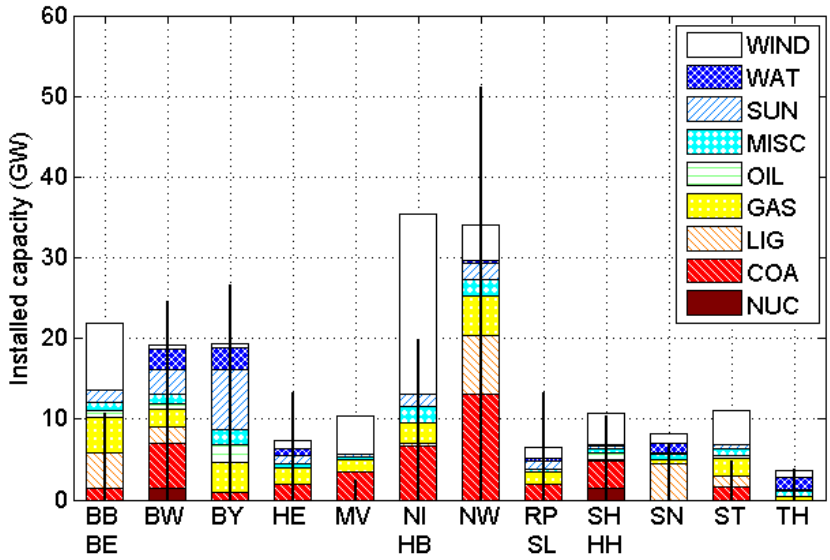

Figure 3.5.: Installed capacities in German regions (2020)

Apart from wind power, significant "excess" capacities can also be seen in Brandenburg (BB), Mecklenburg-Vorpommern and Sachsen-Anhalt (ST). Hydro-power is mainly located in the South which may be disadvantageous in terms of balancing the wind power input.

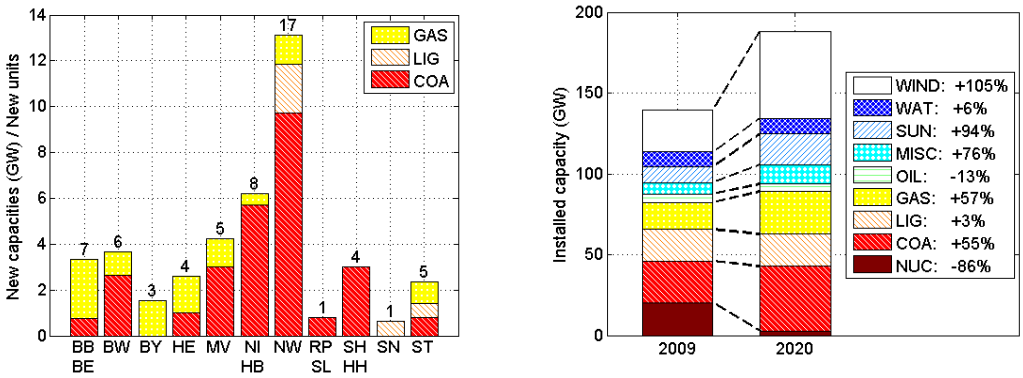

(a) Planned conventional capacities

(b) Portfolio change

Figure 3.6.: Development of installed capacities in Germany

The conventional capacities that are expected to be built between 2010 and 2020 and their locations are given in Figure 3.6-a. They sum up to 41.5 GW. Coal power plants account for 27.5 GW, so two third. 10.7 GW of new gas power plants are built and 3.3 GW lignite plants. Most of the capacities are planned in Nordrhein-Westphalen, but large amounts of new coal capacities are also assumed in the Northern regions Niedersachen, Schleswig-Holstein and Mecklenburg-Vorpommern. New lignite power plants are only given in three regions. Most of the gas power capacities are added in the Southern regions (Bayern, Baden-

Württemberg and Hessen) and in Brandenburg. The numbers on top of the bars in Figure 3.6-a give the number of added units in each region.

Figure 3.6-b shows the change between the German portfolio in 2009, [96], and the portfolio that is projected for 2020. As mentioned above, the portfolio for 2020 takes the new capacities and the ageing of the old ones into account. In total, the installed capacity significantly rises, above all due to wind power. High growth rates are also given for the renewable sources photovoltaic and biomass ("Misc"), whereas hydro power stays relatively constant. A slight increase of the conventional capacities can be seen, but by far not in the order of the 41.5 GW of new built capacities. Most of them only replace the capacity that is disconnected due to ageing or the nuclear phase out. Both coal and gas power thereby show a growth rate of about 50%.

Power plant parameters

In the model, operation constraints due to start-up times, minimum operation and minimum shutdown times are considered. Minimum load levels and part load efficiency as well as start-up fuel usage and start-up costs are also considered. The corresponding parameters are given in Table 3.2. They are reference values that are used in case that no other values are stored in the database. All parameters are derived from the analysis in Section 2.2.1. The values are based on the most suitable literature indications keeping a consistent relation between the different power plant types. In the start-up costs, it is considered that 20% of the costs are already represented by the start-up fuel usage and part-load efficiencies, see Table 2.8. The start-up costs are given in relative terms, so related to the unit size. Gas turbines that are typically smaller than steam power plants therefore have relatively high start-up costs. The sensitivity of the model results to the flexibility assumptions is tested by an flexibility scenario in Chapter 5, also with regard to future power plant designs that may be more suitable for cycling [106].

Table 3.2.: Flexibility parameters of thermal power plants

	Coal	**Lignite**	**Gas**[a]	**CC**	**Turb.**	**Nuc.**
Start-up fuel (MWh/MW)	2.5	2.5	1.2	0.8	0.1	6.5
Start-up[b] costs (€/MW)	25	20	15	50	50	10
Start-up time (h)	5	5	3	2	0	7
Minimum up-time (h)	4	6	4	4	1	1
Minimum down-time (h)	3	6	2	2	1	1
Minimum load factor (%)	40	40	34	33	20	50[c]
Efficiency loss	6	5	5	10	20	6

[a] Steam
[b] excluding start-up fuel and part-load efficiency costs
[c] PWR (Konvoi, Vorkonvoi)

The efficiencies of the existing and future power plants are based on IER databases. The efficiency range of for the future conventional power plants is given in Table 3.3. Coal power plants reach efficiencies of 50% and the future efficiency

Table 3.3.: Efficiency range for new power plants

Coal	0.45 - 0.5
Lignite	0.43 - 0.44
Gas (CC)	0.56 - 0.61

of combined cycle power plants can even exceed 60%.

Fuel and C02 prices

The applied fuel prices are given in Table 3.4. The CO_2 price is assumed to 22.4 €/t. The price assumptions are taken from the baseline scenario in the European energy trends for 2020 [100]. As the fuel prices are free-border prices, transport costs as suggested by Swider, [107], are added to calculate the free-plant prices. The lignite and nuclear fuel prices are also taken from latter source. For biomass, an average humidity rate of 35% with a heat value of 3 kWh/kg is assummed [108]. In 2007, a typical price for wood chips with such a humidity rate was 70€/t, [109], leading to 23 €/MWh as a biomass price. No transport costs are considered for nuclear, lignite and biomass and their prices are assumed to stay constant until 2020. The model parameters that are related to reserve

Table 3.4.: Fuel price assumptions for 2020 (€/MWh)

Fuel type	**Price at border**	**Transport costs**	**Price at plant**
Oil	31.17	0.82	31.99
Gas	23.47	2.02	25.49
Coal	7.50	1.41	8.91
Lignite	-	-	3.77
Nuclear	-	-	1.75
Biomass	-	-	23.00

requirements and transmission are presented in the following two sections.

3.2.2. Calculation of reserve requirements

Generation reserves are required to prevent imbalances in the system as explained in Section 2.2.2. Reserves are considered in the model according to Section 3.1.3.

The reserve requirements are thereby an exogenous input. In the following, the reserve requirements are assessed for 2020. Primary, secondary and tertiary reserves are used in the UCTE system. The primary and secondary reserve requirements are assessed based on UCTE guidelines and literature sources. The tertiary reserve is calculated by a probabilistic model approach.

Primary and secondary reserves

Primary and secondary reserve requirements are derived for the negative and positive direction. The derivation is mainly based on the TSO guidelines in the UCTE and Nordel zone.

Primary reserves The required amount of primary reserves is defined to 3000 MW in the UCTE region which is related to the largest generation units with capacities of about 1500 MW [62, Policy 1]. The outage of two large units at the same time can thus be covered. For each control area, the respective shares of primary reserve are given by multiplying the reserve for the entire zone by the contribution coefficient of the control area. The contribution coefficient of each control area is based on its electricity generation. The contribution coefficients of all areas sum up to one.

$$\text{coefficient} = \frac{\text{electricity generation in area}}{\text{total electricity generation}} \tag{3.25}$$

The coefficients are calculated by the electricity generation of the UCTE countries in 2007 [110]. This leads to 2292 MW of primary reserves for the model regions that belong to the UCTE (all model regions except Finland, Norway, Sweden and a part of Denmark). The total amount of primary reserve in the UCTE is likely to stay the same in the future as it is related to the largest power units. An increase of primary reserve with increasing wind shares is not expected. The wind power fluctuations in the time frame of the primary reserve are considered as negligible [54, 41].

Hence, assuming a constant relation between the generation in the model regions and in the other UCTE regions, the value of 2292 MW can be taken unchanged for the year 2020. A run of the market model with preliminary reserve levels leads to the electricity generation and contribution coefficients for the year 2020. The primary reserve requirements in the Scandinavian countries are defined by the organisation for the Nordic transmission system operators Nordel [111]. Primary reserve is there differentiated between frequency controlled normal operation reserve and frequency controlled disturbance reserve. Their sum corresponds to the primary reserve in the UCTE region [112]. The primary reserve requirements in the Nordel countries are higher than in the UCTE ones as the Nordel zone is relatively small and secondary reserves are not used there.

The resulting primary reserve requirements for the year 2020 are stated in Table 3.5. Primary reserve is activated in the case of frequency deviations in negative

Table 3.5.: Positive and negative primary reserve requirements (MW)

Region	Primary reserve	Region	Primary reserve
D-BB-BE	66	**A**	66
D-BW	62	**B**	87
D-BY	31	**CH**	71
D-HE	14	**CZ**	96
D-MV	37	**DK**	128
D-NI-HB	109	**FIN**	394
D-NW	204	**F**	635
D-RP-SL	18	**I**	390
D-SH-HH	50	**LU**	1
D-SN	47	**NL**	100
D-ST	29	**N**	550
D-TH	3	**PL**	149
D total	669	**S**	625

and positive direction. The maximal frequency deviation that is permitted is equal in negative and positive direction. The same amounts of negative and positive primary reserve are therefore required.[6]

Secondary reserves No strict methodology is defined by the UCTE operation handbook to size the amount of secondary reserves. An approximate assessment of *a part of* the secondary reserves is given by the following equation [62, Policy 1].

$$\text{Secondary reserve margin}_{(\text{maximal value - operation point})} = \sqrt{a \cdot L_{max} + b^2} - b \quad (3.26)$$

L_{max} stands for the maximal expected demand. 10 MW and 150 MW are indicated for the parameters a and b. The equation does not calculate the required secondary reserve as it is sometimes stated. It refers to the margin that should be kept between the activated reserves and the available capacity. It therefore indicates when the activated secondary reserve should be replaced by tertiary reserves [113, Appendix 1][44].

The secondary reserve requirements for Germany assuming one German control area are calculated by Haubrich [44]. Under the assumption of the historical (high) security level, the positive secondary reserve requirements amount to 1794 MW. This is 2.4 times more than the 750 MW that are calculated by Equation (3.26) based on the maximal German load level in 2007. This relation is used to assess the future secondary reserve requirements in Germany and in the other model regions. First, secondary reserve margins are calculated applying the demand profiles of 2020 according to Equation (3.26). Then, the secondary reserves are calculated by multiplying with 2.4. An important increase of secondary reserve due to additional wind power capacities is thereby not considered. The stochastic fluctuations of

[6] In the Nordel zone, only frequency controlled normal operation reserve reacts to positive frequency deviations.

wind power in the time domain below 1/4 h are considered negligible compared to the permanent oscillation of the load [54, 49]. A calculation for the Irish power system for example shows that, even with an installed wind capacity of more than 40% of the peak load, the primary and secondary reserve requirements do not increase [41].

Table 3.6.: Secondary reserves requirements (MW)

Region	Secondary reserve		Region	Secondary reserve	
	pos	neg		pos	neg
D-BB-BE	115	95	**A**	596	494
D-BW	263	218	**B**	677	562
D-BY	286	238	**CH**	539	447
D-HE	142	117	**CZ**	563	467
D-MV	26	22	**DK**	238	197
D-NI-HB	212	176	**FIN**	0	0
D-NW	549	456	**F**	2044	1695
D-RP-SL	142	118	**I**	1732	1437
D-SH-HH	111	92	**LU**	104	86
D-SN	76	63	**NL**	891	739
D-ST	52	43	**N**	0	0
D-TH	40	33	**PL**	996	826
D total	2014	1670	**S**	0	0

Table 3.6 shows the resulting secondary reserves. The negative secondary reserve requirements are assessed according to the relation of negative and positive reserves given by Haubrich (1794 MW to 1488 MW).[7] In Germany, the secondary reserve is first calculated for the country and it is then divided between the model regions according to their peak demands. The lack of secondary reserves in the Nordel model regions is compensated by more primary and tertiary reserves.

Tertiary reserves

A probabilistic approach is applied to derive the tertiary reserve requirements in 2020. The different importance of the input parameters is shown by a sensitivity analysis.

Probabilistic approach combined with optimization The UCTE operation handbook does not give a methodology to size the amount of tertiary reserves [62]. In the literature, probabilistic approaches are normally applied to assess the tertiary reserves for a given security level. The probability of unplanned power plant outages, the forecast errors of load and the forecast errors of wind power are combined to calculate the possible unbalances that have to be covered by tertiary

[7] This relation of 0.83 corresponds well to the reserve capacities currently contracted on the German reserve market. In 2008, the average relation between negative and positive secondary reserves was thereby equal to 0.8 [61].

reserves. The probability function of the possible unbalances is derived by a convolution of the single probability functions. The single probability functions are thereby assumed to be independent.

In the Dena study, [39], the effects of wind power on tertiary and replacement reserves are thus calculated. A later version of the applied model also considers load oscillations and secondary reserves [45]. A similar methodology is used in an expert opinion by Haubrich, [44], and in related papers [50, 53]. A calculation of reserve requirements under consideration of the UCTE requirements is given by [49]. A slightly modified approach based on monte-carlo simulation is proposed in [43]. A mixture of Markov chains and probabilistic methods is proposed in [114]. In [41], the reserve level in each hour is related to the reliability of the system over the year. Reserve levels for the Irish system are then calculated. Methods with a more non-probabilistic focus are also possible. Reserve levels and their costs can for example be calculated by means of a stochastic programming market clearing model [115].

Here, a probabilistic model that combines a probabilistic approach and an optimization is developed.[8] It allows to calculate the reserve requirements according to the wind power capacities, the wind and load forecast error and the power plant portfolio. The calculation is based on the plant outage probabilities and the standard deviation of load and wind power forecasts. All uncertainties are assumed to be independent from another.

First, the discrete probability function of the total capacity loss is derived in an iterative process. The probability function of the sum of two random variables is equal to the convolution of the probability functions of the random variables. Hence, in the first step of the calculation the outage probability function of two power plants are convoluted. The resulting probability function is then convoluted with the outage probability function of the third power plant. The last steps leads to the probability function P_{out} of the capacity loss C_l (see Appendix A for a fast calculation code). $P_{out}(C_l = c_i)$ gives the probability that c_i of the total capacity fails. The capacity margin C_m gives the difference between the reserve R and C_l. The probability function of the capacity margin is given by P_{margin} according to Equation (3.27). Loss of load occurs in case of a negative capacity margin.

$$P_{margin}(C_m = R - c_i) = P_{out}(C_l = c_i) \tag{3.27}$$

Secondly, the probability function of the forecast error is derived. The forecast errors of the load forecast and wind power forecast are assumed to be independent and normally distributed in order to apply an analytical approach. The standard deviation of the total forecast error, σ_{err}, is directly calculated by the standard

[8] The approach is similar to the one in [41]. The main difference is given by the here applied probability function of the total capacity loss. Several simultaneous outages are thus considered and in addition the model formulation is clearer.

deviations of the load and wind forecast errors, σ_{load} and σ_{wind}.

$$\sigma_{err} = \sqrt{\sigma_{load}^2 + \sigma_{wind}^2} \tag{3.28}$$

The probability function of the normally distributed forecast errors is therefore $N(0, \sigma_{err})$ assuming a mean value of zero. The cumulative probability function is noted as $F(x \mid N_{0,\sigma_{err}})$.

Thirdly, the probability distributions of the capacity margin and the forecast errors are combined to calculate the expected loss of load time in a year. For each capacity margin level, the loss of load probability is equal to the probability of having a larger forecast error than the considered capacity margin level. The sum over all capacity margin levels weighted by their probabilities gives the total loss of load probability. Multiplying the loss of load probability by 8760 hours leads to the yearly loss of load expectation measured in hours according to Equation (3.29).

$$LOLE = 8760\,h \cdot \sum_i (1 - F(c_i \mid N_{0,\sigma_{err}})) \cdot P_{margin}(C_m = c_i) \tag{3.29}$$

Equation (3.29) leads to the loss of load expectation for a given reserve level (the reserve level is thereby contained in P_{margin}). The reserve level for a given (reference) loss of load expectation, $LOLE_{ref}$, is found by an optimization. A minimization of $(LOLE - LOLE_{ref})^2$ with $LOLE$ according to Equation (3.29) gives the corresponding reserve level. The approach was implemented in Matlab using the optimization function "fminsearch". On a standard computer, calculation times are in the order of seconds.

The calculated reserve refers to the sum of secondary and tertiary reserve as both secondary and tertiary reserve capacities are able to balance related uncertainties.[9] Only the sum of the two reserve types (here called total reserve) is therefore given by the presented calculation approach. The tertiary reserve is equal to the difference between the total reserve and the secondary reserve (see also [44]). The secondary reserve level is additionally determined by requirements in the shorter time domain that are not considered here.

Application and results The following data is required for the calculation approach: the capacities of the power plants with the corresponding outage probabilities, the standard deviations of the wind and load forecast errors and a reliability target level. Table 3.7 shows the data for the power plants. The power plant capacities are derived from the power plant portfolio in 2020, see Section 3.2.1. The capacities are broken down to single units by means of typical average power plant sizes. The numbers of yearly unplanned and non-relocatable outages are based on the analysis in Section 2.2.2 and division by 8760 leads to the outage probabilities.

[9] The primary reserve being regulated by the UCTE is independent of this reserve consideration.

The standard deviation of the load forecast error is set to 1.2% of the yearly peak

Table 3.7.: Power plant data for reserve calculation

Type	Unit size (MW)	Outage probability	Outages
Coal	450	0.091%	8
Lignite	600	0.103%	9
Gas/Oil	100	0.034%	3
Gas/Oil (cc)	350	0.137%	12
Gas/Oil (turbine)	50	0.040%	3.5
Nuclear	1000	0.034%	3
Hydro power	50	0.046%	4

load, see Section 2.2.2. The standard deviation of the wind forecast errors is set to 3% of the installed capacity referring to a short-term intraday wind power forecast, see Figure 4.5 in Section 4.1.2. An intraday wind power forecast is applied as the market model reschedules the power plant operation every three hours. The wind forecast errors related to longer forecast horizons are therefore balanced by rescheduling. As a matter of fact, tertiary reserve markets with an intraday clearing are already in place, for example in the Eastern US states [116]. The sensitivity of the calculation to the parameters is tested below.

Table 3.8 shows the resulting total reserves (sum of secondary and tertiary reserve) and tertiary reserves. The German reserve is distributed between the regions according to their peak loads.[10]. In total, about 8.5 GW of secondary and

Table 3.8.: Tertiary reserves requirements in 2020 (MW)

Model region	Sec. + tert. reserve	Tertiary resreve	Model region	Sec. + tert. reserve	Tertiary resreve
D-BB-BE	479	364	**A**	1119	524
D-BW	1099	836	**B**	1579	902
D-BY	1196	909	**CH**	1337	798
D-HE	591	449	**CZ**	1551	987
D-MV	109	83	**DK**	1087	849
D-NI-HB	886	673	**FIN**	1542	1542
D-NW	2293	1744	**F**	6359	4315
D-RP-SL	593	451	**I**	4294	2562
D-SH-HH	463	352	**LU**	399	296
D-SN	315	240	**NL**	1852	961
D-ST	217	165	**N**	1297	1297
D-TH	167	127	**PL**	2050	1054
D total	8408	6394	**S**	2047	2047

tertiary reserves is required in Germany. More than 6 GW of them can be provided by tertiary reserve. Tertiary reserves are technically less demanding and normally preferred to secondary reserves. The tertiary reserve requirement is about twice as high as the average level of 3 GW in 2008 [61]. This increase is due to the additional wind power and due to a partial replacement of secondary reserves by

[10]In the model, tertiary reserves can be transferred between the German regions

tertiary reserves.[11] The impact of wind is also shown in the following sensitivity analysis.

Sensitivity analysis There are four input parameters that determine the reserve requirements (standard deviation of the load and wind forecast, the outage probabilities of the power plants and the reliability target). Figure 3.7 shows the sensitivity to each input (only one input is changed in each case). The input parameters are varied between 0% and 200%. The reserves are highly influenced by the quality of the wind and load forecasts. The sensitivity is higher for the wind forecasts as the related standard deviation, $3\% \cdot 56$ GW $= 1.68$ GW, is larger and therefore more important than the standard deviation of the load forecast, $1.2\% \cdot 95$ GW $= 1.14$ GW. An improvement of the wind forecast quality by 50% decreases the reserve by about 25%, whereas it decreases only by about 12.5% in the case of load forecasts.

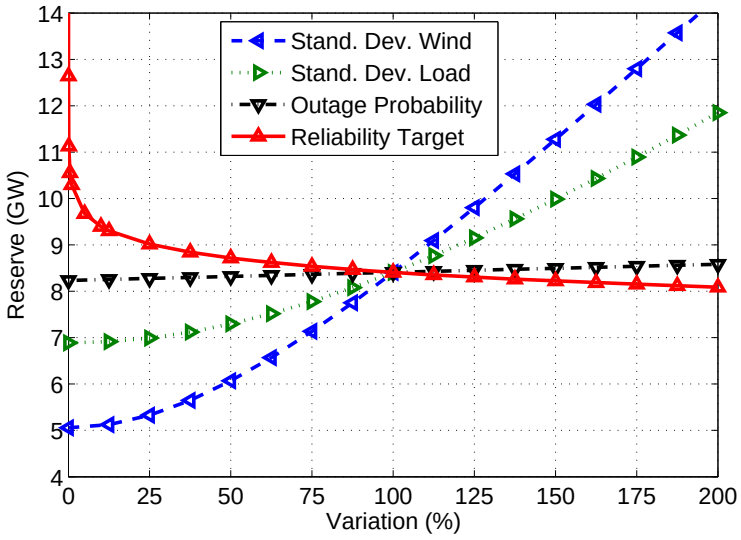

Figure 3.7.: Sensitivity of reserve calculation

The outage probabilities have a remarkably low impact on the reserve requirement. The reserve increases only slightly with higher outage probabilities. This is due to the high influence of the load and wind forecast. Assuming an outage probability of 0.1% and 120 GW of installed capacities, 120 MW of capacity experience an outage in average. The wind forecast error, having a standard deviation of 1.68 GW, is higher than 1.12 GW in fifty percent of the time. The sensitivity is therefore much more accentuated in the case of wind and load forecasts.[12] With

[11] The secondary reserve levels in 2008 apply to a separated consideration of the German control areas leading to higher reserve requirements. They are considered to be too high for Germany and to be partially replaceable by tertiary reserve [117, 44].

[12] The low sensitivity of the reserve to the outage probabilities also justifies that the calculation approach considers the installed capacities and not the actually operating capacities as it would

outage probabilities of zero, the reserve requirement is only due to the wind and load forecast errors. The reliability target has a moderate impact on the reserve requirements. With very high reliability targets (a loss of load expectation near to zero), the reserve requirements start to rise to the infinite.

3.2.3. Modelling of transmission restrictions

The transmission between the German model regions is modelled by a DC load flow approach according to Section 3.1.3. The regions are thereby connected by "hypothetical" lines. The transmission parameters of these lines are found by the following approach that is applied to the German transmission grid. The transmission parameters at the country borders are presented at the end of the section.

Grid reduction approach

The process of the reduction approach leading to the parameters of the "hypothetical" connections (in other words, the reduced grid) are shown in Figure 3.8. The reduction is based on the entire German transmission grid. The load flows for the entire grid are calculated by a DC load flow approach combined with a minimization of the system costs. The installed plant capacities and typical load and wind situations are thereby considered. The resulting generation levels are aggregated to get the balance of each region. In the next step, the parameters for the reduced grid are found. The load flow calculation with the reduced grid should lead to the same results as with the entire grid. The balances of each region are therefore used as targets in the optimization that calculates the transmission parameters of the reduced grid. Finally, the reduced grid is evaluated by an optimization of the reduced power system, minimizing the system costs, and comparing the results with the ones of the initial optimization with all nodes.

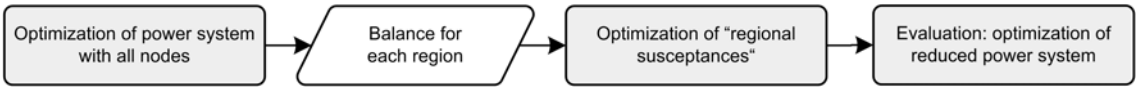

Figure 3.8.: Reduction of transmission grid

Optimization of the power system The representation of transmission constraints by a DC load flow approach allows a linear optimization. The total generation costs are minimized according to Equation (3.30). The costs are given by the cost factor c and generation P of each power plant fleet k at each node n. The installed capacity, Cap, must not be exceeded. In the case of wind power, Cap stands for the wind power capacity that is available with the assumed wind situation. The load L of each node has to be balanced. The transmission between

be more accurate.

two nodes n_i and n_j is defined by their voltage angles, δ_{n_i} and δ_{n_j}. The angle difference multiplied by the susceptance of the connecting branch, B_{n_i,n_j}, is equal to the transmitted power. The transmission is constraint by the thermal transmission capacity, $Transcap_{n_i,n_j}$ and the maximally allowed angle difference, δ_{max}. The voltage angle at an arbitrary reference node is set to zero.

$$
\begin{aligned}
\min \quad & \sum_{k,n} c_{k,n} P_{k,n} \\
\text{s.t.} \quad & \sum_{k} P_{k,n_j} + \sum_{n_i} B_{n_i,n_j}(\delta_{n_i} - \delta_{n_j}) = L_{n_j} && \forall\, n_j \\
& \delta_{n_i} - \delta_{n_j} \leqq \delta_{max} && \forall\, n_i, n_j \\
& B_{n_i,n_j}(\delta_{n_i} - \delta_{n_j}) \leqq Transcap_{n_i,n_j} && \forall\, n_i, n_j \\
& P_{k,n} \leqq Cap_{k,n} && \forall\, k, n \\
& \delta_{n_1} = 0
\end{aligned}
\tag{3.30}
$$

The generation of each region, P_r, is given by aggregating the calculated nodal generation levels. The aggregated load of each region is denoted by L_r and the generation/load balance of each region is equal to $P_r - L_r$. As the optimization is run for several load/wind situations, there is a set of regional balances, $P_{r,s} - L_{r,s}$. The regional balances are denoted by $R_{r,s}$ and they are applied as reference values in the following optimization.

Grid reduction / Optimization of "regional susceptances" In the reduced grid, there is only one branch between each (neighbouring) region pair. For these hypothetical branches, susceptances are found that can be applied in the DC load flow equations of the market model. They are derived by a non linear optimization according to Equation (3.31). Two aspects are considered by the optimization. On the one hand, the regional susceptances B_{r_j,r_i} should be small (restricting) in order to represent the higher restrictivity of the entire grid. On the other hand, the reduced grid should allow all power transmissions that are also possible in the original grid. The first point is given by a minimization of the regional susceptances. The second point is reflected by the first constraint that assures that the regional susceptances allow the same regional balances as given by the original grid. The balances in the original grid, $R_{r,s}$, are calculated for typical and extreme load/wind situations (Equation (3.30)). The wind/load situation is represented by s. Each region (or rather the node that represents the region in the reduced grid) has a voltage angle, $\delta_{r_i,s}$. One arbitrary angle is thereby set to zero. The angle difference can not exceed the maximally allowed angle difference, δ_{max}. In addition, the thermal transmission capacities between the regions, $Transcap_{r_i,r_j}$, that are given by the sum of the crossing lines, have to be respected. In the optimization, the susceptances and the angles are the free variables. The susceptances stay the same in all situations s. The regional voltage angles are unique for each

load/wind situation. The product of regions and situations therefore gives the total number of angles. The angles are free variables that are not used any longer once the optimization has solved. Only the susceptances are regarded as result.

$$
\begin{aligned}
\min \quad & \sum_{r_i,r_j} B_{r_i,r_j} \\
\text{s.t.} \quad & \sum_{r_j} B_{r_i,r_j}(\delta_{r_i,s} - \delta_{r_j,s}) = R_{r_i,s} && \forall\, r_i, s \\
& \delta_{r_i,s} - \delta_{r_j,s} \leqq \delta_{max} && \forall\, r_i, r_j, s \\
& B_{r_i,r_j}(\delta_{r_i,s} - \delta_{r_j,s}) \leqq Transcap_{r_i,r_j} && \forall\, r_i, r_j, s \\
& \delta_{r_1,s} = 0 && \forall\, s \\
& B_{r_i,r_j} = B_{r_j,r_i} && \forall\, r_i, r_j \\
& B_{r_i,r_j} \geqq 0 && \forall\, r_i, r_j
\end{aligned}
\tag{3.31}
$$

In the first instance, the maximally allowed angle difference, δ_{max}, is set equal to the one applied in the entire grid. It may be that this angle difference is too small and the problem is infeasible. No regional susceptances are then found that allow the same regional balances as in the entire grid. In this case, the maximally allowed angle difference is slightly increased and the optimization is restarted. Once the maximal angle difference is large enough, the optimization is feasible and the regional susceptances are found. They are then applied in the market model in combination with the related maximal angle difference.

It is important that the considered load/wind situations give a good representation of all possible transmissions that can occur. Theoretically, the consideration of all possible situations would be optimal. This is not possible due to solvability, calculation time and, being a nonlinear optimization, quality of results. As a first approach, it is sufficient to consider typical situations and the situations with the most extreme transmissions. Considered extreme situations are for example the peak load hour or the peak wind hour. The typical situations are derived by a cluster analysis.

Evaluation Until now, only minimal regional susceptances are found that allow transmissions equal to the ones in the complete grid for different load/wind situations. It still has to be backtested if, after an optimization of the power system with the reduced grid, the results are similar to the ones with the complete grid. The optimization problem according to Equation (3.30) is therefore applied once again, simply replacing the nodes n by regional nodes r. The regional thermal transmission capacities, $Transcap_{r_i,r_j}$ are calculated by aggregating the capacities of the lines connecting the regions. The resulting balances can then be compared to the ones in the original grid.

Table 3.9.: Planned grid developments in Germany

Connection	Region 1	Region 2	TSO	Circuits / Voltage
Hamburg - Dollern	D-SH-HH	D-NI-HB	Eon	2*380kV
Diele - Niederrhein	D-NI-HB	D-NW	Eon / RWE	2*380kV
Wahle - Mecklar	D-NI-HB	D-HE	Eon	2*380kV
Altenfeld - Redwitz	D-TH	D-BY	Eon	2*380kV
Dauersberg - Hünfelden	D-RP-SA	D-HE	RWE	2*380kV
Rommerskirchen - Weißenturm	D-NW	D-RP-SA	RWE	1*380kV
Krümmel - Görries	D-SH-HH	D-MV	Vattenfall	2*380kV
Lauchstädt - Vieselbach	D-ST	D-TH	Vattenfall	2*380kV

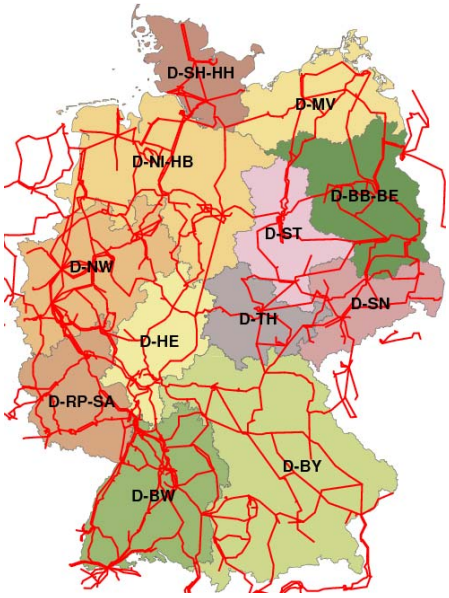

Figure 3.9.: Transmission grid

Application to German transmission grid

The German transmission grid was recorded in a Geographical Information System (GIS) based on the map published by the German association of the electricity network operators (former VDN, now BDEW)according to Figure 2.6, see [118]. The map shows the 380 kV, 220 kV and some of the 110 kV lines and their number of circuits is given. The transformer stations are also shown. Next to the existing lines, the interregional grid developments of Table 3.9 were added to the system. These lines are expected to be realised until 2020 according to the transmission system operators. The grid developments refer to new constructions and to upgrading of circuits to higher voltage levels or adding additional circuits to existing lines. At the beginning of 2009 all lines in Table 3.9 were in the process of regional impact assessment procedure ("Raumordnungsverfahren") or project approval procedure ("Planfeststellungsverfahren") or under construction. The resulting grid is shown in Figure 3.9.

Table 3.10 shows the transmission capacities and the reactances that were ap-

Table 3.10.: Transmission line parameters

	Capacity (MVA)	Reactance (Ohm/km)
380 kV	1400	0.28
220 kV	400	0.3
110 kV	100	0.42

plied. The susceptances are equal to the reciprocal values of the reactances (as resistances are here zero). The parameters are based on the analysis in Section 2.2.3 assuming thin conductors (single conductors for 110 kV circuits, two-conductor bundles for 220 kV and three-conductor bundles for 380 kV circuits) in order to follow a conservative approach. A conservative approach is also important as N-1 security is not considered here. The transformer stations are described by a reactance of 0.0003 per unit to an MVA base of 1, see [119]. A maximally allowed voltage angle difference of 40° is applied [1].

The DC load flow problem of Equation (3.30) is then solved. The load and capacity values of the market model (Section 3.2.1) are thereby applied. These values are only related to the regions. In order to estimate the values at the nodes, the loads and capacities of each region are equally distributed over the nodes that are in the region and that are equipped with a transformer station and a 220 kV or 380 kV connection. The offshore capacities in the North Sea and Baltic Sea, possibly equipped with HVDC transmission systems, are directly allocated to the connecting transformer stations at the coasts [120]. 9500 MW of the 14000 MW in the North Sea are located in the zones "Borkum" and "Borkum II". They are connected to the transmission grid in Niedersachsen. 4500 MW are located in the zones "Helgoland" and "Sylt" that are connected in Schleswig-Holstein. The 2300 MW in the Baltic Sea are mainly connected to stations in Mecklenburg-Vorpommern, except of 150 MW that are connected to Schleswig-Holstein.

Reduced German transmission grid The reduced transmission grid is calculated by the optimization in Equation (3.31). The following extreme situations are considered: the hour with the peak load, the hours with the lowest and highest wind power generation and the hour for that the wind power share related to the load is maximal.[13] In addition to these four hours, six typical load/wind situations are derived by a cluster analysis.[14] All ten situations are considered in the reduction and the susceptances of the reduced grid are derived. The thermal transmission capacities between the regions are given by summing up the capacities of the connecting lines. The resulting susceptances and capacities are shown

[13]The hour with a minimal wind power share related to the load is considered as it is equal to the hour with the lowest wind power generation.

[14]A kmeans clustering is applied. The squared Euclidean distances to the cluster centroids are thereby minimized. For the clustering process, the PV and run-of-river production is subtracted from the load.

Table 3.11.: Susceptances (and transmission capacities) for Germany (GW)

Susceptance (Capacity)	BB-BE	BW	BY	HE	MV	NI-HB	NW	RP-SL	SH-HH	SN	ST	TH
BB-BE	-	-	-	-	1.35 (14.4)	-	-	-	-	1.06 (8.4)	1.06 (11.2)	-
BW	-	-	1.48 (6.2)	1.69 (7.4)	-	-	-	2.55 (6)	-	-	-	-
BY	-	1.48 (6.2)	-	5.29 (11.4)	-	-	-	-	-	-	-	1.33 (5.6)
HE	-	1.69 (7.4)	5.29 (11.4)	-	-	2.54 (4.4)	1.09 (4.2)	1.05 (9.6)	-	-	-	1.2 (2.8)
MV	1.35 (14.4)	-	-	-	-	-	-	-	1.44 (2.8)	-	0.43 (0.8)	-
NI-HB	-	-	-	2.54 (4.4)	-	-	7.11 (23.8)	-	3.19 (11.6)	-	1.42 (2.8)	-
NW	-	-	-	1.09 (4.2)	-	7.11 (23.8)	-	1.79 (16)	-	-	-	-
RP-SL	-	2.55 (6)	-	1.05 (9.6)	-	-	1.79 (16)	-	-	-	-	-
SH-HH	-	-	-	-	1.44 (2.8)	3.19 (11.6)	-	-	-	-	-	-
SN	1.06 (8.4)	-	-	-	-	-	-	-	-	-	0.45 (0.8)	1.91 (6.4)
ST	1.06 (11.2)	-	-	-	0.43 (0.8)	1.42 (2.8)	-	-	-	0.45 (0.8)	-	1.33 (3.6)
TH	-	-	1.33 (5.6)	1.2 (2.8)	-	-	-	-	-	1.91 (6.4)	1.33 (3.6)	-

in Table 3.11. The direction of the exchange has no influence on the parameters and the table is symmetrical. The angle difference that is maximally allowed between the "regional nodes", δ_{max}, also derives from the reduction approach and it is equal to 90°.

Evaluation In the following, the reduced grid is evaluated. The operational costs of the power systems are therefore calculated by the DC load flow approach (Equation 3.30), both for the original grid and the reduced grid. The regional generation and the operational system costs are then compared. In addition, the reduction is compared to a zonal representation of the grid that applies thermal transmission capacities only. This means that the thermal transmission capacities in Table 3.11 are the only limiting factor for the transmission (no DC load flow is considered). The complete grid is denoted by "Reference", the reduced grid by "Zonal DC" and the representation of the reduced grid by thermal transmission capacities only is denoted by "Zonal Thermal". The reduction approach is only useful if it leads to better results than the more straightforward "Zonal Thermal" approach.

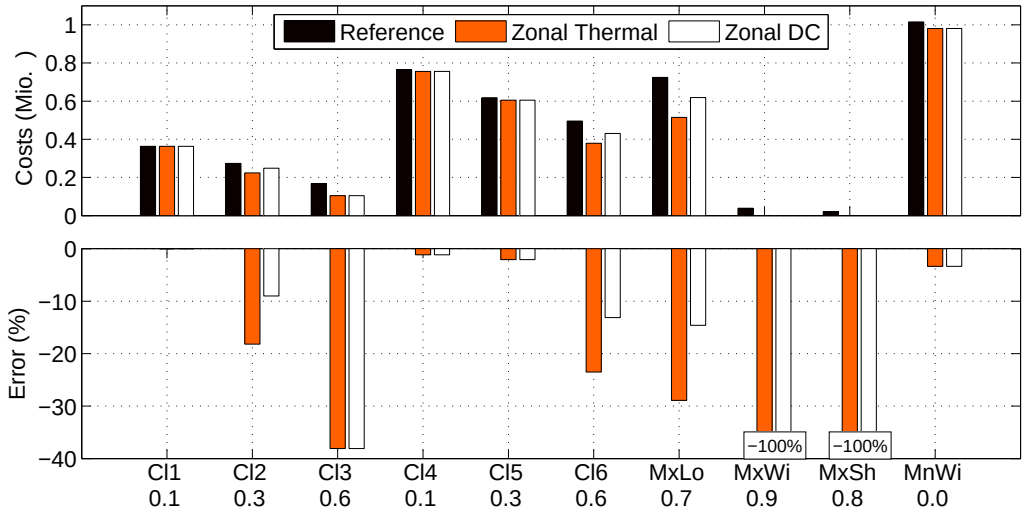

Figure 3.10.: Differences of system costs with nodal and zonal grid representation

The most comprehensive figure to compare the cases are the total system costs that are given in Figure 3.10 for each load/wind situation (the six clusters, “Cl1” to “Cl6”, and the four extreme situations). The number below the situation labels indicate the wind power generation related to the installed capacity. The “Zonal Thermal” and the “Zonal DC” grid representation are always less restrictive than the complete grid and the system costs are therefore lower. The differences are more important for high wind situations. In these cases, transmission issues are more relevant due to the concentration of wind power in the North. Looking at high wind situations, the differences are more important if they occur in low load hours. For example, the wind generation is similar in “Cl3” and “CL6” but the load is lower in “Cl3” (as identified by the lower system costs) and the differences are higher for “Cl3”. With the maximal wind generation or wind share (“MxWi” and “MxSh”), all of the German load can be covered by wind and other renewables in the reduced grids. In the case of the original grid, conventional power plants have to be used due to transmission restrictions.

In all cases, a “Zonal DC” representation always performs as well as or better than a “Zonal Thermal” one. The relative error can be reduced by more than a half in some situations (“CL3”,“MxWi” and “MxSh”). A reduction of the error in these situations is a good result, as the system costs are high in these hours and a large relative error leads to large absolute deviations of the costs. For example, a 100% error at the maximal wind hour (“MxWi”) may seem critical, but in absolute terms the deviation is relatively low. For low wind situations, the different grid representations lead to very similar results and the errors are generally low.

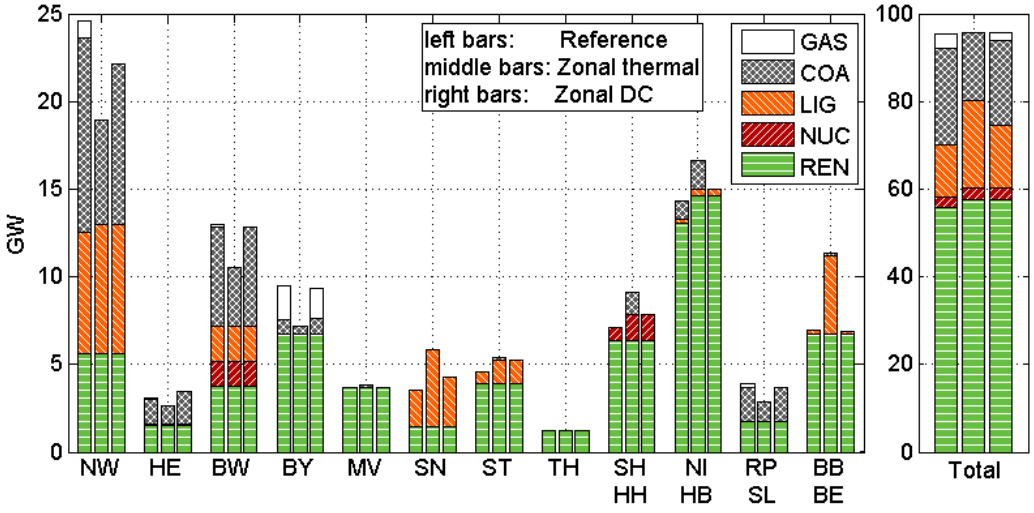

Figure 3.11.: Generation levels at maximal load with nodal and zonal grid representation

The deviations between the three cases are explained in more detail by Figure 3.11 for the maximal load situation. The less restricting “Zonal Thermal”

representation of the grid allows the model to use cheap lignite capacities in Sachsen-Anhalt and Brandenburg. In the two other cases, this is not possible due to the load flows in the grid. In Niedersachsen, the transmission restrictions of the original grid lead to a reduced generation as the maximal export level is reached. In the two other cases, more power can be generated. The "Zonal DC" case is thereby closer to the reference case than the "Zonal Thermal" one. In general, "Zonal DC" gives a much better representation of the generation levels than "Zonal Thermal". This is also shown by the total German generation levels. Only in the "Zonal Thermal" case enough transmission capacities are free to use a large amount of lignite capacities in addition to the renewable energy capacities. As a consequence, no expensive gas capacities and less hard coal capacities are needed and the system costs are underestimated.

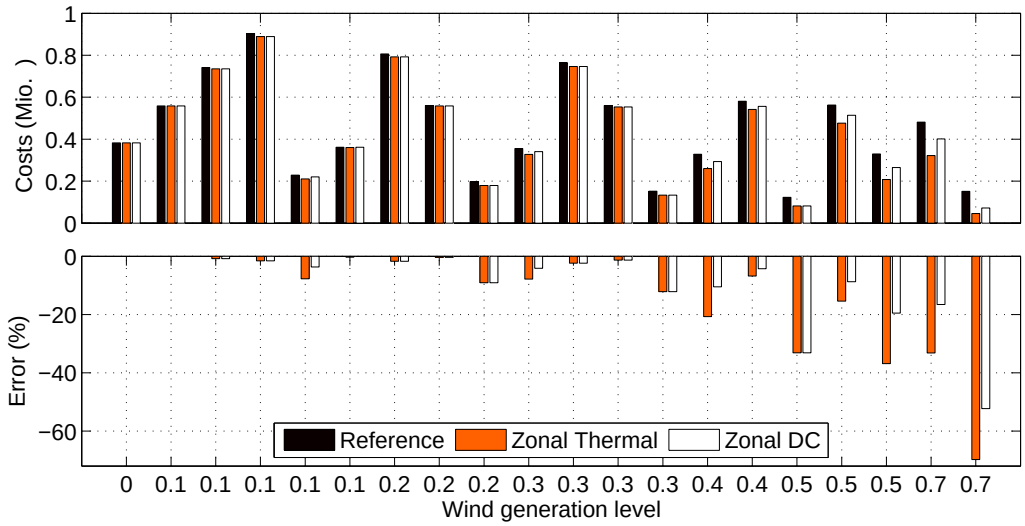

Figure 3.12.: Differences of system costs with nodal and zonal grid representation for 20 clusters

Until now, the reduction was only evaluated for the load situations that were used in the reduction approach. It rests to verify if the reduction is also useful in other situations. A cluster analysis with 20 clusters is therefore applied in order to test more typical load flow situations (next to the extreme situations that were already evaluated above). The total system costs are given in Figure 3.12. The 20 clusters are thereby denoted by the related wind generation level. The total system costs are underestimated if reduced grids are applied. As stated above, the underestimation error increases with higher wind generation levels and, for similar levels, the relative errors are high if the absolute system costs are low. In all cases, the reduction approach ("Zonal DC") leads to better results than applying thermal transmission capacities only ("Zonal Thermal"). For many clusters, the error is significantly reduced by the "Zonal DC" grid representation, in some cases by nearly 50%.

Each cluster represents a number of hours. The costs for each cluster multiplied by the number of hours gives an estimation of the yearly costs. In the reference case, the yearly costs amount to 4388 million €. In the reduced grid without a load flow representation, the costs are underestimated by 5.5%. By considering the loadflow in the reduced grid ("Zonal DC"), the error is reduced by about one third and the total costs are only underestimated by 3.6%. The errors for one year are relatively low as there are many situations for that the grid has no influence on the costs. The costs are only significantly underestimated by the grid reductions in some hours. For these hours, the presented reduction approach leads to an improved representation.

Transmission at country borders

The transmission capacities for international exchanges are modelled according to the net transfer capacity values published by the ETSO (European Transmission System Operators) association. These values allow the market participants to assess the possibilities of international trade. The application of the values in the market model is here explained after a short definition of the values.

NTC values The net transfer capacities (NTC) are calculated in the following way, see [121]. The total transfer capacity between two countries is given by the transfer capacity that would be possible according to operational security standards if future network conditions, generation and load patterns were perfectly known in advance. Security standards include thereby N-1 security conditions. As the input data of the capacity calculations is subject to uncertainties, a security margin (transmission reliability margin) is subtracted from the total transfer capacity resulting in the net transfer capacities. In other words:

> The NTC values represent an ex-ante estimation of the seasonal transmission capacities of the joint interconnections on a border between neighbouring countries, assessed through security analyses based on the best estimation by TSOs of system and network conditions for the referred period. As numerical values, the NTCs constitute the maximum foreseen magnitudes of exchange programmes that can be operated between two areas respecting the N-1 security conditions of the involved areas, taking into account the uncertainties on the assumptions of NTC assessment [122].

In general, the NTV values only give indications for the transfer capacities as they depend on the load flow situation.

Application of NTC values The transfer capacities are based on the NTC values published for the peaking hours in winter 2008/2009 [123]. NTC values are published for peaking hours in winter and summer. The former are normally more

restrictive than the latter due to higher peaks. The winter values are here applied as a conservative approach. As Germany is divided into different regions, the NTC values between these regions and the neighbouring countries are required. Regional NTC values are calculated according to the thermal transmission capacities that cross the region borders. The same linear approach was applied to approximate the total NTC value of Denmark being one region in the model but being divided in East and West Denmark in the ETSO reports. The resulting transfer capacities for the German borders are given in Table 3.12 for the export and import direction.

Table 3.12.: German border transfer capacities (MW)

from\to (to\from)	A	CH	CZ	DK	F	LU	NL	PL	S
D-BB-BE	-	-	-	-	-	-	-	283 (260)	-
D-BW	616 (555)	1500 (3200)	-	-	1262 (1330)	-	-	-	-
D-BY	1384 (1245)	-	425 (1194)	-	-	-	-	-	-
D-MV	-	-	-	252 (345)	-	-	-	-	-
D-NI-HB	-	-	-	-	-	-	1099 (856)	-	-
D-NW	-	-	-	-	-	-	3308 (2578)	-	-
D-RP-SL	-	-	-	-	1488 (1570)	980 (0)	-	-	-
D-SH-HH	-	-	-	1248 (1705)	-	-	-	-	600 (600)
D-SN	-	-	375 (1056)	-	-	-	-	917 (840)	-

Possible future developments of interconnections between the countries are published for the UTCE area, [71], and for the Nordel area, [124]. In general, the planned interconnections are still to be studied or have a mere idea status and their final commissioning is unknown. Moreover, it is difficult to assess the impacts of these grid developments on the NTC values. Not all developments are targeted on an increase of transmission capacity but for example also on N-1 security. As the analyses focuses on Germany, the NTC values are therefore assumed to stay unchanged apart from one exception. A 380 kV transmission line between Doetinchem and Niederrhein (situated in the Netherlands respectively Nordrhein-Westphalen) is in an advanced state of the planning process. It is expected to be commissioned in 2013 earliest. This line is considered in Table 3.12 applying the above mentioned linear projection of the given NTC values.

4. Simulation of wind power generation and forecast errors

Wind power is a stochastic energy source. A stochastic generator is characterized by its fluctuating nature and the existence of uncertainties. The two aspects are not always combined. A power source that is fluctuating but well predictable is for example tidal power. A conventional power plant on the other hand can be scheduled but outages are a relevant risk due to the large plant capacities. In principle, all power sources are stochastic, so fluctuating and unpredictable, to some extent. The schedules of conventional power plants are for example influenced by external natural factors like the river temperature. Outages occur at power plants of all types. The differentiation between fluctuating and unpredictable is nevertheless useful for the purpose of analysis. The fluctuating characteristics of wind power are covered in the second section of the following chapter, the uncertainty characteristics in the third section. The first section gives an overview of the simulation approach, the data assumptions and simulation results. It is worthwhile to note that the developed concepts could also be applied to solar energy.

4.1. Concept and results of overall simulation

The output of the simulation is the wind power generation and the short-term wind power forecasts. The simulation, being based on wind speed data, allows to simulate different wind yields and to consider different forecast qualities. The advantages of using wind speed data are discussed in the first section, together with the simulation concept and the underlying wind speed data. In the second section, the data assumptions for the here scenarios are given and the simulation results are presented.

4.1.1. Overview and wind speed data

The simulation generates time series of wind power generation and related wind power forecast scenarios for each model region. The simulation is based on wind speed series. The simulation concept is pictured in Figure 4.1. For each model region several measured wind speed series are available. These series are transformed and aggregated to a power time series for the region. Before the transformation,

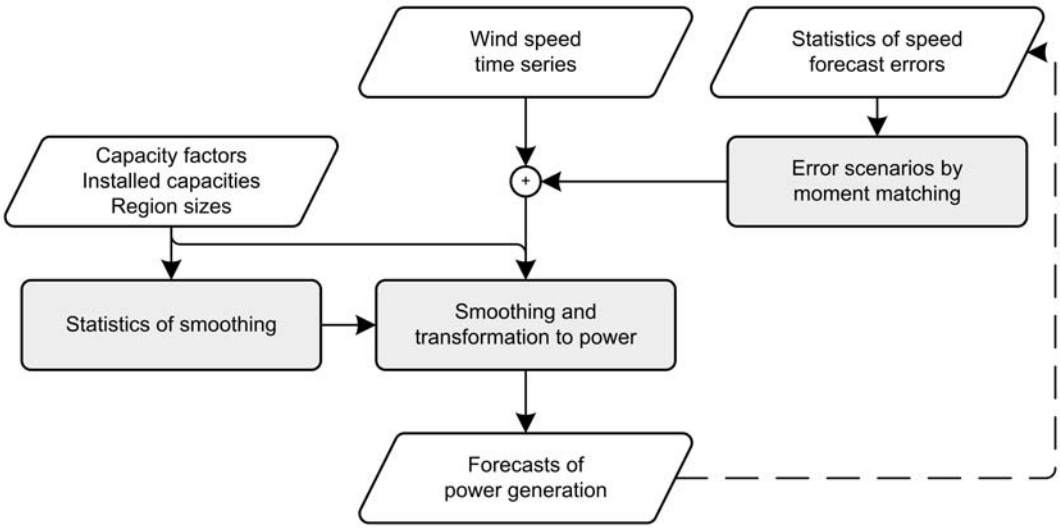

Figure 4.1.: Simulation of wind power generation and short-term forecasts

scenarios of forecast errors can be added to the wind speed series. The scenarios represent typical forecast errors for a forecast horizon of up to 36 hours.

The transformation of wind speed to power is according to the power curves of the wind turbines. The wind power generation at single locations is however more variable than the wind power generation of a complete region that is composed of many wind farms at different locations. A smoothing is therefore integrated in the transformation. The applied smoothing is adapted to typical statistics of variability reduction. These statistics are derived in a separated analysis and take into account the region size. The smoothing is done both by a smoothing of the wind speed series itself and by applying an adapted power curve. The transformation and smoothing also take into account the capacity factors (full load hours) that are achieved in the region. The analysis that leads to typical statistics of variability reduction is explained in Section 4.2.1. The smoothing technique itself is presented in Section 4.2.2.

Forecast errors are simulated and added to the wind speed series. The simulation is based on the statistical parameters of measured wind speed forecast errors. The calculated statistical parameters are mean values, standard deviations, skewness, kurtosis, autocorrelations and spatial correlations between forecast errors at different locations. Theses parameters are applied in a simulation technique that generates the forecast error scenarios. After transformation to power, the root mean square error (RMSE) of the resulting German power forecasts is calculated. This RMSE is compared to historic results of German wind power forecasts and the initial statistics are adapted in an iterative process in order to consider future forecast improvements. The analysis of measured forecast errors and the scenario generation approach are presented in Section 4.3.1 and Section 4.3.2.

An important general characteristic of the simulation is its foundation on wind

speeds. Even though the parameter of interest is wind power, it is advantageous to start from wind speeds for the following reasons:

- Different energy yields can be simulated. With power data, this is difficult as scaling cannot be applied (up-scaling of power time series can for example lead to generation values that exceed the actually installed capacity).
- Regional power generation can be simulated. Wind power time series are often not published for specific regions and down-scaling of higher-level power data (for example the published data for a TSO zone) distorts the variability characteristics, see Section 4.2.2.
- Offshore wind power can be simulated without measured offshore power data.
- The simulation of forecasts based on wind speeds is more "physical" and closer to the real forecasting process.
- Regional power forecasts can be simulated.

The simulation approach therefore corresponds to a bottom-up approach (using aggregated wind power data would correspond to a top-down approach).

Wind speed series measured by the German Weather Service (DWD) are applied. Their locations is given by the (red) circles in Figure 4.2. Additionally, Reanalysis data is applied. The locations of the Reanalysis speed series are given by the (grey) crosses. The Reanalysis data was verified and adjusted to an hourly resolution during the TradeWind project [125] and the resulting data was made available to the author. All speed series are from they year 2006 (corresponding to the demand profiles).

4.1.2. Wind scenario and results

The simulation is based on two types of data input. On the one hand, there are measured wind speed time series at different locations (given above). On the other hand, there are the characteristics of the wind power scenario that is simulates. This covers the installed capacity and average power generation in each region. The related assumptions are given first followed by the simulation results.

Wind scenario assumptions

The future installed wind capacities depend on numerous factors. The usable locations, their wind yield potential and the feed-in tariffs and other political subventions are for example important. In the case of offshore wind power, the availability of materials and construction boats may be a factor. New wind power parks and repowering of old ones has to be considered. Table 4.1 shows the projections of different studies for the future onshore and offshore respectively total wind

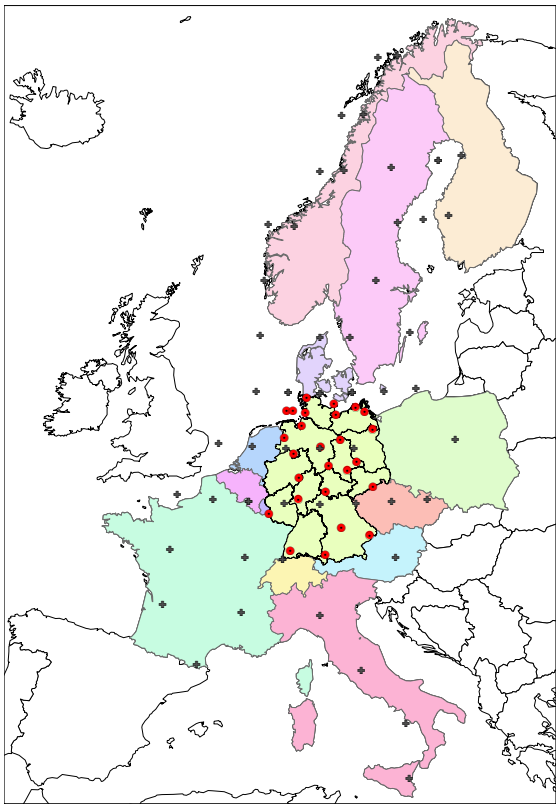

Figure 4.2.: Locations of wind speed series

power capacities in Germany. The DENA I study from 2005 estimates 48.2 GW in 2020 [39]. Scenarios made by the German Energy Agency (DENA) are also applied in the EU study Tradewind from 2007. Additional to the 48.2 GW, a high and low development scenario are there given with 14 GW less respectively 8 GW more [126]. An EU study from 2008 (European energy and transport trends, EETT) gives 32.4 GW of German wind capacities in 2020 [100]. The UCTE system adequacy outlook from 2009 assumes 45.3 GW in its best estimate scenario [97]. A forecast from 2009 by the German Federal Association for Renewable Energies (BEE) estimates 55 GW for 2020 [127]. The DENA II study assumes 56.3 GW for 2020.[1] Looking at all the projections, there is a range from 32.4 GW to 56.6 GW. In this work the assumptions at the upper end of the range (DENA II) are applied in order to analyse the system effects of the wind power generation. The regional distribution of the German capacity in 2020 according to DENA II is resumed in Table 4.2.[1]

Capacity factors are another important input factor for the simulation. The capacity factor multiplied by the 8760 gives the total full load hours. The capacity factors of the German wind power generation from 1999 to 2008 are shown in Figure 4.3. They are based on published figures of installed capacity and energy generation [128]. Two points are important. On the one hand, there are large

[1]Internal communication.

Table 4.1.: Study assumptions for wind power capacities in Germany in 2020 (GW)

	Onshore	**Offshore**	**Total**
DENA I	27.9	20.3	48.2
TRADEWIND Low	24.4	9.8	34.2
TRADEWIND High	32.0	24.6	56.6
UCTE[a]	-	-	45.3
EETT[a]	-	-	32.4
BEE	45.0	10.0	55.0
DENA II - 2020	37.0	16.3	53.3

[a]No specification of onshore/offshore capacities

Table 4.2.: Parameters for simulation of wind power in German regions

	Capacity (MW)	**Full load hours (h)**	**Region size (km^2)**
D-BB-BE	8278	1476	30371
D-BW	612	960	35752
D-BY	569	1204	70552
D-HE	958	1354	21115
D-MV	2571	1574	23180
D-NI-HB	8272	1627	48028
D-NW	4436	1515	34085
D-RP-SL	1382	1456	22422
D-SH-HH	3837	1777	16554
D-SN	1077	1495	18416
D-ST	4228	1730	20446
D-TH	757	1570	16172
D-Off-NO	14000	3200	20000
D-Off-OS	2300	3200	5000

annual variations. The future energy generation is therefore unknown even if all wind farms are known. On the other hand, there is no systematic decrease of the capacity factors, especially not over the last 10 years. This indicates that the energy yield of wind farms installed at a later date is not always inferior to the energy yield of wind farms installed at an earlier date. One reason is that the energy yield is not the only factor for the location choice and other characteristics as potential grid connection or suitable subsoil are also important. Another reason is that new wind power capacities are not only given by new wind farms but also by repowering. Repowering stands for the replacement of an older wind turbine by a more powerful and higher turbine at the same location. Repowering can therefore lead to higher capacity factors as wind speed increases with height. In the following, a capacity factor of 0.18 is chosen to represent a moderate German wind year. This corresponds to the average capacity factor of the last ten years. Earlier capacity factors are not considered as they are based on limited wind power capacities. A higher wind yield is considered by a high wind scenario in Chapter 5.

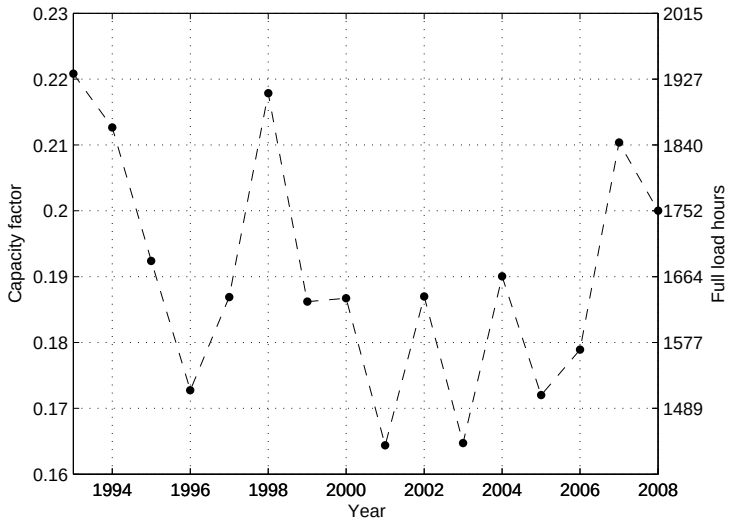

Figure 4.3.: Capacity factor of German wind power from 1993 to 2008

The capacity factors for the German regions are derived from their potential annual energy yields. The potential annual energy yields are published as the annual energy yields that would be achieved in an average wind year according to the IWET wind index [3]. The IWET wind index is a long term statistics monitoring the energy generation of wind farms since 1998 [129, 10]. It allows to rate a wind year compared to the long term average. The annual energy yields are here only used to derive the relation between the regional capacity factors. Their absolute values are adapted to the total German capacity factor of 0.18 applying the installed capacities. The resulting values are given in Table 4.2. There are large

differences between the German regions. The wind farms in Schleswig-Holstein for example generate nearly twice as much energy as the ones in Baden-Württemberg.

Measured data of offshore wind power generation was not available as the first German offshore parks have been installed only recently.[1] A map of the wind resources over open sea gives a range of average annual wind speeds from 8.5 to 10 m/s and a range of wind power densities from 650 to 1100 W/m^2 at a height of 100 m for the German offshore regions. These wind conditions corresponds to annual full load hours between 3000 and 4000 [10]. In the literature, more detailed assessments of the offshore wind power generation can be found. Accurate predictions of the offshore generation are however difficult due to the lack of climatologically representative measurements [130]. In one study speed measurements at an land mast at the Danish coast (3 km from the closest coastline) and at an offshore mast (9 km from the closest coastline) are used to derive the relation between a typical onshore and offshore wind power generation [131]. Three turbine types are applied and, in all cases, the offshore capacity factor is about twice as large as the onshore capacity factor. An estimation of wind power generation based on long-term measurements at a sea mast with an over-water fetch of 2 km from the closest coastline leads to 3200 full load hours [132]. For a proposed UK offshore wind power programme, offshore capacity factors of 38% (3330 full load hours) are assumed for the year 2020 as a conservative assumption [133]. Some results of European offshore parks indicate full load hours between 2000 and 3500 but near-cost offshore parks are thereby included [134]. Only one park in the list is more than 10 km from the coast line and 3000 full load hours are given for it. The planned German offshore parks are mostly 30 to 100 km from the coast line and their full load hours are therefore likely to be higher. A simulation program of wind power generation even leads to 4200 full load hours for the offshore wind park "alpha ventus" [135]. In the future, the potential of offshore wind power is for example further assessed by the "Offshore - Scientific measurement and evaluation program (Offshore-WMEP)" or by the EU project "Windspeed".[2] Here, a value of 3200 is assumed for the offshore wind power. Higher energy yields are considered by a high wind scenario in Chapter 5.

The simulation of the wind power forecasts in 2020 is based on a statistical analysis of measured forecast errors according to Section 4.3.2. The forecast quality will however improve until 2020. In the Dena study, [39], an improvement by 13% to 25% is for example applied. A related study states 10% improvement [136]. Rohrig estimates the potential at 35% to 40% [137]. Here, a more conservative improvement of 20% is assumed.

[1] The first German offshore wind park, "alpha ventus", was completed on 16nd November 2009 (http://www.alpha-ventus.de).

[2] see `http://offshorewmep.iset.uni-kassel.de` and `http://www.windspeed.eu`.

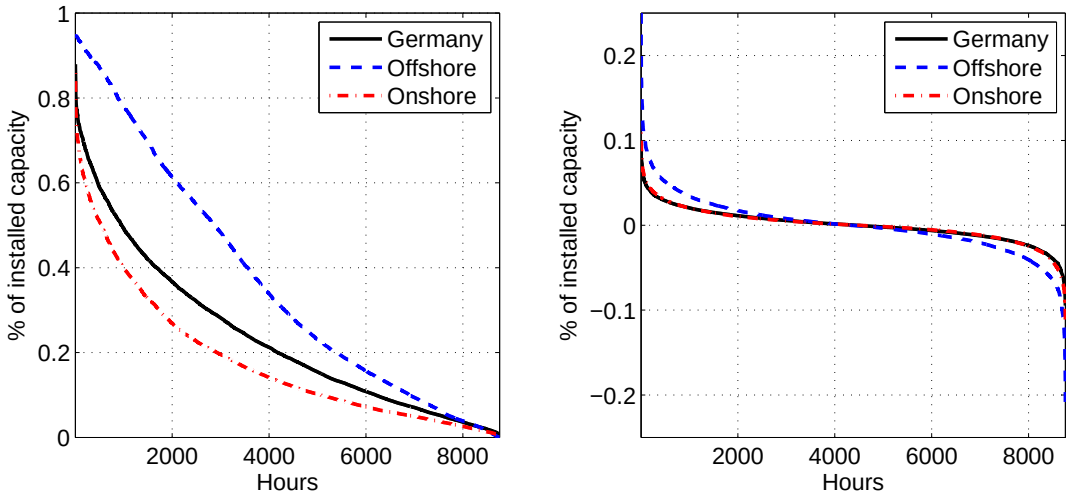

Figure 4.4.: Duration curves of simulated German wind power generation

Results

Wind power generation and wind power forecasts for the year 2020 are simulated. Figure 4.4-a shows the duration curves of the resulting German wind power generation. There are differences between the offshore and onshore generation. The highest generation levels in the offshore region are significantly above the onshore ones due to the steadier wind and the smaller region size. The offshore duration curve is closer to the bisecting line from top left to down right than in the onshore case. This shows that the variability of the offshore generation is higher. A duration curve that is equal to the bisecting line represents generators that use all generation levels equally often which corresponds to a higher variability.

The higher variability of the offshore wind power generation can also be seen by the duration curves of the one hour gradients in Figure 4.4-b. The offshore generation can change by 25% of the installed capacity in one hour. In the onshore case, the maximal changes do not exceed 12%. Interestingly, the jumps are quite similar for the onshore and the German case. This is due to the normalization by the installed capacity and a correlation between the onshore and offshore gradients that is below one (0.22). The maximal hourly change of the German power generation is about 9.5% (corresponding to 5.3 GW). With two-hour jumps, the maximal rise of power generation is about 17% whereas the maximal fall can be 18.5%. In the case of four-hour jumps, rises of up to 27% of the installed capacity can occur and falls of up to 33%.

The quality of the power forecasts are given in Figure 4.5 showing the root mean square error (RMSE). The RMSE in the offshore case can be higher than 10% of the installed capacity. This is due to the concentration of capacity in the offshore regions and their relatively small geographical size (balancing of forecast errors is

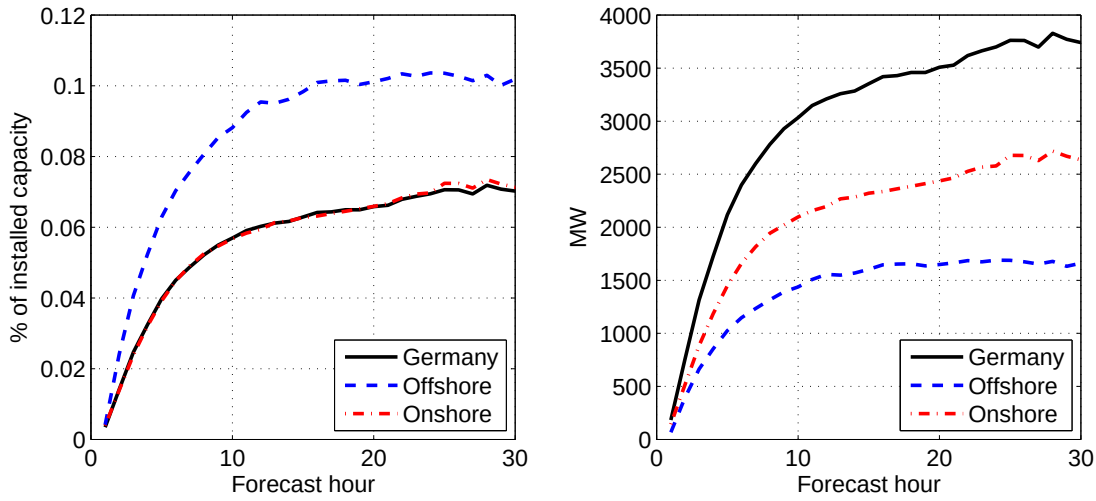

Figure 4.5.: RMSE of simulated German wind power forecasts

less important in smaller regions as weather patterns are similar and correlations higher). The RMSE of the German forecasts and the onshore forecasts are very similar. This is due to the normalization by the installed capacity. In absolute terms, the errors of the German forecasts are significantly higher than in the offshore or onshore case, as Figure 4.5-b shows. If the onshore and offshore forecast errors were perfectly correlated, a offshore RMSE of 1500 MW and a onshore RMSE of 2500 MW would lead to a German RMSE of 4000 MW.[3] If the errors were completely uncorrelated, the German RMSE would be about 3000 MW. Here, the correlation between onshore and offshore forecast errors is about 0.46 and the German RMSE is close to 3500 MW at forecast hour 20. The ratio between the German and onshore RMSE is therefore 1.4 which corresponds exactly to the ratio between the installed capacities (56.3 GW and 40 GW). This explains why the normalized RMSEs of the onshore and German forecasts are equal. The maximal error of the simulated German day-ahead forecasts is 36% of the installed capacity. This applies to an overestimation of the wind power generation. The maximal underestimation of the power generation by a day-ahead forecast goes up to 30% of the installed capacity. In the case of intraday forecasts, for example 4-hour forecasts, the maximal errors in positive and negative direction can be as high as 20% of the installed capacity.

[3] A mean error of zero is thereby assumed and the variance equation for a sum of random variables is applied: $Var(X+Y) = Var(X) + Var(Y) + 2 \cdot Cov(X,Y)$).

4.2. Simulation of wind power generation

The wind power generation is simulated based on measured wind speed series. However, a transformation of speed data at single locations to regional power generation may neglect changes of variability. Theses changes of variability, called smoothing, have to be considered additionally. In the first section, the smoothing effect is analyzed in general. Quantitative measures of the smoothing effect are derived. More precisely, the analysis leads to equations that allow calculating the smoothing effect in dependence of the region size and the generated energy.[4] These equations are applied in the simulation in the second section. The simulation is based on a smoothing of the wind speed time series and on the application of aggregated power curves. The related approaches are presented and the quality of the simulation is evaluated.

4.2.1. General statistics of regional wind power generation

Wind power generation and its fluctuations have been analyzed for specific regions and wind farms [138, 139, 140, 141, 99]. The smoothing effect was also described for the wind power generation of Europe [142, 143, 144]. A common statement is that power output of groups of wind farms is less fluctuating than that of single wind farms. The studies show that the smoothing effect, being due to only partially correlated wind power series, is more important with increasing region size and number of wind farms. It is for example known that the smoothing effect in an area has an upper limit. Additional wind farms will then no longer decrease the fluctuations [145]. But no general quantitative measures of the smoothing effect exist. This topic is here addressed by a general simulation of the smoothing effect. The following approach quantifies the smoothing effect and shows under which conditions the smoothing effect only depends on the region size. Smoothing is thereby evaluated by changes in the central moments of the time series and its gradients.

In the following wind power time series at single stations are considered as random variables. Their sum is equal to the regional wind power generation. The smoothing effect occurs as the power series are not perfectly correlated due to different wind speeds at the wind farms. A functional relation between correlations and distances is derived empirically. This allows calculating the correlations between simulated wind station locations that are distributed randomly in an idealized area shape. Knowing the correlations between all stations allows to deduce the standard deviation for the total wind power generation as the standard deviation of a sum of random variables can be calculated by means of their correlations. The same approach was used to examine standard deviations of wind forecast errors and has inspired the approach here [146, 22]. By extending the approach,

[4] For the first section, see also [90] by the author.

skewness and kurtosis of regional wind power generation can also be derived. For the calculation of the parameters typical values of standard deviations at single wind farms are needed in addition. Equations are therefore derived that allow to determine these standard deviations from the average wind power generation in the regarded region.

Hence, the below derived equations permit to calculate statistical parameters of regional wind power generation only having region sizes and the average generation (full load hours) as input data. The method is applied to hourly time series and to one-, two- and three-hour gradients of them. The equations are tested by data of German and Irish wind power generation. In the first section, the mathematical basis of the approach is explained. The equations themselves are derived in the subsequent section and a summary of the approach is given. In the last section, the equations are verified and their sensitivity is analyzed.

Mathematical basis

The second, third and fourth central moment of wind power generation in a certain region and over a certain time period can be connected to corresponding parameters of wind power generation at single wind farms. Generation is thereby always described relative, so as a percentage of the installed capacity. The regional generation in absolute terms, P^{abs}, is equal to the sum of the absolute generation at all single wind farms P_i^{abs} that are installed in the region. If all N wind farms have the same capacity C, the relative regional generation P is equal to the sum of the relative generation at all farms divided by N.

$$P = \frac{P^{abs}}{NC} = \frac{\sum_i^N P_i^{abs}}{NC} = \frac{\sum_i^N CP_i}{NC} = N^{-1} \sum_i P_i \tag{4.1}$$

The generation time series can be seen as correlated random variables. The correlations of single random variables lead to statistical parameters of their sum, so the regional generation. The variance of a sum of random variables is equal to the sum of their covariances or, more exactly, of all elements in the corresponding covariance matrix [147]. This relation and Equation (4.1) lead to Equation (4.2), where μ_2^P stands for the variance of regional generation.

$$\begin{aligned} \mu_2^P &= \frac{1}{N^2} \sum_i \sum_j E(P_i^c P_j^c) = \frac{1}{N^2} \sum_i \sum_j \frac{\sigma_i \sigma_j E(P_i^c P_j^c)}{\sigma_i \sigma_j} = \sigma^2 F_2 \\ \text{with } F_2 &= N^{-2} \sum_i \sum_j \frac{E(P_i^c P_j^c)}{\sigma_i \sigma_j} = N^{-2} \sum_i \sum_j Corr_{ij} \\ \text{and } P_i^c &= P_i - E(P_i) \quad \text{and } \sigma = \sigma_i = \sqrt{E((P_i^c)^2)} \end{aligned} \tag{4.2}$$

P_i^c refers to the centralized power generation at each single wind farm. It is calculated by subtracting the mean generation $E(P_i)$ from the generation. The correlation $Corr_{ij}$ between two time series is defined by $\frac{E(P_i^c P_j^c)}{\sigma_i \sigma_j}$. The standard deviation σ_i is assumed to be equal at each wind farm. This common standard deviation stands for a typical single wind farm standard deviation.[5] By considering standard deviations, F_2 is based on correlations instead of covariances. This is helpful for the empirical derivation of F_2 below that is based on the region size. Empirical fitting functions are also derived for σ starting from the average generation in the region. With F_2 and σ, the variance of regional power generation, μ_2^P, can then be calculated.

A similar approach is developed for the third and fourth central moment of regional generation, μ_3^P and μ_4^P. This results in Equation (4.3) that corresponds to Equation (4.2). The derivation is given in Appendix B. $Corr3_{ijk}$ and $Corr4_{ijkl}$ are thereby defined in a similar way as $Corr_{ij}$.

$$\mu_3^P = \frac{1}{N^3} \sum_i \sum_j \sum_k E(P_i^c P_j^c P_k^c) = \sigma_3^3 F_3$$

$$\mu_4^P = \frac{1}{N^4} \sum_i \sum_j \sum_k \sum_l E(P_i^c P_j^c P_k^c P_l^c) = \sigma_4^4 F_4 \tag{4.3}$$

$$\text{with } F_3 = N^{-3} \sum_i \sum_j \sum_k \frac{E(P_i^c P_j^c P_k^c)}{\sigma_{3i}\sigma_{3j}\sigma_{3k}} = N^{-3} \sum_i \sum_j \sum_k Corr3_{ijk}$$

$$\text{and } F_4 = N^{-4} \sum_i \sum_j \sum_k \sum_l \frac{E(P_i^c P_j^c P_k^c P_l^c)}{\sigma_{4i}\sigma_{4j}\sigma_{4k}\sigma_{4l}} = N^{-4} \sum_i \sum_j \sum_k \sum_l Corr4_{ijkl}$$

$$\text{and } \sigma_{3i} = \sqrt[3]{E(|P_i^c|^3)} \text{ and } \sigma_{4i} = \sqrt[4]{E((P_i^c)^4)}$$

σ_{3i} and σ_{4i} represent values that are similar to the standard deviation.[6] They are assumed to be equal at all wind farms representing typical single wind farm values (σ_3 and σ_4).[5] The definition of these "standard deviations" is so that $Corr3$ and $Corr4$ stay always between -1 and 1 as normal correlations do (see Appendix B for demonstration). This standardization facilitates the empirical derivation of the factors F_3 and F_4. Empirical relations are derived between the typical single wind farm values σ_3 and σ_4 and the average generation in the region below. Empirical relations are also derived for F_3 and F_4 based on the region size. The third and fourth central moment of regional power generation, μ_3^P and μ_4^P, can then be calculated knowing the region size and the average generation.

Concluding, empirical functions, derived in the next section, allow to relate the

[5] A justification for assuming equal standard deviations is given in the Appendix C.

[6] Absolute values are taken in σ_{3i} as otherwise division by zero occurs in $Corr3$ in the case of symmetrically distributed variables. Now, this can only occur for trivial random variables taking only one value.

factors F_2, F_3, F_4 to the geographical region size and the standard deviations σ, σ_3 and σ_4 to the average generation in the region. The central moments μ_2^P, μ_3^P and μ_4^P of regional power generation are then calculated according to Equation (4.2) and (4.3). Finally, standard deviation, skewness and kurtosis of regional power generation are given by the following Equation (4.4).

$$Std = \sqrt{\mu_2^P} \quad , \quad Skew = \frac{\mu_3^P}{Std^3} \quad , \quad Kurt = \frac{\mu_4^P}{Std^4} \tag{4.4}$$

Two final remarks complete the section. First, the factors F_2 and F_4 are interesting for themselves independent of a calculation of the other parameters. The factor F_2 gives a relation between the variance of regional power generation (μ_2^P) and the variance of single wind farm power generation (μ_2) and F_4 gives the corresponding relation for the fourth central moment.[7] Hence, they can be interpreted as a measure of variability reduction in the region.

$$F_2 = \frac{\mu_2^P}{\sigma^2} = \frac{\mu_2^P}{\mu_2} \quad \text{and} \quad F_4 = \frac{\mu_4^P}{\sigma_4^4} = \frac{\mu_4^P}{\mu_4} \tag{4.5}$$

Secondly, all equations can also be applied to gradients of wind power generation as the gradients at single wind farms sum up to the gradients of regional wind power generation.

Standard deviation, skewness and kurtosis of regional power generation

Equation (4.4) in combination with Equation (4.2) and (4.3) allow to calculate standard deviation, skewness and kurtosis of regional power generation without knowing the actual generation profile. Values for F_2, F_3 and F_4 (called moment factors in the following) and values for σ^2, σ_3^3 and σ_4^4 (called standard deviations in the following) are required to apply the equations. In the following, exponential equations are derived relating the moment factors F_2, F_3 and F_4 to the region size. The moment factors are also interesting for themselves as they give a quantification of the smoothing effect. After that polynomial equations are derived relating the standard deviations σ^2, σ_3^3 and σ_4^4 to the average power generation in the region. The numerical values of all equation parameters are gathered in Table 4.3 at the end of the section and a summary is given.

Applied data Hourly wind speed series from 2006, measured at 10 m height by the German National Meteorological Service (DWD), are applied to derive the following equations. 24 locations distributed over Germany according to the large dots in Figure 4.6-(a) were available. The speed series are transformed to 70 m height as a typical height by the power-law method. The scaling factor

[7] This does not apply for F_3 because σ_3^3 is not equal to the third central moment as σ_3 is based on absolute values.

is $1.476 = (70/10)^{0.2}$ applying a power law exponent of 0.2 as it is proposed for agricultural land with a few trees [148]. The resulting speed series are transformed to power by means of a Vestas V47-660 power curve and the correlations between the power time series are calculated. Only hours are considered for which no location has a missing value so that the data set is reduced to 4575 hours.[8]

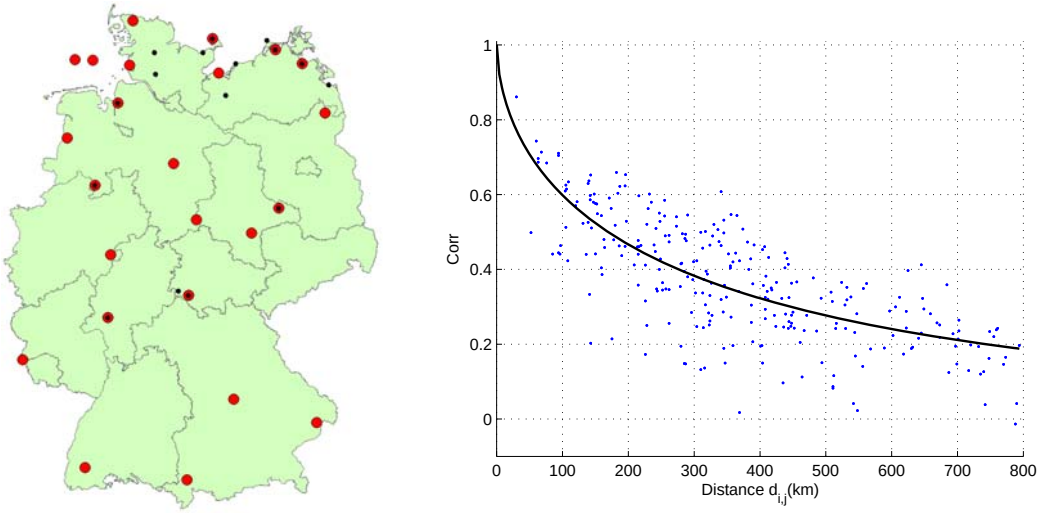

(a) Data locations (b) Correlations over distances

Figure 4.6.: Data locations and correlations

The presented data is applied to calculate correlations of power generation. Additionally to the correlations, relations between the average power generation and its standard deviation are required. For this purpose, the measured time series do not need to cover equal time periods. Therefore wind speed data from other years and partially other locations was added to the data above. The added data covers the years from 2001 to 2004 and the related locations are pictured by small dots in Figure 4.6-(a). Each year and location was considered separately. Thus, together with the data from 2006, 85 pairs of average generation and standard deviation could be calculated.

Deviation of moment factors First, relations linking the distance between wind farms and the correlation of their power generation are derived. Secondly, distributions of point locations representing wind farm locations are simulated in a square shape and their correlations are calculated based on the derived relations. Summing up the calculated correlations between the locations for all combinations results in the moment factors.

The correlation between the generation at location i and location j is equal to $\frac{E(P_i^c P_j^c)}{\sigma_i \sigma_j}$. With 24 data locations according to Figure 4.6-(a), there are 276 pairs.

[8]The influence of the transformation parameters on the equations derived below is discussed in the Appendix B.

For all pairs, the distances and the correlation of the generation time series are calculated. An exponential function according to Equation (4.6) is chosen as fitting function as correlations become one for a distance of zero and approach zero for infinite distances.

$$Corr = \frac{E(P_i^c P_j^c)}{\sigma_i \sigma_j} = e^{-a \cdot d_{i,j}^{\alpha}} \tag{4.6}$$

The distance between two locations is denoted by $d_{i,j}$. The exponential function is defined by a decay constant, a, and a stretching exponent, α, that are derived by least squares fitting. The stretching exponent makes the exponential function more flexible leading to better fitting results. Figure 4.6-(b) shows the correlations and the fitted curve.

In a similar way, fitting functions for $Corr3$ and $Corr4$ are derived. However, they depend on three respectively four locations (equivalent to three respectively six distances). $Corr4$ becomes one if all distances are zero. $Corr3$ and $Corr4$ become zero with increasing distances. Products of exponential functions according to Equation (4.7) are therefore chosen as fitting functions. As the distances should be interchangeable in all functions there are no specific coefficients for specific distances. Due to absolute values in σ_3, see Equation (4.3), $Corr3$ can be smaller than one even if all distances are zero. This is taken into account by the scaling coefficient b_{sc}. All coefficients are derived by least squares fitting.

$$\begin{aligned} Corr3 &= \frac{E(P_i^c P_j^c P_k^c)}{\sigma_{3i}\sigma_{3j}\sigma_{3k}} = b_{sc} \cdot e^{-bd_{i,j}^{\beta}} \cdot e^{-bd_{i,k}^{\beta}} \cdot e^{-bd_{j,k}^{\beta}} \\ Corr4 &= \frac{E(P_i^c P_j^c P_k^c P_l^c)}{\sigma_{4i}\sigma_{4j}\sigma_{4k}\sigma_{4l}} = e^{-cd_{i,j}^{\gamma}} \cdot e^{-cd_{i,k}^{\gamma}} \cdot e^{-cd_{i,l}^{\gamma}} \cdot e^{-cd_{j,k}^{\gamma}} \cdot e^{-cd_{j,l}^{\gamma}} \cdot e^{-cd_{k,l}^{\gamma}} \end{aligned} \tag{4.7}$$

Based on the correlations $Corr$, $Corr3$ and $Corr4$, the moment factors F_2, F_3 and F_4 can now be derived. According to Equation (4.2) and (4.3), summing up the correlations of all location combinations leads to the moment factors. A simulation of 100 randomly distributed points in a square shape represents a spatial distribution of wind farms in an area. Point distributions for side length from 0 to 800 km are simulated. In each case, the distances between all points are calculated, correlations are calculated by Equation (4.6) and (4.7) and the sum of the correlations gives the values F_2, F_3 and F_4. In Appendix C it is shown that the assumption of square shapes does not limit the generality of the approach. It is therefore also valid for other area shapes (apart from very longish shapes). It is also shown that 100 points are sufficient in the simulation and more points do not alter the results. Figure 4.7-(a) shows the results. For a better visualization and application, the results, calculated for selected side lengths, are connected by exponential fitting functions. These functions are given by Equation (4.8) that link the moment factors to the side length s.

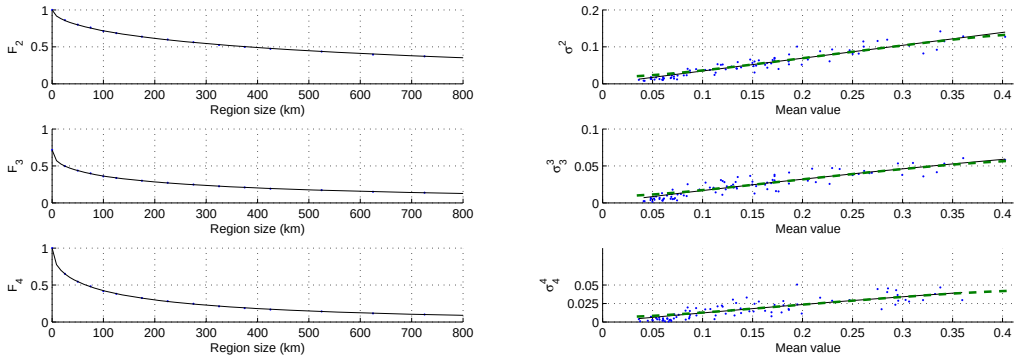

(a) Moment factors F over square size s (b) Standard deviations over mean generation

Figure 4.7.: Moment factors and standard deviations

$$\begin{aligned} F_2 &= e^{-g_2 \cdot s^{r_2}} \\ F_3 &= g_{3sc} \cdot e^{-g_3 \cdot s^{r_3}} \\ F_4 &= e^{-g_4 \cdot s^{r_4}} \end{aligned} \tag{4.8}$$

Standard deviations Equation (4.2) and (4.3) allow to calculate the central moments of regional wind power generation. Next to the moment factors F_2 to F_4, that depend on the region size, values of σ^2, σ_3^3 and σ_4^4 must be known. In the equations these values are assumed to be identical for all wind farms in the region, which is justified in Appendix C. The following approach allows to derive the values knowing the totally generated energy amount in the region. In fact, there is a close relation between the average wind power generation and its standard deviations.

Figure 4.7-(b) gives standard deviations of power generation depending on average generation. The values of σ^2 show an accentuated relation. The values of σ_3^3 and σ_4^4 are more dispersed, but there is still a systematic dependence on the mean values. The following polynomial functions according to Equation (4.9) were chosen to fit the data that give reasonable results for mean values between 0.03 and 0.41 (equal to 300 and 3600 full load hours). These extreme limits are chosen to capture all possible cases. In general, wind farms realize full load hours well above 1400 hours. In the equations m stands for the mean values and k_{21} to k_{42} are derived by least squares fitting. The functions are represented by the solid lines in Figure 4.7-(b).

$$\begin{aligned} \sigma^2 &= k_{21} m + k_{22} m^2 \\ \sigma_3^3 &= k_{31} m + k_{32} m^2 \\ \sigma_4^4 &= k_{41} m + k_{42} m^2 \end{aligned} \tag{4.9}$$

The mean generation values of all wind farms are distributed around a given re-

Table 4.3.: Coefficients for the calculation of the smoothing parameters

Correlations					
a	0.0373	b	0.03889	c	0.0211
α	0.5695	β	0.4574	γ	0.4991
		b_{sc}	0.7093		
Moment Factors					
g_2	0.0264	g_3	0.0857	g_3	0.0867
r_2	0.5499	r_3	0.4494	r_3	0.4974
		g_{3sc}	0.7167		
Standard Deviations					
k_{21}	0.3457	k_{31}	0.1737	k_{41}	0.1271
k_{22}	0.0041	k_{32}	-0.0663	k_{42}	-0.0444

gional average generation value. Some wind farms will generate more power, other less. The influence of this dispersion is evaluated in the following. The distribution of single mean values around the regional mean value is thereby assumed to be a normal distribution that is specified as follows. The mean of the normal distribution is equal to the regional mean value. Its standard deviation is estimated to 0.06 assuming that 99.7 percent of the wind farms (respectively their mean generation values) are in the range of +0.18 and -0.18 around the regional mean. This corresponds to a range of +1577 and -1577 h around the full load hours of the regional generation. The product of Equation (4.9) and the normal distribution function is now integrated over a range from 0 to 0.5. The differences between the mean generation levels in the region are thus considered in the calculation of the typical standard deviation. The dashed line in Figure 4.7-(b), mostly covered by the solid one, shows the resulting values standing for the mean standard deviation in a region. The solid and dashed lines are nearly identical, especially around mean values of 0.2, and differences do not exceed 5 percent. Hence, standard deviations can be calculated directly by Equation (4.9), too.

Summary Table 4.3 summarizes all coefficients of the precedent equations. The derived equations allow to identify a distribution for the regional wind power generation. As it is shown in the Appendix C, there should be at least 50 uniformly distributed wind farms in the region to justify the approach. Data or estimations of following values are required next to the coefficients in Table 4.3: geographical region size and relative average wind power generation over the regarded time horizon (normally given by the total installed wind capacity and total wind energy generation). There are the following steps:

Table 4.4.: Coefficients for 2-h gradients

Correlations					
a	0.2909	b	0.0011	c	0.1345
α	0.4001	β	1.5154	γ	0.3326
		b_{sc}	0.0587		
Moment Factors					
g_2	0.2347	g_3	0.0110	g_3	0.6183
r_2	0.3680	r_3	1.0456	r_3	0.3295
		g_{3sc}	0.0695		
Standard Deviations					
k_{21}	0.1059	k_{31}	0.0337	k_{41}	0.0146
k_{22}	-0.1037	k_{32}	-0.0192	k_{42}	-0.0021

0 Input data: region size and relative average wind power generation.

1 a Moment factors are calculated by Equation (4.8) using region sizes.

1 b Mean standard deviations are calculated by Equation (4.9) using average wind power generation.

2 a Central moments are calculated by Equation (4.2) and (4.3) and transformed to standard deviation, skewness and kurtosis according to Equation (4.4).

These values can be used to adjust a simulation of wind power generation as it is done in Section 4.2.2. In the remaining section here, the equations are verified. In addition to the parameters found by step 2a, distributions of wind power generation are thereby derived. The Pearson System of distributions is applied to select representative distributions. In fact, the Pearson system allows to find a distribution function matching given values of mean value, standard deviation, skewness and kurtosis. The Pearsons distributions cover Normal, Students-t, Gamma and Beta distributions [149]. In Matlab, for instance, the method is implemented by the function 'pearsrnd' that simulates random values that are according to the appropriate distribution. This results in the following step.

2 b A duration curve is generated by simulating wind power generation values according to the identified Pearson distribution function.

The same approach applies to gradients of wind power generation. The equation coefficients for the case of 2-hour gradients are given by Table 4.4.

Verification

Two test cases show the suitability of the described approach.[9] The aggregated German and Irish wind power data, published by the transmission system operators, is applied. German data of the years 2006 and the first half of 2007 and Irish data of the year 2007 were taken. The regarded region in Germany covers the balance areas of Eon, RWE and Vattenfall, in total about 312000 km^2. The transmission grid in Ireland, an area of about 84000 km^2, is operated by Eirgrid. Next to the region sizes, the average power generation is required as input. They were here directly calculated from the published power time series after normalization by the installed wind power capacities. Normally, the approach will be applied if the time series are not given and the average generation level will be calculated from the total wind energy generation and the installed capacity. Knowing the average generation and the region size, steps 1 to 2b described above can be applied.

This leads to the results in Figure 4.8, that are compared to the corresponding values calculated directly from the power time series. The top left plot shows the average generation values. The other plots give the comparison between simulated ('Simulated') and real value ('Measured') for the standard deviation, skewness and kurtosis of the regional power generation. In addition to that, typical values for a single wind farm, as they are also calculated in the approach, are given. Thus, the change of the variability (the smoothing effect) going from generation at a single wind farm to regional generation is illustrated. The top right plot shows standard deviations. σ, calculated by Equation (4.9), stands for the typical standard deviation at a single wind farm in the region. The bottom left plot shows skewness, the bottom right plot kurtosis. σ_4^4/σ^4 gives the typical kurtosis value at a single wind farm. σ_3^3/σ^3 is not equal to skewness, see Equation (4.3), which is indicated by the dashed line. The comparison between simulated and measured parameters of regional generation shows that best results are achieved for standard deviations. The 'Simulated' and 'Measured' bars are nearly equal. Matching of skewness and kurtosis is less accurate. This is explained by the fact that data errors have larger impacts on higher moments. In summary, the results show that the equations lead to good estimations of standard deviation but only to indicative estimations of skewness and kurtosis. Similar results can be seen looking at the parameters of the 2-hour gradients according to Figure 4.9. Again, the standard deviations are well estimated. The same applies to skewness, whereas there is not a good match in the case of kurtosis.

The calculated parameters allow to identify an appropriate distribution function for the wind power generation appyling the Pearson family of distributions (step 2-b above). A distribution of type 1 equal to a four parameter beta distribution fits to the calculated parameter values. Drawing many random values and eliminating

[9] In Appendix C, sensitivity analyses are given showing further how the approach works.

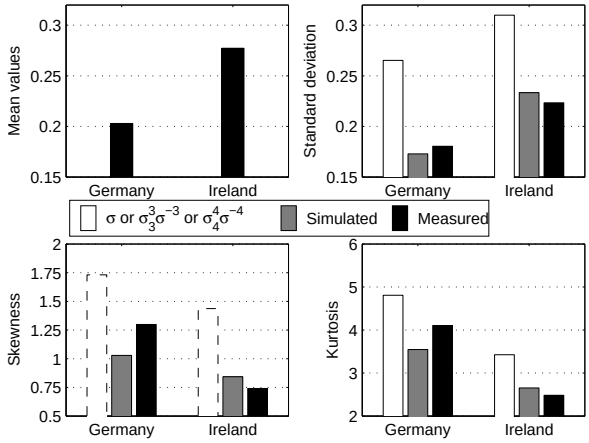

Figure 4.8.: Calculated and measured parameters of generation curve

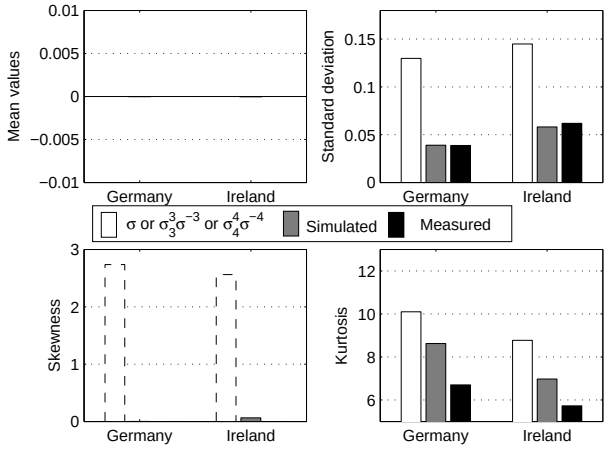

Figure 4.9.: Calculated and measured parameters of 2-hour gradients

values that are outside zero and one, the duration curves can be generated. Figure 4.10-(a) compares these curves ('simu.') with the ones derived directly from the measured data ('meas.'). The duration curves differ slightly. This is not only due to the different parameter values but also due to the simulation method. Even if the original parameters are taken for the simulation there a discrepancies between simulated and measured curves, especially at the borders. Hence, the simulation based on the Pearson system is useful for visualization of the duration curves but not as an accurate representation of the distribution.

The duration curves especially illustrate the variance of power generation. High variances lead to duration curves that are close to the bisecting line from top left to down right. The (relative) wind power generation in Ireland has a higher variance than the one in the larger area of Germany and the duration curve is

therefore closer to the bisecting line.

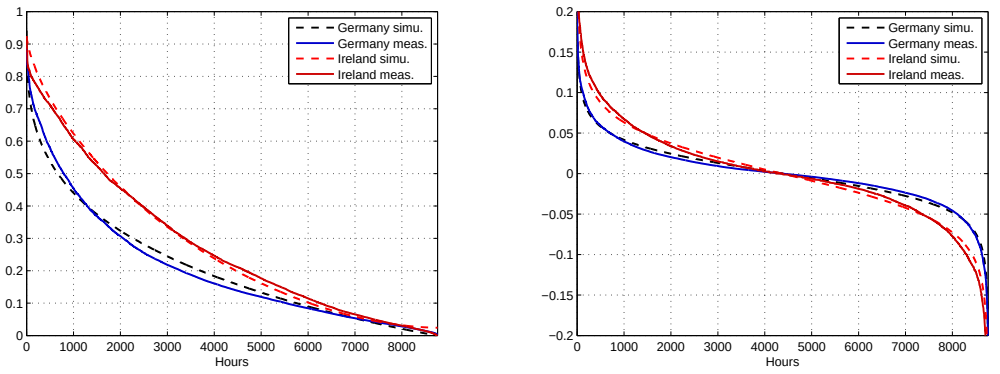

(a) Duration curves of generation

(b) Duration curves of 2-hour gradients

Figure 4.10.: Duration curves of generation and 2-hour gradients

The approach is also applied to 2-hour gradients of power generation. Figure 4.10-(b) shows the simulated and measured duration curves. Distribution functions of type four of the Pearson system are thereby applied. Again, the curves differ only slightly. The results for Ireland for the generation and the 2-hour gradients show that, even though the correlations in Equation (4.6) and (4.7) were derived from German wind data, the approach can also be applied to other regions.

Concluding, the derived equations give an estimation of standard deviation, skewness and kurtosis of regional wind power generation. The same applies to the generation gradients, especially if their standard deviations are estimated. Only indications about the average wind power generation in the region and its geographical size are required to apply the equations. The factor F_2 for example relates the variance of regional power generation to the typical variance of power generation at a single wind farm. Equations are given relating the latter to the average wind power generation in the region and relating F_2 to the region size. Knowing F_2 and the typical variance at a wind farm, the variance (or standard deviation) of regional wind power generation can be derived. Appendix C demonstrates that the equations do not depend on the number of wind farms if there are more than 50 distributed over the region. The low sensitivity to the region shape, to an accumulation of wind farms and to the parameters of the speed to power transformation is also shown.

4.2.2. Simulation approach

The simulation of the wind power generation is presented in the following. The simulation applies to the case that the power generation of a region is not known and only wind speed series are available. The simulation of regional power generation then consists of the transformation of the single speed series to realistic

regional power series. One straightforward approach is given by up-scaling according to the capacity that is installed in the region. The single speed series are transformed to power series applying turbine power curves and the resulting power series are scaled according to the installed capacity. However, smoothing effects are neglected by this approach and the following, more sophisticated methods were developed.

One approach is the application of multi-turbine power curves [150, 151, 152]. There are also called equivalent power curves [153]. The wind speed series are thereby transformed to power by means of power curves, too. However, no standard single-turbine power curve is taken but a multi-turbine power curve. A multi-turbine power curve can be seen as a smoothed single turbine power curve. The application of a multi-turbine power curve takes into account that, at each moment, not only the wind speeds of the regarded time series are present in the region but also other wind speeds. Methods to generate multi-turbine power curves were developed [150, 152]. A method with the same purpose is presented here that has the advantage that it explicitly takes into account the region size and the energy output considering several statistical parameters.

However, the use of a multi-turbine power curve is not sufficient to simulate regional power generation. The gradients of regional power series are normally lower than the gradients of single wind farm power series. This is shown by the decrease of their standard deviation, see Section 4.2.1. The variability decrease is not completely reflected by the application of a multi-turbine power curve. The smoothing effect related to the gradients can for example be simulated by a moving block averaging [150]. Here, it is simulated by overlying several shifted time series that are differently weighted. The weighting parameters are thereby again derived under consideration of statistical parameters that are related to the region size and energy output.

Overview

The simulation approach is summarized by Figure 4.11. For each region, it leads to the time series of power generation. The variability of the time series is thereby adjusted to the region sizes and the generated energy. Basic inputs are one or several wind speed series for each region. Additional input parameters are the region sizes and the total wind energy generation in each region for the considered time period. The wind speed series of a region are scaled according to the assumed energy generation. The scaling can also be interpreted as adjusting the height of the wind speed series. Wind speed series are often not measured at turbine height and the speed is scaled to other heights by means of the power-law method. The power-law method gives a linear scaling factor as a function of the height adjustment. Here, a linear scaling factor is chosen in such a way that, after transformation to power applying a standard single-turbine curve, the resulting power generation gives the energy amount specified for the region. The scaled wind speed series are

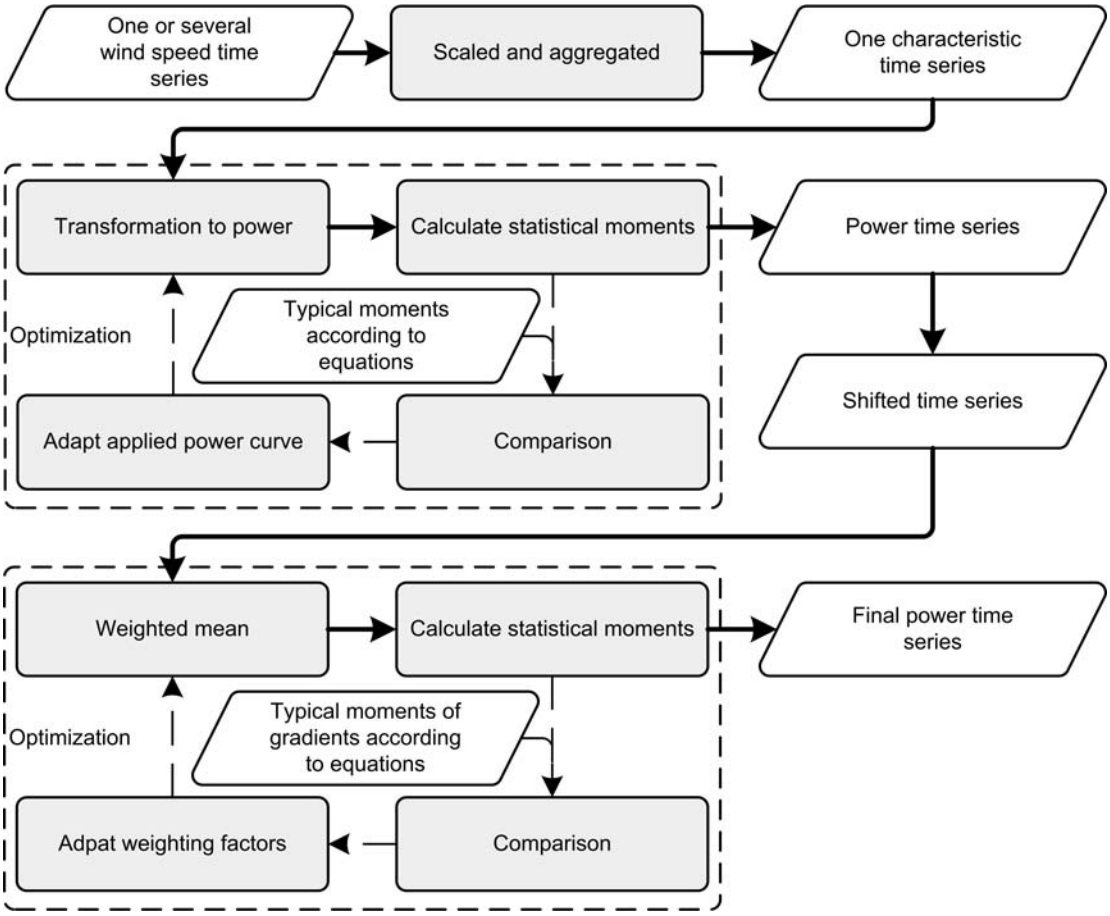

Figure 4.11.: Simulation of regional wind power generation by means of wind speed series

summed up and the average is taken resulting in a characteristic speed time series for the region. If the characteristic time series is based on more than one wind speed series a smoothing has already taken place here.

The characteristic speed time series are transformed to power applying a multi-turbine power curve. The multi-turbine power curve is thereby derived by an optimization in order that the statistics of the resulting power time series are similar to the ones that are typical for the region size and energy generation. The considered statistics are the first four central moments (representing mean, standard deviation, skewness and kurtosis). After that, the resulting power time series is smoothed. The power time series is therefore shifted in time by one or more time steps. The non-shifted and the shifted power time series are combined applying a weighting factor for each of them. The weighting factors are found by an optimization that considers the statistics of the gradients of the resulting power time series. The standard deviations of 1-hour, 2-hour and 3-hour gradients are taken into account. The final power time series represent the regional power generation. The multi-turbine power curve and the weighting factors implicitly

take into account how many wind speed series were considered at the beginning. If more wind speed series are applied for a region less smoothing is necessary in the approach and the multi-turbine power curve and the weighting factors are less accentuated.

Optimization of multi-turbine power curve

The multi-turbine power curve is found by a non-linear optimization. In the objective function the speed time series are transformed to power time series applying the power curve. The discrete power curve is expressed as a lookup table giving a power generation level g_i for each wind speed level w_i (typically in m/s steps). The vector $\mathbf{g}$ (the power generation levels for all wind speed levels from 0 m/s to 30 m/s) defines the power curve. The transformation from speed to power is denoted by $T_{\mathbf{g}}$ in the following. $T_{\mathbf{g}}(\mathbf{v})$ then gives the power time series for the speed time series $\mathbf{v}$. The optimization to find the multi-turbine power curve respectively $\mathbf{g}$ is given by Equation 4.10.

$$
\begin{aligned}
\min_{\mathbf{g}} \quad & \sum_{i=2,3,4} \left(\frac{\frac{1}{n}\sum_j (T_{\mathbf{g}}(v_j) - \frac{1}{n}\sum_k T_{\mathbf{g}}(v_k))^i - \mathrm{MOM}_i}{\mathrm{MOM}_i} \right)^2 \\
\text{s.t.} \quad & \frac{1}{n}\sum_k T_{\mathbf{g}}(v_k) = \mathrm{cf} \\
& g_i - g_{i-1} > 0 && \forall\, i \mid 2 \leqq i \leqq m_{\mathbf{g} \text{ maximal at } g_m} \\
& g_i - g_{i-1} < 0 && \forall\, i > m_{\mathbf{g} \text{ maximal at } g_m} \\
& |g_i - g_{i-2}| < 0.02 && \forall\, i > 3 \\
& g_i \leqq 1 \quad \text{and} \quad g_i \geqq 0 && \forall\, i \\
& g_1 = 0 \quad \text{and} \quad g_{31} = 0
\end{aligned}
\tag{4.10}
$$

The transformation from speed to power applying the multi-turbine power curve should lead to power time series that are smoothed as it is typical for the region size. In the objective function of the optimization problem, the second, third and fourth central moment of the power time series are calculated (the second central moment is the variance). The variance of the resulting time series is for example equal to $\frac{1}{n}\sum_j (T_{\mathbf{g}}(v_j) - \frac{1}{n}\sum_k T_{\mathbf{g}}(v_k))^2$ with n time steps in the time series. The optimization takes the relative differences between the calculated moments and the theoretical moments MOM into account. They are squared and their sum is minimized. The theoretical moments MOM are derived from the region size and capacity factor (average generation) by the Equations (4.2), (4.3) and (4.4), see Section 4.2.1.

The first restriction ensures that the capacity factor of the resulting power time series is equal to the exogenously defined capacity factor cf. The other restrictions take care of the profile of the multi-turbine power curve. They ensure that the curve has a reasonable profile respectively that the curve is still similar to the one

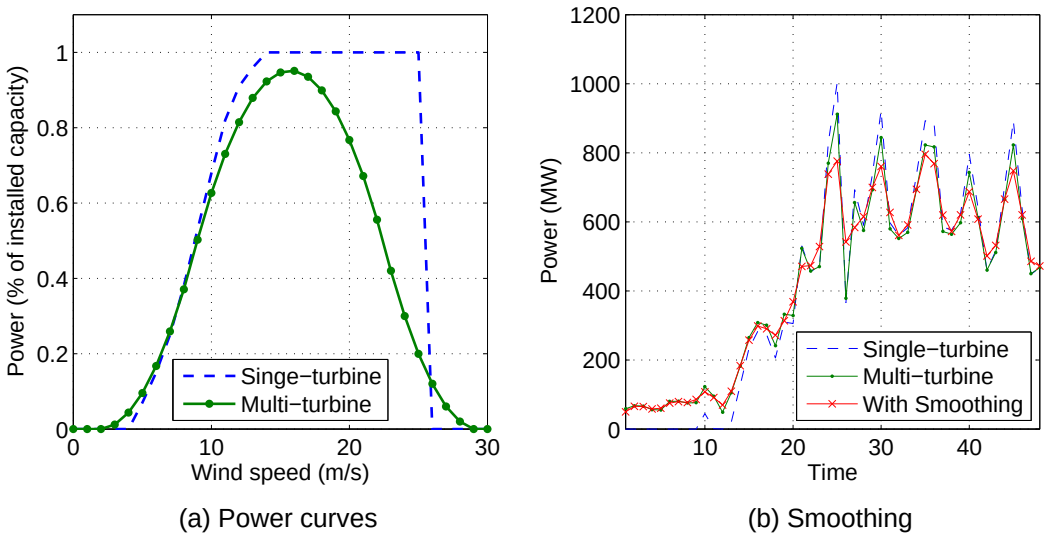

Figure 4.12.: Example of multi-turbine power curve and smoothing of power time series

of a single-turbine power curve and not deformed. Due to the second and third restriction the power curve rises to its maximal value and then falls. m thereby stands for the speed level at that $\mathbf{g}$ is maximal. The fourth restriction binds the absolute differences of second order so that they do not become too large. The differences of second order represent the second derivative. Their restriction ensures that there are no big jumps or sudden changes in the power curve.

Figure 4.12-a gives an example of a resulting multi-turbine power curve. The dots indicate the values that are found by the optimization. For the purpose of comparison a single-turbine power curve (Vesta V47-660) is also shown (dashed line). The multi-turbine power curve reproduces the fact that low speed values in the applied speed time series may be compensated by higher wind speeds in another part of the region and vice-versa. The optimized multi-turbine curve does not only depend on the region parameters but also on the applied wind speed series. If the applied time series is already based on several single speed series, the multi-turbine power curve is more similar to a single-turbine curve.

Figure 4.12-b shows the resulting power time series after application of the single-turbine curve and the multi-turbine curve. The application of the multi-turbine curve leads to less extreme values but the power time series is still relatively unsteady. The composition of shifted time series, denoted by “With Smoothing” and explained below, results in a smoother time series that is more typical for regional power generation.

Optimization of weighting factors

The application of a multi-turbine power curve is not sufficient to simulate the smoothing as it has only a limited effect on the gradients. The reduction of the variability of the gradients that was shown in Section 4.2.1 is therefore considered by combining shifted time series. The power time series that result from the multi-turbine power curve, denoted by $\mathbf{p^0}$ (equal to $T_{\mathbf{g}}(\mathbf{v})$) is shifted by one or several hours in both directions. The resulting shifted power time series (for example $\mathbf{p^{-2}}$, $\mathbf{p^{-1}}$, $\mathbf{p^1}$, $\mathbf{p^2}$) plus the original one ($\mathbf{p^0}$) are weighted and aggregated according to Equation (4.11). The aggregated power time series, depending on the applied weighting factors, is denoted by $\mathbf{p^w}$.

$$\mathbf{p^w} = w_{-2} \cdot \mathbf{p^{-2}} + w_{-1} \cdot \mathbf{p^{-1}} + w_0 \cdot \mathbf{p^0} + w_1 \cdot \mathbf{p^1} + w_2 \cdot \mathbf{p^2} \tag{4.11}$$

The weighting factors are found by an optimization according to Equation (4.12). They are optimized in such a way that the variances of the gradients match theoretical ones. The theoretical variances of the 1-hour, 2-hour and 3-hour gradients are denoted by VAR_1, VAR_2 and VAR_3. They are derived from the region size and the capacity factor by Equations (4.2), (4.3) and (4.4), see Section 4.2.1. The 1-hour gradients of $\mathbf{p^w}$ are given by $\mathbf{p^w_{2,\dots,n}} - \mathbf{p^w_{1,\dots,n-1}}$ with n as the number of hourly time steps in the time series. The 2-hour and 3-hour gradients are given correspondingly. In the objective function, the variances of the gradients are calculated and the relative differences between them and the theoretical variances are squared, summed up and minimized.

$$\begin{aligned}
\min_{\mathbf{w}} \quad & \sum_{i=1,2,3} \left(\frac{\frac{1}{n-i}\sum((\mathbf{p^w_{i+1,\dots,n}} - \mathbf{p^w_{1,\dots,n-i}}) - \frac{1}{n-i}\sum(\mathbf{p^w_{i+1,\dots,n}} - \mathbf{p^w_{1,\dots,n-i}}))^2 - \mathrm{VAR}_i}{\mathrm{VAR}_i} \right)^2 \\
\text{s.t.} \quad & \sum\nolimits_i w_i = 1 \\
& w_{-1} = w_1 \quad \text{and} \quad w_{-2} = w_2 \\
& w_{-2} \leqq w_0 \quad \text{and} \quad w_{-1} \leqq w_0 \\
& w_i \leqq 1 \quad \text{and} \quad w_i \geqq 0 \qquad \forall\, i
\end{aligned} \tag{4.12}$$

The first restriction ensures that the sum of the weighting factors is equal to one. The second restriction ensures that there is no imbalance in the weighting factors. The combination of shifted time series is only applied for the purpose of smoothing but it should not lead to a general shifting of the power time series. According to the third restriction, the weighting factor of the unshifted power time series has to be higher than the others. Figure 4.12-b shows a power time series after application of the weighting factors. The power time series becomes smoother and less variable. The application of the multi-turbine power curve alone does not reduce the short-time variability of the power time series.

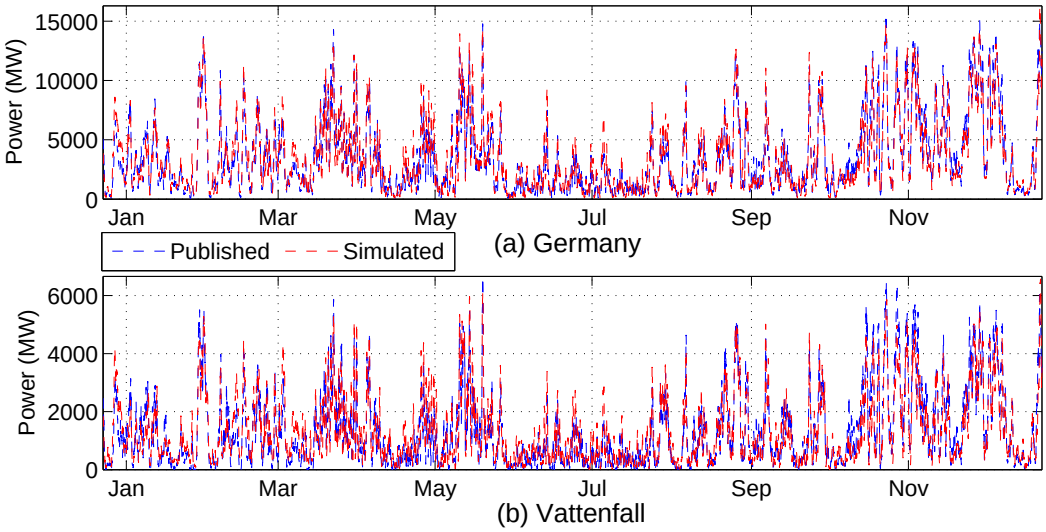

Figure 4.13.: Published and simulated power time series

Evaluation of simulation

The simulated power time series are evaluated by German power generation data. Wind power generation data from 2006 published by the four German transmission operators for their control areas is applied. The data of 2006 is considered as the simulation is based on wind speed data of 2006. The evaluation is limited for two reasons. First, the simulation is based on capacity factors (full load hours) that are exogenously defined for each of the German model regions. The regional capacity factors were however not available for 2006. They are therefore defined according to the theoretical potentials in the regions, see Section 4.1.2, and so that the German energy generation is equal to the published one. Hence, the relation between the regions regarding the generated energy may not be equal to the relation in the published data as the published data is aggregated for each control area and the control areas contain several regions. Secondly, the published data of 2006 is not always based on measured data but it is also based on extrapolation elements. Despite these limitations the evaluation can still show the usefulness of the developed simulation approach, in particular in comparison to the case that no smoothing is applied.

The simulation of German power generation is evaluated first followed by an evaluation based on the Vattenfall control area. The published and simulated power time series of 2006 are shown in Figure 4.13-a. A high correlation can be seen. The correlation coefficient between the two time series is 0.95. Table 4.5 gives additional statistical parameters comparing the two time series. As a matter of fact, the purpose of the simulation lies more in the simulation of statistically realistic power time series than in the exact imitation of actual power time series. The following comparison also looks at power time series that were generated applying

single-turbine power curves without any smoothing. Statistics of the published

Table 4.5.: Statistics of German wind power generation (MW) in 2006

	Mean	**StaDev**	**Skewness**	**Kurtosis**	**Min**	**Max**
Published	3471.47	3118.22	1.32	4.17	74.73	15176.79
Simulated	3471.64	3061.95	1.28	4.07	66.50	16299.30
Deviation (%)	0.01	-1.80	-3.07	-2.28	-11.02	7.40
If only scaled (%)	-0.01	20.34	7.31	4.59	-100.00	23.88

and simulated power generation are given in the first two rows of Table 4.5. The third row shows the deviations between the statistics. The average power generation is equal in both cases as it is an input parameter in the simulation that is defined according to the published data. The evaluation of standard deviation, skewness and kurtosis shows that the simulation leads to realistic results differing only by less than four percent. Skewness and kurtosis are important parameters as they indicate the relation between the values above and below the average and the likeliness of extreme values. The simulated minimal and maximal power generation is also similar to the published one. In fact, the wind power generation never becomes zero. The published data never drops below 75 MW, the simulated data never below 66 MW. The comparison of the parameters shows that there is a high similarity between the two power time series. The last row in Table 4.5 gives the deviations that would result from a pure scaling approach. The scaling approach represents the application of a single-turbine power curve without any smoothing. The high deviations of the parameters show that smoothing effects are neglected by such an approach. The minimal and maximal values for example would be largely under- respectively overestimated. The shortcomings of such an approach become even more obvious with regard to the gradients of power generation.

Table 4.6.: Statistics of German wind power gradients (MW) in 2006

	1h-Gradients			**2h-Gradients**			**4h-Gradients**		
	StaDev	**Mean+**	**Kurtosis**	**StaDev**	**Mean+**	**Kurtosis**	**StaDev**	**Mean+**	**Kurtosis**
Published	375.90	259.88	6.11	671.54	461.10	6.31	1172.01	817.63	6.18
Simulated	379.56	255.83	6.03	703.92	470.38	6.05	1270.88	866.43	5.76
Deviation (%)	0.97	-1.56	-1.29	4.82	2.01	-4.10	8.44	5.97	-6.76
If only scaled (%)	45.91	35.48	14.53	42.52	31.39	12.02	41.15	29.81	6.63

The first two rows in Table 4.6 give statistics of the 1-hour, 2-hour and 4-hour gradients of the published and simulated power generation. The third row shows the deviations between the parameters. The standard deviation, the mean of the positive gradients (denoted by "Mean+") and the kurtosis are given in each case. The means of the negative gradients (not shown here) are similar to the means of the positive gradients. The average increase in wind power generation from one hour to another is approximately equal to 260 MW. The simulated and published data have similar gradients resulting in low deviations between the parameters. In

general they do not differ by more than 5%. Only in the case of 4-hour gradients deviations of up to 8% can be seen. The deviations between the parameters that would result from a scaling approach are given in the fourth row of Table 4.6. A scaling approach, neglecting smoothing effects, leads to much higher gradients and overestimates the variability of the generation significantly.

In the following, the simulation approach is also evaluated based on the data of the "Vattenfall" control area. As the Vattenfall transmission grid covers the five eastern German model regions (MV, BB-BE, S, SA, TH) its power generation can be compared to the simulated one. Figure 4.13-(b) shows the published and simulated wind power time series. Table 4.7 and Table 4.8 give the statistics of the power generation and its gradients. The simulation approach is here not only compared to a pure up-scaling approach but also to a down-scaling approach. In the down-scaling approach, the German power generation is used to simulate the wind power generation in the Vattenfall area. The German power generation is thereby down-scaled according to the energy generation.

Table 4.7.: Statistics of Vattenfall wind power generation (MW) in 2006

	Mean	**StaDev.**	**Skewness**	**Kurtosis**	**Min**	**Max**
Published	1303.34	1282.67	1.39	4.44	0.00	6662.82
Simulated	1303.32	1193.87	1.36	4.37	8.62	6569.27
Deviation (%)	-0.00	-6.92	-1.99	-1.51	-	-1.40
If only scaled (%)	-0.01	18.72	12.74	10.58	-	15.69
Down-scaling (%)	0.00	-8.73	-4.59	-6.00	-	-14.48

Table 4.7 gives the statistics of the power generation. The average generation is equal in all cases as it is an input parameter. The other statistics show that the simulation approach leads to results that are similar to the measured data and the largest parameter deviation is about 7%. In contrast, the scaling methods lead to generation profiles that are too variable (up-scaling) or not variable enough (down-scaling). The maximal generation is then for example by 15% too high or by 14% too low. The shortcomings of scaling become more obvious in Table 4.8. The statistics of the gradients show that the variability is changed sig-

Table 4.8.: Statistics of Vattenfall wind power gradients (MW) in 2006

	1h-Gradients			**2h-Gradients**			**4h-Gradients**		
	StaDev	**Mean+**	**Kurtosis**	**StaDev**	**Mean+**	**Kurtosis**	**StaDev**	**Mean+**	**Kurtosis**
Published	213.23	150.18	6.33	344.85	240.95	6.35	560.56	395.50	6.32
Simulated	188.64	130.10	6.12	338.31	228.37	6.33	604.86	413.64	6.18
Deviation (%)	-11.53	-13.37	-3.36	-1.90	-5.22	-0.24	7.90	4.59	-2.23
If only scaled (%)	49.56	31.67	17.98	51.69	33.14	17.88	51.83	33.74	15.82
Down-scaling (%)	-33.81	-35.02	-3.61	-26.89	-28.17	-0.60	-21.51	-22.39	-2.23

nificantly if a scaling approach is applied. In the case of up-scaling, the variability is largely overestimated. The average positive 1-hour gradient is for example more

than 30% higher than measured. In the case of down-scaling, the variability is largely underestimated. The average positive 1-hour gradient for example is by 35% too low. This over- and underestimation of variability by scaling reflects the general analysis of the smoothing effect in Section 4.2.1. The presented simulation approach considers the changes of variability by taking into account the region size. Realistic generation profiles of single regions can thus be simulated.

4.3. Analysis and simulation of wind forecasts

The simulation of forecast errors requires information about the statistical characteristics of forecast errors. Statistical parameters of measured wind speed forecast errors are therefore analysed in the following. The parameters are related to the forecast quality, to the shape of the error distribution and to temporal dependences. Correlations between forecast errors at different locations are also assessed and they are described by a fitting function. The statistics are then applied in a simulation approach that is based on moment matching. The parameters of the simulated scenarios are thereby matched to the empirical parameters. The forecast quality of regional power forecasts is also considered in the simulation approach. An improvement of forecast quality by 20% until 2020 is applied in the final simulation as discussed in Section 4.1.

4.3.1. Analysis of wind speed forecast errors

The following analysis of measured wind speed forecast errors has two aspects.[10] On the one hand, the analysis delivers the parameters that are needed in the simulation approach in the subsequent section. The considered parameters are standard deviation, skewness, kurtosis, autocorrelations and geographical correlations. For the latter an equation is given that allows their calculation in dependence of the geographical distance and the forecast hour. On the other hand, the following two general points are made by the analysis. First, the standard deviation of the errors does not depend on the wind speed level in a systematic way. As a first approach, the speed forecast errors can therefore be simulated independently from the wind speed series. Secondly, the wind speed forecast errors are not normally distributed which is important for the development of the simulation approach. The analysis is based on one year of data at six different wind farm locations. At each location, a forecast is given every 6 hours with a forecast horizon of 6 hours to 40 hours.

Forecast quality and conditional forecast results

Figure 4.14-a shows the standard deviations depending on the forecast horizon. The standard deviations slightly increase with larger forecast horizons and they

[10] For the analysis, see also [19] and [154] by the author.

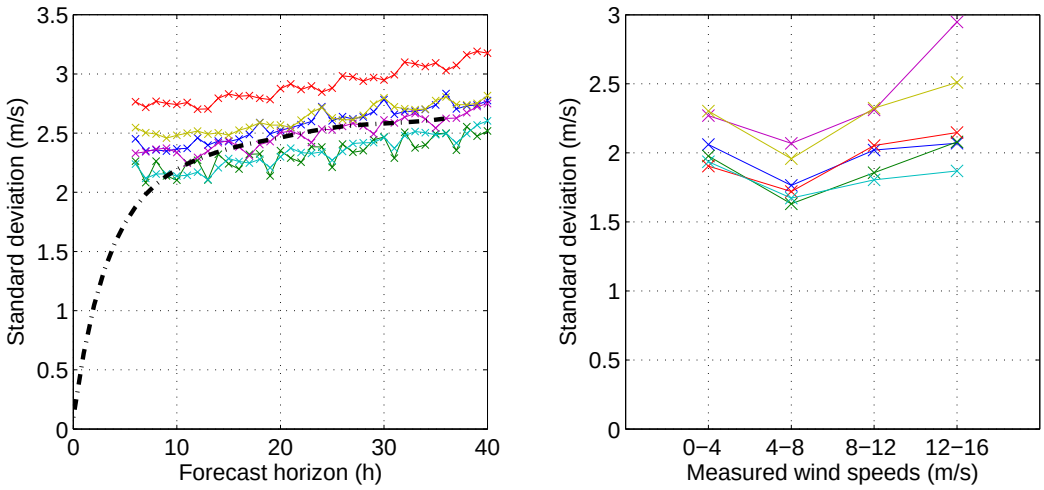

(a) Standard deviation (b) Conditional standard deviation

Figure 4.14.: Standard deviation of wind speed forecast errors

are similar at the different locations. The dash-dotted line indicates the assumed curve for the simulation in Section 4.3.2. The mean errors (not shown here) are either positive or negative over all forecast hours depending on the location, but no general over- or underestimation by the forecast can be observed. The mean errors will therefore balance each other out if forecasts at several locations are aggregated.

Figure 4.14-b shows to which extent the standard deviations depend on the actual wind speed. A hypothesis could be that the forecast errors increase in weather situations with high wind speeds. This hypothesis is analyzed by splitting the measured wind speeds into different partitions (bins). For each bin, the standard deviations of the related forecast errors are calculated.[11] No systematic trend can be observed. Two locations show a clear increase of standard deviation with higher wind speeds but for the other four the standard deviations are similar for all bins. In one case, the standard deviation related to the last bin is even slightly lower than the one related to the first bin. As the available data is limited, the results can only be indicative. The same observation is however also made in the literature. A similar analysis at two locations for example shows that there is no systematic trend between standard deviation and wind speed level [22]. The relative independence between the forecast error and the wind speed level does not apply to power forecasts. Due to the transformation to power by the nonlinear power curve, the power forecast errors systematically depend on the measured power level, as shown by the author, [154] and others, [17].

[11] Figure 4.14-b relates to the forecast error looking at all forecast horizons. Similar results can be seen looking at each forecast hour for itself.

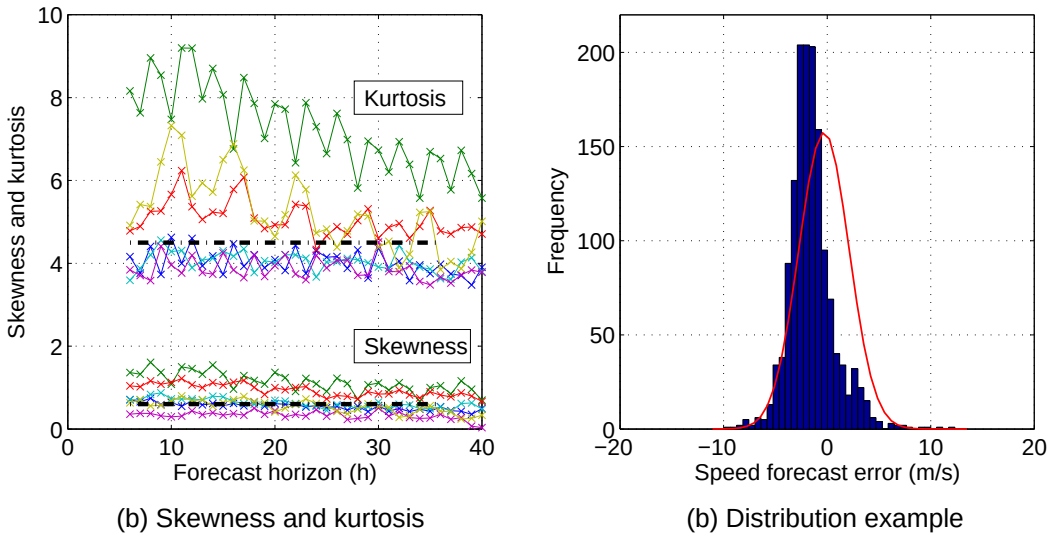

Figure 4.15.: Distribution of speed forecast errors

Distribution of forecast errors

Skewness and kurtosis are important parameters to characterize a distribution. There are given in Figure 4.15-a. In all cases the kurtosis is higher than three so higher than in the case of a normal distribution. The kurtosis stays relatively constant at four locations, whereas it decreases with increasing forecast horizon at two locations. In some cases very high kurtosis values can be seen. Kurtosis values greater than three define leptokurtic distributions. Leptokurtic distributions have sharper peaks and longer, fatter tails. This means that the forecast errors are in general relatively low (high frequency around the average value), but extreme events occur more often than in the case of a normal distribution (fat tails). In other words, large errors happen less often but they are more extreme. Figure 4.15-b gives the distribution of the forecast errors at one location in form of a histogram (ten-hour forecast). In addition, a normal distribution with the same mean value and standard deviation is given by the thin solid line. The example shows that the sharp peak around the mean of the error distribution is balanced by higher frequencies at the tails.

Figure 4.15-a shows that the skewness of the forecast errors is greater than zero and stays relatively constant for different forecast hours (the skewness of a normal distribution is zero). The forecast errors are therefore right-skewed indicating a higher concentration of values below the average. This means that the forecast in general underestimates the future wind speed but in some rare events a high overestimation occurs.[12] The example distribution in Figure 4.15-b illustrates the right-skewness of the forecast errors. The dash-dotted lines in Figure 4.15-a indicate the parameter assumptions for the simulation in Section 4.3.2.

[12]The error is here equal to the predicted value minus the measured one.

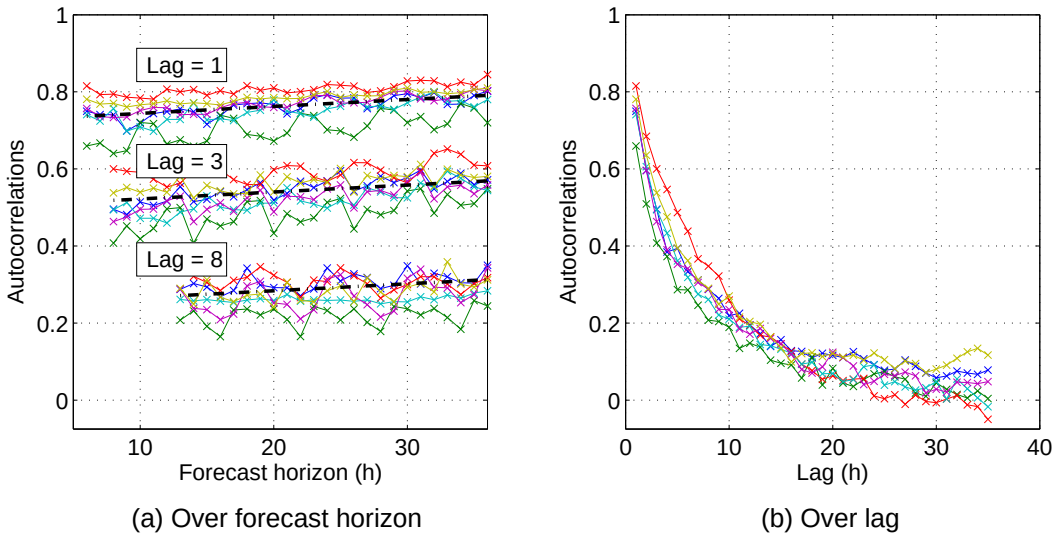

Figure 4.16.: Autocorrelations of wind speed forecast errors

The results show that the speed forecast errors are generally not normal distributed and extreme events occur more often. This observation is important as extreme forecast errors will cause more difficulties for the operation of the power systems. The distribution of the errors was therefore additionally tested by a chi-square test and a Jarque-Bera test. The hypothesis that the errors follow a normal distribution is thereby rejected for all forecast hours for a significance level of 0.1% (the probability that the errors follow a normal distribution is then lower than 0.1%).

Autocorrelations

To simulate forecast errors, it is also important whether the forecast error stays positive (or negative) for the total forecast horizon or whether it rather oscillates. Autocorrelations indicate to which extent the forecast error depends on errors that are related to other forecast hours. Figure 4.16-a shows how the autocorrelations develop with increasing forecast horizon. For example, the autocorrelation at forecast hour three looking at a lag of one hour gives the correlation between the errors of a three-hour forecast and the errors of a two-hour forecast.

The autocorrelations increase only slightly with increasing forecast horizon but they strongly depend on the lag. For a lag of one, the autocorrelations are mainly between 0.7 and 0.8, so relatively high, whereas they are significantly lower for greater lags. This can also be seen in Figure 4.16-b giving the correlation between the error of a one-hour forecast and the errors related to longer forecast horizons. The autocorrelations decrease quickly with increasing lags and the autocorrelations are below 0.2 if the difference between the forecast horizons exceeds twelve hours. The errors of a forecast for one hour are therefore only similar to the er-

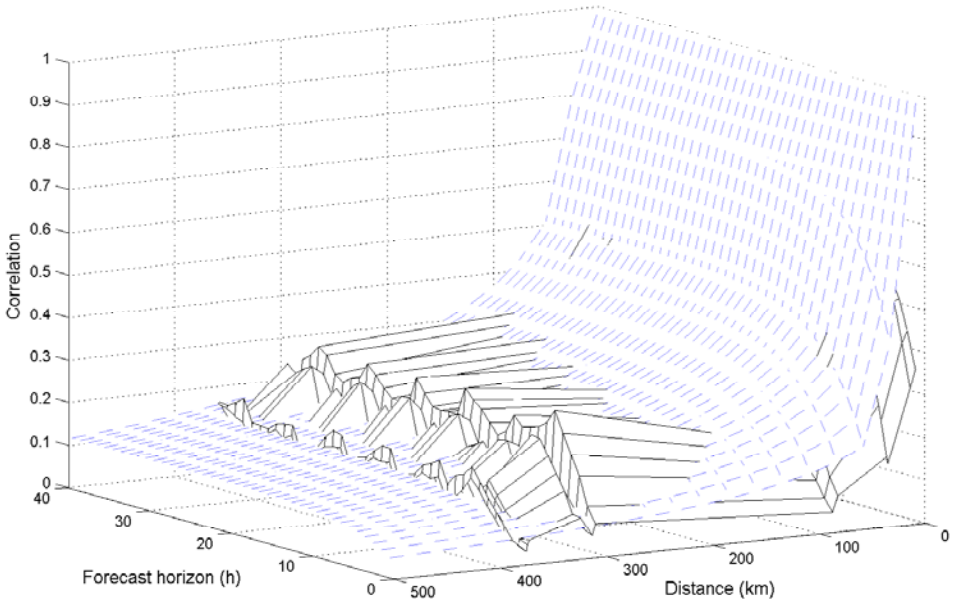

Figure 4.17.: Spatial correlations of speed forecasts and fitted mesh

rors of a forecast for another hour if the lag between the hours is small. The dash-dotted lines in Figure 4.16-a indicate the assumptions for the simulation in Section 4.3.2.

Geographical correlations

The forecasts of regional wind power generation are typically based on the forecasts at selected wind farm locations. Forecast errors at different locations balance each other to a certain extent (only perfectly correlated forecast errors would not level each other out). The correlations between errors at different locations are therefore decisive for the later simulation. The correlation between speed forecast errors and their dependence on the geographical distance is assessed in the following. For each possible pair of wind farms and each forecast hour the correlation between the forecast errors is calculated. The resulting correlation is related to the geographical distance between the locations. The grey mesh (solid lines) in Figure 4.17 shows a graphical representation of the correlations (the z-axis indicates the correlation level).

The results were fitted in order to obtain a general relation. The correlation value is given by a function with three exponential terms, see Equation 4.13, where $\rho_{i,j}$ stands for the correlation between two locations, $d_{i,j}$ for their distance, h for the forecast hour and a_1 to a_4 as fitting parameters. The combination of exponential functions is chosen for the following three reasons. First, the correlations should be zero when the distance is infinite, which is assured by the first exponential term. Secondly, the correlation should increase with the forecast hour, as, with

increasing forecast horizon, the weather situation at a specific location becomes less important and the general weather pattern of the region prevails. This is assured by the second exponential term. Thirdly, the correlation should be one if the distance is zero. The calculated correlation is equal to one if the distance is close to zero as the third exponential term (in the exponent) is then zero.

$$\rho_{i,j} = \exp\left(-a_1 \sqrt{d_{i,j}}\right) \cdot \left(a_2 - a_3 \cdot \exp\left(-a_4 \cdot h\right)\right)^{1-\exp\left(-d_{i,j}*10^5\right)} \tag{4.13}$$

The fitting parameters, found by a least-square optimization, are: $a_1 = -0.0888$, $a_2 = 0.7998$, $a_3 = 0.5034$ and $a_4 = -0.1976$. The blue mesh (dashed lines) in Figure 4.17 shows the correlations calculated by the fitting function.

4.3.2. Simulation of wind power forecasts

A simulation of forecast scenarios by a moment matching approach is presented in the following. After a short overview, the mathematical description of the approach is given. The method is then applied and evaluated by German power forecasts.

Overview

Each optimization of the stochastic market model, see Chapter 3, takes a forecast of the wind power generation into account. The simulation of wind power generation and of the forecasts is based on wind speeds for the reasons given in Section 4.1.1. With regard to the forecasts, one advantage of a simulation based on wind speeds was that it is a more "physical" approach and the statistical changes related to the transformation from speed to power are naturally taken into account. In addition to that, a simulation based on wind speeds also has the advantage that the forecast errors are relatively independent from the wind speed levels, as shown in the precedent Section 4.3.1. The forecast error scenarios are therefore generated independently from the wind speed series. For each optimization of the market model, a forecast error scenario is then drawn and added to the relevant section of the measured wind speed time series resulting in a wind speed forecast scenario and finally in a wind power forecast scenario.

The following simulation approach is applied for two different purposes. On the one hand, error scenarios have to be simulated so that a scenario can be drawn for each market model optimization. Here the number of scenarios that are generated by the simulation approach is not limited. On the other hand, a scenario tree is generated so that stochastic optimization can be applied in the market model. In this case the number of scenarios is limited for the sake of solvability and calculation time of the market model. The first case can be seen as a simulation of an unlimited number of scenario paths representing multivariate, time-dependent random variables in a statistically accurate manner. In the second case, the limitation of the number of scenarios has to be combined with statistical

accuracy as far as possible.

For the first case and with regard to the Wilmar model (a previous version of the market model, see Chapter 3), a method based on ARMA series has been proposed [155]. Auto-regressive moving average (ARMA) series are used in time-series analysis. Auto-regressive expressions are thereby combined with a Gaussian noise and the different parts are weighted by different parameters that define the ARMA series. In the approach the ARMA parameters are derived from exogenously given values of standard deviation and geographical correlations. Many ARMA series are then randomly generated for each location. The generation of a large number of series (scenarios) is thereby necessary to guarantee a good representation of the standard deviation and correlations. Compared to the here developed method, this approach has two drawbacks. First, it is not possible to consider forecast errors that are not Gaussian as ARMA series are based on Gaussian noises. Skewness and kurtosis describing the error distribution and the frequency of extreme events are therefore not taken into account. Secondly, the autocorrelations of the simulated forecast errors are implicitly defined by the ARMA parameters and may not correspond to the autocorrelations of measured forecast errors.

For the second case (the simulation of a limited number of scenarios), one method is scenario reduction, [156, 157, 158], that was implemented in the Wilmar model in combination with the ARMA approach above [159]. The large number of ARMA series is thereby reduced to a small number by eliminating scenarios. The scenarios that are eliminated have to be close to remaining ones (defined by a certain mathematical distance measure) and should have a low probability. Their probability is thereby added to the one of their closest neighbor series. The elimination process is continued until a suitable number of scenarios is reached. In the market model, small scenario trees have to be applied to keep the model solvable. The suitability of the scenario reduction approach to generate small scenario trees was tested by the author in [19, 160]. The scenario trees were thereby evaluated by their performance in the Wilmar market model. Scenario trees generated by a scenario reduction version and by the here applied approach were compared. The performance of the trees was evaluated by comparing the market model results based on small trees to the market model results based on large trees. A scenario tree generation method can be considered as robust if the difference between the results is small. The analysis shows that the moment matching approach (presented below) leads to significantly better results. This is true for the results of the market model applying the trees and also with regard to the statistical accuracy of the trees without looking at the market model results. In general, the later presented approach is useful for the generation of small scenario trees as the considered parameters are specifically selected and defined and the parameters are represented by the generated scenarios in a controlled way. This is important as not all statistical characteristics of the random variable can be considered. Due to the small number of scenarios, only a limited statistical representation of the

random variable is possible. Concluding, the following approach allows to simulate non-Gaussian correlated random variables and to simulate small scenario trees in a statistically robust way. The approach could also be applied to other random variables, for example to simulate photovoltaic or load forecasts.

Moment matching

Moment matching is a general method that applies optimization to match statistical parameters of the scenarios, that are to be found, to the empirical statistical parameters of the random variables, that are to be simulated [161]. In the application examples, see [161], the considered statistical parameters are mean values, standard deviations, skewness, kurtosis and the correlations between the different random variables. The method is here extended by the consideration of autocorrelations and the calculations of the parameters are explicitly given for scenario trees. The following statistical parameters are hence considered in the simulation: mean values, standard deviations, skewness, kurtosis, autocorrelations and geographical correlations. These parameters are equivalent to the mean values, the second, third and fourth central moments, the auto-covariances and the geographical covariances. For technical reasons, the latter are mostly applied in the simulation.

The objective function of the optimization problem calculates the difference between the statistical parameters of the scenarios and the exogenously given parameter assumptions. One possibility of tree generation is to optimize the complete tree in one optimization. As this leads to very large optimization problems a sequential approach is chosen here. In this approach the scenarios of every forecast hour are optimized separately. The optimization problem in Equation 4.14 is solved for forecast hour $h = 1$, where n stands for the number of scenarios and $x_{j,u,h}$ and $p_{j,h}$ give the value and probability of scenario j for wind farm u at the forecast hour h. The statistical parameter k depending on the scenario values and probabilities is calculated by $f_k(x_{j,h}, p_{j,h})$. $SV_{k,h}$ represents the exogenously defined value of the statistical parameter k at forecast hour h. $SV_{k_1,h}$ and $SV_{k_2,h}$ could for example stand for two different statistical parameters at one wind farm or for the same statistical parameters but at two different wind farms. Weighting with w_k allows to emphasize selected statistical parameters.

$$\begin{aligned} \min_{x,p} \quad & \sum_k w_k(\mathrm{f_k}(x_{j,h}, p_{j,h}) - SV_{k,h})^2 \quad , j \in \{1, \ldots, n\} \\ \text{s.t.} \quad & \sum_j p_{j,h} = 1 \\ & p_j > 0 \quad \forall\ j \end{aligned} \tag{4.14}$$

Equation (4.14) applies to the scenarios of the first forecast hours. In the following optimizations, the scenarios of the subsequent forecast hour are simulated. Two

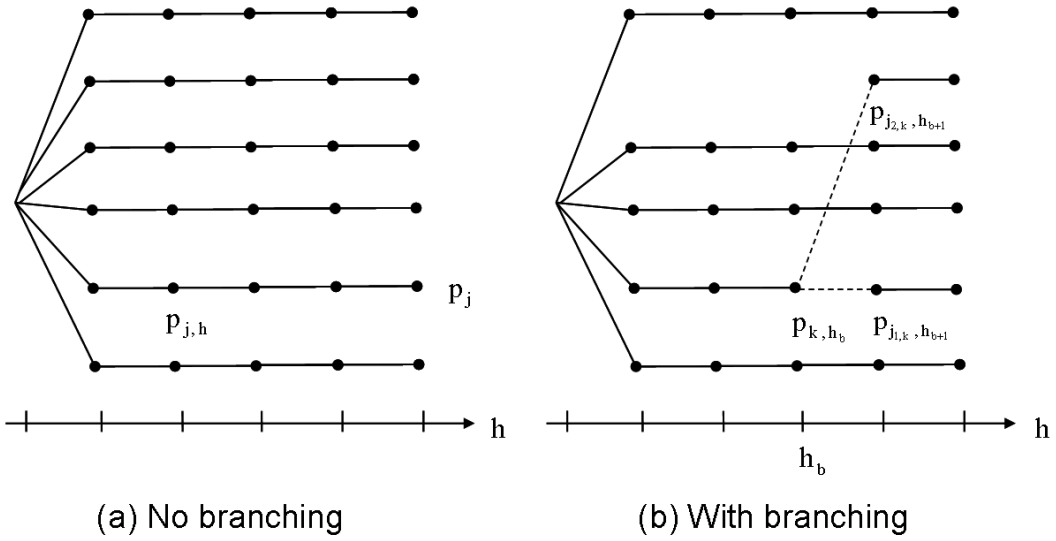

Figure 4.18.: Probabilities in the scenario tree

cases are thereby differentiated. If the scenario paths do not branch, the probabilities are fixed to the ones of the precedent forecast hour. This case is shown in Figure 4.18-a and the corresponding optimization is given by Equation (4.15) (the objective function is equal to the one of Equation (4.14).

$$\begin{aligned} \min_{x,p} \quad & \dots \\ \text{s.t.} \quad & p_{j,h} = p_{j,h-1} \quad \forall\ j \end{aligned} \tag{4.15}$$

In the case that a scenario tree in its literal meaning is generated the scenario paths have to branch. A scenario tree with more scenarios at the end may be wanted to reduce the number of scenarios at the beginning without neglecting the increase of variance with increasing forecast horizons. Figure 4.18-b shows the branching of a scenario. A "parent" scenario path branches into two "child" scenario paths and their probabilities sum up to the probability of the parent. The related restriction in the optimization problem is given by Equation (4.16).

$$\begin{aligned} \min_{x,p} \quad & \dots \\ \text{s.t.} \quad & \sum_{j_k} p_{j_k,h} = p_{k,h-1} \quad \forall\ k \\ & p_{j_k} > 0 \quad \forall\ j,k \end{aligned} \tag{4.16}$$

where the parent scenarios k split into the child scenarios j_k

In the following, the calculation of the parameters in the objective function is explained. For the purpose of readability the parameters are presented separately. The calculation of standard deviation and mean value is shown by the example

objective function in Equation (4.17). It refers to the case of a single wind farm, considering a given mean value, denoted by SV_M, and a given standard deviation, denoted by SV_S, without the application of weighting factors.

$$\min_{x,p} \quad (\sum_j x_j p_j - SV_M)^2 + (\sqrt{\sum_j p_j (x_j - \sum_j x_j p_j)^2} - SV_S)^2 \tag{4.17}$$

The third or fourth central moment are also considered. Their calculation under consideration of probabilities is given by Equation 4.18.

$$\begin{aligned} \text{3th Central Moment} &= \sum_j p_j \left(x_j - \sum_j x_j p_j\right)^3 \\ \text{4th Central Moment} &= \sum_j p_j \left(x_j - \sum_j x_j p_j\right)^4 \end{aligned} \tag{4.18}$$

Autocovariances are added to capture the dependencies between scenario values of different forecast hours. Equation (4.19) and (4.20), show the calculation of autocovariances ("AutoCov") with a lag of one for the case without branching and with branching. Autocovariances with different lags are considered in a corresponding way.

$$\text{AutoCov} = \sum_j p_j \left(x_{j,h} - \sum_j p_j x_{j,h}\right)(x_{j,h-1} - \sum_j p_j x_{j,h-1}) \tag{4.19}$$

In the branching case, k stands for the parent scenarios and j for all children scenarios whereas j_k refers to the children scenarios of a specific parent k. There are fewer parents than children and, for each parent, the children have to be summed up first in the calculation.

$$\text{AutoCov} = \sum_k p_k \left(x_{k,h-1} - \sum_k p_{k,h-1} x_{k,h-1}\right)(\sum_{j_k} p_{j_k,h} \left(x_{j_k,h} - \sum_j p_{j,h} x_{j,h}\right))$$

where the parent scenarios k split into the child scenarios j_k

(4.20)

Finally, the covariances between the scenarios at different wind farms are considered. There is a scenario tree for each wind farm location. The values of the scenarios are different for each tree but the probabilities are equal. With $x_{j,h}^{\text{Wf1}}$ and $x_{j,h}^{\text{Wf2}}$ standing for the scenario values at wind farm one respectively wind farm two the covariance ("Cov") between the scenarios at the two wind farms can be calculated by Equation (4.21).

$$\text{Cov} = \sum_j p_j \left(x_{j,h}^{\text{Wf1}} - \sum_j p_j x_{j,h}^{\text{Wf1}}\right)(x_{j,h}^{\text{Wf2}} - \sum_j p_j x_{j,h}^{\text{Wf2}}) \tag{4.21}$$

With n wind farms the number of independent geographical covariances for one forecast hour is $0.5 \cdot n \cdot (n-1)$. In addition to that, the mean values, standard

deviations, third and fourth central moments and autocovariances are given at each wind farm. For the case that only autocoavariances with a lag of one are considered, the total number of parameters in the objective function is equal to $(4+1) \cdot n + 0.5 \cdot n \cdot (n-1)$.

Application of moment matching

The presented moment matching approach is applied to simulate scenarios of wind speed forecast errors at 36 German locations according to Figure 4.2. The parameter values that are used in the simulation are indicated in the previous Section 4.3.1. The values of the standard deviations are thereby adapted in two ways. They are adapted to the size of the area that is represented by the wind farm location as forecast errors in an area partially level themselves. There are several wind farm locations in a model region and each wind farm represents a sub-area of the region. Focken, [146], gives a relation of the improvement of forecast quality in dependence of the area size. This relation is used to adapt the standard deviations to the size of the aub-area that is represented by the wind farm. Additionally, the value of the standard deviations can be adapted to adjust the forecast quality, for example simulating future forecast improvements. The standard deviations are thereby scaled by a linear scaling factor (equal for all locations). The linear scaling factor is also used to calibrate the simulation to the forecast quality of measured German power forecast.

Two kinds of scenario bundles are generated by the moment matching approach: a large bundle with 50 scenarios that is used to draw single forecast scenarios for the deterministic optimizations in the market model and a small bundle with 6 scenarios that is additionally used if stochastic optimizations are applied in the market model. In the case of the large bundle, no special weighting of the statistical parameters is required in the moment matching process as all parameters can be matched without difficulties. This is a convenient result that is not self-evident for all simulation techniques. In simulation methods that are based on random elements, a high number of draws may be necessary to have a statistically accurate result. However, the error distribution is then not fully considered in the application if only a limited number of random scenarios are selected for it. This is for example the case if one year is modeled and 365 day-ahead forecasts are drawn, but the simulation of the forecasts is based on many more random scenarios than 365.

In the case of the small scenario bundle, all parameters can not be matched equally well as there are not enough scenarios or, in other words, enough degrees of freedom [161]. Having 36 locations with 6 scenarios plus the probabilities (equal at all locations) results in $36 \cdot 6 + 6 = 222$ degrees of freedom. On the other side, 9 parameters at each location and the spatial correlations have to be matched, in total $36 \cdot 9 + 630 = 954$ parameters. This comparison indicates that all parameters cannot be matched accurately. The standard deviation are therefore

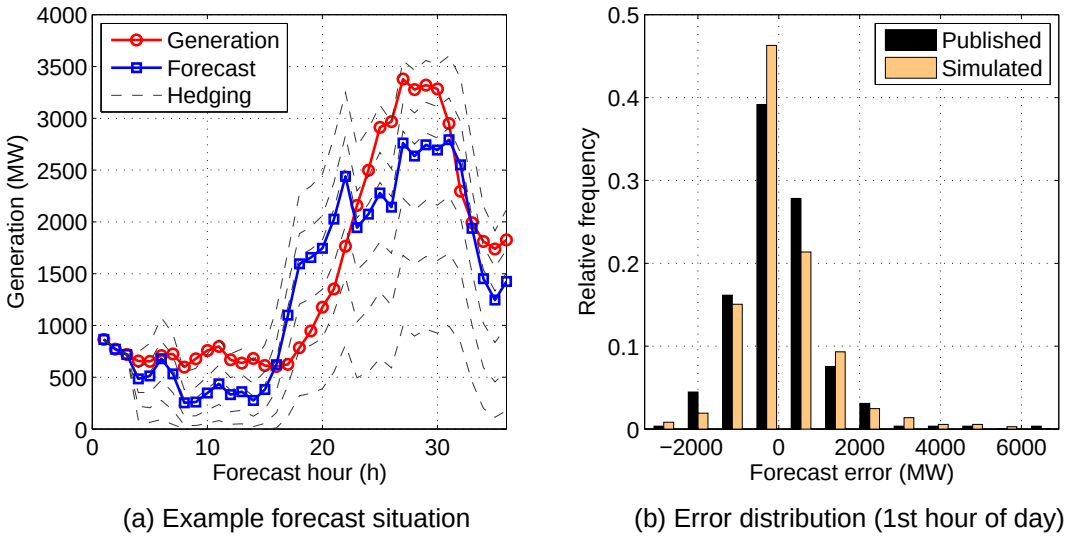

(a) Example forecast situation (b) Error distribution (1st hour of day)

Figure 4.19.: Error scenarios and their distribution

considered by a higher weighting parameter in the moment matching approach of Equation (4.14). An accurate matching of the standard deviations is important as they represent forecast quality.

Evaluation of power forecasts

The simulation of forecasts is based on wind speed forecasts. In the market model, only the wind power forecasts are of relevance. The simulated wind power forecasts are therefore evaluated in the following comparing simulated power forecasts to day-ahead forecasts in Germany. The four German transmission operators publish the wind power generation and the corresponding day-ahead forecasts for each hour of the day. Data from November 2006 to August 2007 is applied in the evaluation. The evaluation is limited as data before November 2006 was not available and the simulation is based on speed data from 2006. It can however be tested if the simulated power forecasts show the same statistical behavior as the measured ones. Figure 4.19-(a) shows a typical simulated forecast situation. The expected value forecast is given by the line with squares. The wind power generation that will actually be available is indicated by the line with circles. If the market model applies stochastic optimization, the scenarios indicated by the dashed lines are also considered in the optimization. The scenarios thereby have different probabilities with very low probabilities for the extreme scenarios. The distributions of the German day-ahead forecast errors, simulated and published, are shown in Figure 4.19-(b). The distributions of the forecast errors are similar. In both cases, large positive forecast errors can occur representing an overestimation of the wind power generation. In the most extreme cases, the wind power generation is about 6000 MW (equal to about 30% of the installed capacity) lower than it was pre-

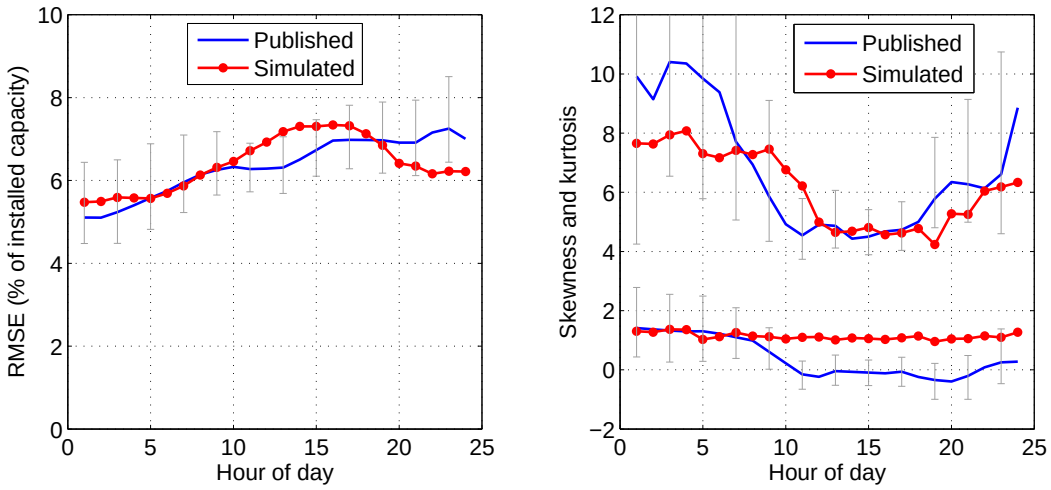

(a) Root mean square error (b) Skewness and kurtosis

Figure 4.20.: Parameters of measured and simulated German day-ahead forecast

dicted. These distributions can only be indicative as they are based on relatively small samples (291 data points for the published data).

Statistical parameters of the simulated and published day-ahead forecasts are compared by Figure 4.20. The root mean square errors representing forecast quality as well as skewness and kurtosis describing the distribution shape are given for each hour of the day. As the applied published data is based on 291 data points only (for each hour of the day), 95% confidence intervals (given by the grey error bars) are also shown.[13] The root mean square errors of the simulated and published forecasts are very similar especially considering the confidence intervals. The simulated and published forecasts also have similar characteristics looking at skewness and kurtosis. The decrease of the kurtosis at the middle of the day is for example well matched. A high kurtosis, as it is especially given at the earlier hours, indicates an increased frequency of extreme events in comparison to a normal distribution. The skewness of the simulated and published forecast errors are very similar at the beginning of the day but a skewness decrease in the second half of the day is not followed by the simulation. Looking at all parameters, the simulated forecasts can be considered as representative for the German power forecasts (also considering that the comparison is based on different time periods for the simulated and published forecasts).

An important advantage of the simulation is that it allows to model power forecasts for single regions. The simulation of regional power forecasts is evaluated applying the published forecasts for the Vattenfall control area. This control area corresponds to the five eastern German model regions (MV, BB-BE, S, SA, TH) so that a comparison of the simulated and published forecasts is possible. The

[13]The confidence intervals are computed using a Matlab bootstrapping function.

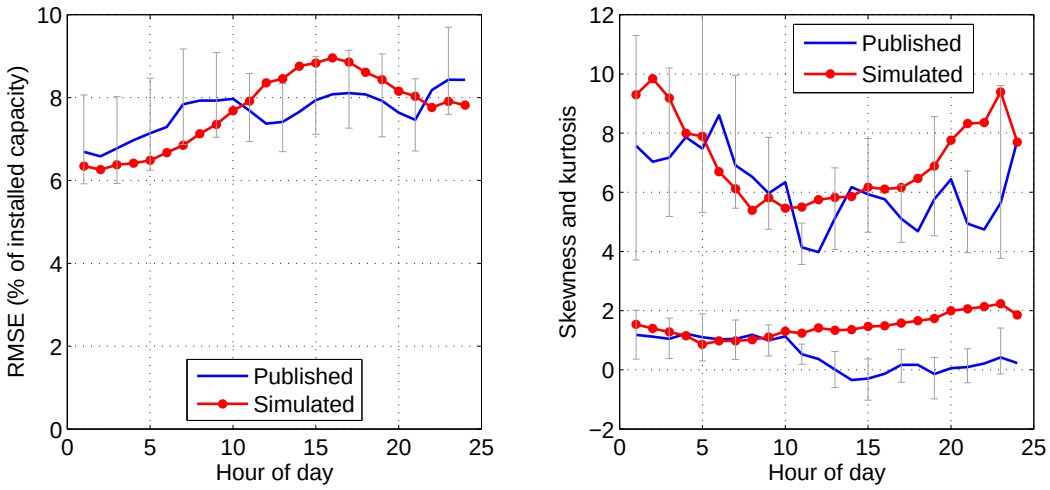

(a) Root mean square error (b) Skewness and kurtosis

Figure 4.21.: Parameters of measured and simulated Vattenfall day-ahead forecast

considered time periods are however not equal as explained above allowing only a general comparison of the statistical behavior. Figure 4.21 shows the root mean square errors and the distribution parameters for both cases. Again, confidence intervals are also indicated. As for the German case, the root mean square errors and kurtosis are similar whereas there is a discrepancy of the skewness for the second half of the day. The root mean square errors are by about one percent point higher than in the case of German forecasts as forecast quality decreases with decreasing region size. Concluding, the presented simulation being based on wind speeds and on a moment matching approach leads to statistically representative wind power forecasts. Power forecasts for single model regions can thus be simulated.

5. Analysis of base scenario and integration measures

In the following, different scenarios of the German power system in 2020 are analysed. The presented power system model (Chapter 3) and wind power simulation (Chapter 4) are thereby applied. The model results show how the power system is operated with high shares of wind power and the amount of curtailment that is required. The base scenario is compared to a high wind year and a high fuel price scenario and the influence of wind forecasts is discussed. The costs of forecast errors, hedging of errors and different levels of tertiary reserves are evaluated. In the subsequent sections integration measures are analysed by modifications of the base scenario. First, integration measures are regarded that are related to an increase of flexibility in the system. Additional storage capacities, changes in the demand curve due to demand side management and a higher thermal flexibility are covered here. The importance of stochastic modelling for the evaluation of these measures is also shown. A second type of integration measures is related to power transmission. Infrastructural changes like grid extensions or an adapted geographical allocation of power plants are thereby evaluated. Additionally, the maximal potential of grid expansions is assessed by a copperplate grid. All integration measures are compared in the last section, both for the base and for the high wind case.

5.1. Base scenario with price and wind variation

Two modifications of the base scenario are analysed. The base scenario is thereby defined as described in Section 3.2 and Section 4.1. The scenarios are analysed with regard to system costs, power generation, curtailment, transmissions and the average and regional electricity prices.

Definition

The two scenario variations evaluate the influence of higher fuel prices and higher wind yields. In the high price scenario, the oil and gas prices are increased by 20% according to Table 5.1. These price variations as well as the unchanged coal price are in accordance with the price differences that are indicated by a reference and a high growth scenario in the World Energy Ooutlook [162]. The high wind

Table 5.1.: Fuel prices for 2020 (€/MWh)

Fuel type	Base scenario	High price scenario
Oil	31.99	38.40
Gas	25.49	30.60
Coal	8.91	8.91
Lignite	3.77	3.77
Nuclear	1.75	1.75
Biomass	23.00	23.00

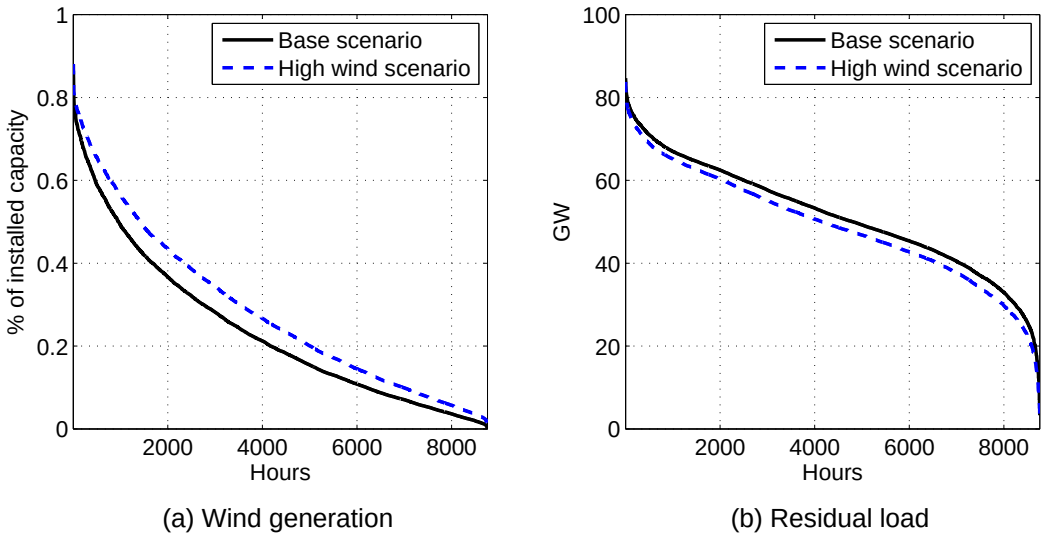

Figure 5.1.: Duration curves of wind power generation and residual load

yield scenario is defined by a stronger wind year resulting in a 20% higher yearly generation for all countries. Compared to the base scenario, the German onshore capacity factor is then 0.216 instead of 0.18 (1892 full load hours instead of 1577) and the offshore capacity factor is 0.438 instead of 0.365 (3837 full load hours instead of 3197). The duration curve of the wind power generation rises due to the higher capacity factor according to Figure 5.1-a. The resulting residual load curve (the demand minus the photovoltaic, wind and hydrorun generation) is given in Figure 5.1-b for both cases. In some hours the residual load values are near to zero but they are never negative.

Results

The German system costs, shown in Figure 5.2-a, aggregate all fuel costs, emission taxes and other operational costs. The international imports or exports are thereby considered as income or expense (the exchanges are multiplied by the day-ahead

prices of the importing region). The costs do not include any investment costs or any renewable energy feed-in tariffs. They only represent the operational costs that are required to cover the residual load for a given renewable energy feed-in.

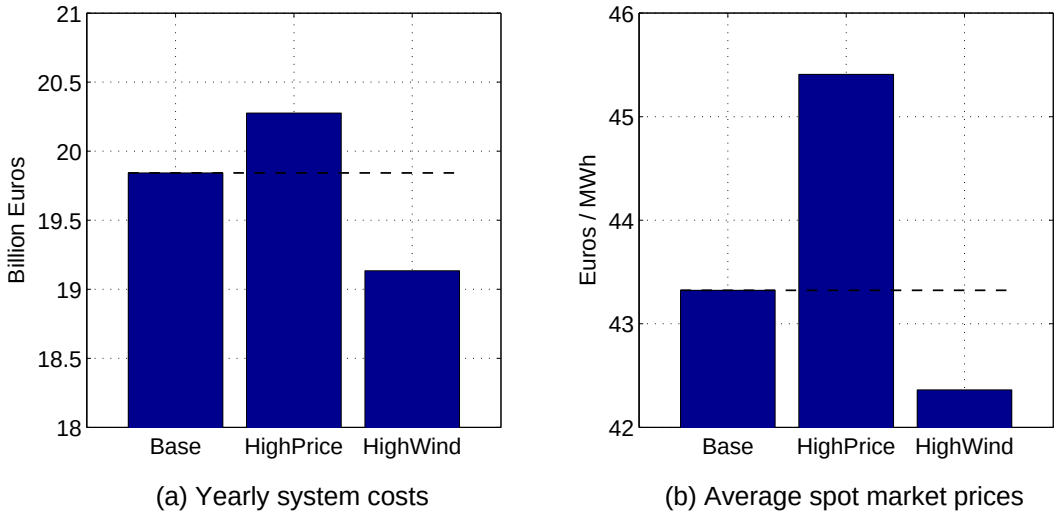

(a) Yearly system costs

(b) Average spot market prices

Figure 5.2.: Total system costs and day-ahead electricity prices

With higher gas and oil prices, the system costs increase by 2%. The average day-ahead electricity price rises by 5%, from about 43 €/MWh to more than 45 €/MWh. The price increase is more important than the cost increase as the marginal units are often gas units. The electricity prices (so the marginal system costs) are often set by the gas power plants but gas is less important with regard to the aggregated power generation. In the base case, only 5% of the generation is given by gas, see Figure 5.3-a. The influence of the gas price on the system costs is therefore small. In addition, with higher gas prices, gas generation is avoided and shifted to other power plants.

In a high wind year, the system costs decrease by 3.5%. Due to the large wind power capacities, the wind yield has a noticeable influence on the system costs. The wind power generation in the two scenarios differs by more than 20 TWh. The average prices only decrease by 2% in the high wind scenario. This is because the additional wind power generation is compensated by less coal and lignite power, see Figure 5.3-a. The use of gas power plants is similar to the base scenario.

In general, the power mix is characterized by high coal and lignite power shares. Wind power is the third power source. The rest is shared between biomass (misc), PV, gas, nuclear and water power. The renewable energy sources count for 31% of the generation. In all scenarios, Germany is a net exporter. In the high wind year, 1 TWh of the additionally available 20 TWh are exported. A significant amount of wind power is also curtailed, see Figure 5.3-a. The aggregated German residual load curve (Figure 5.1-b) does not suggest such an curtailment as there are no negative residual load levels. The curtailment results from the limited transmission

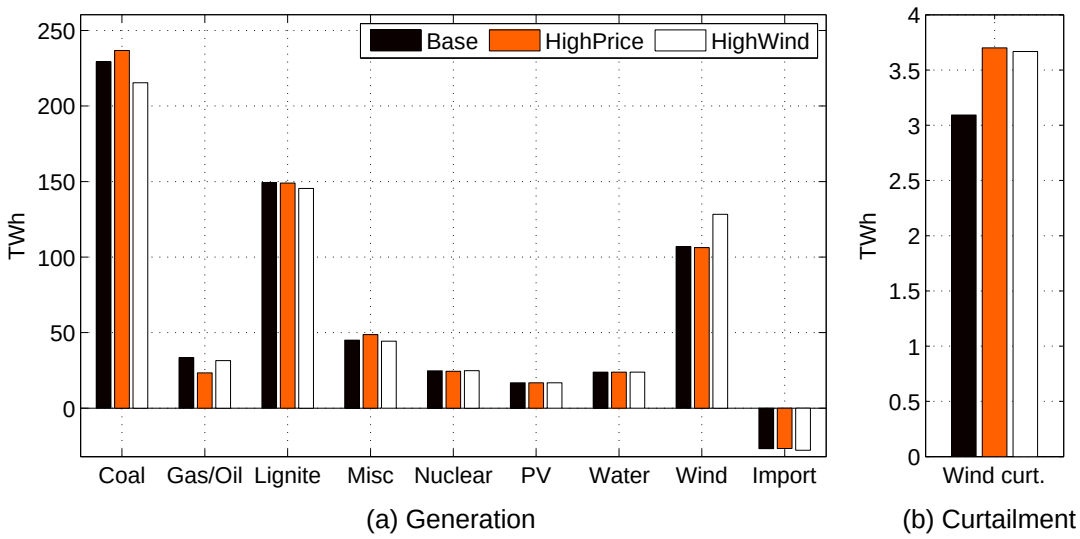

Figure 5.3.: Power generation with imports and curtailment of wind power

capacities that are analysed in detail in Section 5.4. More than 3 TWh of available energy are curtailed in one year. The curtailment rises to 3.7 TWh in the high wind scenario. Higher gas prices also lead to more curtailment. Due to the higher prices more coal capacities are used. As their flexibility is lower, curtailment is more often required. The results show that the modelled power system is not optimally designed for the high wind power shares. The transmission capacities are for example not sufficient to transport the electricity to the regions where the highest costs reductions could be achieved.

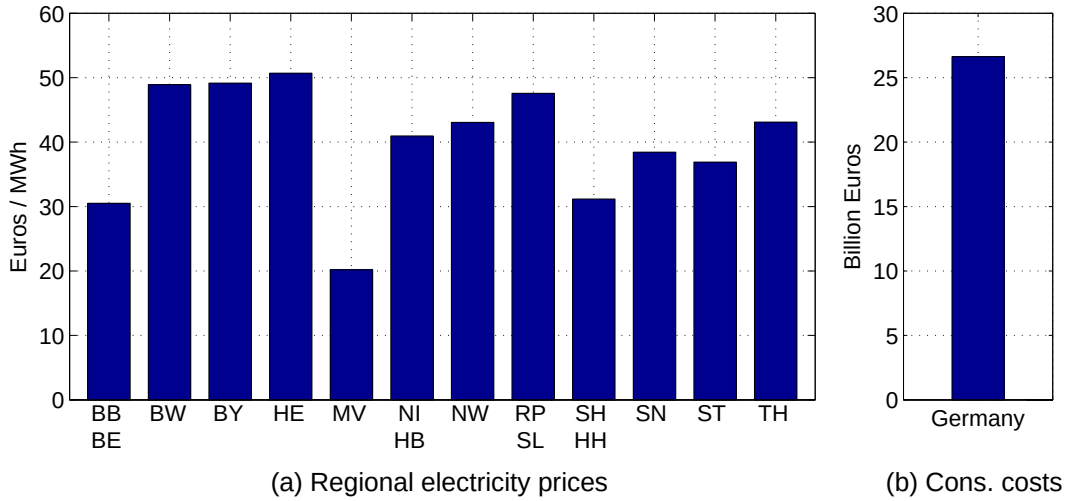

Figure 5.4.: Regional prices and consumer costs in the base scenario

Transmission constraints are also shown by the significant price differences be-

tween the German regions, see Figure 5.4-a. The average prices differ by more than 100% in the most extreme cases. With infinite transmission capacities, the prices would be equal in all regions. The lowest prices occur in Mecklenburg-Vorpommern. In this region, high amount of capacities and especially lignite capacities are installed compared to the demand level (see Figure 3.5). In Hessen, the high electricity prices are explained by the lack of capacities compared to the demand. In addition, there are high shares of gas power. A low level of installed capacity also explains the high prices in Bayern, Baden-Württemberg or Rheinland-Pfalz.

The electricity costs for the consumers (without grid tariffs or taxes) are calculated by multiplying the regional prices with the regional electricity demands. A market design with regional electricity prices is thereby assumed. The German consumer costs amount to about 26 billion Euros per year, see Figure 5.2-b. The difference between consumer costs and operational system costs indicates how much money is available in the system to cover the fix costs. With total operational costs below 20 billion Euros and consumer costs above 26 billion Euros, more than 6 billion Euros remain for the investment costs and profits.

The electricity exchanges within Germany and at the German borders are shown in Figure 5.5. For each connection, the aggregated yearly exchanges are indicated in both directions (in the positive and negative direction of the arrow) and their sum is equal to the net balance between the two related regions. The general transmission direction within Germany is from North to South and from East to West. This is due to the wind power in the North and the lignite power plants in the East. The electricity demands are also lower in these regions. An exception is Baden-Württemberg (BW) that is a net exporter due to its nuclear capacities and the electricity arriving from the country borders. The electricity therefore goes from BW to the North and East. At the South-Western borders of Germany high exchanges can be seen in both directions. This is due to reimported electricity that originally comes from the North. In fact, high shares of wind power arrive that from the North Sea to Niedersachsen (NI) are then exported to the Benelux countries, either directly from NI or via Nordrhein-Westphalen (NW). At these Western borders, no electricity is imported at all. At the Eastern borders of Germany electricity is exported reflecting the East-West direction within Germany.

5.2. Forecast quality, reserves and risk hedging

The influence of wind forecast errors is analysed in the following section by a comparison of the base scenario and a scenario with perfect forecasts. The effects of forecast errors can be attenuated by the application of risk management and hedging. Related benefits are estimated by a model run based on stochastic optimizations.

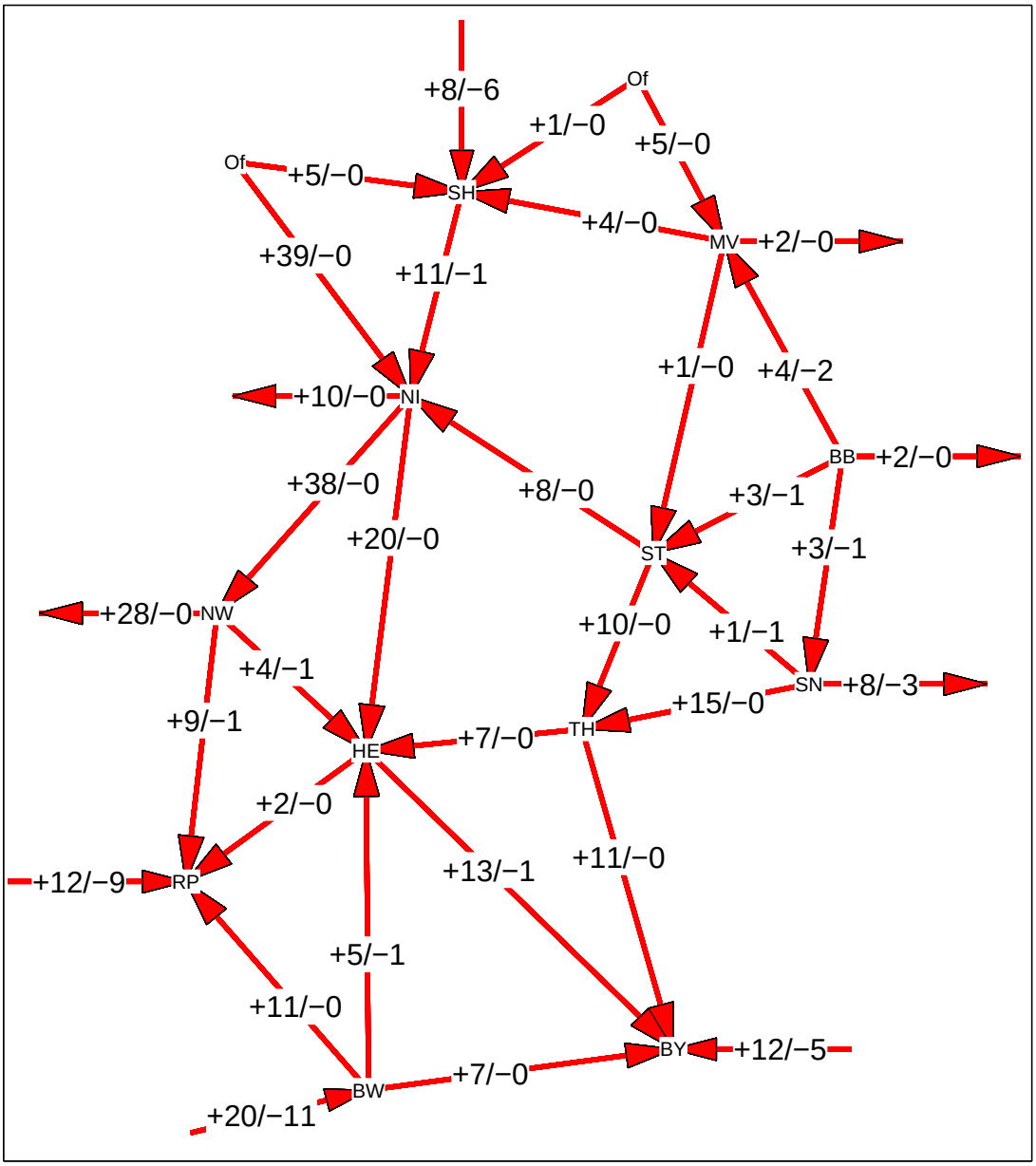

Figure 5.5.: Yearly exchanges in positive and negative direction (TWh)

Definition

The stochastic model concept allows to estimate the costs of wind forecast errors and the potential benefits of risk hedging methods. In the base scenario, the model is exposed to wind forecast errors as it is also the case for the operation in reality (Figure 3.1-a). In a "perfect forecast" scenario, the model has perfect foresight on the future wind power generation.[1] Two cases are here differentiated. In the first case, the tertiary reserve requirements are equal to the base scenario. The reserve requirements are therefore calculated with wind forecast errors and perfect foresight is only given on the energy markets (day-ahead and intraday). In the second case, the reserve requirements are calculated without wind forecast errors resulting in lower reserve levels. The reserve requirements for both cases (denoted by "Perfect" and "Absolutely Perfect") are shown in Table 5.2. The comparison of the base and the "perfect forecast" scenario allows to evaluate the influence of forecast errors.

Table 5.2.: Tertiary reserves requirements (MW)

Model region	With Wind Forecast Error	No Wind Forecast Error
D-BB-BE	364	173
D-BW	836	398
D-BY	909	433
D-HE	449	214
D-MV	83	39
D-NI-HB	673	320
D-NW	1744	830
D-RP-SL	451	214
D-SH-HH	352	168
D-SN	240	114
D-ST	165	79
D-TH	127	60
D total	6394	3042

The effects of forecast errors can be attenuated by risk hedging methods. In the model, this is represented by the use of stochastic optimization (see Figure 3.1-b). The stochastic optimization mode stands for an ideal application of risk hedging methods. It is an ideal representation for the following reasons. The scenario trees that are used in the stochastic optimizations are simulated based on perfect knowledge of the forecast error distribution. In reality, perfect distribution information is not available. Moreover, the delivered information of the error distribution is fully exploited by the model and it is considered in the dispatch of all power plants. In reality, power plant operation is determined by many factors in the markets and hedging of risks will not always have the highest priority. Besides, it is questionable if the market participants are able to apply hedging if there are

[1] A 20% improvement of forecast quality is already considered in the base scenario.

many small bids in the market from many different participants. The scenario with stochastic optimization is denoted by "Hedged". The reserve requirements are thereby equal to the base scenario.

Results

Forecast errors only have a small impact on the system costs. 0.9% of the system costs are caused by forecast errors. The difference is small in relative terms as the costs are mainly determined by the energy demand. In absolute terms, the costs due to forecast errors amount to 178 million Euros per year, see Figure 5.6-a. The application of hedging methods can reduce the yearly costs to 38 millions. This is a cost reduction of 80% but it can only indicate the maximal potential of hedging as explained above. Interestingly, higher tertiary reserve requirements have nearly no influence on the system costs ("Perf." and "Abs.Perf."). Tertiary reserve requirements cause nearly no costs in the system as, most of the time, some capacities (like gas turbines) are idle in the system and can be used as tertiary reserves. The average price on the tertiary reserve market is therefore only 0.005 €/MW.

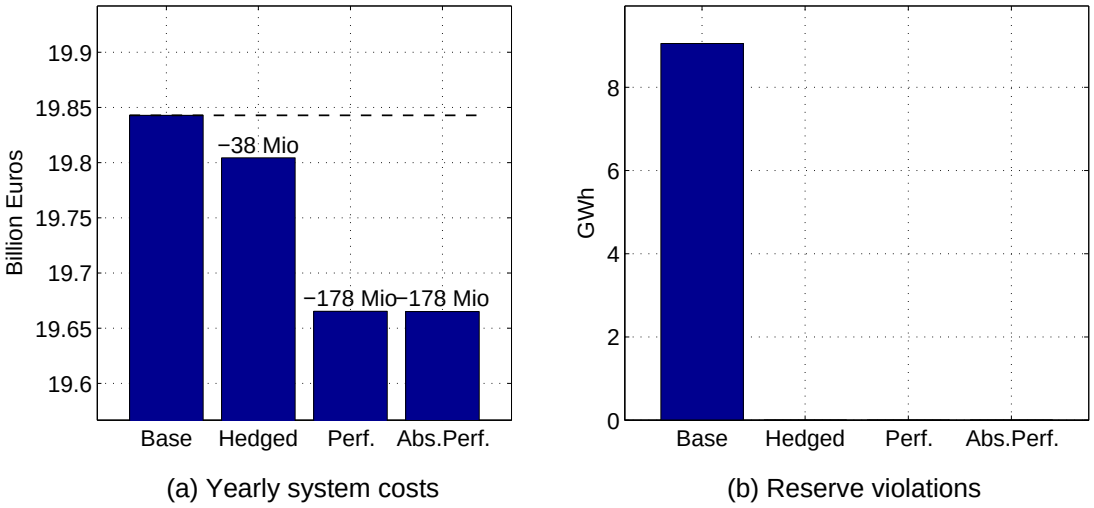

Figure 5.6.: Total system costs and reserve violations

The benefits of better forecasts are more significant looking at the reserve violations. Reserve violations indicate hours when the system cannot balance the demand or forecast errors. The reserve requirements are then no longer respected.[2] The penalties for the system violations are not considered in the system costs.[3] In the base case, the violations occur in 8 hours corresponding to a total energy

[2]This holds if the system violations do not exceed the reserve capacities as it is the case here. Otherwise, they would stand for loss of load situations.

[3]A discussion of the penalties is given in the final section of the chapter.

of about 8 GWh. Without forecast errors, violations no longer occur. Also with hedged forecast errors the system becomes stable and violations are prevented. This shows one important benefit of hedging methods. The system is not so sensitive to extreme forecast errors and system imbalances can be prevented.

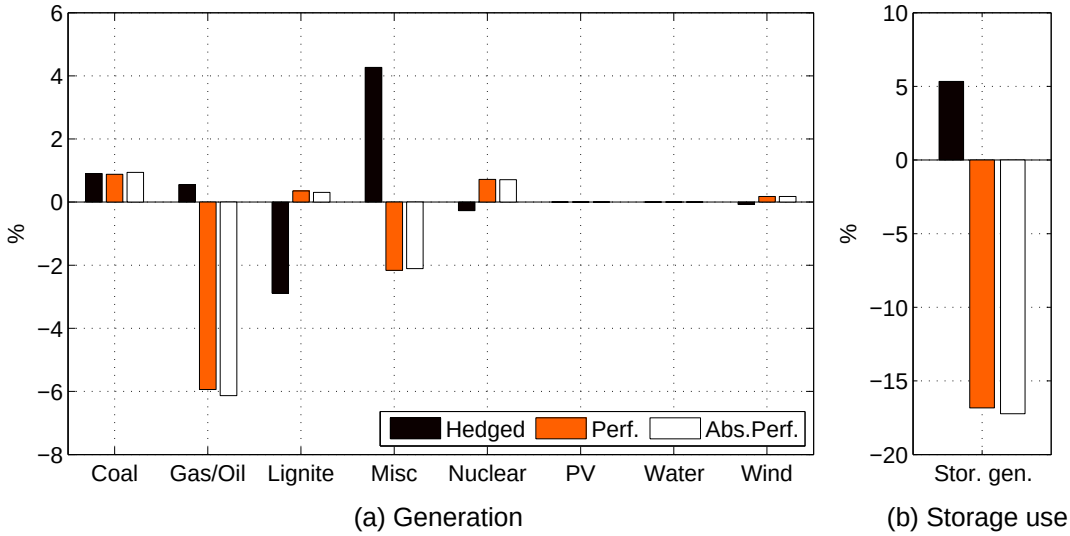

Figure 5.7.: Percentage changes of the generation compared to the base scenario

The generation mix is only slightly influenced by the forecast errors as shown by Figure 5.7. The most important changes are given for gas. With perfect forecasts, the gas use is reduced by 6% as there is no need of balancing actions. The gas is mostly replaced by coal capacities. The hedging case leads to an interesting misceallonous picture. Lignite is less used than in all other cases. This is due to the stochastic optimization approach that takes into account different realizsations of the wind input. The model plans the operation in such a way that it can react to different scenarios. This planning approach is distinct for the hedging case. The relatively inflexible lignite plants are therefore less used. Correspondingly, more gas power plants are chosen in the planning to be more flexible in the case of forecast errors. The storage generation shows the largest differences between the scenarios. With forecast errors, the use of storage is clearly reduced indicating the reduced flexibility requirements. In the hedging mode, the model uses more storage generation in the planning phase so that it can react to potential forecast errors.

The different planning approaches are also illustrated by generation curves of one exemplary day according to Figure 5.8. Negative values stand for the energy that is stored. The two smooth red lines show the wind energy that was predicted by the precedent day-ahead forecast. In Figure 5.8-a and -b, more wind was predicted than it is now available. In the perfect forecast case, Figure 5.8-c, the lines are equal to the available wind power. A comparison of the base and the perfect foresight scenario shows that the missing energy is mainly balanced by gas

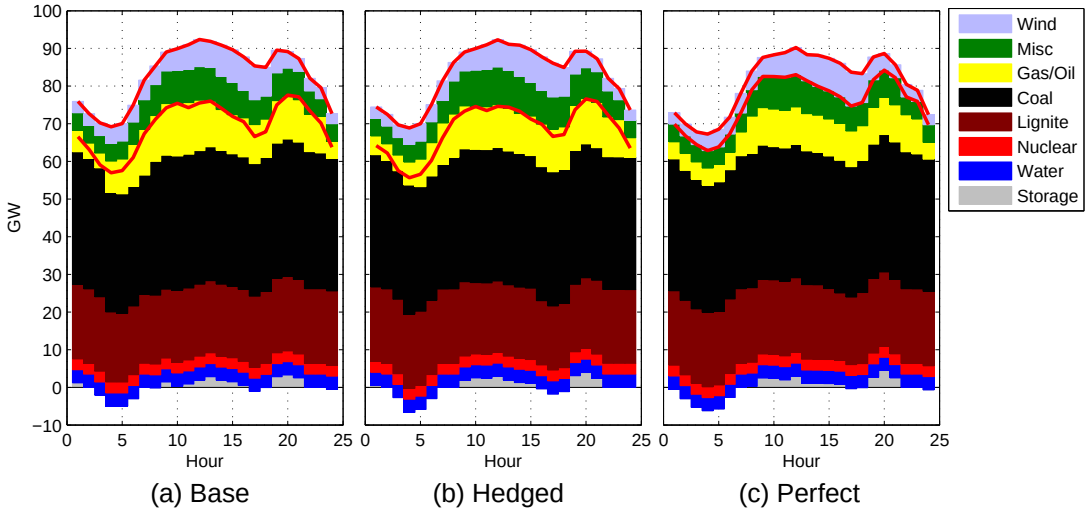

Figure 5.8.: Generation of one exemplary day for the "Base", "Hedged" and "Perfect" case

power generation. The differences are however small. This is also due to the fact that three intraday optimizations have already taken place between the day-ahead planning and the intraday optimization results shown here. These precedent intraday optimizations were already based on updated forecasts correcting the errors of the day-ahead forecasts and reducing the effects of forecast errors. In Figure 5.8, the forecast errors also have a small influence on the cross-border transmission. The maximal generation is slightly higher (just above 90 GW) with forecast errors than without. Due to an optimistic wind power forecast, more export was planned in the day-ahead optimization. The international cross-border changes are fixed in the day-ahead market and they cannot be adapted in the intraday loops. The generation is therefore slightly lower in the case of perfect forecasts.

5.3. Flexibility improvements: CAES, DSM and thermal flexibility

The benefits of CAES power plants and of peak shifting (demand side management) are evaluated in the following. Additionally, a scenario with a higher thermal power plant flexibility is regarded to estimate the potential of thermal flexibility improvements.

Definition

Adiabatic storage capacities with a total capacity of 1 GW are added to the model in the "CAES"-scenario. The capacities are placed in Niedersachsen. Most of the

German caverns that are suitable for gas storage are located there [163]. The energy storage capacities of a CAES plants reach from 2000 to 20000 MWh [164]. For the here added CAES plants, a total storage capacity of 50000 MWh is chosen. This figure is related to an assessment of the German cavern capacity that is assumed to be available for CAES [165]. Related estimations are however difficult as the caverns can also be used for the storage of CO_2 or natural gas [166]. The overall efficiency of the CAES plants is set to 0.7 [167, 168]. The CAES parameters are summarised in Table 5.3.

Table 5.3.: CAES plants in "CAES"-scenario

Parameter	**Value**
Location	D-NI
Total capacity (GW)	1
Total storage capacity (MWh)	50000
Efficiency	0.7

Demand side management (DSM) can be classified into two types that are often addressed at the same time [169]. First, DSM can lead to a reduction of energy demand by encouraging energy saving behaviour. Secondly, DSM can lead to a temporal shifting of the demand keeping the total demand constant. The shifting thereby leads to increased system efficiency on the supply side so that, ultimately, energy is also saved. Here, only the second type of DSM is regarded. The total electricity demand is then equal in the scenarios and a comparison is possible. DSM measures that shift energy demand from one sector to another are therefore not regarded (e.g. heat pumps or electrical vehicles that shift energy demand from the heat or traffic sector to the electricity sector). Temporal shifting of demand within the electricity sector is motivated by price differences. Flexible electricity tariffs with higher prices in high demand hours are required for it. According to the costumer type, the tariffs can be more or less sophisticated. Peak shifting becomes more practical by using automated services that control selected appliances as for example washing machines.

The potential of German peak shifting is uncertain. Studies from other countries may be misleading as the shifting potential can be much higher. Air conditioning units are for example not so important in Germany. A study assigned by the German grid operator ("Bundesnetzagentur") states that there are only a few studies explicitly analysing the German conditions for DSM [170]. Comparing the different studies, a potential of 5% for demand shifting in households is regarded realistic. As households represent less than one third of the electricity demand and assuming that the remaining potential for flexible tariffs and shifting is limited in the industry sector, the shifting potential related to the total demand will be lower. A shifting of 1% of the total demand, equal to 6 TWh, is here assumed.

After applying the following smoothing approach, the maximal peak clipping in single hours does not exceed 7% and the maximal raise in low demand hours does not exceed 11%.

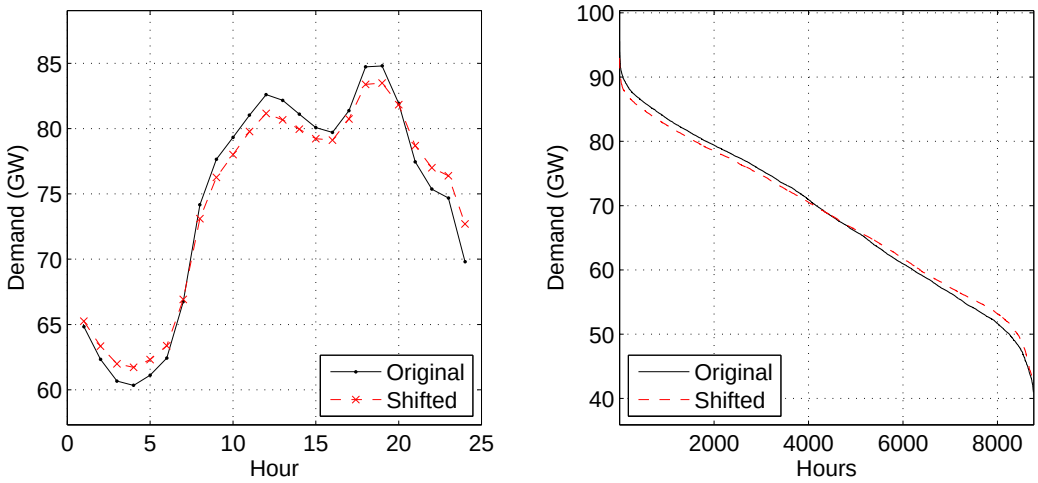

(a) Exemplary day (b) Duration curve

Figure 5.9.: Shifting of demand

In the smoothing approach the residual demand (the demand minus the wind, PV and run-of-river power) is considered first. The residual demand is smoothed for each day by reducing the demand values above the daily average and raising the values below the daily average. The relative reduction or raise is thereby equal in all days and it is calculated so that the total shifted residual demand is equal to 6 TWh. The observed changes in the residual demand are then added to the original demand and the resulting demand curve is applied in the model. Figure 5.9-a shows the shifting for one exemplary day. The resulting duration curves are given in Figure 5.9-b.

The design of new power plants could be adapted to a more flexible operation. The analysis in Section 2.2.1 showed that there is already a high uncertainty about the flexibility of existing power plants. The potential for future flexibility improvements is therefore difficult to estimate. A Siemens product study states that the flexibility of combined cycle power plants can be improved by 50% [106]. This value is here used as an indication for a thermal flexibility scenario. The new power plant capacities that are expected to be built between 2010 and 2020 (Figure 3.6) are thereby modified. Their flexibility is raised by 50%. The flexibility of turbines, being already highly flexible, stays unchanged. The related operational parameters are given in Table 5.4 together with the ones of the base scenario.

In the following, the scenario with CAES capacities is denoted by “CAES”, the peak shifting scenario is denoted by “DSM” and the flexibility scenario is denoted by “Flexi”.

Table 5.4.: Operational parameters of new capacities in the base and flexibility scenario

	Base			Flexibility		
	Coal	**Lignite**	**CC**	**Coal**	**Lignite**	**CC**
Start-up fuel (MWh/MW)	2.5	2.5	0.8	1.25	1.25	0.4
Start-up costs (€/MW)	25	20	50	12.5	10	25
Start-up time (h)	5	5	2	2.5	2.5	1
Minimum up-time (h)	4	6	4	2	3	2
Minimum down-time (h)	3	6	2	1.5	3	1

Results

The system costs are compared in Figure 5.10-a. All three flexibility improvements lead to cost reductions. The additional CAES capacities have a small influence on the system costs. The yearly cost reduction is three times lower as in the "DSM" or "Flexi" scenario. The CAES capacities are concentrated in one region. Demand side management or improved plant flexibility are more global measures that have more influence on the costs. Both scenarios lead to cost reductions of about 70 millions. It is however important to note that the costs of reserve violations are not considered here. The CAES plant is more benefitial with regard to these violations as shown below.

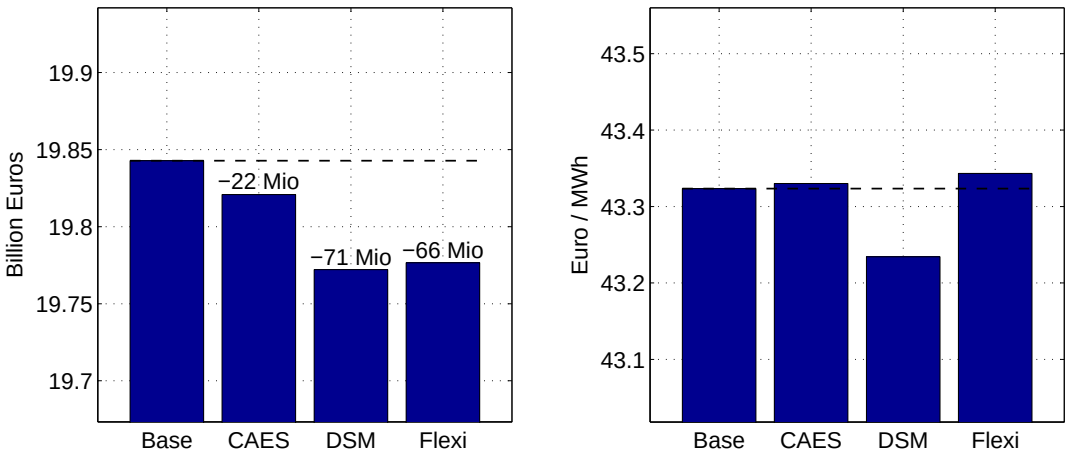

(a) Yearly system costs

(b) Average spot market prices

Figure 5.10.: Total system costs and day-ahead electricity prices

The cost reductions are analysed in more detail by Figure 5.11-a. The differences of the cost curves related to the base scenario are shown.[4] The small plot at the top shows the cost curve of the base scenario. In the CAES and DSM scenario, high costs occur less often, either by using stored electricity or by the reduced demand

[4]The sum of the differences is equal to the total cost difference.

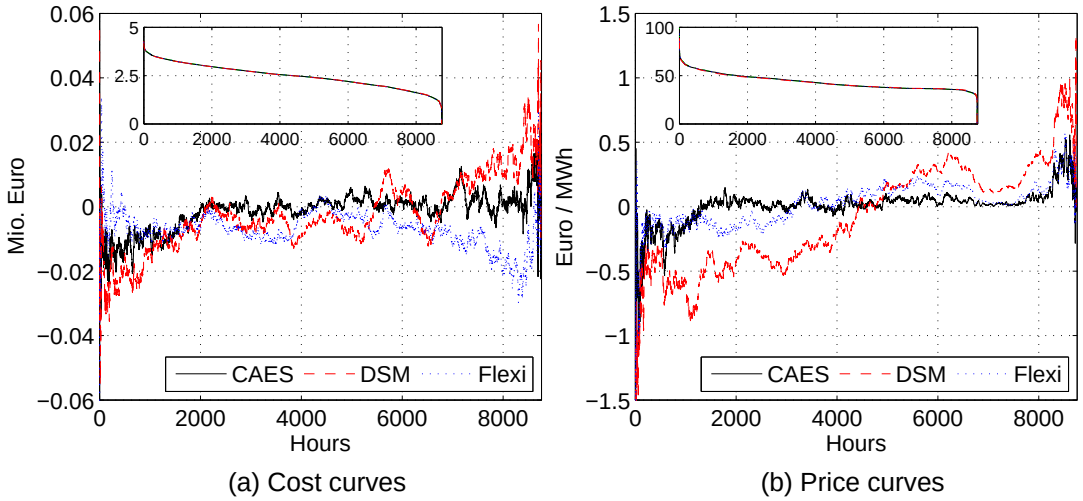

Figure 5.11.: Differences in the cost and price curves related to the base scenario

levels (left end in the figure). This is partially balanced by higher costs in the low cost hours (right end). In the CAES case, the cost reduction is less important as the storing losses have to be compensated. The "Flexi" scenario shows a different behaviour. The cost reduction is achieved over all hours and especially in the low cost hours. The improved thermal flexibility leads to an increased use of coal and lignite power plants (see also below). In the high cost hours (the hours with a high residual load), these plants are also used in the base scenario. In the hours with a low residual load, the flexibility of the running power plants becomes more important as less power plants are generally activated.[5] More coal and lignite power plants can therefore be used and the cost reduction is more important in the low cost hours.

Figure 5.10-b compares the average electricity prices. The differences are small and rest below 0.1 €/MWh. The changes are more noticeable in an hourly resolution. Figure 5.11-b shows the price differences to the base price curve. The latter is given in the small plot at the top. The peak shifting by demand side management or storage leads to lower prices in high price hours and higher prices in low price hours. In the CAES case, only 1000 hours at both ends of the price curve are affected as the price spread has to be large enough to compensate the storage losses.

The flexibility improvements result in a change of the generation mix according to Figure 5.12-a. In all cases, less gas power plants are needed due to the increased flexibility (or the modified demand curve). Coal and lignite power plants replace the gas plants. The nuclear power generation slightly increases. This also applies to the "Flexi" scenario. Even though the flexibility of the nuclear power plants is

[5] See Section 2.2.1 for an analysis of the residual load levels and the related gradients.

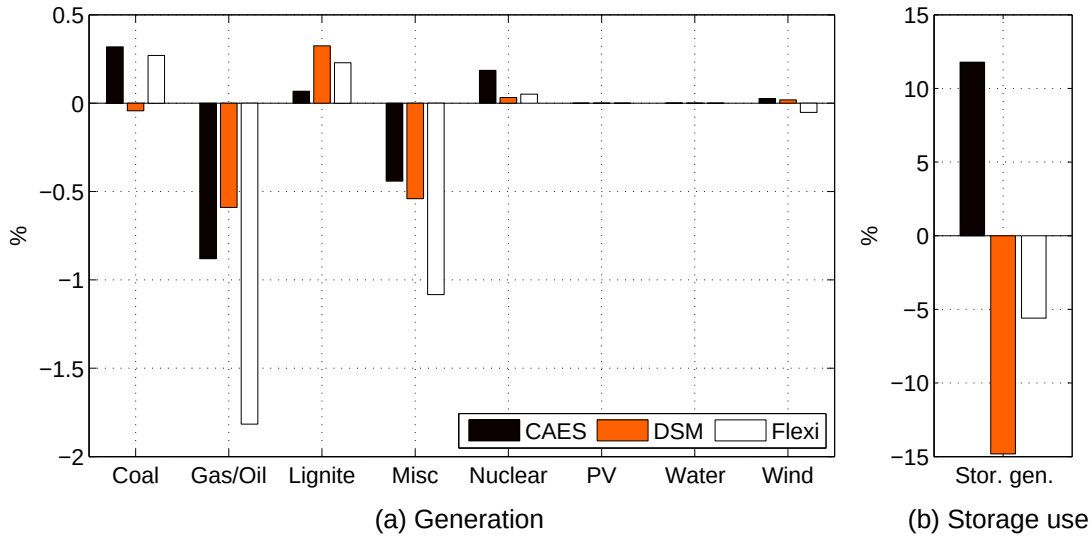

Figure 5.12.: Percentage changes of the generation compared to the base scenario

not changed, they are used more due to the higher flexibility of the other plants. Less storage is needed with more flexible power plants or a shifted peak demand, see Figure 5.12-b. Especially the DSM scenario shows a reduction by 15%. The smoothing of the demand curve leads to reduced price spreads and the use of storage becomes less attractive. The additional CAES capacities naturally lead to more storage generation. The increase of the generation is 12%, so lower than the increase of the installed capacity (16%). The CAES capacities have lower full load hours than the pump storage plants. In the base scenario, the full load hours of the pump storage plants are equal to 1170 hours in average (related to the generation only). The CAES capacities operate at full load in 1014 hours, so 14% less, and the average of all storage plants is reduced to 1130 full load hours. The use of pump storage plants is preferred as they are more efficient than the CAES capacities.

The flexibility improvements do not reduce the wind power curtailment in a significant way, see Figure 5.13-a. The curtailment is mainly caused by transmission constraints. The CAES scenario however has a noticeable effect on the reserve violations, see Figure 5.13-b. The system violations occur in the base case due to forecast errors that cannot be balanced on the intraday market. The added storage capacities, being highly flexible, are helpful in these hours. The system violations, measured in missing energy, are reduced by more than 25%.

Until now, the flexibility scenarios and their cost reductions were evaluated with regard to the case with forecast errors. It is interesting from a modelling point of view whether the scenarios can also be evaluated without the effort of modelling forecast errors. The system costs of the scenarios are therefore calculated both for the case with forecast errors and for the case without forecast errors. In Figure 5.14, the percentage cost changes are given related to the corresponding

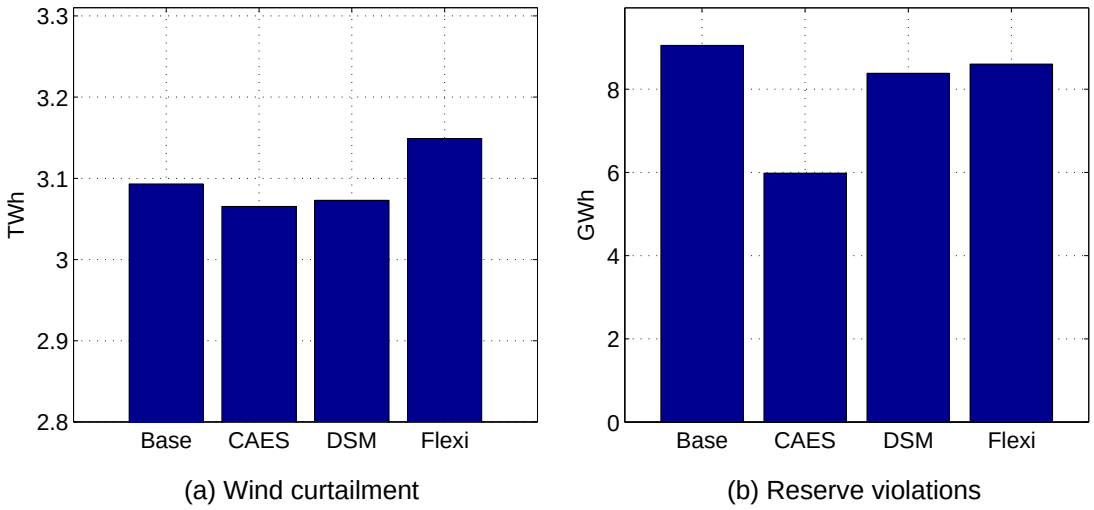

Figure 5.13.: Wind power curtailment and reserve violations

base scenario. Without forecast errors, the benefits of the CAES power plant and the flexible power plants ("Flexi") are clearly reduced. The achieved cost reduction is about one third lower than in the case with forecast errors. For example, the cost reduction by flexible power plants is 0.33% if forecast errors are considered, but only 0.13% without forecast errors. In contrast, the cost reduction by demand side management is similar in both cases. The DSM scenario was derived by a shifting of the demand curve without any consideration of forecast errors. The potential contribution of demand side management to the balancing of forecast errors is therefore not modelled and the system benefits are similar in the two cases.

5.4. Infrastructure changes: Grid expansion and power plant allocation

New transmission lines contribute to a more efficient power supply by connecting low-cost generation centres and demand centres. Similar effects could also be achieved by reallocating power plants. The related benefits are evaluated in the following. The maximal potential of grid extensions is estimated by the application of a copperplate grid.

Definition

In order to simulate grid expansions, useful new transmission lines have to be identified. An optimization of the grid expansion is however not in the scope of this work. A promising extension of the grid is therefore identified by the results

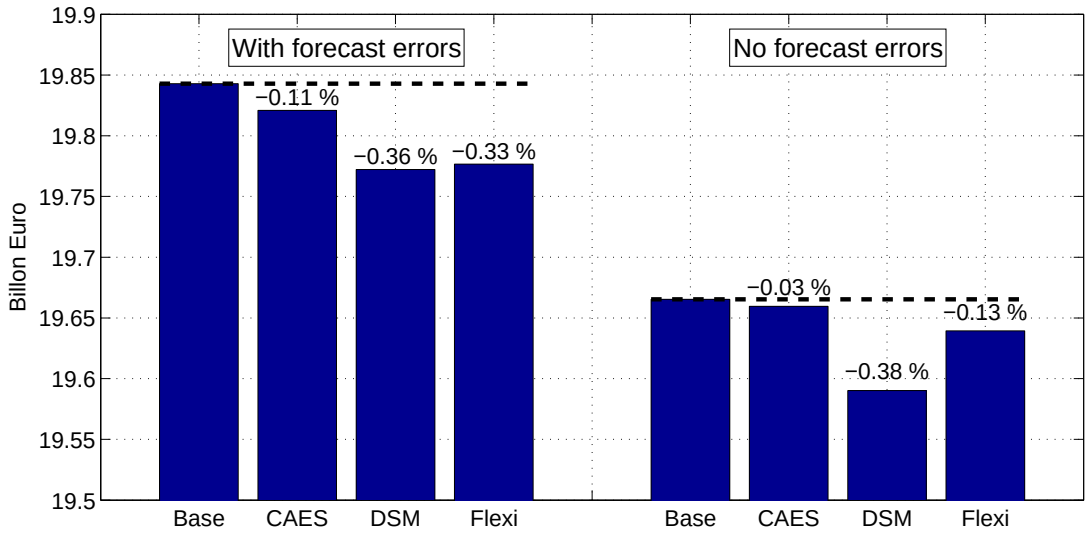

Figure 5.14.: Comparison of system costs with and without forecast errors

of the "Base" scenario. The marginal values of the transmission constraints[6] indicate for each connection the cost reduction that could be achieved with additional transmission capacity. The marginal values are given hourly and they are aggregated to calculate the yearly potential. Transmission lines are then added to the connections that have the highest marginal values. This is not an optimized grid expansion as the cost potential of a line may for example vanish by adding another line. In addition, only connections between regions and no exact line locations are identified. In a second scenario, an extreme grid expansion is therefore modelled to estimate the maximal benefits of new transmission lines.

The marginal values of all German connections are given in Figure 5.15. The offshore connections have no marginal values as they are not affected by the load flow constraints. High values indicate the lines that are often congested. Due to the load flow approach, it is also possible that high marginal values indicate lines that are mainly responsible for congestions in other lines. Niedersachsen, receiving most of the offshore wind power from the North Sea, lacks connection to the South and Sachsen-Anhalt. Counter-intuitively, the north-eastern regions Schleswig-Holstein and Mecklenburg-Vorpommern (MV) seem to be less congested. On the one hand, there are only few offshore capacities in the Baltic Sea and the regions have some exchange possibilities to Poland and Scandinavia. On the other hand, there are loop flows that go from Brandenburg (BB) via Sachsen or Sachsen-Anhalt (ST). The marginal value of the MV-ST connection is for example zero as more power can be transmitted via BB. Due to the power exchange via BB, the MV-ST exchange is then always fixed by the DC load flow representation and the marginal value is zero. In general, the transmission from North to South is more constraint

[6]Equation (3.11) of the model formulation in Section 3.1.

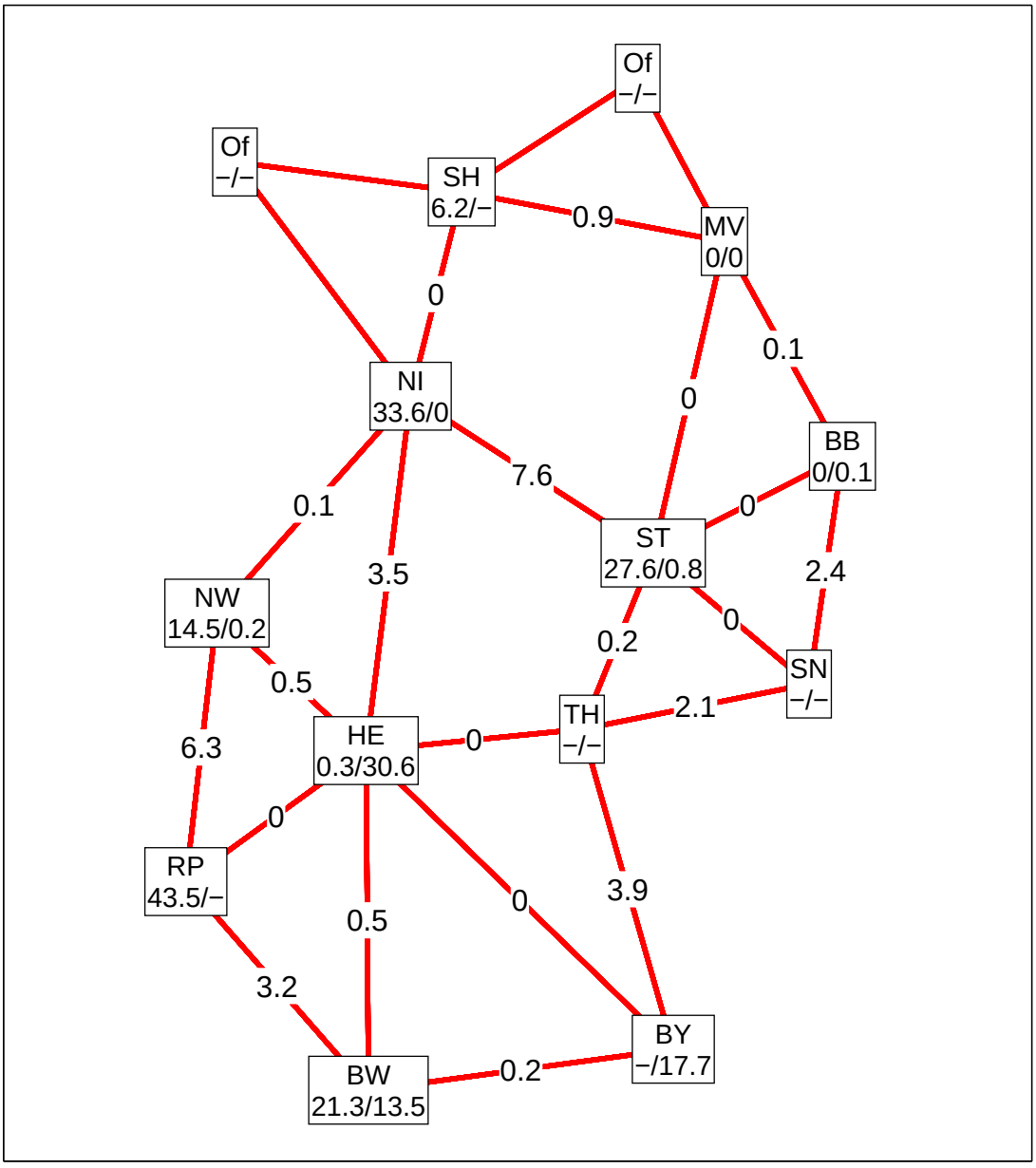

Figure 5.15.: Marginal values of capacities and transmission in the base scenario

due to congestions in Middle and South Germany. The connection between Bayern (BY) and Thüringen (TH) is one example. The connections to Rheinland-Pfalz are also congested resulting from the frequent exchanges with the Western neighbour countries.

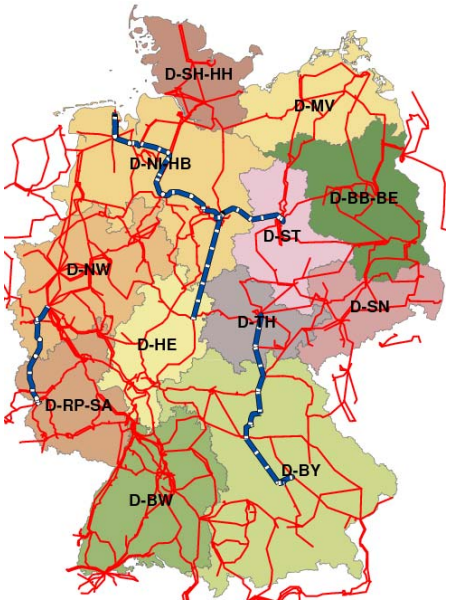

Figure 5.16.: New transmission lines in the grid extension scenario

A total length of about 1000 km is here chosen as limit for the added transmission lines. The following connections, selected in the order of their marginal values, are strengthened: NI-ST, NI-HE, TH-BY, NW-RP. The specific locations of the new lines are required in order to apply the DC load flow and grid reduction approach. Transmission lines according to Figure 5.16 are therefore added to the transmission grid. The selection of these lines is here to some extent arbitrary. In general, they are placed in such a way that the demand centres of the regions are covered. In NI, the new transmission line also connects the offshore parks and the exchange with the neighbour countries is facilitated in RP. One 380 kV line with two circuits is added in all cases. The new lines have a total length of 1080 km. The grid reduction approach of Section 3.2.3 is then applied to calculate the new transmission parameters between the German regions. The resulting scenario is denoted by "Gr.Ext." in the following.

The subsequent results show that the grid extension only leads to limited cost reductions. For more general results, a copperplate scenario is therefore considered. All regional transmission parameters (susceptances and thermal capacities) are set unlimited in the scenario (denoted by "Gr.Total"). The resulting grid represents a system without any transmission constraints within Germany. The maximal benefits of German grid expansions are thus estimated.[7]

[7]The scenario comparison only refers to transmission constraints between the German re-

Another possibility to attenuate the effects of regional imbalances is an adjusted allocation of power plants. A comparison of the regional electricity prices could be a way to identify useful changes of plant locations. However, this would not allow to see differences between the plant types, for example if a region lacks flexible gas plants. The marginal values of the capacity constraints are therefore considered. They indicate for each region and power plant type the cost reduction that could be achieved with more installed capacity. The base scenario gives the marginal values for the coal and combined-cycle capacities. Power plant capacities that were built before 2010 are not considered as their location is fixed. Figure 5.15 shows the aggregated marginal values. In each region, the first value refers to the coal and the second value to the gas capacities. High values indicate lacking capacity and regions with low values are likely to have over-capacities.[8]

Table 5.5.: Changes of installed capacities for the allocation scenario (MW)

	BB-BE	BY	HE	MV	NI-HB	RP-SL
Coal	-376	0	0	-1510	943	943
Gas	0	425	425	-600	-250	0

In the case of gas, high marginal values are for example given in Hessen and Bayern, whereas Niedersachsen and Mecklenburg-Vorpommern have marginal values of zero. In these regions, the subtraction of capacity will cost the least. It is however unknown how much capacity can be subtracted without causing high costs and turning the situation around. Only half of the future capacity is therefore reallocated. It is added to the two regions with the highest marginal values. The final reallocation of new capacities is given by Table 5.5. In the case of Niedersachsen, this leads to added coal capacities but subtracted gas capacities. This is not a contradiction as a region, having over-capacities in gas, may lack cheap coal capacities. The opposite is also possible if a a region lacks flexible plants as it is the case in Hessen. The resulting scenario is denoted by "Alloc." in the following.

Results

The infrastructure changes lead to a more efficient system operation. Expensive generation in previously congested regions is replaced and the system costs decrease in all scenarios according to Figure 5.17-a. Obviously, the assumption of a copper plate ("Gr.Total") has the biggest effects in the system. The costs are reduced by nearly one billion Euros per year. A perfect grid has clear advantages for the system operation. A moderate grid extension by some transmission lines

gions. Grid expansions that may be necessary within the regions are not regarded here.

[8] The marginal values of the capacity constraints are not comparable with the marginal values of the transmission constraints as they are related to different unit sizes.

leads to cost reductions of 84 million Euro per. The cost reduction is about 10% of the one with a perfect grid. The cost reductions by a new allocation of power plants are even higher. The coal power plants that were shifted to Niedersachsen and Rheinland-Pfalz can now be more productive (see below for the generation mix). Transmission constraints are therefore partially eliminated in an effective way without a grid extension.

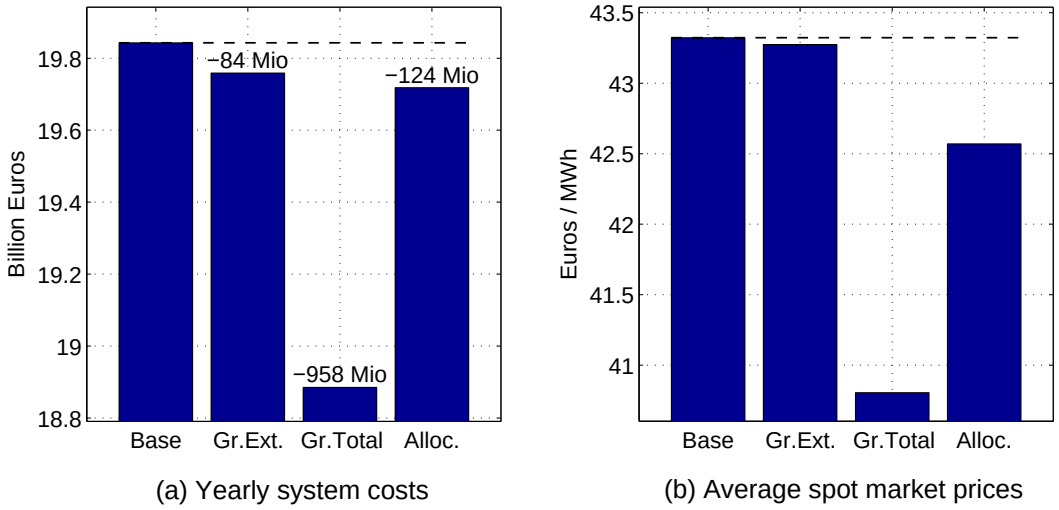

Figure 5.17.: Total system costs and day-ahead electricity prices

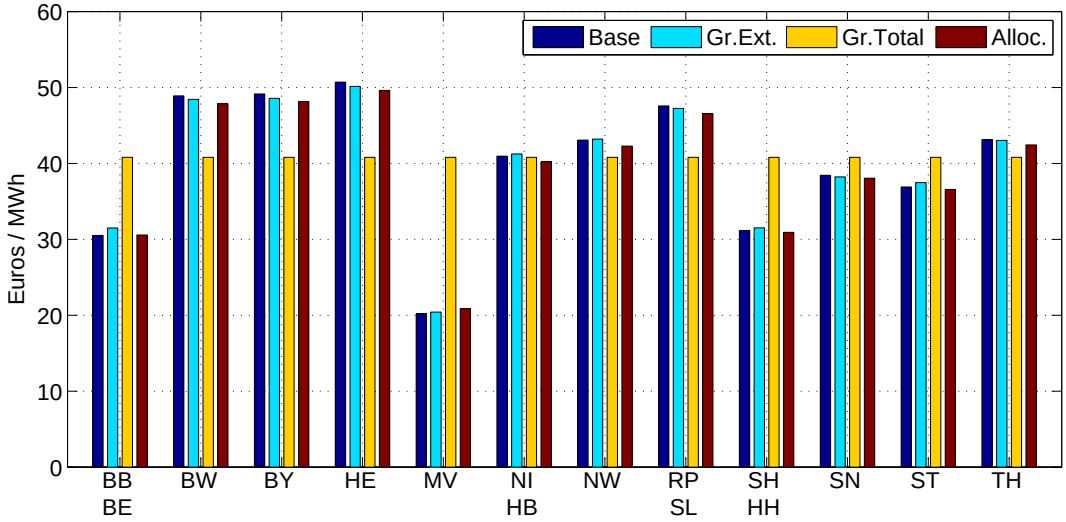

Figure 5.18.: Regional day-ahead electricity prices

The cost reductions are reflected by the change of the regional prices according to Figure 5.18. Regions with additional capacities (RP, BY) have slightly lower electricity prices than in the base scenario. The contrary applies to regions with

diminished capacities (BB, MV). This indicates a decrease of the system costs as the demand in the latter regions is much lower than the one in the former. The reduction of the average German electricity price is one cent per MWh, see Figure 5.17-b. The copper plate scenario has the biggest effects on the regional prices. All regions have the same price as differences between the regional marginal costs are eliminated. Higher marginal costs in one region motivate a transmission of generation to another region until all differences are balanced. The resulting reduction of the average German price is 2.5 cent per MWh. The price changes in the grid extension scenario are small. Slightly higher costs for example occur in Brandenburg and Niedersachsen, whereas the prices in the regions in the South-West (Bayern, Baden-Württemberg, Hessen, Rheinland-Pfalz) decrease. This corresponds to the improved East-West and North-West connection that is given with the added transmission lines. The grid extension therefore leads to a slight decrease of the regional price differences. In the price comparison, it has to be considered that the exports increase in all scenarios. More exports are equivalent to more generation within Germany leading to smaller price reductions. In the base scenario the German net balance is minus 26.8 TWh. In the three infrastructure scenarios, the exports rise to 28.6 TWh, 30.5 TWh and 31.3 TWh, see Figure 5.19-a. These increased exchanges at the border are only due to inner-German infrastructure changes that allow or motivate higher transmissions at the borders.

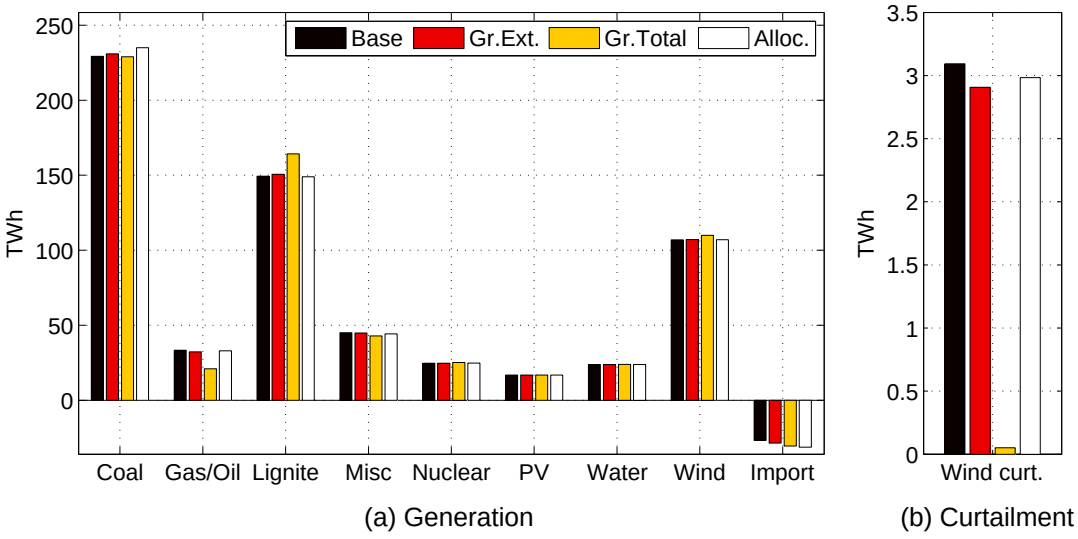

Figure 5.19.: Power generation and curtailment of wind power

Figure 5.19-a shows the generation mix. The cost and price reductions are mainly due to gas savings. Especially in the perfect grid case 40% less gas is needed. It is replaced by coal, lignite and nuclear plants. In the allocation scenario, the coal power plants that were relocated can produce more than in the base scenario. The wind generation also changes due to a different curtailment. In all scenarios less curtailment is required, see Figure 5.19-b. The infrastructure

changes facilitate the transport of wind power from Mecklenburg-Vorpommern and the Baltic Sea to the other regions. In the allocation and grid extension scenario, the transport is facilitated even though Mecklenburg-Vorpommern is not directly affected by the infrastructure changes. Congestions are therefore reduced even though the system is expanded at another place. With a perfect grid, the curtailment is nearly zero.

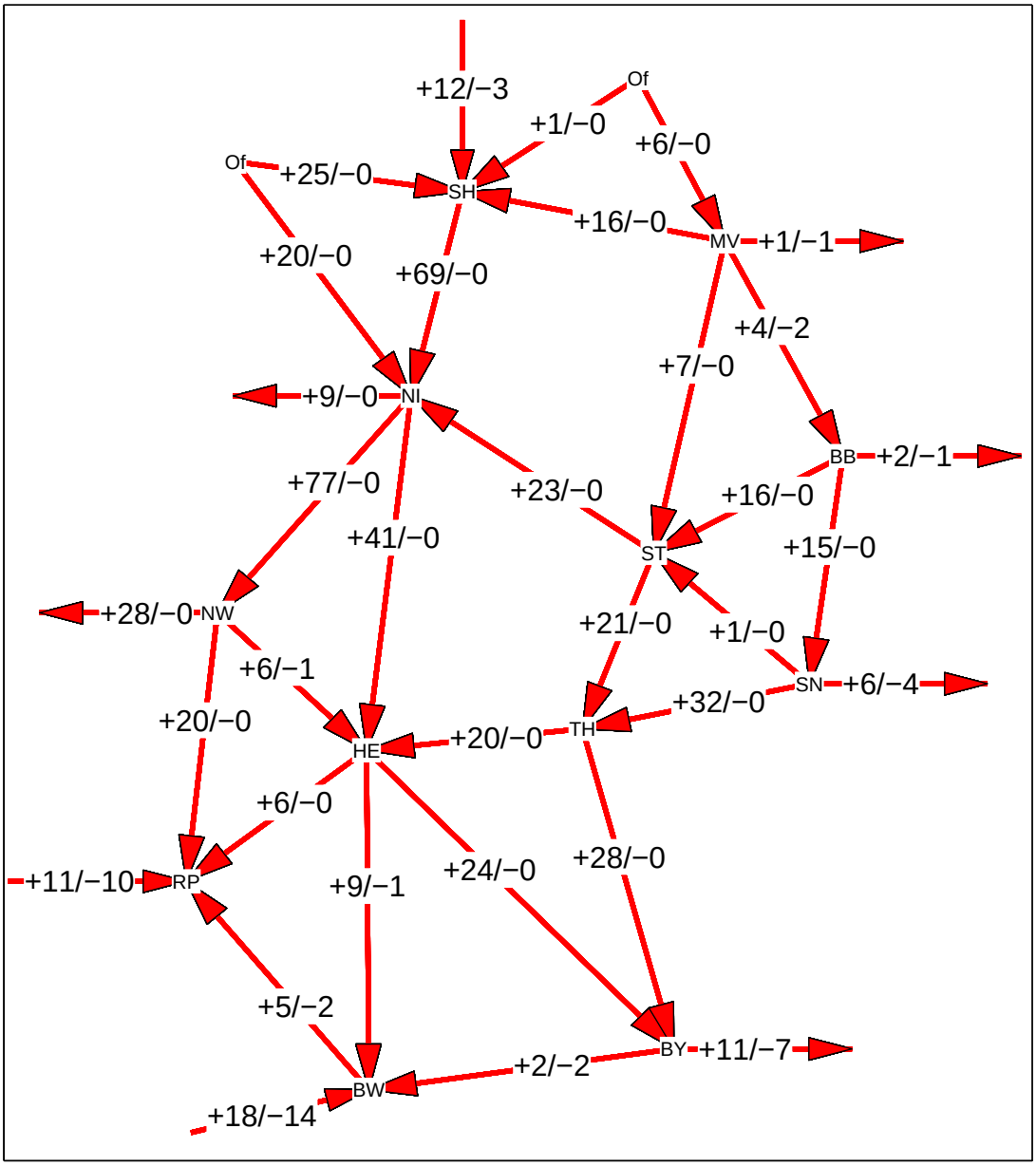

Figure 5.20.: Yearly exchanges with copperplate grid

Figure 5.20 shows the yearly exchanges for the perfect grid case (see Figure 5.5 for the base scenario). The exchanges are indicated in both directions (in the positive and negative direction of the arrow). The exchanges are much higher than in

the base case. The North-South direction and East-West direction of the power flows within Germany are now even more accentuated than in the base scenario. The highest transmission increase is given between Schleswig-Holstein and Niedersachsen. The exchanges from Niedersachsen to Hessen and to Rheinland-Pfalz over Nordrhein-Westphalen are doubled. The same holds for the exchanges to Bayern coming from the North. Even higher transmission increases can be seen in the East where the amount of power transmitted from Mecklenburg-Vorpommern and from Brandenburg to the South more than triples. More power is also transmitted at the borders. Especially the net balance at the border between Schleswig-Holstein and Denmark is different. In the base scenario, 2 TWh are net imported from Denmark. Now, the net import is 9 TWh. The eliminated transmission constraints within Germany therefore allow to import more wind power from Denmark. The large exchanges that occur with a perfect grid show to which point the unexpended grid is insufficient for high wind power shares.

5.5. Comparison and discussion

All integration measures are compared in the following. The operational system costs are regarded indicating the efficiency of the measures. In contrast to the analyses above, reserve violations are here monetized and added to the system costs. A violation price of 3000 €/MWh is taken according to the maximal price at the EEX, [171, 65], assuming that controlled load shedding would be offered at the market for this price. The influence of the violation costs on the cost reductions only exceeds ten percent for the scenario with hedged forecasts and the CAES scenario (see below).

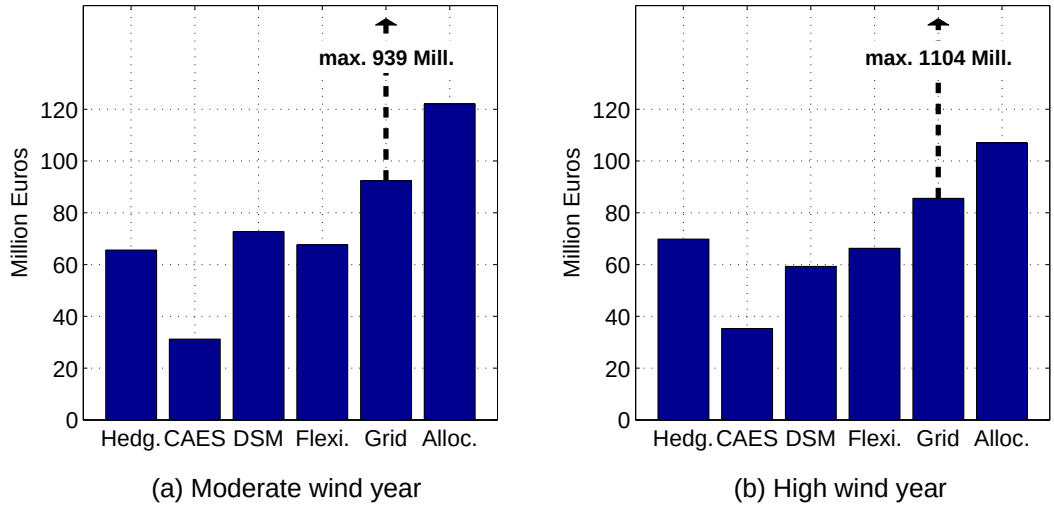

Figure 5.21.: Cost reductions by integration measures

All presented development options lead to a reduction of the operational system costs. Figure 5.21 shows that costs between 25 and 125 million Euros per year are saved in all cases (apart from the copperplate scenario). The system costs and cost reductions were calculated for a moderate and a high wind year (see Figure 5.1 for high wind year). The cost reductions by additional transmission lines ("Grid" scenario) or a new allocation of power plants ("Alloc." scenario) are lower in the second case. This is due to their definition that was derived based on the system results of the base scenario in a moderate wind year. They are therefore not optimized for the high wind year and the resulting cost reductions are lower. In general, the cost reductions are however similar for all scenarios. The influence of the wind year on the cost reductions is therefore not important. This is not the case for the system costs themselves that differ by more than one billion between a moderate and a high wind year, see Figure 5.2. The system is hence highly influenced by the wind year but the integration measures and their benefits are effective independently from the wind year.

Hedging of forecast errors leads to a cost reduction of about 60 million. A large part, 40%, is thereby due to reserve violations. This indicates that hedging could help to cope with uncertainties especially with regard to system stability. Neglecting the reserve violations, the cost reduction is only equal to 38 million. This is still a relatively high value considering that a future improvement of forecast quality by 20% is already considered in the base scenario. The application of hedging measures should therefore be encouraged in the intraday trading. One possibility could be that the transmission system operators publish not only the expected value forecasts but also the related error quantiles (density forecasts). The market participants would then be informed about the possible under- or oversupply of wind power and they could optimize their bids accordingly. It is however important to note that the hedging scenario represents an ideal, market-wide application of stochastic optimization with perfect knowledge of the forecast error distribution as discussed in Section 5.1. The achieved cost reduction can therefore only indicate the potential of related measures.

The additional 1 GW of CAES capacity has the lowest effects on the system costs. The added CAES plant is a local measure and not a system-wide change as in the other scenarios. The efficiency of the plant, 0.7, is not as high as for pump storage plants. The cost reduction is therefore relatively small. The CAES plant however helps to reduce the reserve violations by 33% (this accounts for 30% or 9 million Euros). In a high wind year, the cost reduction rises from 31 million to 35 million Euros equal to an increase of 13%. This indicates that CAES power plants could become more important with more renewable energy in the system. Here, with 53 GW of wind and 19 GW of photovoltaic, CAES has limited effects. The benefits are limited even though the capacities are located in the North, so near to the main wind power areas. Yearly costs saving of 35 million Euros correspond to investment costs of 317 million Euros (assuming a life time of 25 years and a

interest rate of 10%). The investment costs of CAES power plants are estimated to 1000 €/kW, [172, 167, 168], which is equal to 1 billion Euros per Gigawatt. The results therefore suggest that larger amounts of CAES capacities (1 GW or more) are not cost-efficient from a system point of view. They could become more valuable with higher shares of renewable energy.

Both demand side management and flexible power plants lead to significant cost reductions. The thermal flexibility improvement was thereby applied to new power plants only. The cost reductions are between 59 and 73 million Euros per year. More flexible power plants are helpful both for the normal dispatch and for the balancing of forecast errors in the intraday market. Demand side management was simulated without any consideration of forecast errors. The cost reduction could be higher if DSM also reacts to forecast errors.

The grid scenario simulates additional transmission lines in the grid. New lines with a total length of 1000 km are added. They lead to cost reductions of about 90 million Euros per year. This is more than in all previous scenarios. Taking 50 years of life time and an interest rate of 10%, 90 million Euros of cost savings per year are equivalent to investment costs of 900 million Euros. A conservative figure for a 380 kV line is 1 million Euro per km (depending on the territory the investment costs can decrease to 400000 Euro per km) [172, 73, 72, 39]. The price for 1000 km is then 1 billion Euro. The added transmission lines are therefore close to being economical. Moreover, the lines were derived by an evaluation of the base scenario results but no grid optimization was applied. The scenario can therefore only give a lower indication of the cost effects.

In the base and in the grid expansion scenario, curtailment of wind power takes place. About 3 TWh of wind energy are curtailed per year in both cases. A grid expansion can therefore be interesting regardless of curtailment respectively economical without a reduction of curtailment. The curtailment is nearly reduced to zero with a copperplate grid. The related cost saving potential is indicated by the arrows in Figure 5.21. The yearly costs are reduced by about 1 billion Euros. Perfect grid connections between all regions are therefore economical if the total investment costs do not exceed 10 billion Euro (assuming a life time of 50 years and 10% interest rate) corresponding to 10.000 km of new transmission lines. This high number indicates that the limiting factor for new transmission lines is not their economical potential but other reasons. In fact, the long administrative procedures to build transmission lines resulting from local interest conflicts make it difficult to build new lines. Another point is that the future power plant portfolio is always subject to uncertainties. A grid that is optimally designed for all future allocations of capacities is therefore difficult to achieve.

Another way to improve the system infrastructure is an allocation of power plants according to the system requirements. The potential of such an approach is shown by the high cost reduction in the related scenario ("Alloc."). The scenario is only based on a different allocation of coal and gas capacities but no capacities are

added. The required investment costs are therefore only related to the different locations and their suitability for investment. A different allocation of capacities could be encouraged by a regional price model. The location of a power plant then has influence on its revenue and potential disadvantages of the location could be compensated. The necessity of grid expansions could thus be delayed. A regional price model follows the approach that the production is adapted to the grid instead of adapting the grid to the production. The transformation of the power system would therefore be more flexible as the production capacities can be planned in a more dynamic way.

Concluding, all integration measures show positive effects for the power system operation. Storage capacities are not necessary at this stage of renewable shares but they may become essential with higher renewable shares. The hedging of wind forecast errors in the general dispatch, measures related to demand side management and a higher flexibility of thermal power plants are additional elements for a future power system. The enforcement of the grid has great potential and it is very beneficial for the power system operation. A guided allocation of power plants, for example encouraged by a regional price model, could be a promising way to reduce the necessity of new transmission lines.

6. Conclusion

The previous chapters focused on the power system operation with high shares of wind power and related modelling issues. The variability of wind, forecast uncertainties and the geographical concentration of wind power were identified as main aspects of the analysis. The following results are presented according to these aspects. The results refer to content and to modelling orientated questions. Further conclusions about wind power integration in Germany and related development options follow at the end. They are derived from the scenario analysis in the precedent chapter. The scenario analysis and the comparison of integration measures are based on a specific scenario of the year 2020. The related conclusions can therefore be only indicative for other scenarios and systems.

It was proposed to measure the variability of fluctuating generation by several statistical parameters (central moments) both of the generation and of its gradients. A general simulation approach shows that the variability of wind power in a region only depends on the region size if more than 50 wind farms are distributed over the region. Equations are given to calculate the decrease of variability depending on the region size and on the average wind power generation. The equations are used in a simulation approach that gives the wind power generation based on wind speed time series and that allows to consider different wind year qualities. Multi-turbine power curves are thereby defined in accordance to the equations and the region size. The simulation results were compared to published data and the shortcomings of scaling approaches are shown.

The variability becomes especially important in combination with the variability of the demand. A positive correlation between wind and load however does not necessarily mean that the variability is balanced. In fact, the positive correlation between wind and load in Germany is due to a positive seasonal correlation but the daily correlation is negative. The variability of the residual load therefore increases. This can be seen by the absolute gradients but it becomes especially important looking at the gradients related to the residual load level. The residual load level defines how many power plants are operating. Operating power plants are more flexible than power plants that are offline. The realization of large gradients at low residual load levels is therefore more difficult than the load following at high load levels.

The capability of load following is defined by the flexibility of the power plants. A literature research from different sources compared the parameters that are related to the flexibility of power plants. A general statement in the sources is

that the costs of a flexible power plant operation are difficult to estimate. There is therefore a large range of values. The indications for the start-up costs for example differ by a factor of 10 and more. From a system point of view, the costs of cycling are however relatively low compared to the fuel and CO2 costs. A scenario with more flexible new thermal power plants therefore only leads to a 0.33% decrease of the total operational system costs.

The uncertainty of wind power prediction was described in several ways. An analysis of measured wind speed forecast errors defines the statistical behaviours of the forecasts. Several parameters are calculated that can be used in the simulation of forecast scenarios. The correlation between errors at different locations is for example given by an equation that depends on the distance and the forecast horizon. Moment matching is proposed as a suitable approach to simulate forecast scenarios or scenario paths. The approach allows to consider non-normal distribution parameters so that a higher frequency of extreme events can be represented. The simulation is here also calibrated to the quality of German wind power forecasts. A main result of the final simulation is that, with 53 GW wind power (16 GW offshore) and an improvement of forecast quality by 20% to 2020, the root mean square error of the German forecasts is similar to the current one. The improvement of forecast quality is compensentated by the offshore concentration of wind farms.

The forecast errors are partially balanced by the intraday market. It is shown that, with high shares of wind power, the influence of the wind forecast errors is dominant on the intraday market and the load forecast error can be neglected. The intraday market is modelled by a rolling planning approach that simulates the exposure of the power system operation to uncertainties. In the base scenario with a forecast improvement of 20% until 2020, the forecast errors cause about 1% of the total operational system costs. The redispatch in the intraday market also changes the generation mix slightly. About 6% of the gas generation is for example due to rebalancing actions. In general, the influence of forecast errors on the generation mix is however small. The consideration of forecast errors is especially important for the evaluation of integration measures. The benefits of additional storage capacities or more flexible thermal power plants are for example underestimated by a factor of three with a determinstic approach.

Load forecast errors and the outages of power plants are considered in the calculation of the reserve requirements. The primary and secondary reserve requirements are derived according to the UCTE requirements and literature sources, whereas a calculation approach is developed to find the tertiary reserve requirements. The calculation approach is based on probabilistic methods in combination with an optimization. This includes a fast calculation code for the convolution of the power plant outages. The relevant outage type is thereby specified as an unplanned and non-relocatable outage according to the literature. The calculation results show that, with high wind power shares, the tertiary reserve requirements

depend above all on the wind forecast errors. In contrast, the probabilities of the power plant outages only have a small impact. The power system operation is however only marginally influenced by the level of tertiary reserves. The model results for 2020 show that the provision of tertiary reserves is nearly cost free and the reserve price is close to zero most of the time due to the available capacities in the system. The activation of the reserves and related costs are not considered here.

The concentration of wind power in the North causes higher exchanges in the transmission grid. Large wind parks and especially offshore parks are directly connected to the transmission grid. A grid reduction approach is applied to consider the transmission grid in the regional market model. The reduction approach derives susceptances between regions based on the complete grid. The susceptances can then be applied in the market model for the DC load flow representation between the aggregated regions. It is estimated that considering only thermal transmission capacities between the regions underrates the operational system costs by about 5.5% in average for the German 2020 scenario. The proposed grid representation reduces the average error to 3.5%. In both cases the errors can however be much higher in single hours. A possibility for future work could be to apply a reduced grid first and to redispatch, for selected hours, the operation results based on a complete grid.

Different integration measures were tested that are related to the discussed aspects of wind power generation. First of all, the analysis of the base scenario shows that the power system can integrate high shares of wind power but it is not optimally designed for it. A condition for the integration is that curtailment is possible. 53 GW of wind power and 19 GW of photovoltaic are integrated with 3 TWh of curtailment. Biomass is thereby modelled as dispatchable. In a high wind year, the curtailment rises by 20%. The same is true with 20% higher gas prices due to the increased use of base load power plants. The German net export in the base scenario amounts to 27 TWh, so, depending on the developments in the other countries, more or less curtailment may be necessary. Another aspect of high wind power shares is that the wind year can have an important influence on the system performance. For example, the additional energy in a good wind year, replacing coal and lignite generation, leads to a 3.5% decrease of the operational system costs.

System changes could help to optimize the power system operation and to avoid unnecessary energy losses. The transmission constraints are for example responsible for most of the curtailment that can be seen in the base scenario. As the model only considers the transmission grid, curtailment due to constraints in distribution grids is not considered here. The complete integration of all renewable energy without tolerating any curtailment would therefore require an substantial grid enforcement. In the model here, an exemplary addition of some transmission lines leads only to a slight decrease of the curtailment (the transmission lines were

however not chosen with regard to curtailment) and the curtailment is only suppressed by a copperplate grid. The related costs for such a grid are unknown. The scenario analysis suggests that, from a system costs point of view, such a grid, saving about 1 billion Euro of operational system costs per year, should not cost more than 10 billion Euro to to be economical.

Less important cost reductions are made by other integration measures. The flexibility in the system can for example be improved by more flexible thermal power plants or demand side management. The yearly cost reduction is similar and in the order of 80 million Euro. The addition of CAES capacities, even though located near to the wind power centres, proved to be the least cost-efficient measure. The here assumed residual load curve does not show any negative values and storage capacities are not required. They can however contribute to the system stability with regard to forecast errors. The same is true for the application of hedging techniques. Hedging of forecast errors or risk management techniques could potentially help to reduce the costs from forecast errors by 80%. This refers to the ideal case with perfect distribution information. In a market with many participants, the bids will be orientated towards the expected value forecast and hegding will only be realized in a limited way. Neverthelss, the hedging of forecast errors by the market dispatch should be encouraged by publishing risk quantiles of wind power forecasts.

An interesting system change is given by the re-allocation of power plants. The related cost reduction is in the order of the one achieved by an exemplary addition of 1000 km new transmission lines. The guided allocation of new power plants could therefore be a promising measure to deal with transmission constraints. This is especially true considering the long procedures and large uncertainties that are related with grid investments. One way to guide such an allocation process without applying centralised planning could be the introduction of a regional price model. The investors would then have an incentive to build the power plants at locations that are not optimal at first glance. A regional price model, for example similar to the market coupling models between the European countries, could therefore be an interesting development option for a German power system with congested transmission capacities. It should however be investigated if such a model still leads to sufficient profitability margins for the investors so that new investments and an appropriate system adequacy can also be guaranteed for the future.

A. Fast code for convolution of power plant outages

The outage combinations of single power plants lead to the capacity levels that are out of order in a portfolio mix and the related probabilities. This is expressed by the cumulative probability function (CPF) stating the probability of each possible generation state [173]. The CPF is for example required in Section 3.2.2 to calculate the reserve requirements. The CPF is derived by convolution of the probability functions of the single power plants. The two-sate probability function of a single power plant is given by its outage probability (see Section 3.2.2 for values of unplanned and non-relocatable outages). The following code was developed to calculate the convolution in a fast way (also presented in [102] by the author). The CPF is represented by a table composed of the vectors $\mathbf{p}$ and $\mathbf{c}$ giving the probability p_j for each capacity level c_j. In the first step it is given by the capacity and outage probability of the first power plant. In each step i a new power plant with capacity c^* and outage probability p^* is added according to Equation (A.1). The resulting probabilities and capacity levels are given by the vectors $\mathbf{p'}$ and $\mathbf{c'}$. The corresponding table is twice as big as the old one and it will normally contain rows with equal capacity levels.

$$\begin{bmatrix}\mathbf{c}^i & \mathbf{p}^i\end{bmatrix} \rightarrow \begin{bmatrix}\mathbf{c}^i + c^* & \mathbf{p}^i \cdot (1-p^*) \\ \mathbf{c}^i + 0 & \mathbf{p}^i \cdot p^*\end{bmatrix} \rightarrow \begin{bmatrix}\mathbf{c'} & \mathbf{p'}\end{bmatrix} \tag{A.1}$$

The rows with equal capacity levels have to be merged to avoid an exponential increase of the table size over the iterative process (the table would for example have more than 1 billion rows after 30 power plants). Rows with equal capacity levels are merged by summing up the associated probabilities. This merging after each iteration makes the calculation time consuming. The following merging code was therefore implemented. First, the table is sorted in ascending order of the capacity levels using some pre-implemented sorting function according to Equation (A.2). The resulting vectors are given by $\mathbf{p^s}$ and $\mathbf{c^s}$.

$$\begin{bmatrix}\mathbf{c'} & \mathbf{p'}\end{bmatrix} \xrightarrow{\text{sort}} \begin{bmatrix}\mathbf{c^s} & \mathbf{p^s}\end{bmatrix} \tag{A.2}$$

Then, the temporary vectors $\mathbf{h}$, $\mathbf{k}$ and $\mathbf{q}$ are calculated according to Equation (A.3). $\mathbf{h}$ stands for the vector of the cumulative sums of the probabilities subtracted from 1. $\mathbf{k}$ gives the differences between adjacent capacity levels. If the differences are

zero the capacity levels are equal. $\mathbf{q}$ is equal to $\mathbf{h}$ but without the rows where $\mathbf{k}$ is zero.

$$\mathbf{h} = 1 - \begin{bmatrix} 0 \\ p_1^s \\ \vdots \\ p_1^s + \cdots p_{n-1}^s \end{bmatrix}, \ \mathbf{k} = \begin{bmatrix} 1 \\ \mathbf{c}^s_{2,\cdots,n} - \mathbf{c}^s_{1,\cdots,n-1} \end{bmatrix}, \ \mathbf{q} = \mathbf{h}_{j|k_j \neq 0} \tag{A.3}$$

Finally the new vectors of capacity levels and probabilities $\mathbf{c}^{i+1}$ and $\mathbf{p}^{i+1}$ are calculated by Equation (A.4). All capacity levels in $\mathbf{c}^{i+1}$ are different keeping the size of the table as small as possible.

$$\mathbf{c}^{i+1} = \mathbf{c}^s_{j|k_j \neq 0} \quad \text{and} \quad \mathbf{p}^{i+1} = \begin{bmatrix} \mathbf{q}_{1,\cdots,m-1} - \mathbf{q}_{2,\cdots,m} \\ q_m \end{bmatrix} \tag{A.4}$$

After all iterations the probability function of conventional generation capacity is known.

B. Higher statistical moments for regional smoothing

The relations related to the higher central moments and correlations that were used in Section 4.2.1 are derived in the following (also presented in [90] by the author). Equation (4.3) giving the third central moment is derived as follows. The fourth central moment can be derived in the same way.

$$\begin{aligned}
\mu_3^P &= \frac{\mu_3^{P^{abs}}}{(NC)^3} = \frac{E((\sum_i P_i^{abs} - \sum_i \mu_i^{abs})^3)}{(NC)^3} \\
&= \frac{E(\sum_i \sum_j \sum_k (P_i^{abs} - \mu_i^{abs})(P_j^{abs} - \mu_j^{abs})(P_k^{abs} - \mu_k^{abs}))}{(NC)^3} \\
&= \frac{E(\sum_i \sum_j \sum_k C^3 (P_i - \mu_i)(P_j - \mu_j)(P_k - \mu_k))}{(NC)^3} \\
&= \frac{1}{N^3} \sum_i \sum_j \sum_k E((P_i - \mu_i)(P_j - \mu_j)(P_k - \mu_k))
\end{aligned}$$

P^{abs} and P stand for the absolute regional generation respectively the regional generation normalized by the installed capacity. P_i^{abs} and P_i give the absolute respectively relative generation at each wind farm. μ_i and μ_i^{abs} stand for the expected values $E(P_i)$ and $E(P_i^{abs})$. Each wind farm of the N wind farms has an installed capacity of C.

As mentioned in Section 4.2.1, the quantities $Corr3$ and $Corr4$ stay, like correlations, always between -1 and 1. This is shown using the inequality of arithmetic and geometric means.

$$\begin{aligned}
Corr3 &= \frac{E(P_i^c P_j^c P_k^c)}{\sigma_{3i}\sigma_{3j}\sigma_{3k}} \\
&= \frac{E(P_i^c P_j^c P_k^c)}{\sqrt[3]{E(|P_i^c|^3)E(\left|P_j^c\right|^3)E(|P_k^c|^3)}} \leq \frac{E(\left|P_i^c P_j^c P_k^c\right|)}{\sqrt[3]{E(|P_i^c|^3)E(\left|P_j^c\right|^3)E(|P_k^c|^3)}} = E(Z_i Z_j Z_k) \\
&= E(\sqrt[3]{Z_i^3 Z_j^3 Z_k^3}) \leq E(\frac{Z_i^3 + Z_j^3 + Z_k^3}{3}) = 1 \\
&\quad \text{with } Z_i = \frac{|P_i^c|}{\sqrt[3]{E(|P_i^c|^3)}} \text{ and } E(Z_i^3) = 1
\end{aligned}$$

By introducing a minus after the first inequation and replacing $\leq$ with $\geq$ it is also shown that $Corr3$ is always greater than -1. The same demonstration can be applied to $Corr4$.

C. Sensitivity analysis of smoothing

The moment factors F_2, F_3 and F_4, derived in Section 4.2, give relations between the central moments of regional power generation and of single wind farm generation. By means of the derived equations, the moment factors are calculated for given region sizes without knowing the number of wind farms. Installed capacities and standard deviations were assumed to be equal at all wind farms. Moreover, the approach is based on square shapes even though real regions have other shapes. These points will be tested by the following sensitivity analyses and reflections (see also [90] by the author). In general, the moment factors can only describe general tendencies as they are derived from approximate exponential functions of correlations. The dependency of the correlations on the adjustment of wind speed to hub heights is assessed first.

Adjustment of wind speed

The available wind speed data is measured at 10 m height. It is transformed to 70 m height by applying an exponent of 0.2 in the power law. The influence of the transformation parameters is shown in Figure C.1. Correlations are calculated for 50 m or 100 m hub heights assuming 0.14 or 0.24 as exponents. The resulting correlations are nearly identical in most cases. Only a transformation to 100 m height based on an exponent of 0.24 leads to slightly lower correlations. The calculated correlations are therefore valid for most typical wind farm configurations.

The derived exponential function of the correlation has a decay of 322 km. The decay value allows comparing the calculated correlations to the ones of other studies. In [143], correlations of power generation are calculated based on European data. The resulting exponential fit shows a decay of 723 km. However, the author points out that this decay is too slow giving results of other studies. A cited study based on data from the German National Meteorological Service (DWD) gives a decay of 375 km which is similar to the decay here. A cited study based on Danish data results in a decay of 500 km. The author explains his slow decay by the large number of coastal locations being exposed to similar weather patterns. A recent study based on power data in Ontario gives a decay of 333 km [174]. The decay of the correlations that was derived here is therefore in line with the literature results.

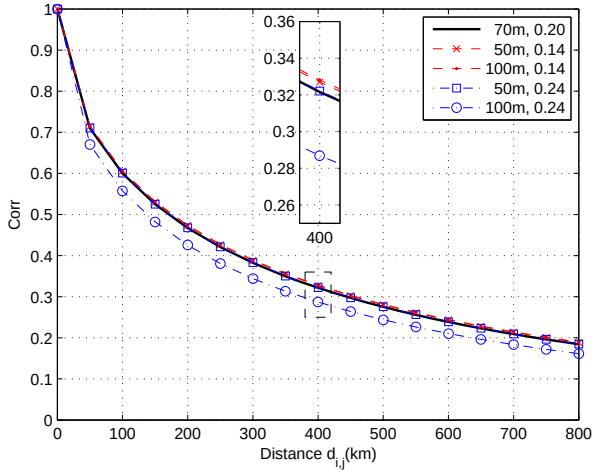

Figure C.1.: Correlations and adjustment of wind speed

Number of wind farms

One could suppose that the derived moment factors depend not only on the region size but also on the number of installed wind farms. But this is only true for small numbers of wind farms and a saturation value is attained quickly with increasing numbers. Figure C.2 shows F_2 and F_3 for a region size of 400 km (square shape) for increasing number of wind farms. Calculation of F_4 is time consuming and not part of this analysis. The error bars indicate the deviation of results having performed different simulations of point patterns. Similar results are obtained for other region sizes. The figure shows that the results differ only slightly with more than 50 wind farms. Hence, the moment factors are nearly independent of the simulated point pattern and they depend only on the region size if there are more than 50 randomly distributed wind farms. In the case of gradients, the saturation value is also attained with 50 wind farms.

This can also be seen by the application of random distance distributions that are known for different geometric shapes. Equation (C.1) gives the probability distribution of distances d between random points in a square with square size s, see for example [175].

$$f = \begin{cases} \frac{\pi}{s^2} - \frac{4d}{s^3} + \frac{d^2}{s^4}, & 0 \leq d \leq s \\ \frac{2}{s^2}\operatorname{asin}(\frac{2s^2}{d^2} - 1) + \frac{4\sqrt{d^2 - s^2}}{s^3} - \frac{2s^2 + d^2}{s^4}, & s < d \leq \sqrt{2}s \end{cases} \tag{C.1}$$

An integration of the product of Equation (C.1) and (4.6) leads to F_2. This can be seen by Equation (C.2). The distribution of distances between all points in the area is denoted by the function f. In the case here, this would be as if an infinite number of wind farms were installed everywhere in the area. The arrow

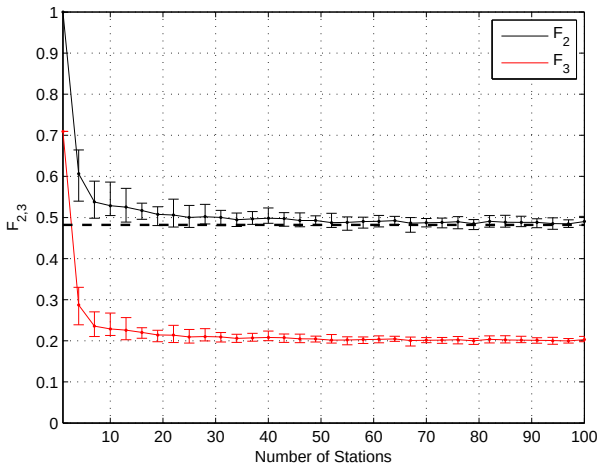

Figure C.2.: Moment factors F_2 and F_3 over number of wind farms

symbolizes the change from discrete to continuous case.

$$F_2 = N^{-2} \sum_i \sum_j Corr = E(Corr) \rightarrow \int (Corr \cdot f) \tag{C.2}$$

For a region size of 400 km the resulting value is shown in Figure C.2 as dashed line. Hence, even in the case of an infinite number of wind farms, F_2 is not smaller as in the case of 50 wind farms. This demonstrates the existence of a saturation value being like an expected value. As the simulation results show the value is already achieved with a small number of wind farms.

The relations above show that, from 50 uniformly distributed wind farms onwards, additional wind farms in a given region do no longer change the variability substantially.[1]

Accumulation of wind farms

Until now it was assumed that the wind farms are randomly distributed in the region. In the following, the more realistic case of accumulated wind farm locations is tested. First it is shown that this point is connected to the question whether it is justified to assume equal standard deviations and capacities at all wind farms.

In Equation (4.2) and (4.3) the installed capacities and standard deviations at each wind farm were assumed to be equal. The following Equation (C.3) calculates the variance μ_2^P according to Equation (4.2) but with different capacities and

[1] The correlations in Section 4.2 were derived based on 24 locations only. However, it can be assumed that the dependency of correlations on the number of locations has no trend and that no systematic error is made by deriving correlations from a limited number of locations.

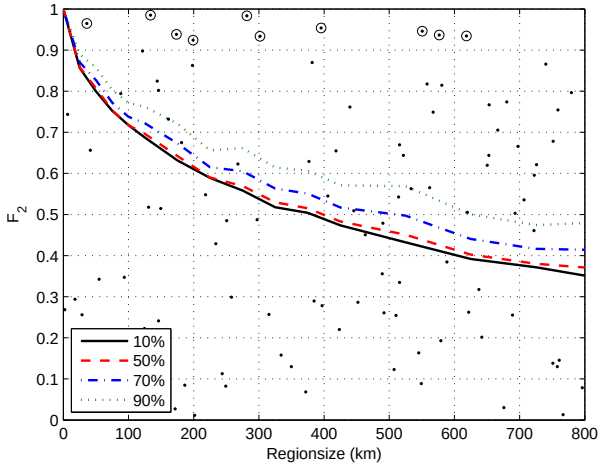

Figure C.3.: F_2 for different capacity concentrations

standard deviations at each location.

$$\mu_2^P = \frac{\sum_i \sum_j C_i C_j \sigma_i \sigma_j \frac{E(P_i^c P_j^c)}{\sigma_i \sigma_j}}{\sum_i C_i} = \frac{\sum_i \sum_j C_i C_j \sigma_i \sigma_j \tau_{ij}}{\sum_i C_i} \tag{C.3}$$

τ_{ij} stands for the empirically derived correlation. Different values of standard deviations lead, like different values of capacity do, to a weighting of the correlations τ_{ij}. As different values of installed capacities can be interpreted as an accumulation of wind farms, the influence of different values of standard deviations and that of different values of capacities can be tested by an accumulation of wind farms.

In the following test cases, the 10 locations (out of 100) that are situated in the north of the area are simulated with higher capacities but the total installed capacity rests equal. The 10 locations thereby represent 10 percent (no accumulation), 50, 70 and 90 percent of the total capacity. Figure C.3 shows the resulting moment factor F_2. Similar results are achieved for the other moment factors and looking at gradients of wind power generation. The figure also shows a simulation example for a square of 800 km side length where the 10 northern locations having more capacity are highlighted.

Hence, the accumulation of wind farms has only a limited influence, as long as there are enough other wind farms that are uniformly distributed over the total region. Even a concentration of 50 percent of the capacity in approximately 10 percent of the area produces no significant change in the moment factor F_2. Only if the concentration exceeds 50 percent or more the smoothing effect is reduced.

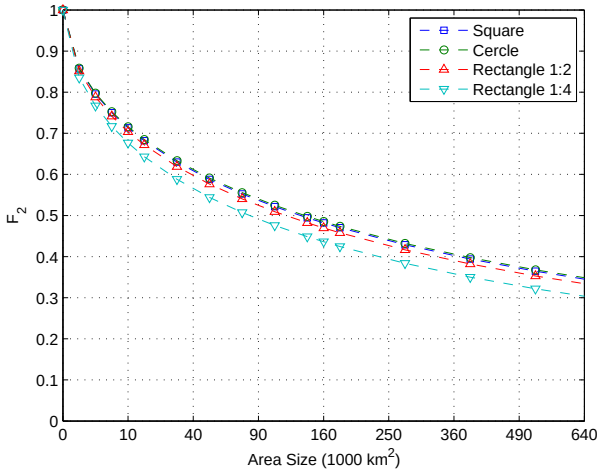

Figure C.4.: F_2 for different region shapes

Region shape

The equations in Section 4.2.1 are based on square shapes. Real regions or countries have different shapes. To test the influence of the region shape, the moment factor F_2 is calculated for different shapes applying distance distributions. The probability distribution of distances d between random points in a square is given in Equation (C.1). Corresponding functions for circles and rectangles are also known [176, 175]. Figure C.4 shows F_2 for the different shapes. One rectangle has an aspect ratio of 2, the other of 4. The moment factors are nearly identical for the square, the circle and the first rectangle. In the case of the second rectangle F_2 is smaller corresponding to a larger decrease of variance respectively an increased smoothing. Similar results are achieved for the moment factor F_3 by means of simulation. Hence, considering that the second rectangle shape is relatively extreme and the differences are generally small, the moment factors derived in Section 4.2.1 should be suitable for most region shapes.

Bibliography

[1] A. J. Schwab, *Elektroenergiesysteme - Erzeugung, Transport, Übertragung und Verteilung elektrischer Energie*. Berlin: Springer, 2006.

[2] ISET, "Windenergie Report Deutschland 2008," ISET e. V., Tech. Rep., 2008. [Online]. Available: http://reisi.iset.uni-kassel.de [Retrieved 14.5.2009].

[3] DEWI, "Windenergie in Deutschland - Aufstellungszahlen für 2006," Deutsches Windenergie-Institut GmbH, Tech. Rep., 2007. [Online]. Available: http://www.dewi.de [Retrieved 20.7.2009].

[4] BWE, "Repowering von Windenergieanlagen - Effizienz, Klimaschutz, regionale Wertschöpfung," Bundesverband WindEnergie e. V., Tech. Rep., 2010. [Online]. Available: http://www.wind-energie.de [Retrieved 10.9.2010].

[5] DEWI, "Status der Windenergienutzung in Deutschland," Deutsches Windenergie-Institut GmbH, Tech. Rep., 2009. [Online]. Available: http://www.dewi.de [Retrieved 7.1.2010].

[6] EEG, "Gesetz für den Vorrang Erneuerbarer Energien (Erneuerbare-Energien-Gesetz - EEG)," 2008.

[7] P. Konstantin, *Praxisbuch Energiewirtschaft: Energieumwandlung, -transport und -beschaffung im liberalisierten Markt*. Berlin: Springer, 2006.

[8] T. Burton, D. Sharpe, N. Jenkins, and E. Bossanyi, *Wind Energy - Handbook*, 4th ed. West Sussex: John Wiley and Sons, 2004.

[9] BNetzA, "Monitoringbericht 2009," Bundesnetzagentur, Tech. Rep., 2009. [Online]. Available: www.bundesnetzagentur.de [Retrieved 1.2.2010].

[10] E. Hau, *Windkraftanlagen - Grundlagen, Technik, Einsatz, Wirtschaftlichkeit*. Berlin: Springer, 2008.

[11] M. Kaltschmitt, W. Streicher, and A. Wiese, Eds., *Erneuerbare Energien - Systemtechnik, Wirtschaftlichkeit, Umweltaspekte*, 4th ed. Berlin: Springer-Verlag, 2006.

[12] G. Giebel, "The State-of-the-Art in Short-Term Prediction of Wind Power. A Literature Overview." Deliverable Report D1.1 in the ANEMOS Project: Development of a Next Generation Wind Resource Forecasting System for the Large-Scale Integration of Onshore and Offshore Wind Farm, Tech. Rep., 2003. [Online]. Available: http://anemos.cma.fr/ [Retrieved 10.12.2005].

[13] L. Landberg, G. Giebel, H. A. Nielsen, T. Nielsen, and H. Madsen, "Short-term Prediction - An Overview," *Wind Energy*, vol. 6, no. 3, pp. 273–280, 2003.

[14] G. Kariniotakis, I. Marti, D. Casas, P. Pinson, T. S. Nielsen, H. Madsen, G. Giebel, J. Usaola, I. Sanchez, A. Palomares, R. Brownsword, J. Tambke, U. Focken, A. Lange, P. Louka, G. Kallos, C. Lac, G. Sideratos, and G. Descombes, "What performance can be expected by short-term wind power prediction models depending on site characteristics?" in *European Wind Energy Conference*, London, UK, 2004.

[15] B. Lange, K. Rohrig, B. Ernst, F. Schlögl, U. Cali, R. Jursa, and J. Moradi, "Wind power forecasting in Germany - Recent advances and future challenges," *Zeitschrift für Energiewirtschaft*, vol. 30, no. 2, pp. 115–120, 2006.

[16] B. Ernst, "Wind Power Forecast for the German and Danish Networks," in *Wind Power in Power Systems*, T. Ackermann, Ed. Chichester, England: John Wiley and Sons, 2005, pp. 365–383.

[17] I. Marti, G. Kariniotakis, P. Pinson, I. Sanchez, T. S. Nielsen, H. Madsen, G. Giebel, J. Usaola, A. Palomares, R. Brownsword, J. Tambke, U. Focken, M. Lange, G. Sideratos, and G. Descombes, "Evaluation of Advanced Wind Power Forecasting Models - Results of the Anemos Project," in *European Wind Energy Conference*, Athen, 2006.

[18] J. Tambke, L. Bremen von, R. Barthelmie, A. Palomares, T. Ranchin, J. Juban, G. N. Kariniotakis, R. Brownsword, and H.-P. Waldl, "Short-Term Forecasting of Offshore Wind Farm Production - Developments of the Anemos Project," in *European Wind Energy Conference*, Athen, 2006.

[19] B. Hasche, R. Barth, and D. J. Swider, "Effects of improved wind forecasts on operational costs in the German electricity system," in *EcoMod Conference on Energy and Environmental Modeling*, Moscow, Russia, 2007.

[20] P. Pinson, C. Chevallier, and G. Kariniotakis, "Trading Wind Generation From Short-Term Probabilistic Forecasts of Wind Power," *IEEE Transactions on Power Systems*, vol. 22, no. 3, pp. 1148–1156, 2007.

[21] P. Pinson, J. Juban, and G. N. Kariniotakis, "On the quality and value of probabilistic forecasts of wind generation," in *9th International Conference on Probabilistic Methods Applied to Power Systems*, KTH, Stockholm, Sweden, 2006.

[22] M. Lange and U. Focken, *Physical Approach to Short-Term Wind Power Prediction*. Berlin: Springer, 2005.

[23] C. Johnston, M. A. Cooper, and R. J. Martin, "An Approach to Power Station Boiler and Turbine Life Management," in *16th World Conference on Nondestructive Testing (WCNDT)*, Montreal, 2004.

[24] K. Le, R. R. Jackups, J. Feinstein, H. H. Thompson, H. M. Wolf, E. C. Stein, A. D. Gorski, and J. S. Griffith, "Operational Aspects of Generation Cycling. A Report Prepared by the IEEE Current Operating Problems Subcommittee (COPS)." *IEEE Transactions on Power Systems*, vol. 5, no. 4, pp. 1194–1203, 1990.

[25] F. J. Berte, D. S. Moelling, and U. A. Craig, "Assessing the true cost of cycling operation is a challenging assignment." *Combined Cycle Journal*, no. 4, pp. 3–4, 2003.

[26] S. A. Lefton, P. M. Besuner, G. P. Grimsrud, A. Bissel, and G. L. Norman, "Optimizing Power Plant Cycling Operations While Reducing Generating Plant Damage and Costs at the Irish Electric Supply Board," in *International Conference on Plaint Maintenance for Managing Life and Performance - Baltica IV*, Stockholm, 1998.

[27] K. Heuck and K.-D. Dettmann, *Elektrische Energieversorgung: Erzeugung, Übertragung und Verteilung elektrischer Energie für Studium und Praxis*, 6th ed. Wiesbaden: Vieweg, 2005.

[28] A. Shibli, J. Gostling, and F. Starr, "Damage to Power Plants Due to Cycling," EPRI, Tech. Rep. 1001507, 2001.

[29] J. Gostling, "Two Shifting of Power Plant: Damage to Power Plant Due to Cycling - A brief overview," *OMMI*, vol. 1, no. 1, 2002.

[30] S. A. Lefton and P. M. Besuner, "The Cost of Cycling Coal Fired Power Plants," *Coal Power Magazine*, pp. 16–20, 2006.

[31] M. Vollmer, "State of the Art of Combined Cycle Power Plants," in *EU-GCC Seminar: Natural Gas Technologies – Realities & Prospects*, Doha, Quatar, 2005.

[32] J. Bowring, "Operating Reserves Rules," PJM, Tech. Rep., 2005. [Online]. Available: http://www.monitoringanalytics.com/reports/Presentations/2005/20051116-oper-res-rules.pdf [Retrieved 11.6.2009].

[33] M. Fischedick, "Erneuerbare Energien und Blockheizkraftwerke im Kraftwerksverbund: technische Effekte, Kosten, Emissionen." Ph.D. dissertation, Universität Stuttgart, 1995.

[34] IEEE, "The IEEE Reliability Test System - 1996," *IEEE Transactions on Power Systems*, vol. 14, no. 3, pp. 1010–1020, 1999.

[35] M. Hundt, R. Barth, N. Sun, S. Wissel, and A. Voß, "Verträglichkeit von erneuerbaren Energien und Kernenergie im Erzeugungsportfolio - Technische und ökonomische Aspekte," Tech. Rep., 2009. [Online]. Available: http://www.ier.uni-stuttgart.de/ [Retrieved 20.11.2009].

[36] DVG, "Das versorgungsgerechte Verhalten von thermischen Kraftwerken," Deutsche Verbundgesellschaft e. V. (DVG), Tech. Rep., 1991.

[37] CER, "Market Simulation Model Validation," Commission for Energy Regulation (CER), Tech. Rep., 2007. [Online]. Available: http://www.allislandproject.org/en/modelling-group-minutes-presentations.aspx [Retrieved 23.3.2008].

[38] A. J. Wood and B. F. Wollenberg, *Power Generation, Operation and Control*, 2nd ed. New York: John Wiley & Sons, 1996.

[39] Dena, "Energiewirtschaftliche Planung für die Netzintegration von Windenergie in Deutschland an Land und Offshore bis zum Jahr 2020," Deutsche Energie-Agentur GmbH, Tech. Rep., 2005. [Online]. Available: http://www.dena.de [Retrieved 24.02.2006].

[40] V. Viswanathan and D. Gray, "Damage to Power Plants Due to Cycling," EPRI, Tech. Rep. 1001507, 2001.

[41] R. Doherty and M. O'Malley, "A New Approach to Quantify Reserve Demand in Systems With Significant Installed Wind Capacity," *IEEE Transactions on Power Systems*, vol. 20, no. 2, pp. 587–595, 2005.

[42] VGB, "Verfügbarkeit von Wärmekraftwerken 1997-2006," VGB PowerTech e. V. (VGB), Tech. Rep., 2007.

[43] O. Brückl, "Wahrscheinlichkeitstheoretische Bestimmung des Regel- und Reserveleistungsbedarfs in der Elektrizitätswirtschaft," Ph.D. dissertation, Technische Universität München, 2006.

[44] H. J. Haubrich, "Gutachten zur Höhe des Regelenergiebedarfs," Bundesnetzagentur, Tech. Rep., 2008. [Online]. Available: http://www.bundesnetzagentur.de/media/archive/15435.pdf [Retrieved 9.8.2009].

[45] M. Lienert, "Leistungsvorhaltung auf Regelmärkten - Excel Add-in, Beschreibung und Anleitung," Energiewirtschaftliches Institut an der Universität zu Köln, Tech. Rep. Nr. 08.03, 2008. [Online]. Available: http://www.ewi.uni-koeln.de [Retrieved 29.7.2009].

[46] K. Hufendiek, *Systematische Entwicklung von Lastprognosesystemen auf der Basis neuronaler Netze.* Fortschritt-Berichte VDI Reihe 6 Nr. 455. Düsseldorf: VDI-Verlag, 2001.

[47] E. A. Feinberg and D. Genethliou, "Load forecasting," in *Applied Mathematics for Restructured Electric Power Systems: Optimization, Control, and Computational Intelligence*, ser. Power Electronics and Power Systems, J. H. Chow, F. F. Wu, and J. A. Momoh, Eds. Berlin: Springer-Verlag, 2005.

[48] D. J. Swider, B. Hasche, K. Rudion, and C. Heyde, "Verteilungsdichteprognosen von Netzlast und Preisen," Report of the BMBF project: Reduced models of complex electrical networks with dispersed generation (Netmod), Tech. Rep., 2006. [Online]. Available: http://www.netmod.org/ [Retrieved 22.10.2006].

[49] J. Büchner, T. Türkucar, W. Nick, F.-R. Graf, E. Handschin, W. Horenkamp, D. König, D. Waniek, and W. Schulz, "Gutachten - Bestimmung des regelzoneninternen Regelleistungsbedarfs für Sekundärregelung und Minutenreserve," Bundesnetzagentur, Tech. Rep. D06-79, 2006. [Online]. Available: http://www.bundesnetzagentur.de/media/archive/8224.pdf [Retrieved 3.1.2010].

[50] G. Dany, H. J. Haubrich, and D. Schlecht, "Bemessung des Regelleistungsbedarfs im liberalisierten Strommarkt," in *Int. ETG-Kongress – Energietechnik für die Zukunft.* Hamburg: Energietechnische Gesellschaft im VDE (ETG), 2003.

[51] B. Hasche, "Wirtschaftliche Einschätzung des Ausbaus der Windenergie und der resultierenden Auswirkungen auf die Regelenergieversorgung." Diploma thesis, Technische Universität München, 2005.

[52] SEI, "Operating Reserve Requirements as Wind Power Penetration Increases in the Irish Electricity System." Sustainable Energy Island (SEI), Tech. Rep., 2004. [Online]. Available: http://www.sei.ie [Retrieved 8.12.2008].

[53] C. Maurer, S. Krahl, and H. Weber, "Dimensioning of secondary and tertiary control reserve by probabilistic methods," *European Transactions on Electrical Power*, vol. 19, pp. 544–552, 2009.

[54] G. Dany and H. J. Haubrich, "Anforderungen an die Kraftwerksreserve bei hoher Windenergieeinspeisung," *Energiewirtschaftliche Tagesfragen*, vol. 50, no. 12, pp. 890–894, 2000.

[55] E. Lorenz, D. Heinemann, H. Wickramarathne, H. G. Beyer, and S. Bofinger, "Forecast of ensemble power production by grid-connected PV systems," in *20th European PV Conference*, Milano, 2007.

[56] H.-K. Breitkreuz, "Solare Strahlungsprognosen für energiewirtschaftliche Anwendungen - Der Einfluss von Aerosolen auf das sichtbare Strahlungsangebot," Ph.D. dissertation, Universität Würzburg, 2008.

[57] P. Bacher, H. Madsen, and H. A. Nielsen, "Online short-term solar power forecasting," *Solar Energy*, vol. in press, 2009.

[58] C. M. Zealand, D. H. Burn, and S. P. Simonovic, "Short term streamflow forecasting using artificial neural networks," *Journal of Hydrology*, vol. 214, pp. 32–48, 1999.

[59] T. Stokelj, D. Paravan, and R. Golob, "Short and mid term hydro power plant reservoir inflow forecasting," in *Fourth International Conference on Power System Technology (PowerCon 2000)*, Perth, Australia, 2000.

[60] Z. X. Xu and J. Y. Li, "Short-term inflow forecasting using an artificial neural network model," *Hydrological Processes*, vol. 16, pp. 2423–2439, 2002.

[61] regelleistung.net, "Internetplattform zur Auschreibung von Regelleistung," 2010, [Retrieved 9.6.2010]. [Online]. Available: https://www.regelleistung.net

[62] UCTE, "UCTE Operation Handbook," Union for the Coordination of Transmission of Electricity (UCTE), Tech. Rep., 2009. [Online]. Available: http://www.entsoe.eu/resources/publications/ce/oh/ [Retrieved 18.11.2009].

[63] V. Crastan, *Elektrische Energieversorgung 2*, 2nd ed. Heidelberg: Springer, 2009.

[64] StromNZV, "Verordnung über den Zugang zu Elektrizitätsversorgungsnetzen (Stromnetzzugangsverordnung - StromNZV)," 2008.

[65] EEX, "Internetpräsenz der European Energy Exchange," 2010, [Retrieved 25.4.2010]. [Online]. Available: http://www.eex.com

[66] EnWG, "Gesetz über die Elektrizitäts- und Gasversorgung (Energiewirtschaftsgesetz - EnWG)," 2005.

[67] H. Schumacher, "Durchbrechung des Vorrangs für erneuerbare Energien?: Das Einspeisemanagement im Erneuerbare-Energien-Gesetz und das Verhältnis zu den Regelungen des Energiewirtschaftsrechts," *Zeitschrift für Umweltrecht: Das Forum für Umwelt- und Planungsrecht.*, vol. 20, no. 11, pp. 522–530, 2009.

[68] K. Heuck, K.-D. Dettmann, and D. Schulz, *Elektrische Energieversorgung: Erzeugung, Übertragung und Verteilung elektrischer Energie für Studium und Praxis*, 7th ed. Wiesbaden: Vieweg, 2007.

[69] V. Crastan, *Elektrische Energieversorgung 1*, 1st ed. Heidelberg: Springer, 2007.

[70] v. A. Meier, *Electric Power Systems - A Conceptual Introduction.* New Jersey: John Wiley & Sons, 2006.

[71] UCTE, "Transmission Development Plan," Tech. Rep., 2008. [Online]. Available: http://www.ucte.org/resources/publications/otherreports/ [Retrieved 19.2.2009].

[72] H. Brakelmann, "Netzverstärkungs-Trassen zur Übertragung von Windenergie: Freileitung oder Kabel?" Bundesverband WindEnergie e.V., Tech. Rep., 2004. [Online]. Available: http://www.wind-energie.de [Retrieved 7.7.2006].

[73] B. R. Oswald, "Vergleichende Studie zu Stromübertragungstechniken im Höchstspannungsnetz," ForWind, Tech. Rep., 2005. [Online]. Available: http://www.forwind.de [Retrieved 5.4.2006].

[74] F. Leuthold, I. Rumiantseva, H. Weigt, T. Jeske, and C. Hirschhausen, "Nodal Pricing in the German Electricity Sector – A Welfare Economics Analysis, with Particular Reference to Implementing Offshore Wind Capacities," Tech. Rep. WP-EM-08a, 2005. [Online]. Available: http://papers.ssrn.com [Retrieved 24.9.2007].

[75] C. Rehtanz, "Vorlesung - Einführung in die Elektrische Energietechnik," Technische Universität Dortmund - Lehrstuhl für Energiesysteme und Energiewirtschaft, Tech. Rep., 2009.

[76] W. F. Tinney and C. E. Hart, "Power Flow Solution by Newton's Method," *IEEE Transactions on Power Appartus and Systems*, vol. 86, no. 11, pp. 1449–1460, 1967.

[77] B. Stott, "Review of Load-Flow Calculation Methods," *Proceedings of the IEEE*, vol. 62, no. 7, pp. 916–929, 1974.

[78] J. Sun and L. S. Tesfatsion, "DC Optimal Power Flow Formulation and Solution Using QuadProgJ," Iowa State Universitz, Tech. Rep., 2006. [Online]. Available: http://www2.econ.iastate.edu/tesfatsi/dc-opf.jslt.pdf [Retrieved 4.8.2008].

[79] B. Stott, J. Jardim, and O. Alsac, "DC Power Flow Revisited," *IEEE Transactions on Power Systems*, vol. 24, no. 3, pp. 1290–1301, 2009.

[80] T. J. Overbye, X. Cheng, and Y. Sun, "A Comparison of the AC and DC Power Flow Models for LMP Calculations," in *37th Hawaii International Conference on System Sciences*, vol. 37, Hawaii (US), 2004.

[81] K. Purchala, L. Meeus, D. v. Dommelen, and R. Belmans, "Usefulness of DC Power Flow for Active Power Flow Analysis," in *IEEE PES General Meeting*, San Francisco, 2005.

[82] P. Meibom, P. E. Morthorst, L. H. Nielsen, C. Weber, K. Sander, D. J. Swider, and H. Ravn, "Power System Models – A Description of Power Markets and Outline of Market Modelling in Wilmar," Report of the EU Project: Wind Power Generation in Liberalised Electricity Markets (Wilmar)., Forschungsbericht, 2003. [Online]. Available: http://www.risoe.de/rispubl/sys/ris-r-1441.htm [Retrieved 10.2.2006].

[83] H. Brand, R. Barth, D. J. Swider, and C. Weber, "Ein stochastisches Modell zur Berechnung der Integrationskosten der Windenergie," in *VDI-Fachtagung: Optimierung in der Energiewirtschaft*, ser. VDI-Berichte, Stuttgart, 2005, pp. 103–129.

[84] R. Barth, H. Brand, P. Meibom, and C. Weber, "A Stochastic Unit-commitment Model for the Evaluation of the Impacts of Integration of Large Amounts of Intermittent Wind Power," in *9th International Conference on Probabilistic Methods Applied to Power Systems*, vol. 9, KTH, Stockholm, Sweden, 2006.

[85] P. Meibom, J. Kiviluoma, R. Barth, H. Brand, and C. Weber, "Value of Electric Heat Boilers and Heat Pumps for Wind Power Integration," *Wind Energy*, vol. 10, no. 4, pp. 321–337, 2007.

[86] C. Weber, P. Meibom, R. Barth, and H. Brand, "WILMAR: A Stochastic Programming Tool to Analyze the Large-Scale Integration of Wind Energy," in *Optimization in the Energy Industry*, J. Kallrath, P. M. Pardalos, S. Rebennack, and M. Scheidt, Eds. Berlin: Springer, 2009, pp. 437–458.

[87] P. Meibom, R. Barth, H. Brand, B. Hasche, D. J. Swider, H. Ravn, and C. Weber, "Final Report for All Island Grid Study Work-Stream 2b: Wind Variability Management Studies," Tech. Rep., 2007. [Online]. Available: http://www.dcenr.gov.ie [Retrieved 20.10.2008].

[88] TradeWind, "Integrating Wind - Developing Europe's power market for the large-scale integration of wind power," European Wind Energy Association, Tech. Rep., 2009. [Online]. Available: http://www.trade-wind.eu [Retrieved 11.1.2010].

[89] R. Barth, "DISEM2-Net: Modell zur Einsatzoptimierung der verteilten Stromerzeugung," Report of the BMBF project: Reduced models of complex electrical networks with dispersed generation (Netmod), Tech. Rep., 2009.

[90] B. Hasche, "General statistics of geographically dispersed wind power," *Wind Energy*, vol. 13, no. 8, pp. 773–784, 2010.

[91] BNetzA, "Eckpunkte der Ausgestaltung der Öffnung des Marktsegmentes EEG-Veredelung," Bundesnetzagentur, Tech. Rep., 2008. [Online]. Available: www.bundesnetzagentur.de [Retrieved 16.3.2009].

[92] J. R. Birge and F. Louveaux, *Introduction to Stochastic Programming*. New York: Springer, 1997.

[93] P. Kall and J. Mayer, *Stochastic Linear Programming - Models, Theory, and Computation*. New York: Springer, 2005.

[94] C. S. Buchanan, K. I. M. McKinnon, and G. K. Skondras, "The Recursive Definition of Stochastic Linear Programming Problems within an Algebraic Modeling Language," *Annals of Operations Research*, vol. 104, no. 1-4, pp. 15–32, 2001.

[95] J. Kiviluoma and P. Meibom, "Power System Models – A Description of Power Markets and Outline of Market Modelling in Wilmar," Report of the EU Project: Wind Power Generation in Liberalised Electricity Markets (Wilmar)., Tech. Rep. Deliverable D6.2, 2006. [Online]. Available: http://www.wilmar.risoe.dk/ [Retrieved 10.8.2006].

[96] UCTE, "System Adequacy Retrospect 2008," Union for the Coordination of Transmission of Electricity, Tech. Rep., 2008. [Online]. Available: http://www.ucte.org [Retrieved 13.6.2009].

[97] ——, "System Adequacy Forecast 2009 – 2020," Union for the Coordination of Transmission of Electricity, Tech. Rep., 2009. [Online]. Available: http://www.ucte.org [Retrieved 1.9.2009].

[98] ENTSO-E, "Country Data Packages - Production, Consumption, Exchange Package," 2010, [Retrieved 10. January]. [Online]. Available: http://www.entsoe.eu

[99] ISET, "Wind Energy Report Germany 2006," ISET e. V., Tech. Rep., 2006.

[100] P. Capros, L. Mantzos, V. Papandreou, and N. Tasios, "European Energy and Transport - Trends to 2030 - Update 2007," European Commission - Directorate General Energy and Transport, Tech. Rep., 2008. [Online]. Available: http://ec.europa.eu [Retrieved 23.8.2008].

[101] AGFW, "Hauptbericht der Fernwärmeversorgung," Arbeitsgemeinschaft für Wärme und Heizkraftwirtschaft - AGFW - e.V., Tech. Rep., 2006.

[102] B. Hasche, A. Keane, and M. O'Malley, "Capacity Value of Wind Power, Calculation and Data Requirements: the Irish Power System Case," *IEEE Transactions on Power Systems*, vol. 26, no. 1, pp. 420–430, 2011.

[103] BMU, "Langfristszenarien und Strategien für den Ausbau erneuerbarer Energien in Deutschland - Leitszenario 2009," Bundesministerium für Umwelt, Naturschutz und Reaktorsicherheit, Tech. Rep., 2009. [Online]. Available: http://www.erneuerbare-energien.de [Retrieved 10.4.2010].

[104] L. Mez, S. Schneider, D. Reiche, S. Tempel, S. Klinski, and E. Schmitz, "Zukünftiger Ausbau erneuerbarer Energieträger unter besonderer Berücksichtigung der Bundesländer," Forschungsstelle für Umweltpolitik, Tech. Rep., 2007. [Online]. Available: www.erneuerbare-energien.de [Retrieved 2.11.2009].

[105] BNetzA, "PV Leistung pro Bundesland," Bundesnetzagentur, Tech. Rep., 2009. [Online]. Available: www.bundesnetzagentur.de [Retrieved 8.4.2010].

[106] N. Henkel, E. Schmid, and E. Gobrecht, "Operational Flexibility Enhancements of Combined Cycle Power Plants," in *POWER-GEN Asia 2008*. Kuala Lumpur: Siemens, 2008.

[107] D. J. Swider, I. Ellersdorfer, M. Hundt, and A. Voß, "Anmerkungen zu empirischen Analysen der Preisbildung am deutschen Spotmarkt für Elektrizität," Gutachten im Auftrag des Verband der Verbundunternehmen und Regionalen Energieversorger in Deutschland - VRE - e.V., 2007. [Online]. Available: http://elib.uni-stuttgart.de [Retrieved 3.5.2008].

[108] L. Eltrop, J. Moerschner, M. Härdtlein, and A. König, "Bilanz und Perspektiven der Holzenergienutzung in Baden-Württemberg," *Forschungsberichte des IER*, vol. 98, 2006.

[109] CARMEN, "Preisentwicklung bei Waldhackschnitzeln," 2008, [Retrieved 11.09.2008]. [Online]. Available: http://www.carmen-ev.de

[110] UCTE, "Statistical Yearbook 2007," Union for the Coordination of Transmission of Electricity, Tech. Rep., 2008. [Online]. Available: http://www.ucte.org [Retrieved 19.6.2009].

[111] Nordel, "Agreement (Translation) regarding operation of the interconnected Nordic power system (System Operation Agreement)," Organisation for the Nordic Transmission System Operators, Tech. Rep., 2006. [Online]. Available: http://www.entsoe.eu [Retrieved 22.11.2009].

[112] Y. G. Rebours, D. S. Kirschen, M. Trotignon, and S. Rossignol, "A Survey of Frequency and Voltage Control Ancillary Services—Part I: Technical Features," *IEEE Transactions on Power Systems*, vol. 22, no. 1, pp. 350–357, 2007.

[113] UCTE, "UCTE Operation Handbook," Union for the Coordination of Transmission of Electricity (UCTE), Tech. Rep., 2004. [Online]. Available: http://www.ucte.org/ [Retrieved 2.5.2008].

[114] E. M. Gouveia and M. A. Matos, "Operational Reserve of a Power System with a Large Amount of Wind Power," in *8th International Conference on Probabilistic Methods Applied to Power Systems (PMAPS)*, Iowa, 2004, pp. 717–722.

[115] J. M. Morales, A. J. Conejo, and J. Pérez-Ruiz, "Economic Valuation of Reserves in Power Systems With High Penetration of Wind Power," *IEEE Transactions on Power Systems*, vol. 24, no. 2, pp. 900–910, 2009.

[116] Y. G. Rebours, D. S. Kirschen, M. Trotignon, and S. Rossignol, "A Survey of Frequency and Voltage Control Ancillary Services—Part II: Economic Features," *IEEE Transactions on Power Systems*, vol. 22, no. 1, pp. 358–366, 2007.

[117] S. Riedel and H. Weigt, "German Electricity Reserve Markets," Dresden University of Technology, Tech. Rep. WP-EM-20, 2007. [Online]. Available: http://papers.ssrn.com [Retrieved 29.06.2009].

[118] VDN, "Deutsches Höchstspannungsnetz 01.01.2007," Verband der Netzbetreiber, VDN e. V., Tech. Rep., 2007.

[119] Eirgrid, "Transmission Forecast Statement 2008 - 2014," Tech. Rep., 2008. [Online]. Available: http://www.eirgrid.com [Retrieved 19.03.2009].

[120] BSH, "Offshore-Windparks (Pilotgebiete)," Bundesamt für Seeschifffahrt und Hydrographie, Tech. Rep., 2009. [Online]. Available: http://www.bsh.de [Retrieved 10.9.2009].

[121] ETSO, "Definitions of Transfer Capacities in Liberalised Electricity Markets," European Transmission System Operators, Tech. Rep., 2001. [Online]. Available: https://www.entsoe.eu [Retrieved 1.9.2009].

[122] ——, "Explanatory notes for the interpretation of NTC values," 2009, [Retrieved 9.5.2009]. [Online]. Available: http://www.etso-net.org/NTC_Info/prototype/ntc_matrix/e_default.asp

[123] ——, "Indicative values for Net Transfer Capacities (NTC) in Europe," 2008, [Retrieved 9.5.2009]. [Online]. Available: http://www.etso-net.org/NTC_Info

[124] Nordel, "Prioritized cross sections - Reinforcement measures within the Nordic countries," Tech. Rep., 2008. [Online]. Available: http://www.nordel.org [Retrieved 10.9.2009].

[125] J. McLean and G. Hassan, "Tradewind Project, WP2.4 – Characteristic Wind Speed Time Series," Tech. Rep., 2008. [Online]. Available: http://www.trade-wind.eu [Retrieved 2.4.2009].

[126] G. v. d. Toorn and G. Hassan, "Tradewind - Work Package 2: Wind Power Scenarios - WP2.1: Wind Power Capacity Data Collection," Tech. Rep., 2007. [Online]. Available: http://www.trade-wind.eu [Retrieved 2.4.2009].

[127] BEE, "Stromversorgung 2020 - Wege in eine moderne Energiewirtschaft," Bundesverband Erneuerbare Energie e.V., Tech. Rep., 2009. [Online]. Available: www.bee-ev.de [Retrieved 26.11.2009].

[128] BWE, "Die Entwicklung der Windenergie in Deutschland 2008," Bundesverband WindEnergie e. V., Tech. Rep., 2009. [Online]. Available: http://www.wind-energie.de/de/statistiken/ [Retrieved 10.8.2009].

[129] W. Winkler, M. Strack, and A. Westerhellweg, "Normierung und Bewertung von Winddaten und Energieerträgen von Windparks," *DEWI Magazin*, vol. 23, 2003.

[130] R. Barthelmie and S. Pryor, "Challenges in Predicting Power Output from Offshore Wind Farms," *Journal of Energy Engineering*, vol. 132, no. 3, pp. 91–103, 2006.

[131] S. Pryor and R. Barthelmie, "Comparison of Potential Power Production at On- and Offshore Sites," *Wind Energy*, vol. 4, pp. 173–181, 2001.

[132] R. Barthelmie, O. F. Hansen, K. Enevoldsen, J. Hojstrup, S. Frandsen, S. Pryor, S. Larsen, M. Motta, and P. Sanderhoff, "Ten Years of Meteorological Measurements for Offshore Wind Farms," *Journal of Solar Energy Engineering*, vol. 127, pp. 170–176, 2005.

[133] G. A. Boyle, "UK Offshore Wind Potential," *Renewable Energy Focus*, 2006.

[134] IWES, "Windenergie Report Deutschland 2009 - Offshore," Fraunhofer Institut für Windenergie und Energiesystemtechnik (IWES), Tech. Rep., 2010. [Online]. Available: http://offshorewmep.iset.uni-kassel.de [Retrieved 17.1.2010].

[135] J. Tomaschek and H. Kollmann, "Windenergie - Bewertung von Kosten und Potenzialen," *BWK*, vol. 61, no. 6, pp. 48–52, 2009.

[136] B. Ernst, M. Hoppe-Kilpper, K. Kurt Rohrig, and M. Michael Scheibe, "Zeitreihen der Windeinspeisung und deren statistische Analyse - Zusatzuntersuchung im Rahmen der dena-Netzstudie," Institut für Solare Energieversorgungstechnik e. V. (ISET), Tech. Rep., 2004.

[137] K. Rohrig, "Dezentrale Energieversorgung - Entwicklungschancen, Voraussetzungen, Pilotprojekte," in *VWEW/VDE-Fachtagung*, Mainz, 2007.

[138] B. Ernst, Y. Wan, and B. Kirby, "Short-Term Power Fluctuation of Wind Turbines: Analyzing Data from the German 250-MW Measurement Program from the Ancillary Services Viewpoint," in *Windpower'99*. Burlington, Vermont: National Renewable Energy Laboratory, 1999.

[139] Y. Wan and D. Bucaneg, "Short-Term Power Fluctuations of Large Wind Power Plants," *Journal of Solar Energy Engineering*, vol. 124, pp. 427–431, 2002.

[140] Y. Wan, "Wind Power Plant Behaviours: Analyses of Long-Term Wind Power Data," Tech. Rep. NREL/TP-500-36551, 2004. [Online]. Available: http://www.nrel.gov [Retrieved 6.10.2008].

[141] P. Norgaard, G. Giebel, H. Holttinen, L. Söder, and A. Petterteig, "Fluctuations and predictability of wind and hydropower," Risoe National Laboratory, Tech. Rep. Riso-R-1443(EN), 2004. [Online]. Available: http://www.risoe.dk [Retrieved 30.3.2007].

[142] L. Landberg, "The availability and variability of the European wind resource," *International Journal of Sustainable Energy*, vol. 18, no. 4, pp. 313–320, 1997.

[143] G. Giebel, *On the Benefits of Distributed Generation of Wind Energy in Europe*, ser. Schriftenreihe Energietechnik. Düsseldorf: VDI-Verlag, 2001.

[144] P. Kiss and I. M. Jánosi, "Limitations of wind power availability over Europe: a conceptual study," *Nonlinear Processes in Geophysics*, vol. 15, pp. 803–813, 2008.

[145] H. Holttinen and R. Hirvonen, "Power System Requirements for Wind Power," in *Wind Power in Power Systems*, T. Ackermann, Ed. Chichester, England: John Wiley and Sons, 2005, pp. 143–169.

[146] U. Focken, M. Lange, K. Mönnich, H.-P. Waldl, H. G. Beyer, and A. Luig, "Short-term prediction of the aggregated power output of wind farms - a statistical analysis of the reduction of the prediction error by spatial smoothing effects," *Journal of Wind Engineering and Industrial Aerodynamics*, vol. 90, no. 3, pp. 231–246, 2002.

[147] D. Wackerly, W. Mendenhall, and R. Scheaffer, *Mathematical Statistics with Applications*, 5th ed. New York: Duxbury Press, 1996.

[148] D. A. Bechrakis and P. D. Sparis, "Simulation of the Wind Speed at Different Heights Using Artificial Neural Networks," *Wind Engineering*, vol. 24, no. 2, pp. 127–136, 2000.

[149] C. Rose and M. Smith, *Mathematical statistics with Mathematica*. New-York: Springer, 2002.

[150] P. Norgaard and H. Holttinen, "A Multi-Turbine Power Curve Approach," in *Nordic Wind Power Conference*, Chalmers University of Technology, 2004.

[151] M. Gibescu, B. C. Ummels, and W. L. Kling, "Statistical Wind Speed Interpolation for Simulating Aggregated Wind Energy Production under System Studies," in *9th International Conference on Probabilistic Methods Applied To Power Systems (PMAPS)*, KTH, Ed. Stockholm, Sweden: KTH, 2006.

[152] M. Gibescu, A. J. Brand, and W. L. Kling, "Estimation of Variability and Predictability of Large-scale Wind Energy in The Netherlands," *Wind Energy*, vol. 12, pp. 241–260, 2009.

[153] J. McLean and G. Hassan, "Tradewind Project, D2.4 – Equivalent Wind Power Curves," Tech. Rep., 2007. [Online]. Available: http://www.trade-wind.eu [Retrieved 2.4.2009].

[154] B. Hasche, "Analyse von Prognosen der Windgeschwindigkeit und Windstromeinspeisung," Report of the BMBF project: Reduced models of complex electrical networks with dispersed generation (Netmod), Tech. Rep., 2007. [Online]. Available: http://www.netmod.org [Retrieved 29.1.2008].

[155] L. Söder, "Simulation of Wind Speed Forecast Errors for Operation Planning of Multi-Area Power Systems," in *8th International Conference on Probabilistic Methods Applied to Power Systems*, vol. 8, Iowa State University, Ames, Iowa (US), 2004.

[156] J. Dupacova, N. Groewe-Kuska, and W. Roemisch, "Scenario reduction in stochastic programming - An approach using probability metrics," *Mathematical Programming*, vol. 95, no. 1, p. 493–511, 2003.

[157] N. Groewe-Kuska, H. Heitsch, and W. Roemisch, "Scenario Reduction and Scenario Tree Construction for Power Management Problems," in *IEEE Bologna Power Tech Conference*, Bologna, Italien, 2003.

[158] H. Heitsch and W. Roemisch, "Scenario Reduction Algorithms in Stochastic Programming," *Computational Applications and Optimization*, vol. 24, no. 2-3, pp. 187–206, 2003.

[159] R. Barth, L. Soeder, C. Weber, A. J. Brand, and D. J. Swider, "Methodology of the Scenario Tree Tool - Deliverable 6.2 (d)," Report of the EU Project: Wind Power Generation in Liberalised Electricity Markets (Wilmar)., Tech. Rep., 2006. [Online]. Available: http://www.wilmar.risoe.dk

[160] B. Hasche, "Scenario Tree Generation for an Electricity Market Model," Report of the BMBF project: Reduced models of complex electrical networks with dispersed generation (Netmod), Tech. Rep., 2008. [Online]. Available: http://www.netmod.org/ [Retrieved 20.7.2008].

[161] K. Hoyland and S. W. Wallace, "Generating Scenario Trees for Multistage Decision Problems," *Management Science*, vol. 47, no. 2, pp. 295–307, 2001.

[162] IEA, *World Energy Outlook 2007 - China and India Insights*. Paris: International Energy Agency, 2007.

[163] R. Sedlacek, "Untertage-Gasspeicherung in Deutschland," *Erdöl Erdgas Kohle*, vol. 124, no. 11, 2008.

[164] F. Crotogino, "Druckluftspeicher-Gasturbinen-Kraftwerke / Geplanter Einsatz beim Ausgleich fluktuierender Windenergie-Produktion und aktuellem Strombedarf," in *Kasseler Symposium Energy-Systemtechnik 2002*, Kassel, 2002.

[165] A. Kampke, "Druckluftspeicher," *Energieperspektiven*, no. 1, p. 4, 2008.

[166] D. Oertel, "Energiespeicher - Stand und Perspektiven," TAB - Büro für Technikfolgenabschätzung beim Deutschen Bundestag, Tech. Rep., 2008. [Online]. Available: http://www.tab.fzk.de [Retrieved 26.3.2009].

[167] D. J. Swider, "Compressed Air Energy Storage in an Electricity System With Significant Wind Power Generation," *IEEE Transaction on Energy Conversion*, vol. 22, no. 1, pp. 95–102, 2007.

[168] C. Kruck, "Integration einer Stromerzeugung aus Windenergie und Speichersystemen unter besonderer Berücksichtigung von Druckluft-Speicherkraftwerken," Ph.D. dissertation, University of Stuttgart, 2008.

[169] C. Nabe, G. Papaefthymiou, and A. Mullane, "All Island Grid Study - Updated to Include Demand Side Management," Tech. Rep. PPSMDE082653, 2009. [Online]. Available: http://www.dcenr.gov.ie/Energy [Retrieved 22.3.2010].

[170] C. Nabe, C. Beyer, N. Brodersen, H. Schäffler, D. Adam, C. Heinemann, T. Tusch, J. Eder, C. de Wyl, J.-H. vom Wege, and S. Mühe, "Einführung von lastvariablen und zeitvariablen Tarifen," Bundesnetzagentur, Tech. Rep., 2009. [Online]. Available: www.bundesnetzagentur.de [Retrieved 25.2.2010].

[171] A. Ockenfels, V. Grimm, and G. Zoettl, "Strommarktdesign - Preisbildungsmechanismus im Auktionsverfahren für Stromstundenkontrakte an der EEX - Gutachten im Auftrag der European Energy Exchange AG zur Vorlage an die Sächsische Börsenaufsicht," EEX, Tech. Rep., 2008. [Online]. Available: www.eex.com [Retrieved 11.7.2010].

[172] P. Denholm and F. Sioshansi, "The value of compressed air energy storage with wind in transmission-constrained electric power systems," *Energy Policy*, vol. 37, pp. 3149–3158, 2009.

[173] R. Billinton and R. N. Allan, *Reliability evaluation of power systems*, 2nd ed. New York: Plenum Publishing Corporation, 1996.

[174] T. Adams and F. Cadieux, "Wind power in Ontario: Quantifiying the benefits of geographic diversity." in *2nd Climate Change Technology Conference*. Ontario: Engineering Institute of Canada, 2009.

[175] M. S. Bartlett, "The Spectral Analysis of Two-Dimensional Point Processes," *Biometrika*, vol. 51, no. 3/4, pp. 299–311, 1964.

[176] B. Gosh, "Random distances within a rectangle and between two rectangles," *Bulletin of the Calcutta Mathematical Society*, vol. 43, pp. 17–24, 1951.